CHALMERS
UNIVERSITY OF TECHNOLOGY

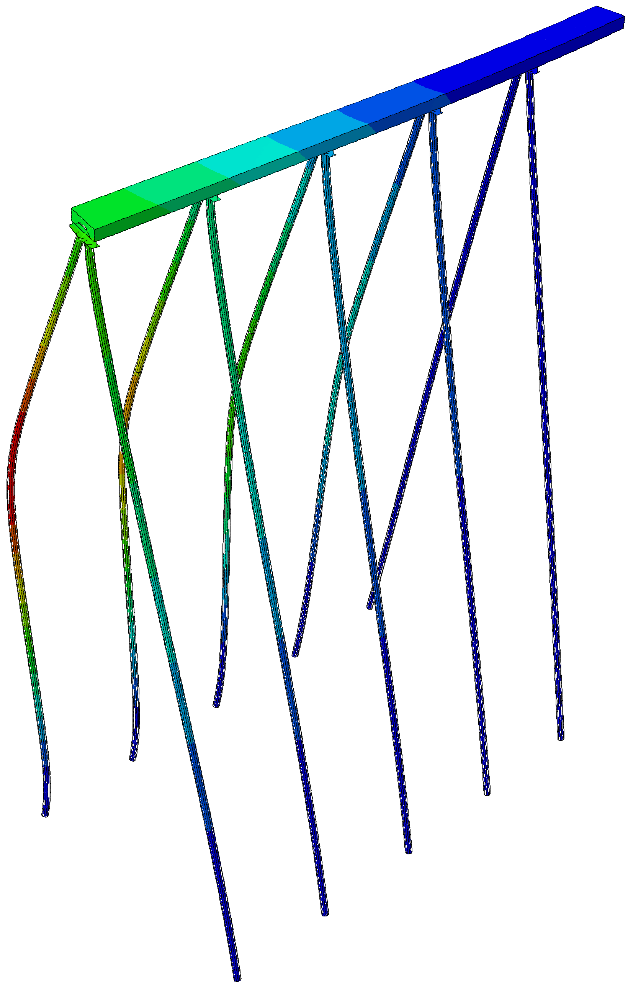

Non-linear analysis of bridge protective piers exposed to ship collision

Energy absorbing capacity of the protective piers at Hisingsbron

Master's Thesis in the Master's Programme Structural Engineering and Building Technology

JOHAN FORSGRAN
ANDREAS LAMTON

Department of Civil and Environmental Engineering
Division of Structural Engineering
Concrete Structures
CHALMERS UNIVERSITY OF TECHNOLOGY
Gothenburg, Sweden 2015
Master's Thesis 2015:50

MASTER'S THESIS 2015:50

Non-linear analysis of bridge protective piers exposed to ship collision

Energy absorbing capacity of the protective piers at Hisingsbron

Master's Thesis in the Master's Programme Structural Engineering and Building Technology

JOHAN FORSGRAN

ANDREAS LAMTON

Department of Civil and Environmental Engineering

Division of Structural Engineering

Concrete Structures

CHALMERS UNIVERSITY OF TECHNOLOGY

Göteborg, Sweden 2015

Non-linear analysis of bridge protective piers exposed to ship collision
Energy absorbing capacity of the protective piers at Hisingsbron

Master's Thesis in the Master's Programme Structural Engineering and Building Technology

JOHAN FORSGRAN

ANDREAS LAMTON

Examensarbete 2015:50/ Institutionen för bygg- och miljöteknik,
Chalmers tekniska högskola 2015

Department of Civil and Environmental Engineering
Division of Structural Engineering
Concrete Structures
Chalmers University of Technology
SE-412 96 Göteborg
Sweden
Telephone: + 46 (0)31-772 1000

Cover:
Deformation figure of the FE-model representing the protective pier, created in FE-software Abaqus/CAE 6.13-3.

Chalmers Reproservice. Göteborg, Sweden, 2015

Non-linear analysis of bridge protective piers exposed to ship collision

Energy absorbing capacity of the protective piers at Hisingsbron

Master's thesis in the Master's Programme Structural Engineering and Building Technology

JOHAN FORSGRAN
ANDREAS LAMTON
Department of Civil and Environmental Engineering
Division of Structural Engineering
Concrete Structures
Chalmers University of Technology

ABSTRACT

Series of historical ship-bridge collisions exposed the need for protective measures. One of these is protective piers that are sacrificial structures and defend the bridge supports against ship collisions. The purpose of this report was to study the non-linear structural response of these piers, which are to be built at Hisingsbron in Gothenburg, during collision progress. This was done by setting up a non-linear finite element model of the protective piers in the software Abaqus and analyse deformation pattern, critical events and resisting capacity.

It was found hard to model the ship load in a representable way and so the incoming kinetic energy from the design ship was compared to the protective piers' energy resisting capacity. The analysis gave an indication of how the structure would deform and computations proved that the energy absorbing capacity was insufficient. However, as the defined clay springs could not be verified, the results are not completely valid and cannot be used in design process of the protective piers. A powerful model, from which interesting data can be extracted, is obtained by correcting the springs and redefine the boundary conditions to resemble the reality better.

Key words: FE-modelling, FEM, Finite element model, Non-linear, Ship collision, Energy absorption, Protective pier, Hisingsbron, Concrete Damaged Plasticity, Structural response, Displacement control, Abaqus, Clay springs, Concrete, Steel, Reinforcement, Beam, Pile

Icke-linjär analys av påsegling utav ledverk
Energiabsorberande kapacitet för ledverket vid Hisingsbron

Examensarbete inom masterprogrammet Structural Engineering and Building Technology

JOHAN FORSGRAN
ANDREAS LAMTON
Institutionen för bygg- och miljöteknik
Avdelningen för Konstruktionsteknik
Betongbyggnad
Chalmers tekniska högskola

SAMMANFATTNING

Flera historiska kollisioner mellan fartyg och bro har påvisat ett behov av skyddande åtgärder. En sådan är ledverk vilka är offerkonstruktioner och hindrar fartyg från att köra in i brostöd. Syftet med denna rapport var att studera den icke-linjära responsen för Hisingsbrons ledverk under kollisionsförloppet. Detta gjordes genom att bygga en finit-element modell av ledverket i mjukvaran Abaqus och därefter analysera deformation, kritiska händelser och mothållande kapacitet.

Då det visade sig vara komplicerat att modellera fartygslasten på ett representativt sätt jämfördes istället dimensionerande fartygs inkommande energi med ledverkets energiabsorberande förmåga. Analysen gav en indikation på hur ledverket skulle ha deformerats och beräkningar visade att den energiabsorberande kapaciteten var otillräcklig. Eftersom lerfjädrarnas korrekta funktion inte kunde säkerställas så är resultaten inte pålitliga och borde därmed inte användas i ledverkets projektering. En bra modell, utifrån vilken man kan hämta intressanta data, erhålls om fjädrarna korrigeras och randvillkoren ändras för att bättre efterlikna verkligheten.

Nyckelord: FE-modellering, FEM, Finit element modell, Icke-linjär, Skeppskollision, Energi absorbering, Ledverk, Hisingsbron, Concrete Damaged Plasticity, Strukturell respons, Förskriven deformation, Abaqus, Lerfjädrar, Betong, Stål, Armering, Balk, Påle

Contents

Preface

This Master's thesis investigates energy absorbing capacity of protective piers exposed to ship collision. It was carried out at COWI AB, Göteborg in the spring of 2015, in collaboration with the Department of Civil and Environmental Engineering, Division of Structural Engineering, Concrete Structures research group. The thesis was carried out at the office of COWI, in Göteborg during the spring of 2015.

First of all we would like to thank our supervisor/examiner at Chalmers Joosef Leppänen for his continuous feedback during this thesis project. We would also like to thank our supervisor at COWI Magnus Bäckström for his guidance. A special thanks goes out to our co-supervisors Isak Svensson and Hanna Jansson who has been very helpful during the thesis process every time a question arose.

Finally we would like to thank all the employees at the department of Bridge engineering at COWI for the good atmosphere at the office and our opponents Niclas Görander and Cristopher Halldén for their feedback on the thesis work.

Göteborg June 2015

Johan Forsgran and Andreas Lamton

Notations

Roman upper case letters

C	Consequence [-]
DWT	Dead weight tonnage of the ship [metric ton]
E_a	Total available kinetic energy [J]
E_c	Young's modulus for concrete [Pa]
E_{def}	Deformation energy [Nm]
E_h	Young's modulus for steel at strain hardening [Pa]
E_s	Young's modulus for steel [Pa]
F	Force that displaces the structure [N]
F_{dyn}	Impact force on the structure following from impact analysis [N]
K	Stiffness [N/m]
N	Total number of incidents in the period of consideration [-]
N	Annual number of bridge passages for the vessel type under consideration [-]
P	Probability [-]
P_y	Yield pressure
PA	Probability of the vessel being aberrant per bridge passage, and successful evasive action not being taken [-]
PC	Probability of bridge collapse due to a collision by an aberrant vessel [-]
PG	Geometric probability of a collision between an aberrant vessel and a bridge pier or span [-]
R	Risk [-]
R	Resistance of the structure [-]
T	Reference period (usually 1 year) [years]
W	Work done on the structure [Nm]

Roman lower case letters

f_{cc}	Concrete compressive strength [Pa]
f_{ct}	Concrete tensile strength [Pa]
f_y	Yield strength (stress) [Pa]
f_u	Ultimate strength (stress) [Pa]
k	Equivalent elastic stiffness of the ship [N/m]
m	Mass of the ship [kg]
m	Mass of the object [kg]

n Number of ships per time unit (traffic intensity) [-]

p_a Probability that a collision is avoided by human intervention [-]

v Ship velocity [m/s]

v Velocity of the object [m/s]

x Coordinate of the point of the fatal error or mechanical failure [-]

Greek lower case letters

α Angle [°]

δ Displacement [m]

ε Strain [-]

ε_c Concrete strain [-]

ε_{c1} Maximum strain (the strain at the top of the curve) [-]

$\varepsilon_{c,el}$ Compressive elastic strain for concrete [-]

ε_h Strain at start of strain hardening [-]

$\varepsilon_{t,el}$ Tensile elastic strain for concrete [-]

ε_u Ultimate strain for concrete [-]

ε_y Yield strain [-]

λ Probability of a failure per unit travelling distance [-]

σ Stress [Pa]

σ_{b0} Initial equibiaxial compressive yield stress [Pa]

σ_{c0} Initial uniaxial compressive yield stress [Pa]

σ_c Compressive stress for concrete [Pa]

σ_t Tensile stress for concrete [Pa]

1 Introduction

1.1 Background

In the year 2010 a series of investments in roads, railroads and public transportation called West Swedish Agreement (Västsvenska paketet) were launched. The Swedish Road Administration’s (Trafikverkets) goal is to create a modernized society which can grow and be more attractive but at the same time be sustainable (Trafikverket, 2014).

One of the larger investments is to build a new bridge over Göta älv in Gothenburg, replacing the current bridge named Göta älvbron which was erected in the years 1936-1939 (Göteborgs stad, 2015). Due to the degradation of the steel in this construction action must take place in 2020 at the latest because of the calculated risk of failure. A great need of transportation over the river has kick-started the plans for the new bridge Hisingsbron and are currently in the making.

Included in the new bridge concept is the design of protective piers which is executed by the consulting company COWI AB. Protective piers are barriers that are erected in the river to guide the ships in the channel or to protect structures from collision. At Hisingsbron these piers will lead the ships through the bridge opening and prevent impact with the foundations. A study made by Trafikverket shows that the waterway traffic is predicted to increase (Trafikverket, 2013). The unused capacity of Göta älv cannot be utilized unless, for example, the protective piers along the fairway meet the requirements for the new traffic. The construction of Hisingsbron is planned to start in the beginning of year 2016.

It is of importance that the piers absorb the energy from the collision in an accurate way so that a catastrophe can be averted. This is done by deformation, both globally by the whole structure and also locally in the different parts. The behaviour of this collision should therefore be analysed so that the piers can be designed to withstand a collision. The response of the protective piers at impact is hard to predict with regular linear-elastic model and is for that reason proposed to be executed with a non-linear FE-setup (Finite Element-setup).

1.2 Purpose and objectives

The purpose of this report is to study the non-linear structural response of protective piers throughout the whole collision progress. The aim is to make a FE-model of the protective piers in a finite element program and to analyse deformation pattern, critical events and energy resisting capacity. Subsequent analyses should map the sensitivity of the system and design.

Another objective is to map how these piers have been designed before and how they can be modelled in an effective way. Therefore a profound literature study will be made to find reference projects and research in the field of study.

1.3 Limitations

The pier system is very large and for that reason only a 50 meter part of the construction will be studied in the final model. Ice, wind and temperature load will not be treated in the analysis, only the self-weight and the accidental collision load including the displaced water and the effects from the clay is treated.

1.4 Method

The project is divided into three sections. The first part is a literature study on protective piers and how this problem has been handled before. A case study will also be performed on the protective piers at the planned Hisingsbron to facilitate the behavioural study on the piers. The case study will provide dimensions for modelling of the protective piers. In addition to this a literature study will be made on FE-modelling to support understanding for how the model and loads will be set up in the software Abaqus. This is done by looking at previous reports, articles and Chalmers lectures containing FE-modelling of similar problem and contact with cunning people in the area.

In the second part simplified hand-calculations in 2D will verify the model and show approximate results to be expected from later analyses. The FE-model will be simple to start with but extended by the time by including more parts of the total guide structure into 3D.

Last part will be designated to model the final structure and run analyses to interpret the structural behaviour in the finite element program Abaqus/CAE 6.13-3. Evaluation whether the global response is reasonable or not along with refinement of model takes place.

2 Protective Measures

When building a bridge over water it might be exposed to various vessels crossing the waters under the bridge, which put the bridge in risk for a collision. One way to prevent this is to introduce a protective system to protect the bridge structure.

During the 1970's the ship-bridge accidents increased in America (U.S. Department of Transportation, 1983) and in 1980 one occurred outside Tampa in Florida, USA, as a freighter hit the Sunshine Skyway Bridge (Svensson, 2009). The impact caused the unprotected support to collapse along with an essential section of the bridge and 38 people died. A national investigation was on-going for more than a decade before standards regarding evaluation of vessel collision to structures were proposed (U.S. Department of Transportation, 1983). Not only in America but many ship-bridge collisions have also been recorded in China since the 70's till present. Waterways of Zhujiang River, Heilongjiang River and Yangzi River have been subject to over 300 incidents (Dai, et al., 2002).

During this period of research, computer software was developed to specifically analyse the effectiveness of bridge- and bridge protective structures subject to impact load. Experience from real accidents and crash tests had given the knowledge until then (Svensson, 2009). Still the problem exists in present time as these early approaches mostly treated the probability of ship collisions or were very conservative. Thanks to the better processing computers, the most accurate way to compute impact forces today would be to perform simulations and analyses using FEM (Finite Element Method).

2.1 Different types of protective methods

In the Swedish Road Administration's technical demands document TRVK BRO 11 it is clarified that it is up to the contractor whether the bridge should be designed to withstand impact loads from waterway traffic or instead to take measures that prevent collision with supports (Trafikverket, 2011).

Due to the extensive costs and complications of trying to retrofit protective systems for already existing bridges, the prediction and planning of a potential ship collision should be introduced at an early state of bridge concept creation. It is also important to decide what kind of protective measure that is going to be used (Kuzmanovic & Sanchez, 1992).

Which type of protective system that is needed depends on many factors (U.S. Department of Transportation, 1983). These factors include navigational matters such as currents, winds, visibility and channel geometrics. Moreover the variation in type and recurrence of the waterway traffic do matter as well as the localization of bridge supports in relation to the water. Furthermore the traffic on top of the bridge can be highly prioritized or not. The variation of the latter factor can increase the total bridge project cost to between 5 – 20 % as an accepted level in Sweden (Olnhausen, 1983).

The type of protective measures used can be divided into three categories. Firstly the bridge supports can be placed out of reach from collision of ships (e.g. on land), secondly the supports themselves can be constructed so that they can resist a direct impact from a ship and thirdly the ships can be halted or guided away from the supports either with a structure or an artificial island (Svensson, 2009). A risk assessment should be done to increase knowledge of the site before measures are taken.

2.1.1 Out of reach

A way to avoid collision is to build the bridge in such a way that a collision is impossible to occur. This can be done by placing the piers on land. An increased span length rather than support protection may for some projects be even cheaper (Svensson, 2009). Learning from the Tjörnbro-catastrophe, where a ship rammed into an arch bridge in western Sweden in 1980 (Brodin, 1984), the bridge should additionally be constructed so that the structural elements are unreachable from the fairway.

2.1.2 Strong piers

When designing the bridge piers they can be constructed in such a way so that they can withstand a collision from a ship, assuming that the ground conditions are sufficient (Svensson, 2009). Additional development of this protection method includes a structure mounted on the bridge support to take some of the impact see Figure 2.1 [a]. It can be made of thin steel membranes (Larsen, 1993) or as a combination of steel and rubber elements. Recent research reports show that analysis involving advanced FEM is on-going for this scientific area (Wang, et al., 2008).

A similar alternative is to make the foundation shallow so that the vessel runs aground before reaching the actual bridge pier, see Figure 2.1 [b]. The filling can for example be of sand or rocks and is an effective method but do take up a lot of space in the vicinity of the support and is only possible if the water depth isn't too great. This alternative may not be an option for channels where the natural current gets prohibited by the reduced cross sectional area due to the filling.

Another option is to design cofferdam cells, external strong points located outside the bridge supports, which usually are made up by driven circular steel sheets filled with crushed stone and a reinforced concrete cap on top for bracing (Kuzmanovic & Sanchez, 1992), see Figure 2.1 [c]. This solution is of good use provided a reasonable depth ending with a firm bottom and is, as an example, used for the Incheon Bridge in South Korea (Flett, et al., 2007) and at the new Sunshine Skyway Bridge.

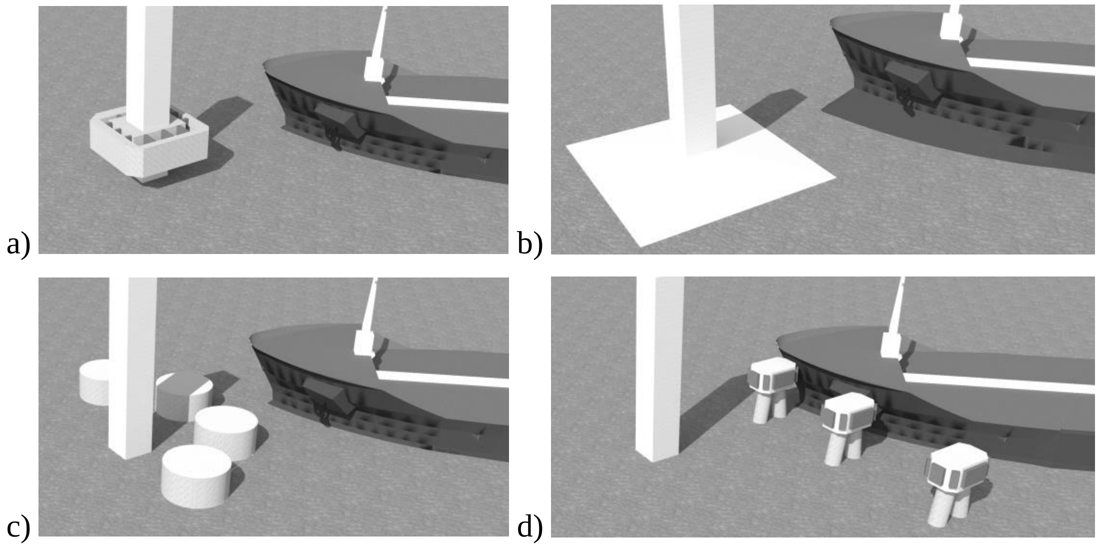

Figure 2.1 Different protective measures for bridge supports.

2.1.3 Guide structures

A guide structure is a structure that will overt a ship from a direct collision. An example of this is protective piers that are constructed in the waterway and will lead the ships through the passageway and thereby defend the bridge supports. These elongated structures are built in slightly different ways depending on what forces they are exposed to. A dolphin is a similar assembly but designed to be an independent structure that basically works in the same way, reminding of cofferdam cells, see Figure 2.1 [d].

Considering all stated facts in this chapter so far it is obvious that the most suitable protective system is dependent on the site conditions and no general conclusion regarding the best one can be stated. This report will however only focus on protective piers further on.

2.2 Risk assessment

The direct consequences of a ship collision with a bridge are determined by the incoming angle, speed and mass of the vessel and the shape, dimensions and type of the bridge (SSPA, 2014). The probability can depend on navigational matters but also channel geometrics and unforeseen ship faults. Indirect consequences may be heavy traffic jam due to closing of the bridge as inspection and/or repair need to be done, pollution due to substances from boat- or road traffic and also human casualties.

An example of an indirect consequence states that closing Gröndalsbron in Sweden's capital city Stockholm would cost the society correspondingly 7 million Swedish kronor per hour (Lindqvist, 2015).

A simple visualization of how protective piers reduce the risk can be illustrated as in Figure 2.2 (SSPA, 2009). It states that if point a) represents for example the risk of a ship-bridge collision, then a protective pier would lower the consequence and hence move the dot to the left of the diagonal line to point b) which symbolizes an acceptable level of risk. Other risk reducing methods would be to lower the probability to c) by taking measures against operating errors. The risk is generally calculated as the product of probability and consequence, see Equation (2.1).

$$R = P \cdot C \tag{2.1}$$

Where:

R is the risk

P is the probability

C is the consequence

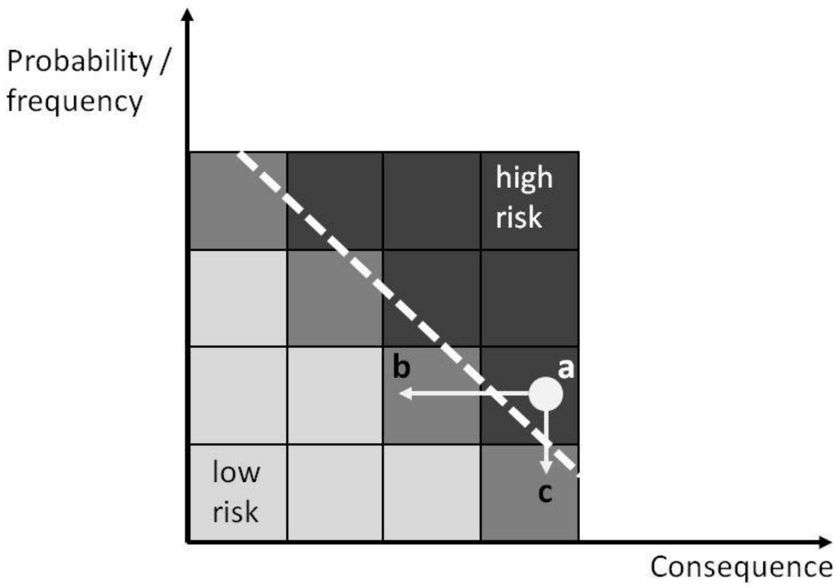

Figure 2.2 Risk assessment of a collision between ship and protective pier adapted from SSPA (SSPA, 2009).*Moving from a) to b) is a consequence reducing measure while moving from a) to c) reduces the probability.*

A more detailed assessment can be used to get a better understanding of how to reduce potential accidents. Eurocode treats an approach on how to compute occurrence of failure under a time period regarding ship impacts (Eurocode, 2010), see Equation (2.2).

$$P_f(T) = N \int P\{F_{dyn}(x) > R\}\, dx \tag{2.2}$$

Where:

$N = n\lambda T(1 - p_a)$ is the total number of incidents in the period of consideration

n is the number of ships per time unit (traffic intensity)

λ is the probability of a failure per unit travelling distance

T is the reference period (usually 1 year)

p_a is the probability that a collision is avoided by human intervention

x is the coordinate of the point of the fatal error or mechanical failure

F_{dyn} is the impact force on the structure following from impact analysis

R is the resistance of the structure

A parameter accounting for the ship's initial position in y-direction may also be introduced if appropriate, as made visible by the distribution diagram in Figure 2.3.

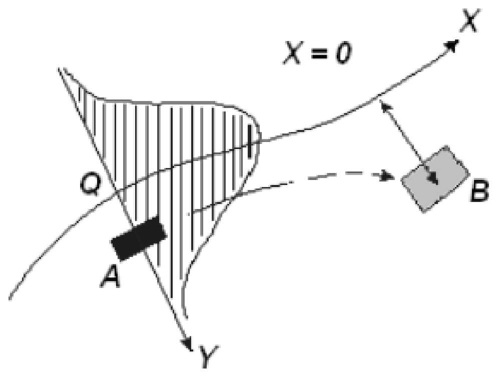

Figure 2.3 Scenario of ship collision, showing a vessel A steering away from its planned course X towards structure B (Eurocode, 2010).

The principle of using a probabilistic methodology in the design process is for instance used in the American standard AASHTO (American Association of State Highway and Transportation Officials) where the demanding criteria of the structure is chosen as an annual frequency of collapse, also referred to as return period of critical events (PIANC, 2001). Below is the general formula for computing the annual frequency of bridge collapse, see Equation (2.3).

$$AF = (N)(PA)(PG)(PC) \tag{2.3}$$

Where:

N is the annual number of bridge passages for the vessel type under consideration

PA is the probability of the vessel being aberrant per bridge passage, and successful evasive action not being taken

PG is the geometric probability of a collision between an aberrant vessel and a bridge pier or span

PC is the probability of bridge collapse due to a collision by an aberrant vessel

Highly prioritized bridges are for example decided to have such periods of 10000 years and the bridge resistance is calculated thereafter. In parallel, an indication of general accepted risks is presented in Figure 2.4 for common structures (Larsen, 1993).

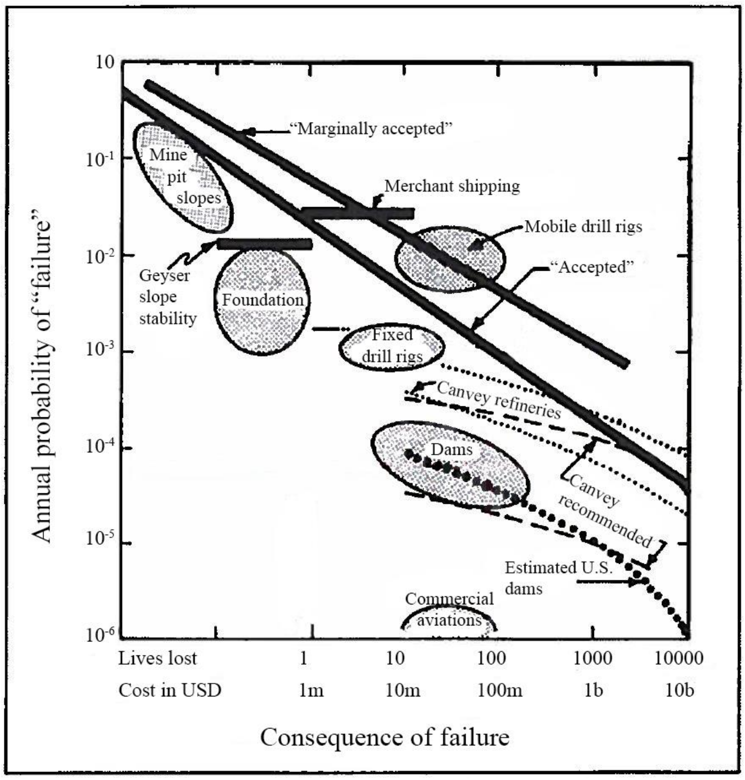

Figure 2.4 Risk diagram for selected engineering projects and the lines separating "accepted" and "marginally accepted" areas (Larsen, 1993).

2.3 Protective piers design

Swedish Road Administration demands the protective piers to fulfil the requirements according to the Eurocodes by the regulations from Swedish National Board of Housing, Building and Planning (Boverket) (Trafikverket, 2011). However, the general design can vary depending on the extent of each project.

2.3.1 General concepts

The universal pier design needs a foundation also called a substructure for support. This foundation generally consists of piles. It also needs a superstructure that consists of some sort of longitudinal beams for taking vessel forces.

By looking at existing protective piers, simpler constructions may consist of only pillars and collision beams made of timber as seen in Figure 2.5. These could work well for a less important structure or fit where only smaller boats can pass. Large ships naturally demand a more complex structure at a larger scale.

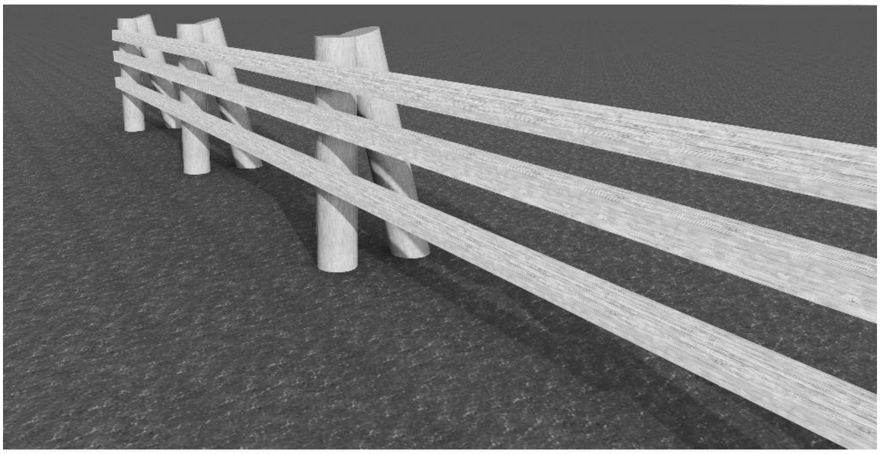

Figure 2.5 Simple protective piers made solely out of timber.

A large scale pier has a main longitudinal beam favourably made in a heavy material, such as concrete, to withstand a heavy collision. The stiffer construction that a concrete beam implies has its advantages since forces are better distributed within the structure, allowing more connecting members to contribute to the bracing.

The main purpose of the protective pier is to transfer the load from a ship-collision into the ground, essentially creating a load carrying system.

The first part of the system that will receive the ship load is responsible for taking care of the service state loads. This is advantageously done by some kind of energy absorbing parts, referred to as fenders, which are mounted on the face of the longitudinal beam. Fenders are typically made out of rubber or possibly foam elastomer that have high energy absorption capacity. The fenders can either be connected via external longitudinal beams that distribute the loads to several units, see Figure 2.6 [a], or be mounted with panels for distribution to a single or to a group of fenders, see Figure 2.6 [b].

a) b)

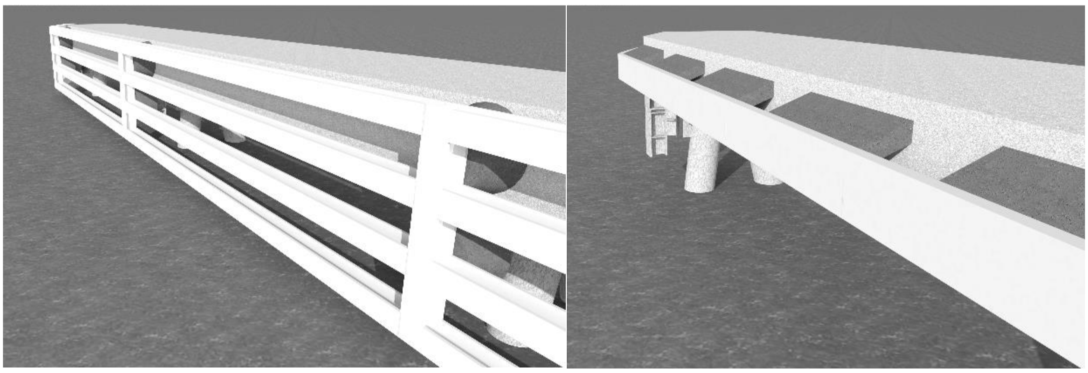

Figure 2.6 Different fender systems. a) Shows fenders with load distributing beams. b) Shows panel like fenders.

In the case of an accidental load the first part of the system will only manage to take up a very small portion of the total load. Instead the second part of the system a main beam will receive and distribute the load and absorb some of the impact as the element's extensive mass is moved.

From the beam the load is transferred into the piles, which is the third part of the system, and from the piles the load is transferred into the ground, see Figure 2.7. Depending on the type of bottom the piles will behave slightly different. A clay bottom will reduce the horizontal movements in the pile through the soils' passive pressure and the vertical movements through cohesion. While a pile in clay that is anchored in solid rock will reduce the horizontal movements' trough the soil and the vertical movements will be hindered by the rock. The piles will work in bending and compression/tension.

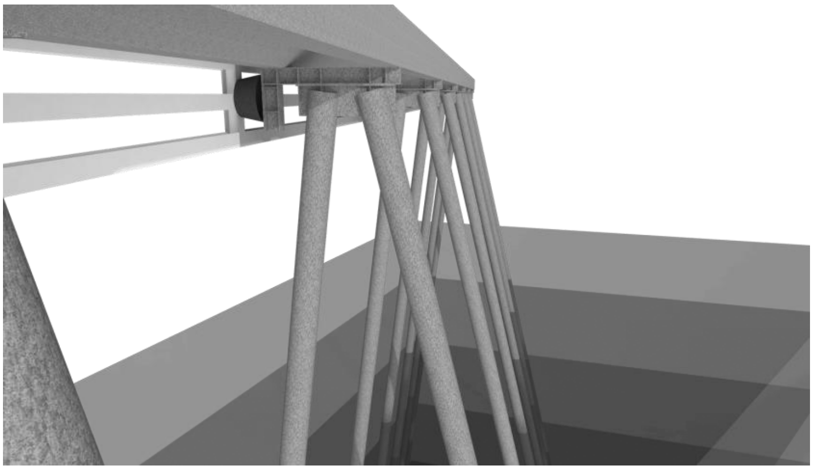

Figure 2.7 Protective piers standing on piles in clay.

2.3.2 Loads on piers

There are several loads that can act on the piers. Pressure from water, ice and earth are more easily found while ship loads tend to be more complex, especially the accidental ones as they are harder to predict.

One reason for the complexity is due to how the load is applied to the structure. Since the ship deforms during impact the surface on where the load acts varies over time. At first it acts as a point load but over time as the ship deforms the load will act as a distributed load on the pier, the time is therefore a crucial factor on which the load's size is dependent on. Knowledge about the ship's hull geometry and mechanics would be required along with the structural data of the protective pier to fully capture the impact in an advanced nonlinear FE-analysis. To make it even more complex the ship will move along the pier and thus the load will act on different parts of the pier over time. This movement will also give rise to a friction force that will act at the interface between the two objects. How big the friction force is depends on the incoming angle of the ship. All these factors make the application of load onto the structure complicated and difficult to model.

2.3.3 Energy absorption

The main purpose of the structure is to bring the incoming ship to a halt or force it back on track. The way that the incoming ship is brought to a halt or given a change in direction is through energy absorption.

Energy is absorbed in several ways during a collision.

- The protective structure can deflect, rotate and slide (Larsen, 1993) globally and/or by its internal components (Algers, et al., 1966).
- The ship can deform.
- The concrete can be crushed.
- The ship's body can be lifted up.
- Friction between hull and structure can occur.
- The ships' rotational movement through the water will consume energy from collision start to end.

If all energies mentioned above are summed and equals the ships' incoming kinetic energy, the ship will come to a stop or be forced back on track.

An impact can be classified as hard or soft (Eurocode, 2010). A hard impact is when the energy is consumed by the striking object, that is when the pier is considered as completely rigid and all of the ship's incoming kinetic energy will be absorbed by the ship's hull, Figure 2.8 [b].

A soft impact occurs if the pier is considered as a flexible structure, in this case the energy will be absorbed more mildly by the sacrificial piers through deflection and plastic deformations (Svensson, 2009), Figure 2.8 [c]. As an example, research at Tongji University in Shanghai show this action in FEM computations where a collision between a ship and an elastic foundation on piles only reaches about half the values than that of a collision between a ship and a rigid wall, when looking at the peak collision force (Svensson, 2009). When designing a flexible structure either the piles or the beam can be the more flexible part. Advantages and disadvantages can be weighted but a heavy argument points at the advantage of having a structural failure above water level since a repair would be easier (Hogström, 2015).

The resulting interface forces depend on the cooperation of the structure and the striking object. Important parameters for an impact analysis are construction of the moving object, its velocity and movement after collision (Eurocode, 2010). Factors regarding both the moving object and the structure are properties concerning damping and deformation along with mass and angle of collision. Characteristic values should be used when setting up the material parameters, because the intention is to model the behaviour that takes place in reality.

a)

b)

c)

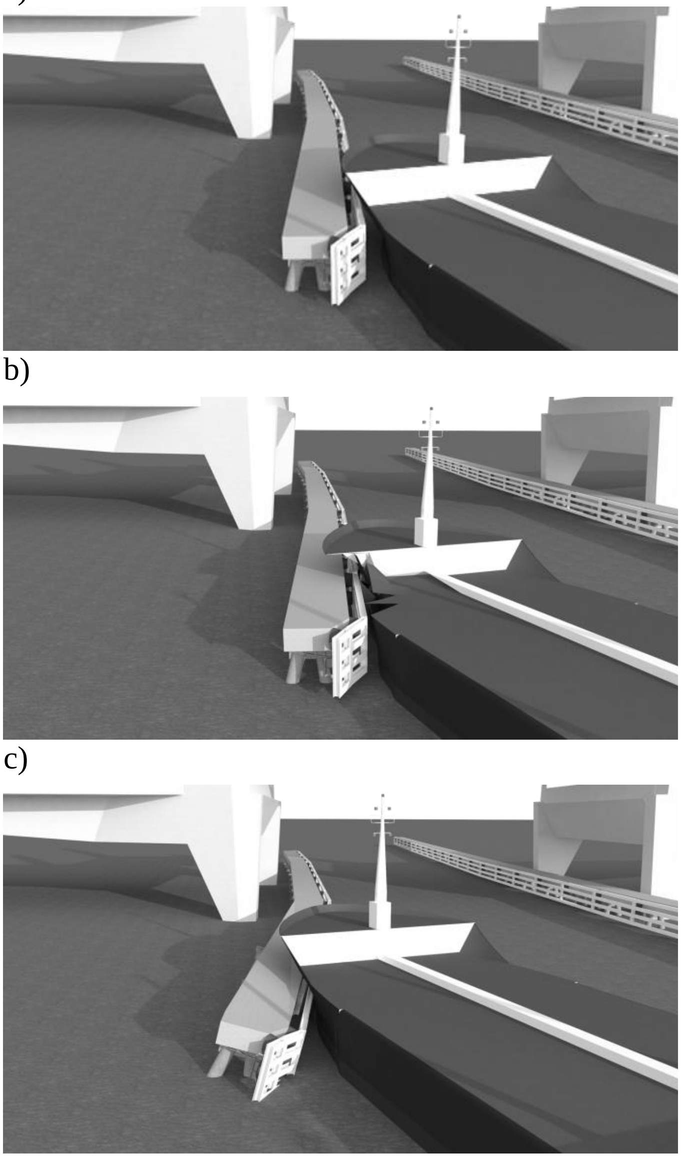

Figure 2.8 Three graphics showing a ship to pier collision at different scenarios. a) Right before impact, b) hard impact and c) soft impact.

The desired design alternative between a stiff or a damped behaviour is case dependent. Similar construction projects have had estimated collision energies so high that it would not be feasible to design a system that could take those impacts (SSPA, 2009). It was instead recommended to design the piers for two scenarios where one was a low energy case in the elastic range where an impact made no harm to the protective piers, typically caused by smaller boats or minor hits. Another would be a high energy case, using the plastic capacities, where protective piers were sacrificed to save the bridge supports from ships and heavy collisions.

Yield limits will be reached when the plastic capacities are used which might cause the superstructure to deflect towards the bridge support. This deflection must generally not be greater than the distance to bridge supports unless they are designed to take a part of the load. This can be exemplified by the two adjacent bridges Marieholmsbron and Hisingsbron in Göta älv. The design of the protective piers at

Hisingsbron is taken from the earlier constructed Marieholmsbron but enhanced. Even though the same traffic passes the two bridges, the ship guides are designed for different loads since Marieholmsbron allow some of the impact load to be transferred into the bridge foundation (Thorsell, 2015).

It is not unusual that some assemblies give the design for other projects. Inspiration for the protective piers at Gröndalsbron was found from a structure that protected a sensitive embankment from ship collision at a nearby location, as an example (Lindqvist, 2015). Analogously, the design of the protective piers fits well for berths and ferry ports where an impact on the docking structure is expected. Similar phenomena can be truck to road barrier contact or explosions which create analogous actions with different time scopes (Eurocode, 2010).

2.4 Mathematical interpretation of load

Real world forces always act dynamically but these problems are often too complex to model (Kang, et al., 2001). The consequence of a time and resource consuming problem is that it is hard to be economically justifiable for companies. A real world load must therefore be interpreted in an appropriate way to be incorporated in a mathematical model. The better the model is the more realistic results will be generated. Some problems must nevertheless be simplified more as the complexity is extensive and demands a lot of time to compute. The simplification of a problem can result in several different models, each with a unique result, and hence an engineering judgment is required. A linear elastic model is commonly used along with static loads when calculating actions on structures (Vrouwenvelder, et al., 2005).

The protective piers are exposed to the waterway traffic and statistics of passing vessels makes it possible to predict what forces may occur. Vessel collisions to these structures create forces that last for a short period of time. For this reason, it is interesting to look at force-time models and in particular the two extreme cases characteristic impulse load, Figure 2.9 [a], and characteristic pressure load, Figure 2.9 [b]. A characteristic impulse I_k is a high force applied over a short time period when two or more bodies collide. On the contrary, a pressure force F_k displays lower force acting during a longer period of time.

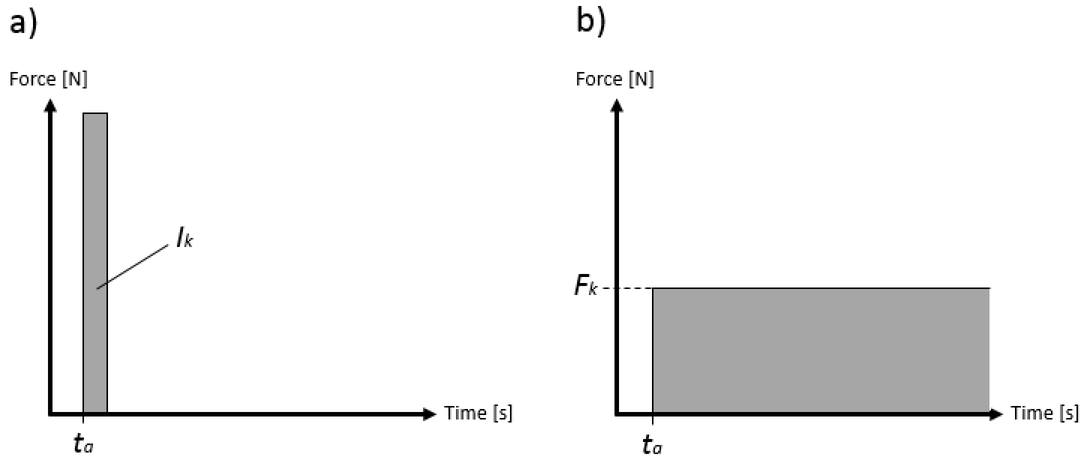

Figure 2.9 *Graphics showing dynamic extreme cases which starts acting at time t_a: a) characteristic impulse and b) characteristic pressure force.*

The ship collision progress for protective piers is likely to be on-going on the scale of seconds thus placing it somewhere in between the two extremes. The interaction is dynamic but it is common to translate the forces into equivalent static forces as a conservative simplification (Eurocode, 2010). This will be further developed in the following section. An advanced design of structures exposed to an impact could however include dynamic effects and/or non-linear material behaviour. Figure 2.10 below shows how an impact to an arbitrary structure can be represented in different ways.

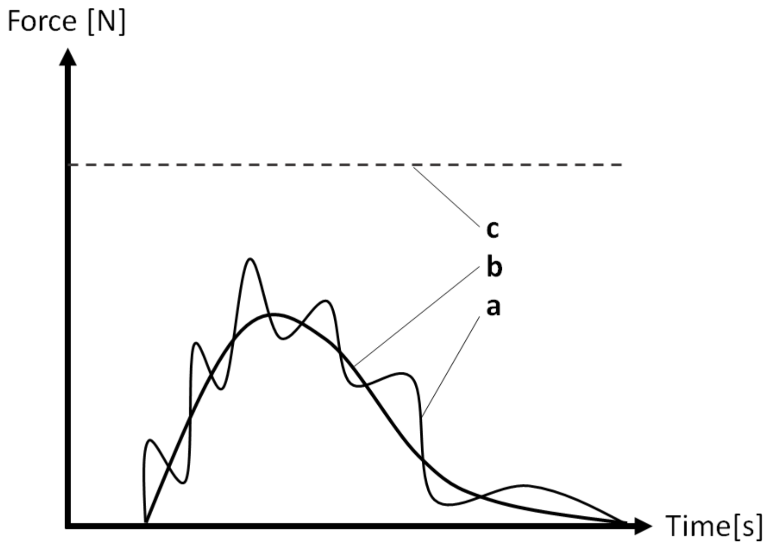

Figure 2.10 *Different mathematical representations of an impact to a structure. a) Structural response, b) dynamic force and c) equivalent static force.*

2.4.1 Equivalent static force

In a soft impact, where a structure go through elastic-plastic deformations, equivalent static forces can be formed which comprises the structures' dynamic response by matching plastic capacities and deformation pattern of the structure as when it is exposed to the actual load. This is done by using dynamic amplification factors for different loading situations which unfortunately in many cases are uncertain or very conservative since they are based on personal knowledge or general design codes (Kang, et al., 2001).

A lot of researches treat the conversion of dynamic loads into equivalent static ones and how to make them accurate. In the report "Design of bridge pier pile foundation for ship impact" (Kuzmanovic & Sanchez, 1992), several sources are stated which treat the methods and procedures for this transformation. "Structural optimization under equivalent static loads transformed from dynamic loads based on displacement" is the name of a more general report regarding the subject (Kang, et al., 2001).

2.4.2 Dynamic force

Today when calculating the impact force of a ship collision the equations often used are based on quasi static and elastic analyses that are simplified. These equations are not based on the dynamic behaviour that is present in a ship collision and thus it will not describe it correctly (Wang, et al., 2008). Standard guidelines, as Europe's design code Eurocode 1991-1-7 Annex C or America's AASHTO, have been developed to present an informative approach on how to calculate dynamic impact forces. Formulas for a hard impact are in Equation (2.4) and Equation (2.5) as a comparison between the two approaches of simpler kind.

$$F = 1.11 \cdot 0.88\sqrt{DWT} \cdot \frac{v}{8} \tag{2.4}$$

according to AASHTO

$$F = v\sqrt{k \cdot m} \tag{2.5}$$

according to Eurocode

DWT is the dead weight tonnage of the ship [metric ton]

v is the ship velocity [m/s]

k is the equivalent elastic stiffness of the ship [N/m]

m is the mass of the ship [kg]

The highly estimated forces according to Eurocode and AASHTO can be seen in an example, Figure 2.11, by Tongji University, as mentioned in Section 2.3.3, in the case of a collision between a bridge pier and ship.

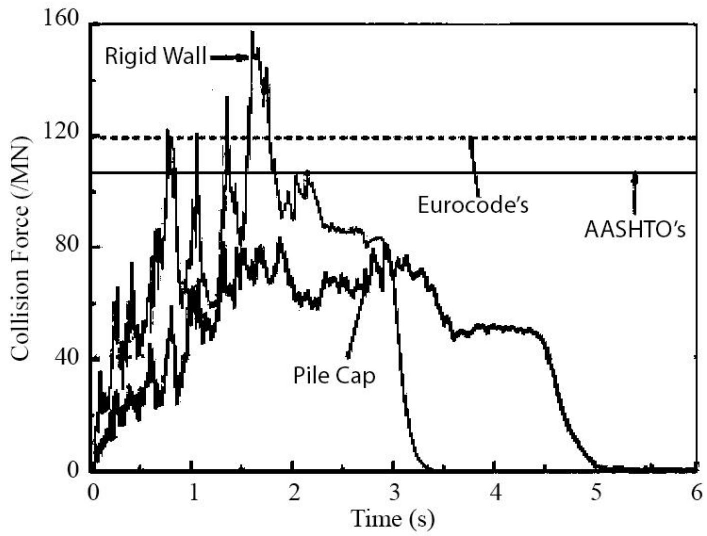

Figure 2.11 Collision force on rigid and elastic pier (Svensson, 2009). *Comparison between real measurements versus the codes Eurocode and AASHTO.*

2.4.3 Load application techniques

An important aspect concerns the load application on the structure and how this affects the calculation of energy absorption. Energy is found as force multiplied by displacement and during FE-analysis one of the parameters is increased through several increments while the other is read, giving two options for computations.

2.4.3.1 Load control

One approach is to continuously apply the force in small steps and see what structural displacement this gives. The problem with this approach is that it cannot describe post-peak behaviour due to how the relation between the force and displacement looks, see Figure 2.12.

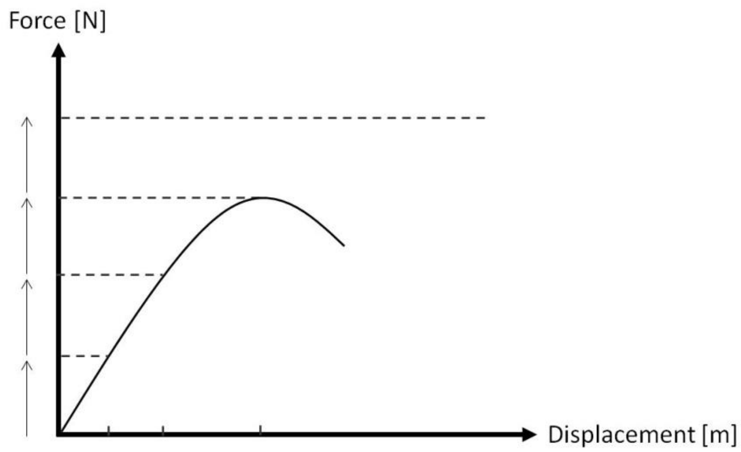

Figure 2.12 Concept of load controlled load application.

2.4.3.2 Displacement control

Another approach is not to apply the load itself but rather to increase the displacement and then read what reaction force it corresponds to. This is done in small increments where the reaction forces are calculated after every increment. From this, one can plot the reaction forces against the displacements to obtain how much energy the structure can absorb as this is the area under the graph. One benefit with this approach is that it, in contrast to the load control approach, can describe the structure at post-peak behaviour see Figure 2.13. This method is called displacement control and is often used in non-linear models and has previously been used in protective pier design (Lindqvist, 2015).

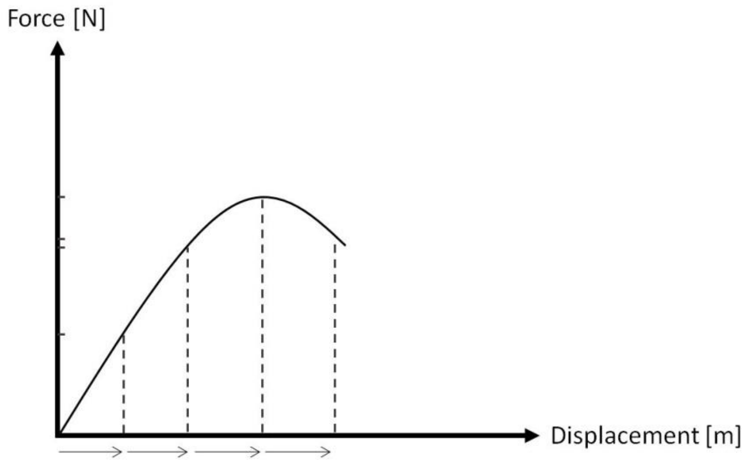

Figure 2.13 Concept of displacement controlled load application.

3 The Case Study Hisingsbron

The case study for this report is about the protective piers for Hisingsbron in Gothenburg. COWI have preliminary dimensions of the piers which form a basis for calculations and modelling in this report. This chapter provides important background to assumptions and input for the FE-modelling.

3.1 Site conditions

The new bridge will be located in the centre of Gothenburg and will cross the river Göta älv from the mainland to the island of Hisingen. The geotechnical surveys show that the ground consists of a deep deposit of clay that varies from 50 to more than 80 meters down before the bedrock is reached. Given data reveal variations in clay properties depending on the depth, see Appendix A. The depth of the river is assumed to be 7.05 meters (COWI, 2014). A principled description of the site conditions are shown in Figure 3.1.

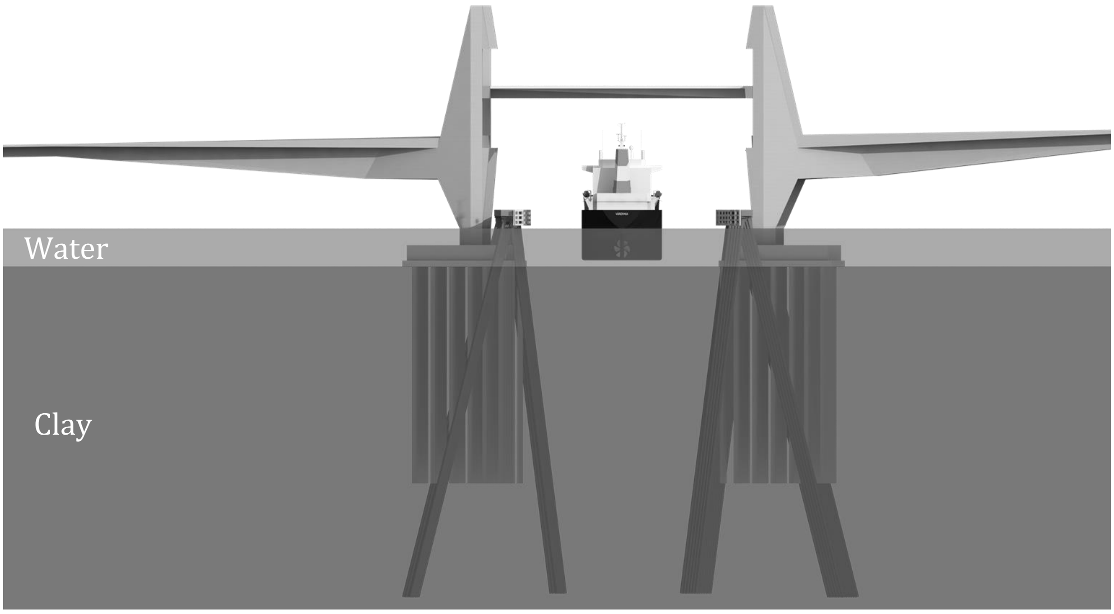

Figure 3.1 A principled description of the site conditions at Hisingsbron.

Passage at the bridge opening has been simplified and made less risky in the new bridge concept by increasing the fairway width from 20 to 30 meters. Free sailing height varies between 12.5 m when the bridge is closed and 29m when the bridge is fully opened.

3.2 Protective system

The presented different methods of bridge protection in Section 2.1 are not all suited for Hisingsbron and hence reasoning needs to be done to find the most appropriate one considering all of the aspects. It has to be mentioned that it was not COWI's task to decide whether protective piers were to be used or not as that choice was part of Trafikverkets conditions in the new bridge concept to be produced. This chapter rather strengthen the argument for using protective piers at Hisingsbron.

3.2.1 Suitable protection method

There are several reasons that have influenced the choice of protection method for Hisingsbron. The desire of a low bridge concept and lack of area at the landings motivates the choice of an opening mechanism and that the bridge supports are placed in the water (Göteborgs Stad, 2013). Göta älv geometry reveals that a course correction is necessary when crossing the bridge, leading to a greater risk of collision see Figure 3.2. In combination with a sensitive opening mechanism, these arguments justifies a separate protective system as a collision may result in a dislocation of mechanical parts even though the force is relatively small (SSPA, 2014).

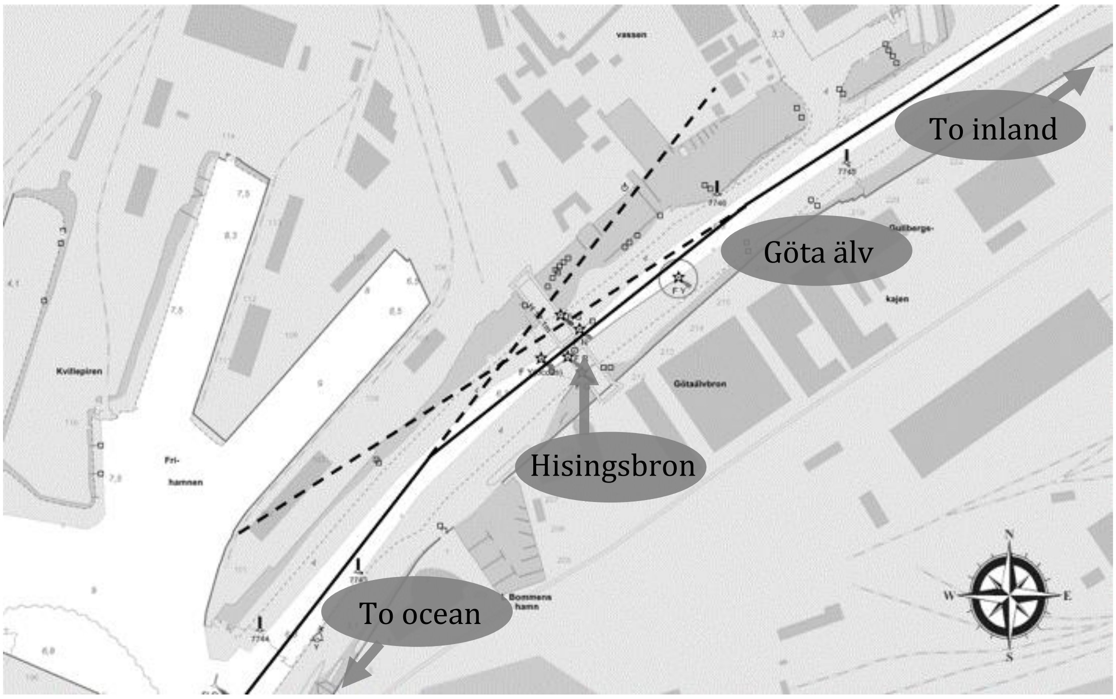

Figure 3.2 Course correction due to the geometry of Göta älv.

A structure on piles is favourable due to the weak clay bottom whilst the alternative with padding around the foundations would take up too much space in the narrow fairway to be a viable option. Flexible protective piers (soft impact) on piles will allow some deflections to take place if a collision occurs. A great advantage of this is that a strong structure would cause the ship to absorb all of the energy, potentially resulting in a rip in its hull. The risk of fire, leakage from cargo and disrupt in traffic below or on top of bridge could be the consequence and is not acceptable at Hisingsbron as both types of traffic are highly prioritized. Concerns like these have indeed been decisive in the evaluation of other projects were upgrades of protective piers got motivated (SSPA, 2014). Altogether, it is concluded that protective piers are appropriate for Hisingsbron.

3.2.2 Protective piers

Two protective piers are considered in the new bridge concept as the supports on both sides of the opening are exposed to the fairway. The northern pier will extend 50 meters in both the upstream and downstream directions from the bridge supports while the southern pier will extend 50 meters in the downstream direction and 150 meters upstream (COWI, 2014), see Figure 3.5.

The protective piers consist of external longitudinal steel beams, fenders, a massive concrete beam and groups of piles. The steel in the structure is made of S355 quality, the concrete is C35/45 and the reinforcement is B500B. The external longitudinal beams (Figure 3.3 [a]) are coated with a low friction material that allows the ship to slide along the beams better and thereby reduce contact forces. The longitudinal beams are connected to cone shaped fenders (Figure 3.3 [b]) that are positioned in pairs at every support. These fenders work elastically up to 335 kN each and will take care of service state loads. An attachment ensures the forces to be transferred from fenders to the massive concrete beam (Figure 3.3 [c]) which in turn is continuous over the supports. This means that a great part of the whole structure will work together when a ship hits the system. Couples of piles form the supports for the beam with a spacing of 10 meters, see Figure 3.4. Below the concrete beam is an I-steel-beam (Figure 3.3 [d]), HEB300, with welded studs on top to attach the two parts together. A similar beam (Figure 3.3 [e]) is welded at one end for attachment of the lower fender. The piles are merged with a T-beam (Figure 3.3 [f]), 300x600, in top and will make up a support for the HEB beam. The I- and T-beam stick to each other by bolted connections (Figure 3.3 [g]). If a ship collides, creating a load greater than service load, then the bolts will break and hence the I- and T-beam will be unconnected and interact with each other only by contact surfaces. The piles (Figure 3.3 [h]) are made of 16 mm thick steel pipes with a diameter of 610 mm. The top 20 meters are filled with reinforced concrete to work better in the free water where no clay helps resisting any movement. Since the piles are of cohesion type, the clay will carry vertical loads from the structure due to friction at the pile surface. In short, the interaction between the piles and the clay is of great importance and the properties of the clay are key features for how the entire structure will work during collision. Fenders, concrete beam and pile group are allowed to collapse at collision so that the ship is averted (COWI, 2014).

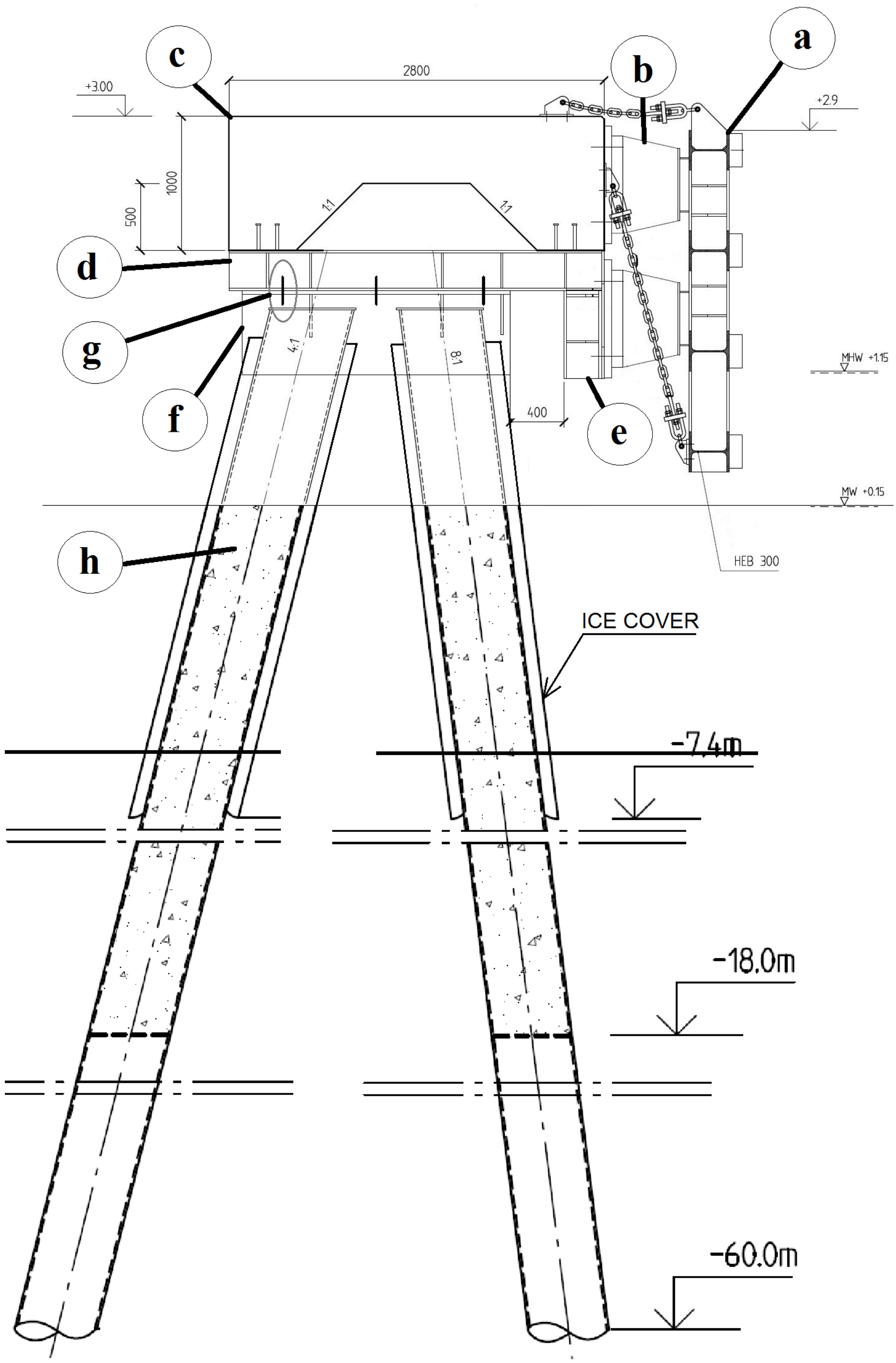

Figure 3.3 Detailed section cut of the protective pier at a pile group.

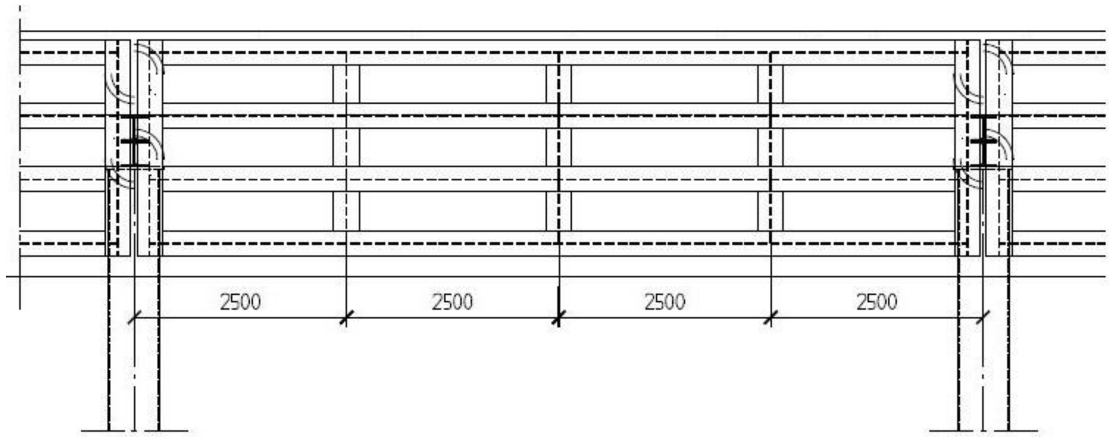

Figure 3.4 Protective pier front view showing the spacing of pile groups.

3.3 Load and application

Ship simulations were made during the design process of the protective piers, prior to this report. SSPA analysed the worst-case collision possible at Hisingsbron as an input for the sizing of the protective piers.

In documentation provided by SSPA, two different scenarios have been evaluated to conclude the worst case. The two scenarios are depicted in Figure 3.5 where scenario A shows a ship collide with the 150 meters long pier and scenario B shows a ship collide with the 50 meters long pier. A linear analysis was made showing that bending moment in the concrete beam was crucial for scenario B, i.e. for collision against the 50 meters long pier (SSPA, 2014). Normally, the ships hit the piers only at hard side winds but their thrust forward in those cases will not cause any noticeable forces except from frictional ones between the hull and the longitudinal steel beams. However, in a rare accidental case, where the rudder is fully turned just before the passage, a larger approach angle will cause greater forces perpendicular to the pier. The size of the force is also dependent on the speed of the ship.

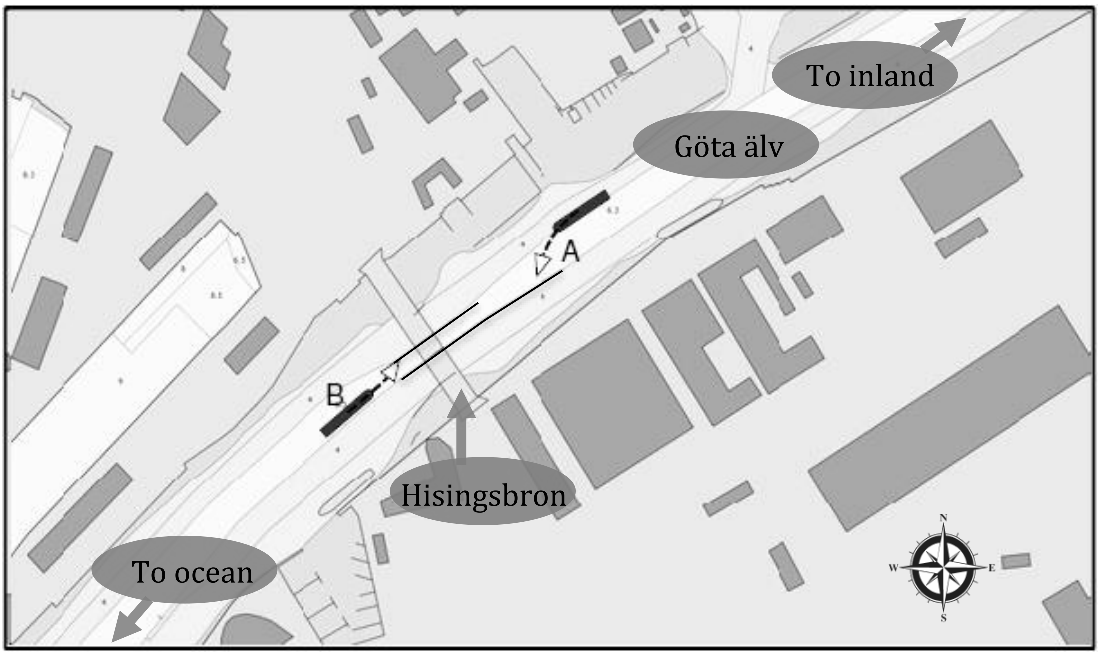

Figure 3.5 Two scenarios describing the collision of the protective piers. One scenario is when ship A collides with the 150 meters long pier. Scenario B is when the ship collides with the 50 m long pier.

As concluded earlier, scenario B is the worst case scenario. This is when a fully loaded, 89 meters long, Vänermax-ship is approaching the 50 meter protective pier at an angle of 20° with a speed of 8 knots (SSPA, 2014). These results were obtained through analysis of simulations made in SEAMAN software. Canal geometry, statistics and predictions were some of the variables leading to the case stated above.

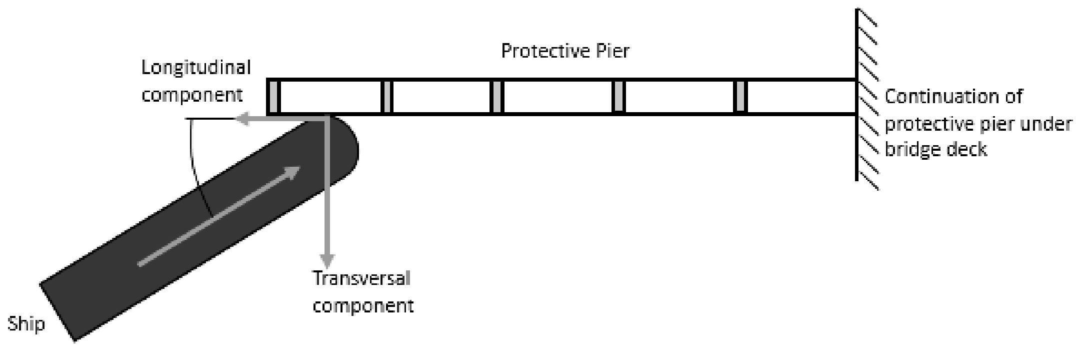

Figure 3.6 Colliding ship with its total force, force components and incoming angle.

The pier is assumed to have a significantly greater stiffness in longitudinal direction hence only the transversal component of the collision force in Figure 3.6 is evaluated in this report.

4 Finite Element Modelling

The reality needs to be mathematically modelled before performing a structural analysis. It is essential to know every assumption, simplification and expression in order to obtain acceptable values that can be applied to a physical construction. Conservative thinking along with safety margins and hand calculations can be used to ensure that the values are on the safe side. Finite element software is an increasingly popular tool for executing advanced mathematical analyses. Its power to perform accurate calculations can easily trick any expert to think the output is correct. The amount of input commands the engineer has to consider is great and requires certain skill. It is therefore important for the engineer to be able to construct a model of the problem and have the knowledge how it can be implemented into the FE-software. Figure 4.1 schematically shows the procedure of how to model a problem and is followed in the project work.

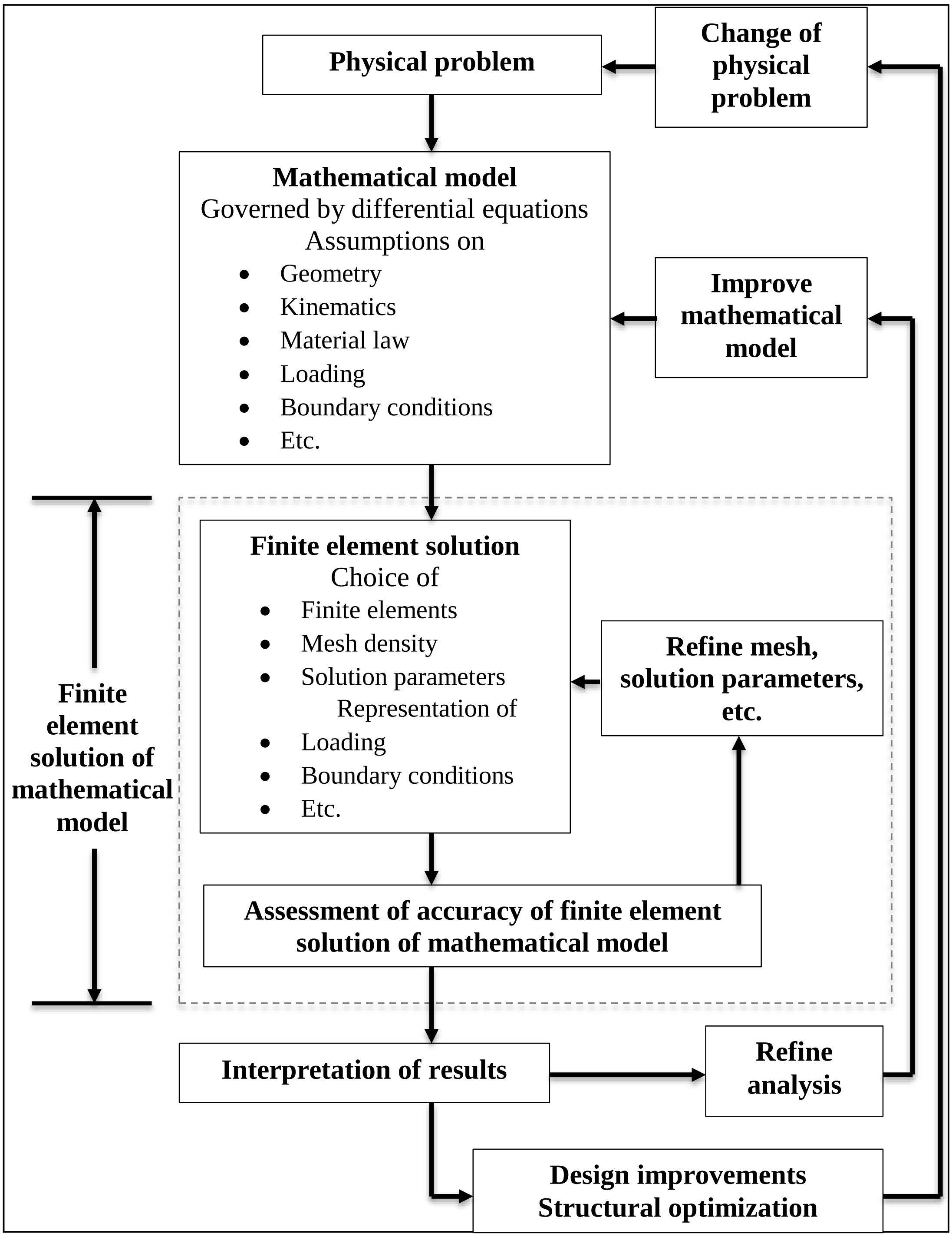

Figure 4.1 An adapted systematic scheme showing the process of finite element analysis (Bathe, 1996).

4.1 Simplification of problem

The protective piers at Hisingsbron have an advanced setup of components in order to get the desired response when a collision occurs. Some of the structural members, for example the fenders, are purely mounted to take care of forces in service state as mentioned in Section 2.3.2. The capacity of the fenders is only about 2 % of the total collision energy, a simple calculation is printed in Appendix B. Since the scope of this report is to investigate the structural behaviour under the action of a ship collision, the contribution of these members are neglected and therefore not included in the model. One should know though that the destruction of these elements in the collision event do contribute to the energy absorption (Darholm, 2015). As all the capacities in service state will be exceeded, ultimate limit state capacities are decisive. Plastic deformations in the structure are of interest when looking at this particular case.

The real failure mode of the protective pier consists of several steps. Fenders will be compressed first. Subsequently, the connectors (Figure 3.3 [g]) between T- and I-beam will be sheared off resulting in a dislocation of 400 mm of the concrete beam in load direction, see gap between part [e] and [f] in Figure 3.3. A concrete beam and pile groups will thereafter start work together to counter the load. The simplification here is to build the model after the 400 mm dislocation occurs. This is done because of the difficulty to model such behaviour in the FE-software and it could be sufficiently described with hand calculations (Darholm, 2015). The I- and T-beam are removed as a result of simplification and replaced with a fictive fixed connection between main beam and piles.

When looking at the parts that are presumed to break, one must not forget the parts that are assumed to stay together. The concrete beam is connected to the I-beam by studs that are welded to the top of the steel flange and grouted into the concrete. At each pile group there are eight studs which are assumed to be enough to keep a fixed connection. A similar connection is provided between T-beam and piles. Web and stiffeners of the T-beam are attached to the pile top as they are inserted into the pile and thereafter grouted and welded to provide a fixed connection.

4.2 Type of analysis and load application

The behaviour of the protective piers is hard to predict with linear-elastic calculations as energy absorption in ultimate state is about utilizing the plastic capacities. It is therefore motivated to execute a non-linear analysis to capture the structural response at and after peak value which gives a more realistic picture.

Displacement controlled load application is chosen to be used in the model. This is done for several reasons. As mentioned in Section 2.3.2, the complexity of the impact variables makes it hard to model the ship load in an accurate way. So instead of looking at an applied load case, the decision was made to treat it as an energy consumption problem i.e. to see how the structure behaves whilst absorbing the incoming collision energy of the design ship. As been said in Section 2.4.3.2 the displacement control method is the only way to do this due to its ability to register post peak behaviour of the structure. The displacement is applied to a Reference Point (RP) as an arbitrary horizontal translation of 6 meters acting perpendicular onto the concrete beam’s face in the outer mid-span, see Figure 4.2. A set of nodes on the beam’s surface form a line and are tied together in a multi-point constraint (MPC). The MPC control point is in turn connected to the RP. This setup works just like a hinged rigid beam trying to push the concrete beam backwards. In doing so, the beam can rotate and translate freely in any direction except for the prescribed displacement direction.

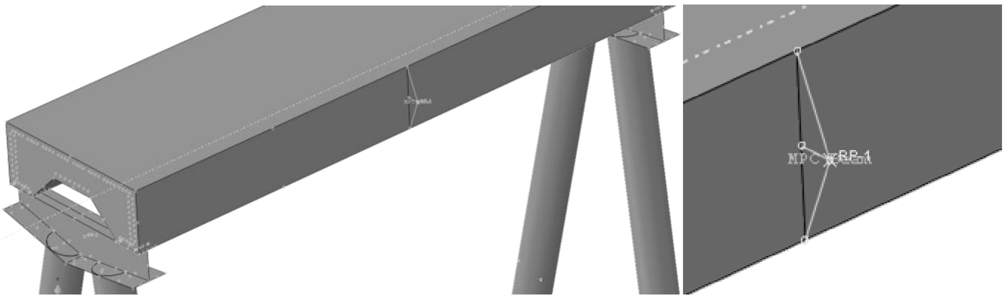

Figure 4.2 *The applied displacement is applied to a Reference Point which in turn affects nodes tied in a MPC.*

A Static General analysis was used in Abaqus to analyse the model at first. Warning messages were generated, pointing at the system matrix not being positive definite, and so the analysis type was changed to Static Riks instead. This option is favourable in cases of negative stiffness response in load-displacement, as in some buckling or collapse behaviour (SIMULIA, 2012). It also has its benefits for ill-conditioned problems treating unstable problems or limit loads.

4.3 Representation of structural members

The modelling process starts by treating each structural part separately before it is put into the global model. Verifications are made along the advancement to ensure reasonable output. A convergence study of chosen mesh sizes will indicate a resolution good enough to capture the non-linear effects and associated output data. Short computation times are not a priority but cannot be unreasonably long.

4.3.1 Modelling of the beam

Beam, shell and solid elements could plausibly all work but their suitability differs. The biggest benefit with one-dimensional beam elements is the low computation time due to the relatively low amount of elements and nodes generated (SIMULIA, 2012). Its response is instead calculated as variables along the beam line. There might be issues when modelling one-dimensional elements in three-dimensional space and one must judge whether it is appropriate or not for each part. Beam elements will in this case not capture the local non-linear concrete behaviour as it is working in one dimension. Other case-related problems which make beam elements inappropriate are the difficulty to model the complex concrete cross-section and the inability to model reinforcement.

Shell elements are preferred elements when the thickness is significantly smaller than the other dimensions (SIMULIA, 2012). This and the fact that shell elements have the ability to cope with the non-linear redistribution are two of the positives for shell elements. Shell elements are also able to model reinforcement with non-linear parameters in Abaqus. The reinforcement is defined in layers as a part of the element section. Nevertheless, the inability to model the complex cross-section of the beam excludes shells as an option.

Solid elements are continuum elements that stretch in 3D. This type of element is good when using non-linear material parameters since the load can redistribute in all three dimensions. Reinforcement is also relatively easy to model in solids as embedded elements. Another upside is the fact that the there is no problem to model the complex cross-section when using 3D-solids. The downside is the increase in amount of elements and nodes that will increase the computational time, especially with non-linear material parameters. Solids are the most suitable elements for the concrete beam when comparing the stated facts. 10-node tetrahedral elements are chosen.

The case study treats only a selection of the whole protective pier and boundary conditions need to be set up. A fixed boundary is set at the end closest to the bridge where shorter piles, attached to the bridge foundation slab, creates a stiffer support for the continued protective pier there.

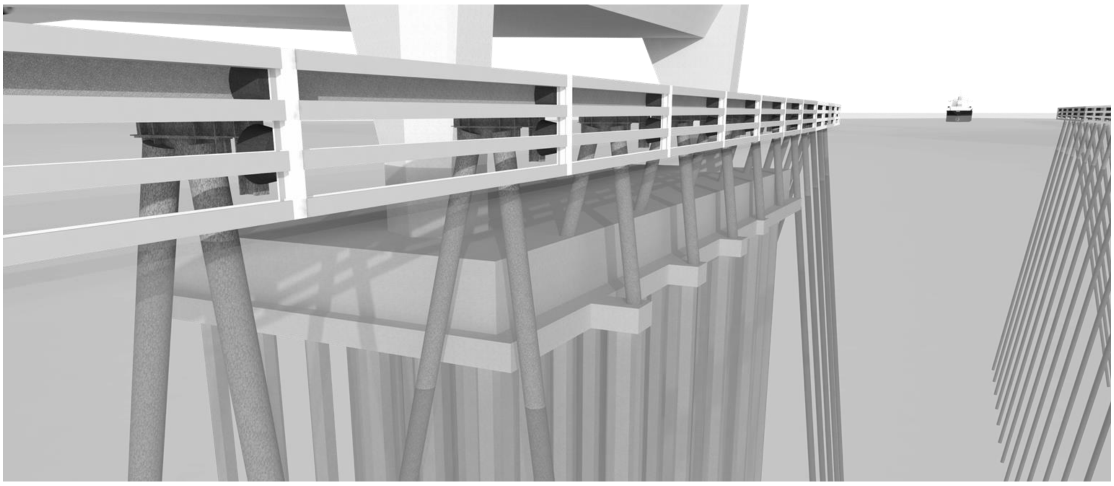

Figure 4.3 Piles supporting the protective piers are attached to the bridge foundation at the opening, giving a stiffer response of the piers.

4.3.2 Modelling of reinforcement

The possibilities to model reinforcement depend on which element type the host element is. As mentioned in Section 4.3.1, shell and membrane elements allow reinforcement to be modelled as smeared layers. These layers have constant thickness which is equal to the total area of the reinforcement (SIMULIA, 2012). In 3D solid elements the preferred way to model reinforcement is as separate parts that can be embedded into the solid element. Full interaction is assumed and means that the steel bars completely follow their host, the concrete beam, without any bond-slip. Only the longitudinal reinforcement is included in Abaqus model, see Figure 4.4, and is assigned 3D truss element type.

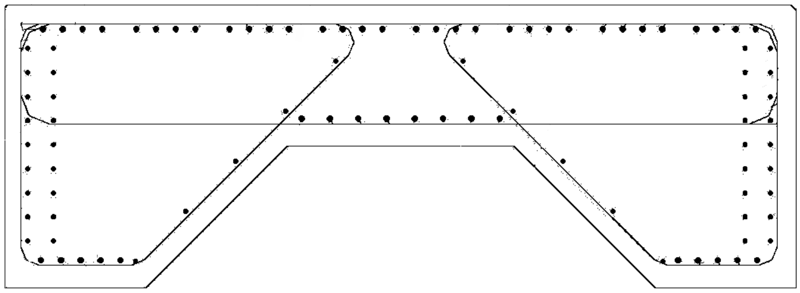

Figure 4.4 Reinforcement drawing of the concrete beam.

4.3.3 Modelling of piles

This section outlines the modelling of the piles themselves and the interaction with surrounding clay soil. In contrast to the beam, the pile modelling consists of more tests to find a good setup, these are found in Appendix C. The real piles consist of one hollow steel part and one concrete filled section.

A hollow steel sheet pile is modelled in two ways using both solid and shell elements for comparison. Due to the fact that the thickness of the pile is significantly smaller than the other dimensions, shell elements are motivated (SIMULIA, 2012). Findings show that the model using solids requires a large number of elements since the thin thickness demand small elements and hence give rise to a large number of elements in other directions due to the elements' depth-length ratio limit. Solids are interesting as they capture the deformation phenomenon well but are excluded since they require a lot more processing power than shells. The choice is also supported by the fact that only global deformation is of interest and hence local variations can be neglected.

The concrete filled steel tube has two test setups. One model has a massive cross section using solid elements. Material properties of steel and concrete are mixed and weighted to create a representable fictitious aggregate. Despite a good behaviour in tests, this solution is still a simplification that will only work for linear material properties and is disregarded further on. The second approach is by separating steel and concrete into two parts and is considered as the appropriate one. A steel sheet shell tube made up by 4-node quad elements and a concrete core of 8-node solid brick elements. Tie constraints connects the inside surface of the steel tube to the outer surface of the concrete core so there is no relative motion between the materials. A setup like this is expected to be able to show large deformations with non-linear behaviour. Beam elements are for this reason neglected and as a consequence of the more complex modelling.

The piles are of about 60 meters length and their boundary conditions are set to be fixed at the bottom edge. This is not the reality but an assumption pointing at the fact that the clay is of great stiffness at that depth.

The piles are standing free in water to a certain depth and remaining length is driven into varying clays. The horizontal passive resistance of the clay against the pile is represented by elasto-plastic springs connected between the piles' outer surface and a fixed point in space in the FE-model, acting in the same direction as the applied displacement. Spring properties are obtained from COWI, see Appendix A, and works according to a bilinear force-displacement relationship where the clay yield pressure, P_y, features the change of slope in Figure 4.5 and K is the spring stiffness. The presence of several clay layers demand depth-varying properties and requires relatively small spring spacing which is set to one every meter, see Figure 4.6. No vertical springs are modelled to represent the vertical resistance from the cohesion forces between the clay and the piles. These would however have a certain impact regarding the pile behavior and hence global deflection of structure.

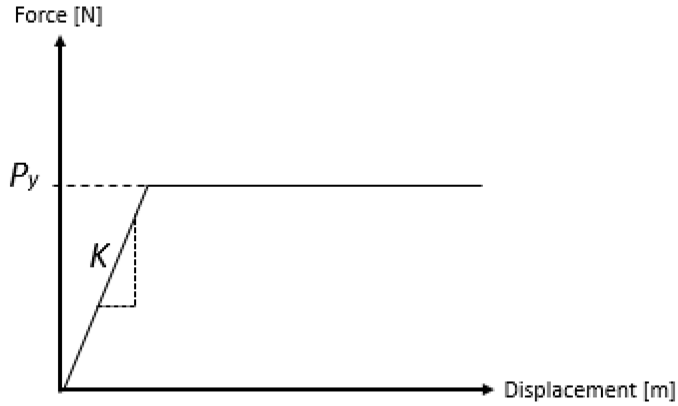

Figure 4.5 Behaviour of a spring representing clay with a linear stiffness K until the yielding point P_y.

Cohesion forces along the pile could probably be modelled by springs as well. Vertical clay carrying capacity is however not considered in this model and thus the reaction forces at the bottom boundary need to be checked and discussed whether these are sufficient or not. The clay-pile modelling is advanced as there might be several unknown parameters which could affect the global behaviour in any direction (Matlock, 1970).

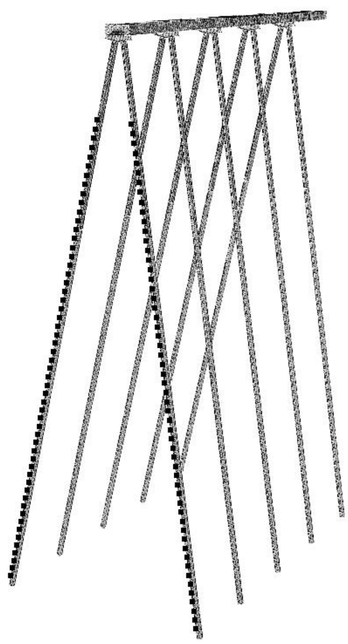

Figure 4.6 Location of the springs represented on two piles. The same distribution is for every pile.

4.3.4 Modelling of connections between structural parts

When the main beam and piles behave as wanted, the parts must act correct together in a global model. It is important to apply an appropriate connection and analyse the structural response to validate the results. A simplification in the model is to disregard the I- and T-beam completely and to use a fictive connection instead. The I- and T-beam are thereby assumed to purely transfer loads, rotations and translations between the concrete beam and piles in a fixed condition. Three different setups are tested to find an appropriate connection. Beam and piles are in all cases fixed in their true relative distance from each other to match a real like behaviour.

Surface-based tie constraints are first tested by connecting a partitioned area of the concrete beam's underside to the top nodes of the pile, see Figure 4.7 [1]. The beam contains the master nodes since it is exposed to the applied displacement and will affect the piles, which contain the slave nodes. The tie constraint is generally defined so that each node on the slave surface will follow the node closest on the master surface. The tolerance distance is set so that the nodes are able to connect.

Another tie constraint is also tested, similar to the first one, except that master and slave nodes are defined as regions, see Figure 4.7 [2]. Backside/frontside of the pile top is constrained to the backside/frontside of its designated concrete area.

A third type of connection is a rigid beam of arbitrary shape to fit the geometry, see Figure 4.7 [3]. In contrast to other parts, this one is a rigid body and will not deform but rather purely transfer loads, rotations and translations as in a fixed connection. The concrete beam and piles are tied to the rigid beam with surface-based tie constraints. A rigid body always contains the master nodes.

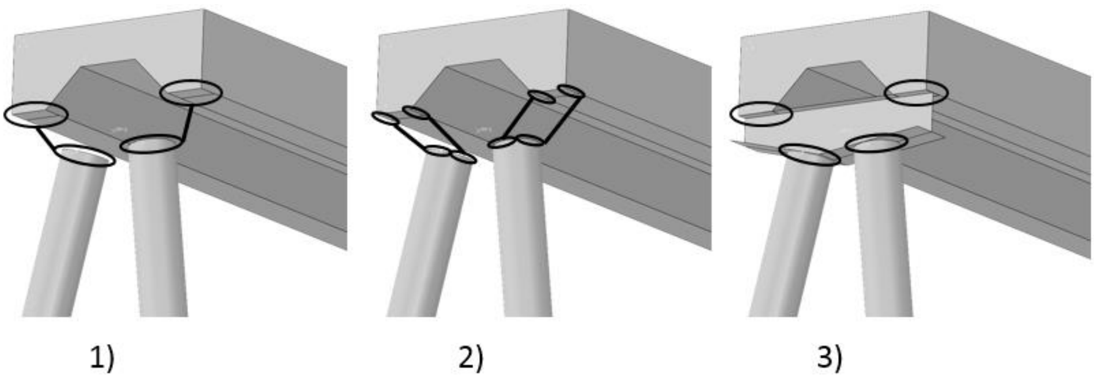

Figure 4.7 Different setups of connections between main beam and piles in Abaqus. 1) Tie constraints between surfaces. 2) Tie constraints between node regions. 3) Tie constraints involving a fictive rigid beam.

The third setup is the most appropriate one as it gives the desired structural response namely a beam and piles that follow each other, see Figure 4.8 [2]. The tie constraint models, in Figure 4.7 [1] and Figure 4.7 [2], do connect the parts but not in a real way, see Figure 4.8 [1]. Because of this the connection involving a fictive rigid beam depicted in Figure 4.7 [3] is the one used in the model.

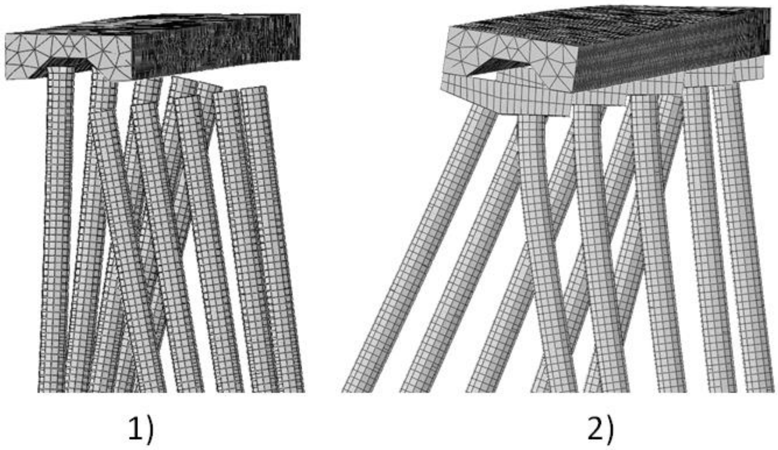

Figure 4.8 *Structural response when using different connections. 1) The use of only tie constraints. 2) The use of tie constraints to a rigid beam.*

4.4 Verification of FE-model

When computing using FEM one should not trust the analysis output without confirming the model first. By performing simple calculations by hand and compare the results with a similar model in FEM software, this concern is averted. The different members of the protective piers will be checked step by step to confirm their behaviour.

4.4.1 Check of concrete beam

An approach is to verify deflection of a simply supported beam. This is done in several sub-steps from the simplest model of the beam to a model that describes the beam completely, see Figure 4.9. All calculations are provided in Appendix D.

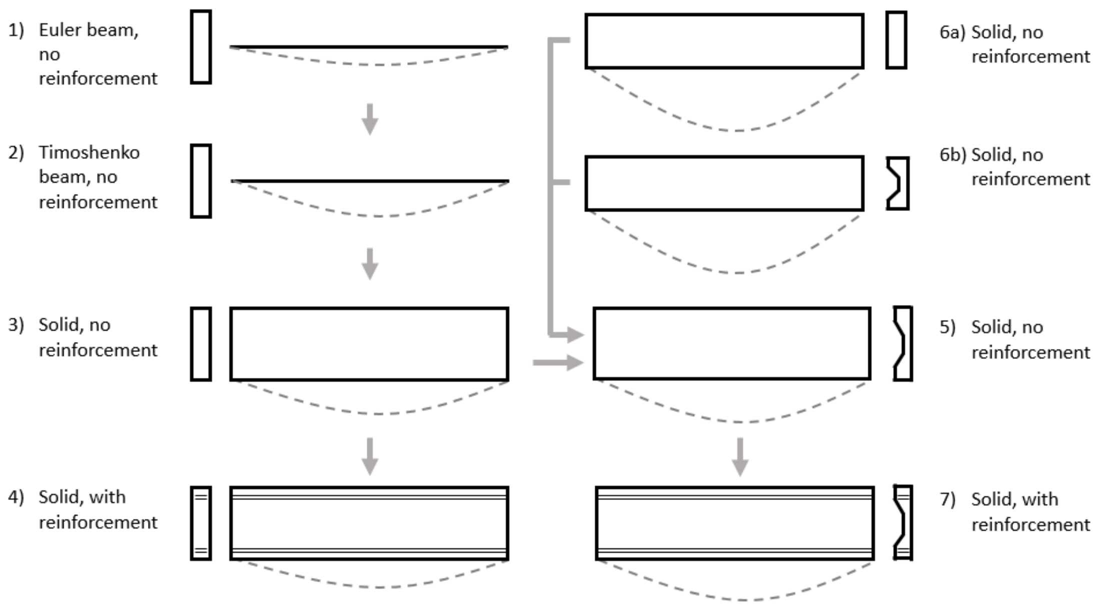

Figure 4.9 Different beam models in Abaqus. 1) Beam elements, no reinforcement, rectangular cross-section. 2) Beam elements that include shear deflection, no reinforcement, rectangular cross-section. 3) Solid elements, no reinforcement, rectangular cross-section. 4) Solid elements, with reinforcement, rectangular cross-section. 5) Solid elements, no reinforcement, complex cross-section. 6a) Solid elements, no reinforcement, rectangular cross-section with lower height. 6b) Solid elements, no reinforcement, complex cross-section with lower height. 7) Solid elements, with reinforcement, complex cross-section.

Both the hand calculation models and the Abaqus models described below use the load controlled approach. The data compared in these verifications is the maximum deflection in the centreline of the lower edge of the beam. In this approach a 10m long simply supported beam is loaded with a point load at the centre of the beam with an arbitrary magnitude of 3200 kN. For the Abaqus model, the point load is modified to a line load with the same resulting magnitude, see Figure 4.10. This is done to best represent the 2D point load in the 3D Abaqus model and also to get rid of the local abnormities under the concentrated load. Only longitudinal reinforcement at short ends of the beam is included in the models accounting for this.

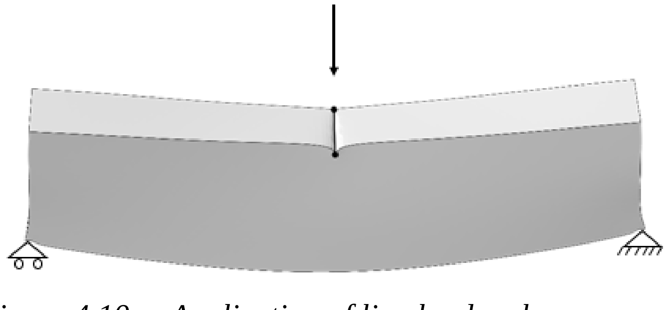

Figure 4.10 Application of line load on beam.

In addition to this, a test of the displacement controlled method is also performed. As the deflection is the applied parameter in Abaqus, the supports' reaction forces are measured instead. The deflection calculated by hand is set to be the applied displacement in Abaqus, the measured reaction forces are then summed up and compared to the applied load in hand calculation. If there is no difference between the forces, the models agree well.

4.4.1.1 Hand calculations

To calculate the deflections by hand for all the different models, see Figure 4.9, elementary cases for simply supported beams are used. These elementary cases are based on the Euler-Bernoulli beam theory which states that plane sections initially normal to the beam's axis will remain plain and normal to the beam axis. This means that the effects of shear deformations are not taken into account while calculating the deflection. For low-depth beams this is not an issue since the influence of shear deformation is not that large, but for deeper beams the shear deformation is evident and has a greater influence.

Deflection calculation for a dynamic analysis, using the same type of beam, is performed to test its dynamic response. Calculations follow the Swedish Civil Contingencies Agency's (Myndigheten för samhällsskydd och beredskap, MSB) impact analysis documents "Bebyggelsens motståndsförmåga mot extrem dynamisk belastning, del 3" (Johansson, et al., 2012) and "Beräkningsanvisning för strukturrespons – Strukturrespons vid impulsbelastning" (Johansson, 2014). Load is chosen to be of same magnitude as for previous cases and of triangular shape, starting at full amplitude and decreasing linearly during five seconds down to zero. Loading time is chosen as an estimated value of the ship impact time.

4.4.1.2 Abaqus models

The first model 1) is a non-reinforced concrete beam with a rectangular cross-section of about the same size as the beam used for the protective pier, see Appendix D. In Abaqus the beam is modelled with one-dimensional beam elements that are solely based on Euler-Bernoulli beam theory. The results seen in Table 4.1 show no difference between the hand calculations and the analysis in Abaqus since the theory behind both models are the same.

Table 4.1 Comparison of deflection between hand calculations and Abaqus.

Beams	Hand calculation deflection [mm]	Abaqus deflection [mm]	Difference [%]
Beam 1)	1.072	1.072	0
Beam 2)	1.072	1.309	22.1
Beam 3)	1.072	1.345	25.5
Beam 4)	0.952	1.209	26.9
Beam 5)	1.137	1.68	47.8
Beam 6a)	1.137	1.401	23.2
Beam 6b)	3.569	4.79	14.04
Beam 7)	1.004	1.53	52.4

The second model uses the same non-reinforced concrete cross-section as model 1 but is modelled with beam elements that include shear deformations. As can be seen in Table 4.1, this change in element property increases the deflection of the Abaqus model with 22.1 %. This increase can be attributed to influence of shear deflections in the global response.

Model 3) also has the same non-reinforced concrete cross-section as model 1 though this model is modelled with tetrahedral 3D solid elements instead. The deflection of this beam increases with 25.5 % which shows that the solid elements also include shear deformation as for the shear flexible beam elements.

In model 4) reinforcement is added to the rectangular concrete cross-section but is apart from that same as model 3). The deflection is lowered for both hand calculations and Abaqus compared to model 3) which is expected due to the increased stiffness, see Appendix D. Even though the results are lowered the difference between hand calculations and Abaqus keeps relatively constant. The difference is 26.9 % which is close to the difference in model three.

The model 5) has the same cross-section as the beam used for the protective pier but is without reinforcement and is modelled with tetrahedral 3D solid elements, see Figure 4.9. This setup increases the difference to 47.8 % compared to hand calculations. Two more tests, 6a) and 6b), are required to see if the cross-section shape is the influencing factor.

In model 6a) a rectangular cross-section with the same area moment of inertia as for model 5), thus resulting in a lower depth, is analysed. Because of the same area moment of inertia, the result of the hand calculations will remain constant but as can be seen in Table 4.1 the deflection in Abaqus is lowered to 1.401 mm. This equates to a margin of error of 23.2 % which is in the same magnitude as for the other models with rectangular shapes. This indicates that the odd shape of model 5) influences the deflection in Abaqus a great deal and that shear deformations are evident.

In model 6b) the shape of model 5) is kept constant but the depth is lowered to 1.8 m from ordinary 2.8 m. This is done to see how much influence the depth has on the deflection. The difference is lowered in this case to 14.04 %, see Table 4.1. This decrease can be contributed to the reduced influence from shear deflection. As mentioned earlier the assumption, that plane sections initially normal to the beam's axis will remain plane and normal to the beam axis, is more valid for less deep beams since the effects of shear deformation are negligible in these beams.

Model 7) has the same cross-section and dimensions as model 5) but reinforcement is added and represents the final setup. As in model 4) the deflections are lowered due to the increased stiffness but the margin of error is kept relatively constant, see Table 4.1.

A dynamic response test is also set up for model 7). Firstly a frequency analysis step is performed to get the beam's natural frequencies. This is followed by a modal dynamic analysis step where the load is applied as described in Section 4.4.1.1. The analysis considers the 10 lowest eigenmodes and a critical damping fraction of 0.055 (Adams & Askenazi, 1999) which is in commonly used range of 1 – 10 % (SIMULIA, 2012). The response of the beam seems reasonable, oscillating at first and rather quickly sticks to the static linear deflection. The initial difference between hand calculation and Abaqus is about 11 %.

4.4.1.3 Conclusion of verification

The reasoning about the shear deformation that has been done throughout the previous section is completely in line with Timoshenko beam theory. This beam theory takes into account the shear deformation that occurs in deeper beams. According to “Introduction to the finite element method” (Ottosen & Peterson, 1992) shear deformation occurs in beams where the span to depth ratio is smaller than 5 which is the case for the tested beam which has a ratio of 3.57. As opposed to Euler-Bernoulli theory, a second order partial derivate is present that describes the rotation of the initial plane sections normal to the beam axis and it is by this that the shear deformation is included (Craig & Kurdila, 2006), see Figure 4.11. Physically all of this effectively lowers the stiffness of the beam with a result that the deflections increase.

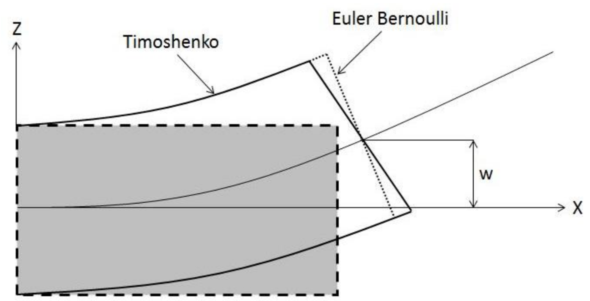

Figure 4.11 Comparison between Euler-Bernoulli and Timoshenko beam theory.

So though the hand calculations and the final model differs as much as 52.4 % the model can be verified by the reasoning about influence of odd cross-section and shear deformation done in the previous sections about Timoshenko beam theory.

The beam's dynamic behaviour is harder to validate as there are many parameters in Abaqus and assumptions in hand calculations that could give rise to the difference. It is also found that the load setup is classified as pressure load rather than a characteristic impulse when looking at this structure, hence the problem should be treated as an equivalent static case (Johansson, 2015). However, results show an indication of good beam properties and natural type of response.

4.4.2 Check of pile

Calculation of piles is made in different setups as defined in Section 4.3.3. In first step all of them are set to be an arbitrary length of 18 meters since this is about the length of the concrete filled part of actual piles. Boundary conditions are set to be a cantilever beam with an arbitrary point load acting on the free edge and the deflection is then measured at the free edge in the direction of the load. Hand calculations are determined from elementary cases. The mesh is fine enough to capture a good resolution.

It is also important to check the clay springs as they have large influence on the total response of the structure. Note that this is only verified in FEM-software and no hand calculations are provided.

4.4.2.1 Hand calculations

The steel sheet's cross sectional constants are computed using formulas assuming a massive circular cross section model which is in accordance with previous COWI calculations. An elementary case gives the deflection of a console beam. Calculations are provided in Appendix C and treat the different pile setups to display how much influence the concrete core has on the overall pile deflection.

4.4.2.2 Abaqus models

The correlation between hand calculations and Abaqus for pile sheet models is good as the errors are below 1 %. The combined steel sheet and concrete core model result in a stiffer pile than for the fictitious and pure steel sheet setups, with a deflection at pile tip 30 % smaller than for hand calculations.

One check is performed on a single-pile model to verify the function of the nonlinear clay springs for the full-length pile of about 60 meters. It is confirmed that springs with a spacing of one meter give a better representation of the clay than for example five meters as they seem to attract a lot of stresses and deformation at the position of the springs otherwise. Non-linearity is checked in Abaqus by plotting stress-strain for the element node of a chosen spring. If the applied action is big enough, some spring elements show a bilinear curve and some elements a linear one. This means that the pile is resisting the force by activating more and more springs along the pile, which is desirable.

A minor check is done to see that forces are transferred correctly when using tie constraints. An arbitrary object is placed in front of the pile with a load acting on it. The object is tied to the pile end and reaction forces in the pile springs and at boundary conditions are summed up. The sum equals the system's added load and hence the load transfer is verified.

4.4.2.3 Conclusions of verification

A 30% difference between hand calculations and Abaqus model could be expected and is explained by at least two reasons. Firstly, a smaller deflection in FE-analysis is logical as steel and concrete are put in their actual position of the cross section. Steel has higher Young's modulus and resist compression and tension better at the edges of the cross section, than if it would be smeared out across the area as in the mixed aggregate pile, see Figure 4.12.

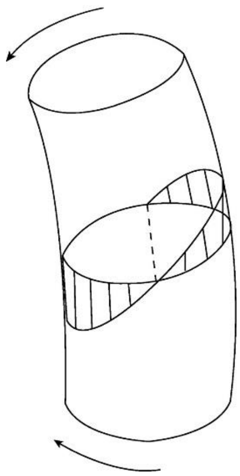

Figure 4.12 Principled sketch of stress distribution in steel tubes. Negative and positive stress on each side of the neutral line.

Secondly the tie constraints lock nodes to each other in the interface between the materials and introduce more stiffness to the pile. An alternative method to connect the materials would be to set up a contact interaction with friction that uses a specified behaviour in the normal and tangential directions (Johansson & Gylltoft, 2002). Friction models do however require much computational resources, can be hard to get to converge and can give rise to critical points (Flansbjer, 2015). Since the pile is probable to have a large deformation, a tie constraint is motivated as the concrete will be squeezed stuck inside the steel sheet when bending occurs and hence reflect a tie constraint well. When local concrete response and cracks are of interest, a friction model is more suitable. To get a good overview of how well a tie constraint resembles the reality, the two extremes are compared namely a tie constraint model and a frictionless contact model. Tests show that the difference in deflection for the chosen pile setup is less than 1% and so the tie constraint is good to use, see Appendix C.

4.4.3 Convergence study

To see that the mesh is of appropriate size for the structure a convergence study is performed. This could be done on the structure as a whole but is chosen to be performed on the individual parts of the structure i.e. the beam and the piles. The choice to split up the study is mainly done to prevent large computing times in the final model of the structure.

4.4.3.1 Beam

The convergence study is performed on a 20 meter long continuous part of the beam over three supports to capture phenomena closer to the real structure. The beam is modelled with solid elements for the beam itself and 3D truss elements for the reinforcement. The beam is loaded with an arbitrary 3200 kN concentrated force located in the centre of one span. In this study four different meshes with different element sizes are tested, 0.5, 0.35, 0.3 and 0.25 meters. For each element size a total number of elements, max deflection and computational time are extracted from Abaqus, see Table 4.2.

Table 4.2 Results of the beam convergence study.

Element size [m]	Total nr of elements	Max deflection [mm]	Computational time [h:mm:ss]
0.5	6793	1.30410	0:05:35
0.35	13525	1.34723	0:17:38
0.3	18235	1.34767	0:21:36
0.25	27763	1.34725	0:58:13

The total number of elements for each mesh size is then plotted against the maximum deflection to see if convergence is reached. The maximum deflection is measured on the bottom edge of the beam see Figure 4.13.

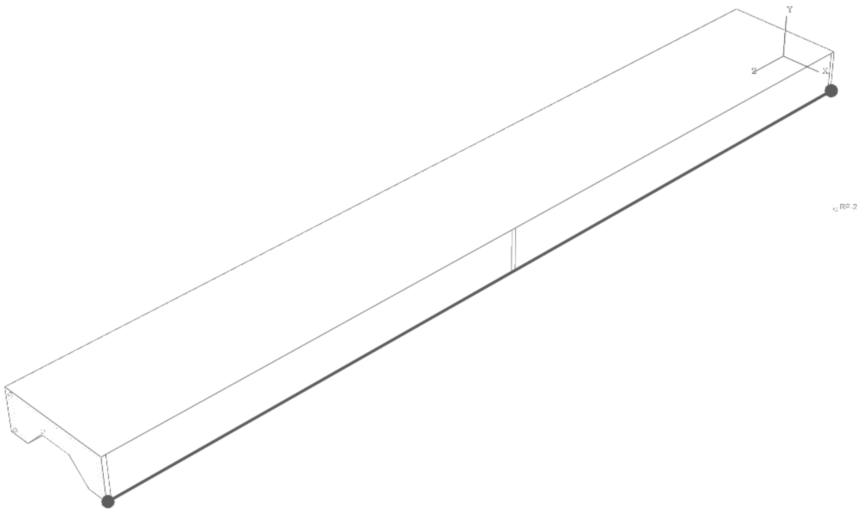

Figure 4.13 Deflection is measured along the marked line.

As can be seen in Figure 4.14 convergence is reached at about 13000 elements which corresponds roughly to an element size of about 0.35 meters, see Table 4.2.

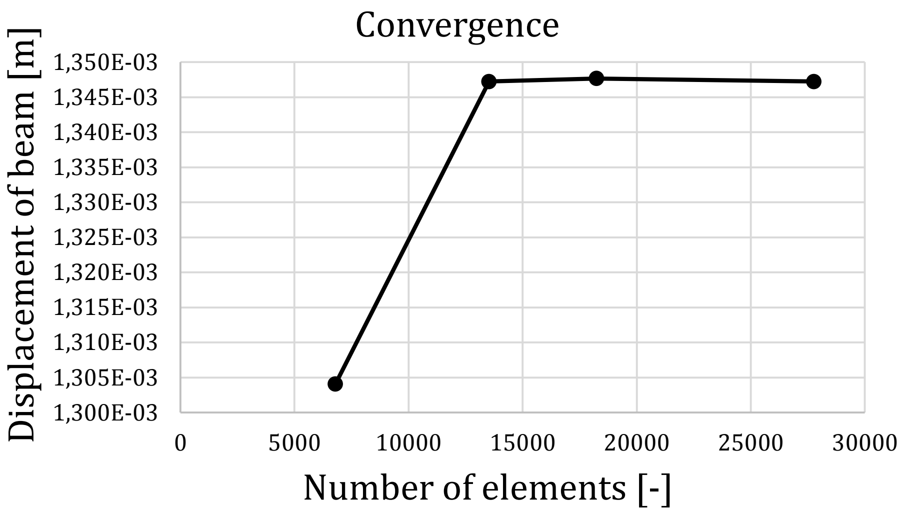

Figure 4.14 Convergence of beam mesh.

The decrease in element size will after this point only increase the computational time as can be seen in Figure 4.15. From this the conclusion is that no larger elements than 0.35 meters have to be used for the beam.

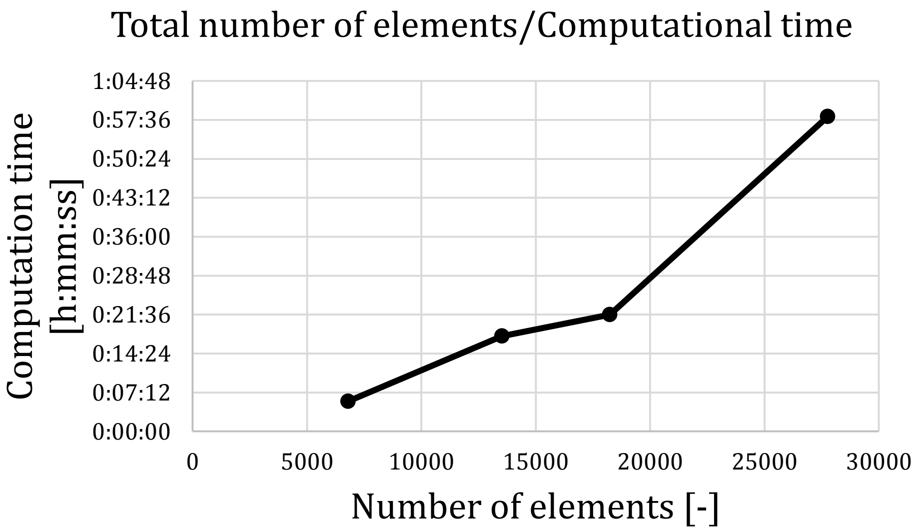

Figure 4.15 The increase in computational time with increase in total number of elements for the beam convergence study.

4.4.3.2 Piles

The convergence study for the piles is done on a single pile with the length of about 60 meters. The pile is modelled with two different elements, 3D solids for the concrete and shell elements for the steel tube. The pile was the fixed at one end and loaded with a 20 kN point load at the other end where deflection also was measured.

In this study 6 different meshes where tested with the element sizes, 0.3, 0.25, 0.2, 0.15, 0.1 and 0.05 meters.

Table 4.3 Results of the pile convergence study.

Element size [m]	Total nr of elements [-]	Max deflection [m]	Computational time [h:mm:ss]
0.3	2444	7.29621	0:01:12
0.25	2496	7.29622	0:01:51
0.2	3854	7.00558	0:01:41
0.15	7698	6.56736	0:04:11
0.1	20055	6.25288	0:17:26
0.05	105820	6.10637	2:55:59

When the number of elements are calculated they are plotted against the maximum deflections, see Figure 4.16.

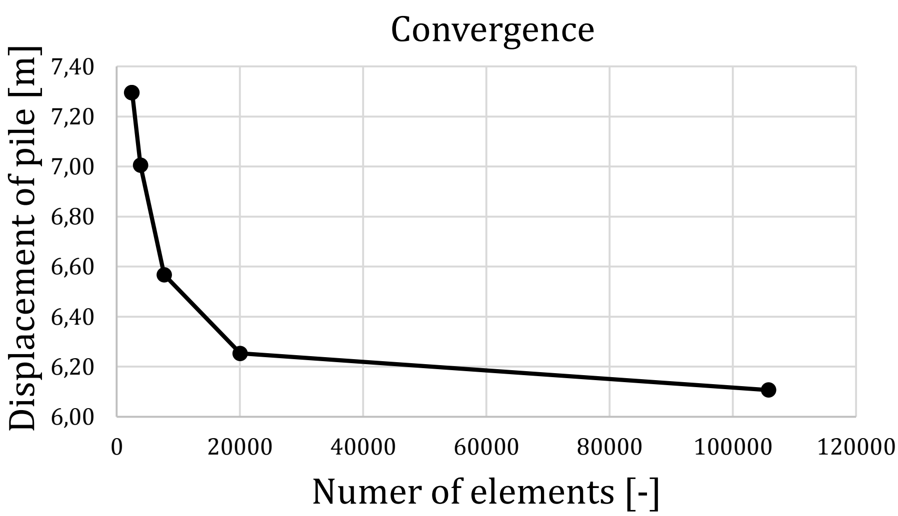

Figure 4.16 Convergence of pile mesh

As can be seen in Figure 4.16, the convergence is not fully developed. Choosing a mesh size of 0.15m results in a less accurate deflection of pile but saves a vast amount of computation time, see Figure 4.17, which weighs more in this case.

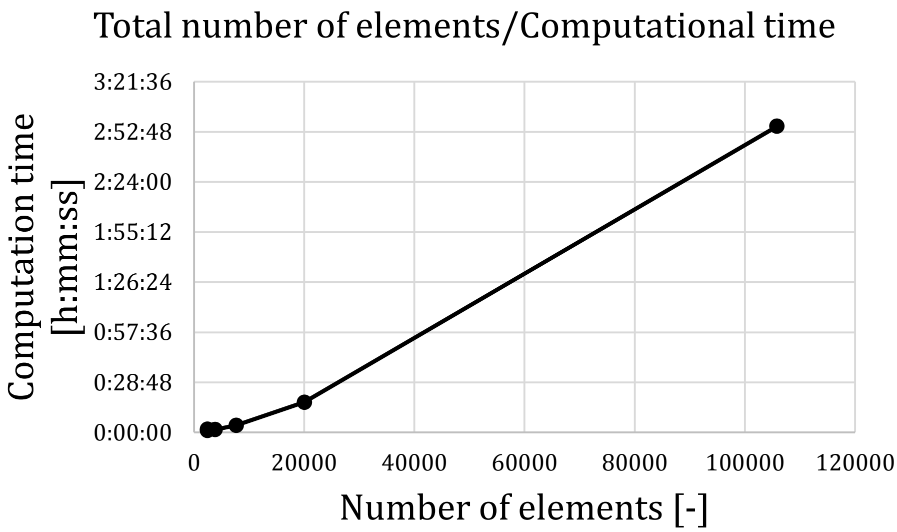

Figure 4.17 The increase in computational time with an increase in total number of elements for the pile convergence study.

4.5 Design energy to be absorbed

Eurocode mentions three design strategies in case of an impact-like accidental situation (Eurocode, 2010);

- Design the structure to have sufficient minimum robustness
- Preventing or reducing the action, e.g. protective measures
- Design structure to sustain the action

Protective piers are a combination of point two and three. The structure protects the bridge supports while it sustains the action itself. One more advanced approach is given in Eurocode 1991-1-7 Annex C Section 4.3 on how to find the resulting dynamic force from an incoming ship. Part of that process treats the computation of deformation energy which is the value to be compared with in final analysis. In case of frontal impact the deformation energy is equal to total available kinetic energy in the collision, see Equation (4.1). SSPA's investigation (SSPA, 2014) gives input regarding hydrodynamic mass due to water and ship's mass and speed. Eurocode do present recommended value for these parameters but are not chosen since the real numbers are more interesting for the case study.

$$E_a = \frac{mv^2}{2} \tag{4.1}$$

Where:

E_a is the total available kinetic energy [J]

m is the mass of the object [kg]

v is the velocity of the object [m/s]

A reduction is performed as the incoming angle is 20° and makes it a sliding impact. The deformation energy perpendicular to the pier is calculated according to Equation (4.2) .

$$E_{def} = E_a(1 - \cos\alpha) \tag{4.2}$$

Where:

E_{def} is the deformation energy [J]

E_a is the total available kinetic energy [J]

α is the incoming angle of the ship [°]

The resistance of the structure will be calculated as the work done by displacing the structure, see Equation (4.3).

$$W = F \cdot \delta \tag{4.3}$$

Where:

W is the work done on the structure [Nm]

F is the force that displaces the structure [N]

δ is the displacement of the structure [m]

The work is measured by energy with the unit Joule [J] and is the same as Newton times meter [Nm]. By the law of energy conservation, it can be stated that the total energy of an isolated system remains constant. In other words, a collision becomes a transformation of ship's kinetic energy into work done by the pier, $W(ship) = W(protective\ pier)$. This is not fully true as some energy will be absorbed by the processes stated in Section 2.3.3.

The energy for the designing Värnermax ship used in this report is calculated to 18.9 MNm according to Equation (4.2). For the complete calculations see Appendix B.

Collision progress starts at time zero and goes on until the kinetic energy from the incoming vessel has been absorbed. The Figure 4.18 shows a simplified expected relation between the objects which in reality would vary non-linearly.

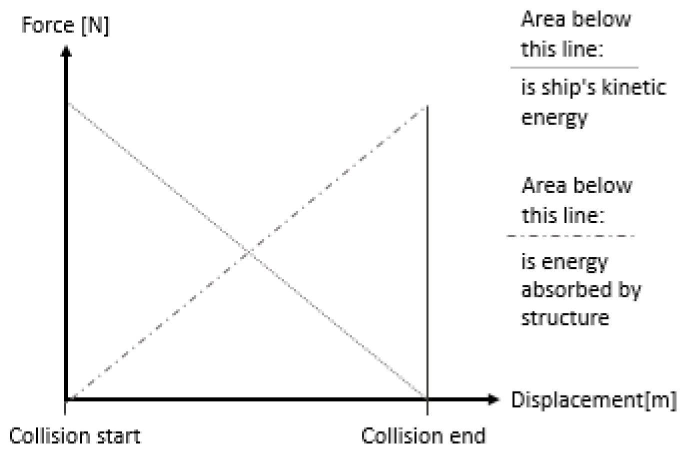

Figure 4.18 Energy relationship between colliding vessel and structure.

Energy transformation is caused by an impact between the two objects. Protective piers are represented by large object 2 and ship by small number 1 in Figure 4.19 below. The vessel's incoming velocity in perpendicular direction v_1 decreases during collision progress until v_2 becomes zero. According to the kinetic energy Equation (4.1) it is clear that a reduced amount of energy will decrease the velocity since the mass is unchanged.

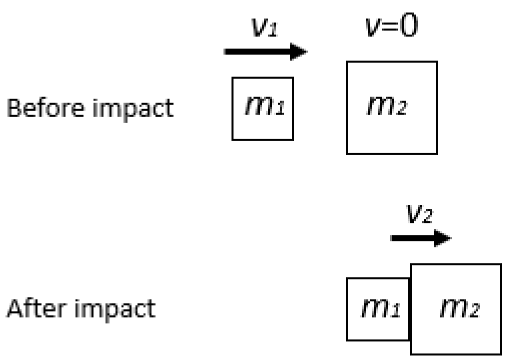

Figure 4.19 Description of collision progress before and after impact.

The sequence can also be visualized by an energy-time diagram, see Figure 4.20 which summarizes the collision progress. It is clear to see that collision end takes place when the structure has consumed all of the ship's kinetic energy.

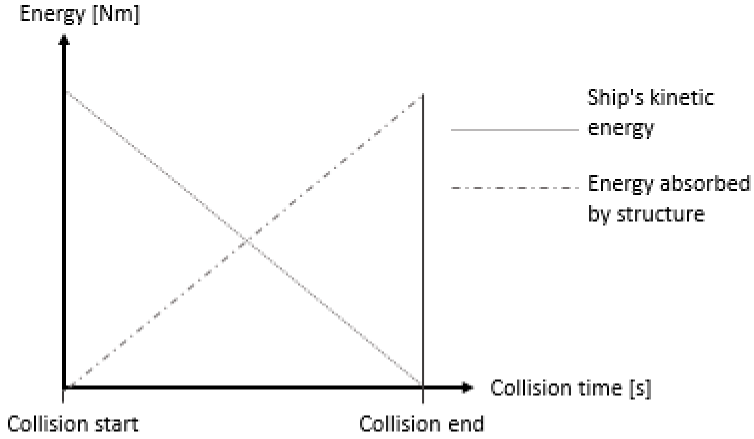

Figure 4.20 Energy-time diagram.

4.6 Non-linear material parameters

When doing non-linear FEM analyses the material properties are extended to better represent the real life behaviour. Gained accuracy is nevertheless paid by longer computation times.

4.6.1 Concrete

The chosen model in Abaqus for describing the non-linear behaviour of concrete is called "Concrete Damaged Plasticity". For this model to work properly some general plastic parameters and the non-linear stress-strain relationship for concrete is described and entered into the model. For a material like concrete that is behaving differently in compression and tension, the parameters describing these states have to be obtained separately. An accurate way to do this is to perform tests of the chosen concrete, however, there are codes and regulations to gain useful values of the sought stress-strain relationships. Because of the absence of tested data in this project a code of principles produced by a collaboration from Lund Tekniska Högskola (LTH), Chalmers Tekniska Högskola (CTH) and Kungliga Tekniska Högskolan (KTH) by (Carlsson, et al., 2008) called "Säkerhetsprinciper för bärighetsanalys av broar med icke-linjära metoder" (Security principles for carrying capacity analysis of bridges with non-linear methods) is used to obtain the non-linear data of the concrete.

4.6.1.1 Compression

In highly compressed parts of the concrete it is important that the internal forces are able to redistribute from the crushed concrete to the reinforcement. It is essential that the model being used is able to exhibit this behaviour in a reasonable way so that non-linear compressive stress-strain curve gets a reasonable shape that describes its behaviour (Carlsson, et al., 2008). The mentioned report by (Carlsson, et al., 2008) has modelled a compressive stress-strain relationship according to the International Federation of Concrete (fib) report from 1990 and is described by Equation (4.4) that is able to do this in a reasonable way.

$$\sigma_c(\varepsilon_c) = \begin{cases} \dfrac{k\dfrac{\varepsilon_c}{\varepsilon_{c1}}\left(1-\dfrac{\varepsilon_c}{\varepsilon_{c1}}\right)}{1+\dfrac{\varepsilon_c}{\varepsilon_{c1}}(k-2)} f_{cc}, & 0 \le \varepsilon_c \le \varepsilon_u \\ \dfrac{f_{cc}}{(\varsigma\varepsilon_u - 2)\left(\dfrac{\frac{\varepsilon_c}{\varepsilon_{c1}}}{\varepsilon_u}\right)^2 + (4-\varsigma)\dfrac{\frac{\varepsilon_c}{\varepsilon_{c1}}}{\varepsilon_u}}, & \varepsilon_c \ge \varepsilon_u \end{cases} \tag{4.4}$$

Where:

$$\varsigma = 4\frac{\varepsilon_u^2\,(k-2) + 2\varepsilon_u - k}{(\varepsilon_u(k-2)+1)^2} \tag{4.5}$$

To make the two parts of the function fit together the value of the strain at the top of the curve ε_{c1} is adjusted (Carlsson, et al., 2008). Using Equation (4.4) this is proved difficult. The first part of the function is defined as Equation (4.6) (The International Federation for Structural Concrete (fib), 2012).

$$\frac{\dfrac{\varepsilon_c}{\varepsilon_{c1}}\left(k-\dfrac{\varepsilon_c}{\varepsilon_{c1}}\right)}{1+\dfrac{\varepsilon_c}{\varepsilon_{c1}}(k-2)} f_{cc} \tag{4.6}$$

So to be able to make the curves to fit together Equation (4.4) and (4.6) are combined to Equation (4.7).

$$\sigma_c(\varepsilon_c) = \begin{cases} \dfrac{\dfrac{\varepsilon_c}{\varepsilon_{c1}}\left(k-\dfrac{\varepsilon_c}{\varepsilon_{c1}}\right)}{1+\dfrac{\varepsilon_c}{\varepsilon_{c1}}(k-2)} f_{cc}, & 0 \le \varepsilon_c \le \varepsilon_u \\ \dfrac{f_{cc}}{(\varsigma\varepsilon_u - 2)\left(\dfrac{\frac{\varepsilon_c}{\varepsilon_{c1}}}{\varepsilon_u}\right)^2 + (4-\varsigma)\dfrac{\frac{\varepsilon_c}{\varepsilon_{c1}}}{\varepsilon_u}}, & \varepsilon_c \ge \varepsilon_u \end{cases} \tag{4.7}$$

The result is a reasonable curve shape that captures the compressed concrete's non-linear behaviour in a good way, see Figure 4.21.

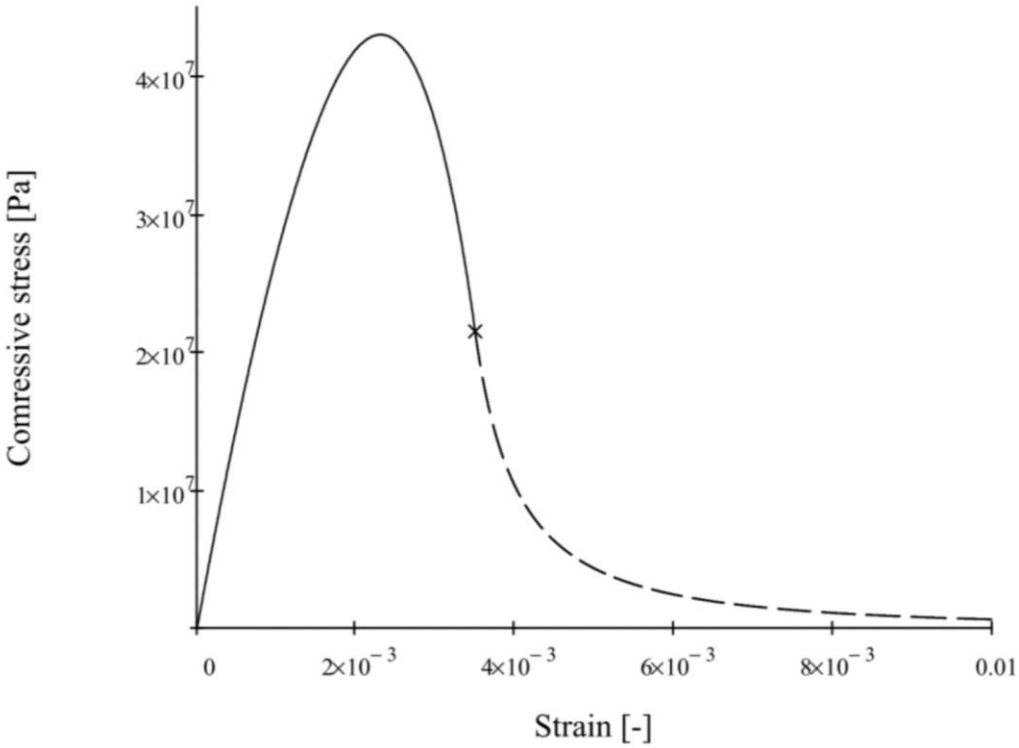

Figure 4.21 Non-linear compressive stress-strain behaviour for concrete used in Abaqus.

The input-data needed to describe the compression in the "Concrete Damaged Plasticity" model are the stress and the inelastic strain. The stress is calculated using Equation (4.7) and the inelastic strain is calculated as the total strain ε_c minus the elastic strain $\varepsilon_{c,el}$ where the elastic strain is calculated according to Equation (4.8).

$$\varepsilon_{c,el} = \frac{\sigma_c}{E_c} \tag{4.8}$$

The limit of elasticity is set to $0.4 \cdot f_{cc}$ (Carlsson, et al., 2008). The input-data is presented in Table 4.4 and the complete calculations in Appendix E.

Table 4.4 Input-data for compressive behaviour in Concrete Damaged Plasticity model.

Yield stress [MPa]	Inelastic strain [-]
17.200	0
27.011	0.0001406
33.026	0.0002492
37.814	0.0003969
41.173	0.00059
42.859	0.0008364
41.966	0.001265
38.422	0.001678
31.832	0.002187
21.500	0.002816
13.245	0.003379
9.222	0.003807
6.881	0.004181
5.372	0.004529
4.330	0.004862
2.447	0.005922
1.586	0.00695
1.116	0.007964
0.830	0.008974

4.6.1.2 Tension

The approach to calculate the non-linear tensile behaviour is rather different than for the compressive part. One way to decide it is to have a curve that gives reasonable fracture energy (Carlsson, et al., 2008). This is done by calculating the start and end point of the plastic part of the curve. The start point is calculated by Equation (4.9) and the end point by Equation (4.10).

$$\varepsilon_{t,el} = \frac{f_{ct}}{E_c} \tag{4.9}$$

$$10 \cdot \varepsilon_{t,el} \tag{4.10}$$

The shape of the curve between these two values is of little significance but if the curve has too much hang it will be hard to reach convergence (Carlsson, et al., 2008). Due to this the values used in this model is chosen so that the curve has a moderate hang, see Figure 4.22.

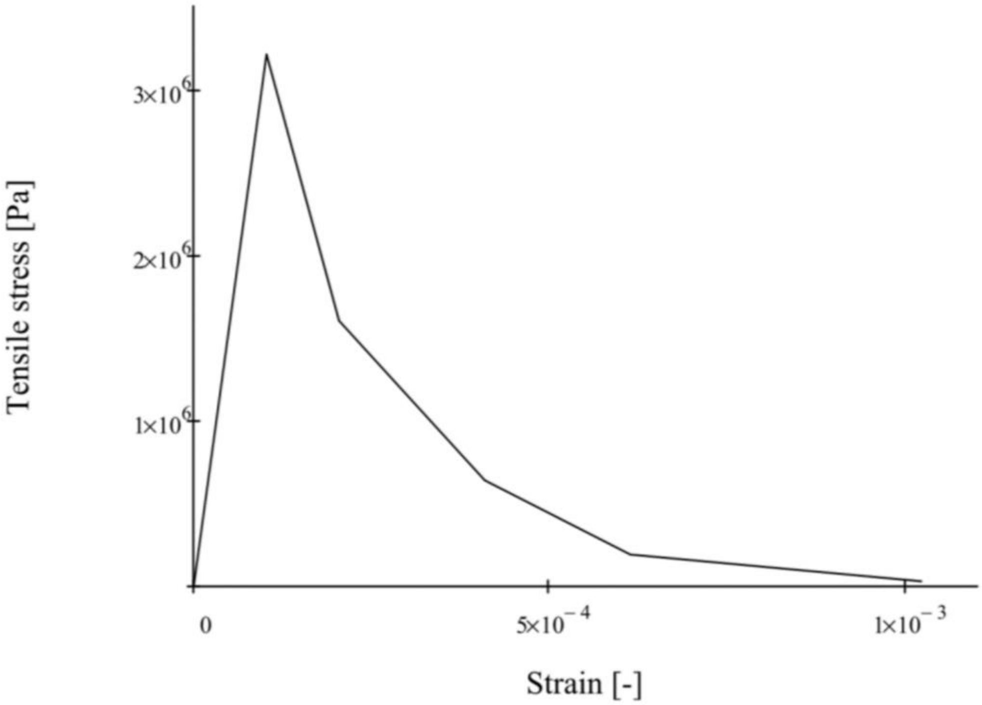

Figure 4.22 Non-linear tensile stress-strain behaviour for concrete used in Abaqus.

As for the compressive part the input-data needed is the stress and the inelastic strain, these values are chosen so that the curve gets the previously mentioned hang, see Table 4.5. Calculations are found in Appendix E.

Table 4.5 Input-data for tensile behaviour in Concrete Damaged Plasticity model.

Yield stress [MPa]	Cracking strain [-]
3.21	0
1.605	0.0002043
0.642	0.0004085
0.195	0.0006128
0.032	0.001021

4.6.1.3 Reinforcement

The reinforcement is modelled in Abaqus with a bi-linear stress-strain relationship with a yield strength $f_y = 500\ MPa$ see Figure 4.23. Because reinforcement has the same behaviour in both compression and tension only one stress-strain curve is needed.

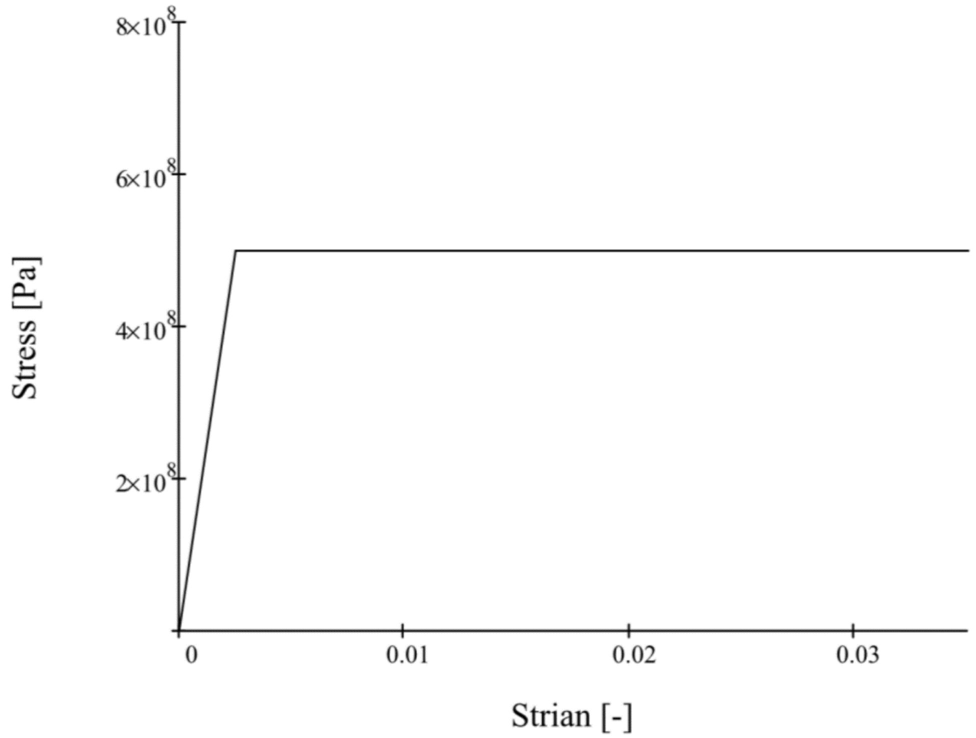

Figure 4.23 Bi-linear stress-strain behaviour for reinforcement used in Abaqus.

4.6.1.4 General plasticity parameters

In addition to the compressive and tensile behaviour parameters of the concrete, several other parameters have to be entered into Abaqus for the model to work properly. The dilation angle ψ and the eccentricity parameter ϵ describe the relationship between hydrostatic pressure and the strength of the concrete. The dilation angle ψ should have a value between 30 and 40 degrees according to the reports “FE-analysis of cracking in transversal support beams of concrete bridges” (Fredriksson & Yhlen, 2010) and “Predicting shear type crack initiation and growth in concrete with non-linear finite element method” (Malm, 2009). The eccentricity parameter ϵ should have the value 0.1 (SIMULIA, 2012). The values for the concrete's compressive and tensile behaviour are described for a uniaxial stress state. Abaqus converts this stress state to a biaxial state with the ratio factor in Equation (4.11). A default value is 1.16 (SIMULIA, 2012).

$$\frac{\sigma_{b0}}{\sigma_{c0}} \tag{4.11}$$

Where:

σ_{b0} is the initial equibiaxial compressive yield stress [Pa]

σ_{c0} is the initial uniaxial compressive yield stress [Pa]

K determines how the yield surface is described in the deviatoric plane. When K changes, the yield surface also changes, see Figure 4.24.

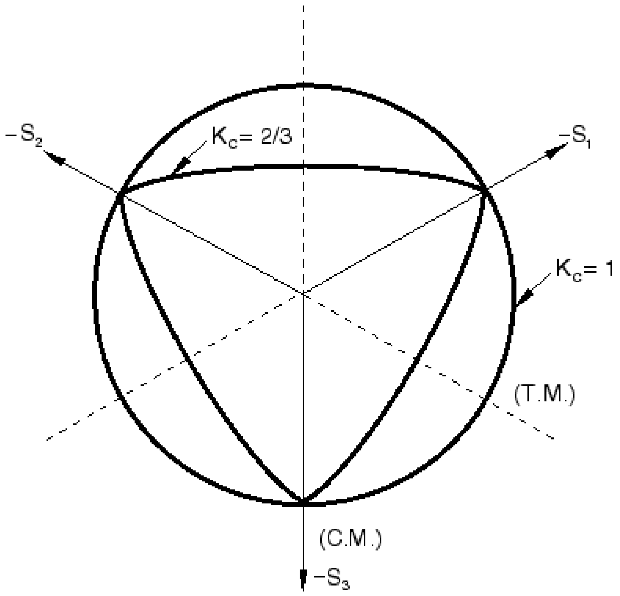

Figure 4.24 Typical yield surfaces on the deviatoric plane (SIMULIA, 2012).

The parameter μ describes the viscoplastic adjustment of the constitutive relationship. This means that the stresses are allowed to be outside the yield surface. This can be of help to avoid convergence problems which can occur when the stiffness decreases. The value of μ should be a small positive value and the larger the value the more outside the yield surface the stresses are allowed to be. The default value is 0 but is set to 0.01 so that convergence can be meet, see Table 4.6 (SIMULIA, 2012).

Table 4.6 General plasticity parameters for concrete.

Dilation angle [°]	Eccentricity	$\frac{\sigma_{b0}}{\sigma_{c0}}$	K	Viscosity Parameter μ
36.31	0.01	1.16	0.6667	0.01

4.6.2 Steel

The stress-strain curve for steel consists of three different regions, the elastic part, the plastic part and the strain hardening part. When modelling steel the difficult part is to model the strain hardening part of the curve. The curve is modelled by Equation (4.12) (Carlsson, et al., 2008).

$$\sigma = \begin{cases} E_s\varepsilon, & \varepsilon < \varepsilon_y \\ f_y, & \varepsilon_y < \varepsilon \leq \varepsilon_h \\ f_y + E_h(\varepsilon - \varepsilon_h)\left(1 - E_h \dfrac{\varepsilon - \varepsilon_h}{4\left(f_u - f_y\right)}\right), & \varepsilon > \varepsilon_h \end{cases} \tag{4.12}$$

Equation (4.12) is used to create the input-data for the stresses into the non-linear material model for steel in Abaqus, see Figure 4.25.

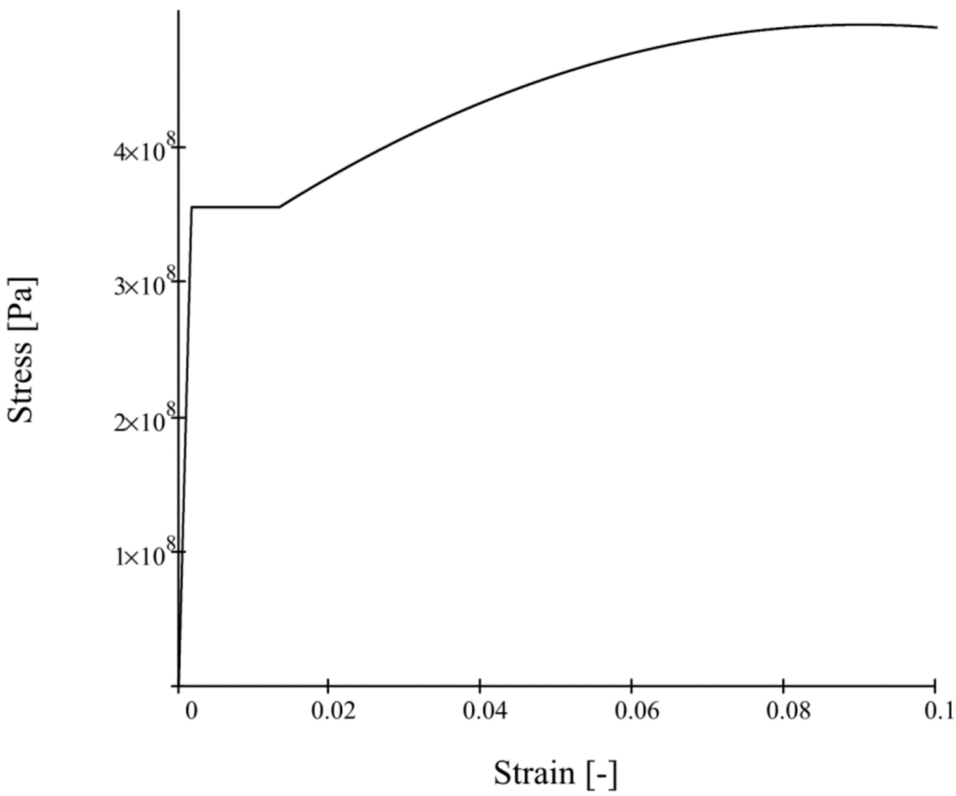

Figure 4.25 Non-linear stress-strain relationship for steel used in Abaqus.

As for the concrete, the strain entered into the model is not the total strain but rather the plastic strain. This strain is calculated as the total strain ε minus the yield strain ε_y. The input-data used for this model is presented in Table 4.7 and the complete calculations in Appendix E.

Table 4.7 Input-data for strain hardening part of steel stress-strain relationship.

Stress [MPa]	Plastic strain [-]
360.77	0.013
407.032	0.028
468.93	0.058
487.51	0.078
487.942	0.098
470.226	0.118
409.624	0.148

5 Results

The results in this chapter is extracted from an Abaqus analysis performed with the Riks method. The analysis took 44 hours whilst running on 16 processors on a computer cluster and stopped at the 229th increment. The arc length is the measurement of incrementation in the used Riks analysis, similarly to time step used in General static analysis. The arc length at and last recorded increment, the 228th, was 2.232 and is such the maximum arc length at 100% of the analysis. Chosen data is presented to indicate how the protective pier model performs under ship collision. Calculated values for the structure's internal energy is also presented and displayed to describe the absorbing capacity. All of this data is then used to analyse the overall structural response as well as the structural response of individual parts.

5.1 Structural response

One of the objectives of the report was to analyse the structural behaviour of the protective pier. This was done by looking at stresses, displacements, reaction forces and the energy absorption capacity of the structure. The data was collected at certain points during the analysis where important structural events occurred such as yielding of different parts. How far the analyses had gone were registered by obtaining the arc lengths at these points.

5.1.1 Overall structural response

The applied displacement generated a deformation on the protective pier. The deformed and undeformed state is shown in Figure 5.1 for comparison.

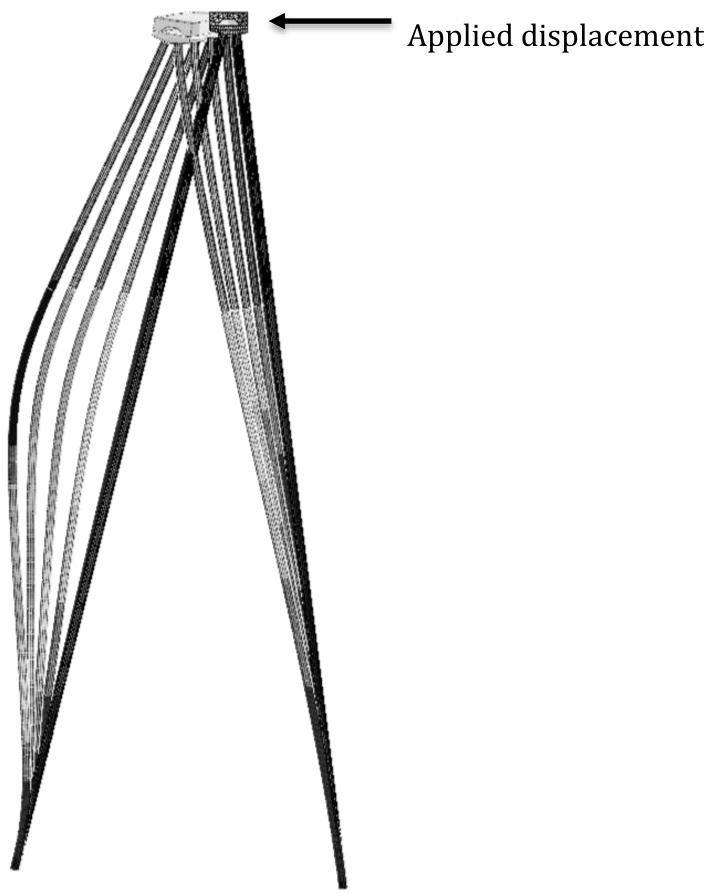

Figure 5.1 Deformed and undeformed shape of the protective pier in the same figure for comparison.

The force needed to create this deformation and move the protective pier was calculated by measuring the reaction force at the reference point where the displacement of the beam was applied since this force equals the total reaction force of the protective pier. These two where then plotted against each other to be able to calculate the total internal energy of the structure and this was done by calculating the area under the graph, see Figure 5.2.

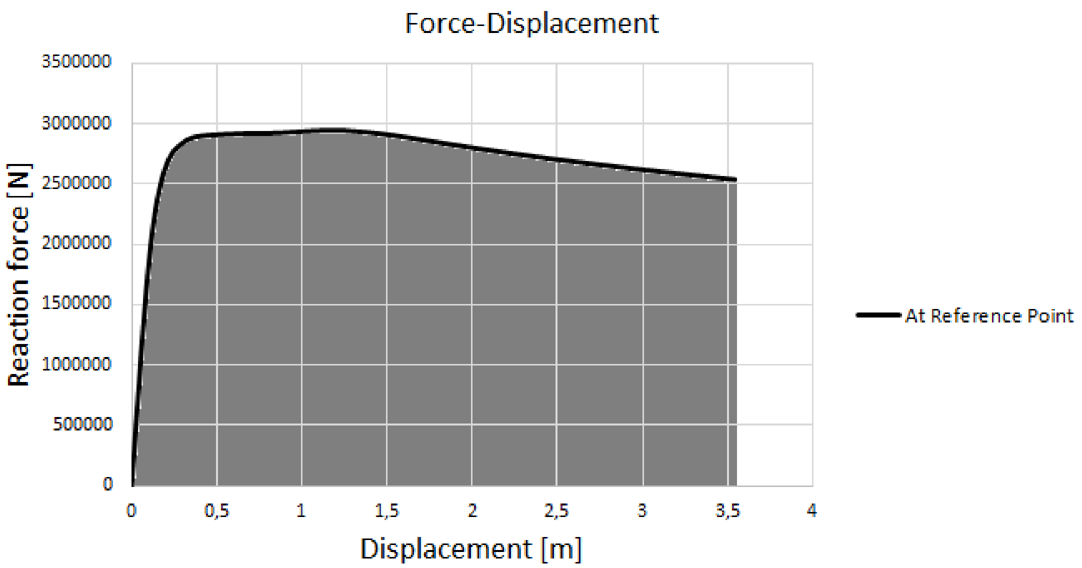

Figure 5.2 Area describing the total energy absorption.

In Abaqus there is a possibility to create an output variable to calculate the entire internal energy of the structure called ALLIE. This value and the approximated hand calculated value were compared as a verification of the energy absorption capacity, see Figure 5.3. The total energy absorption was calculated to 9.902 MNm with ALLIE and 9.651 MNm with the hand calculations. This can be compared with the incoming energy that was calculated to 18.887 MNm.

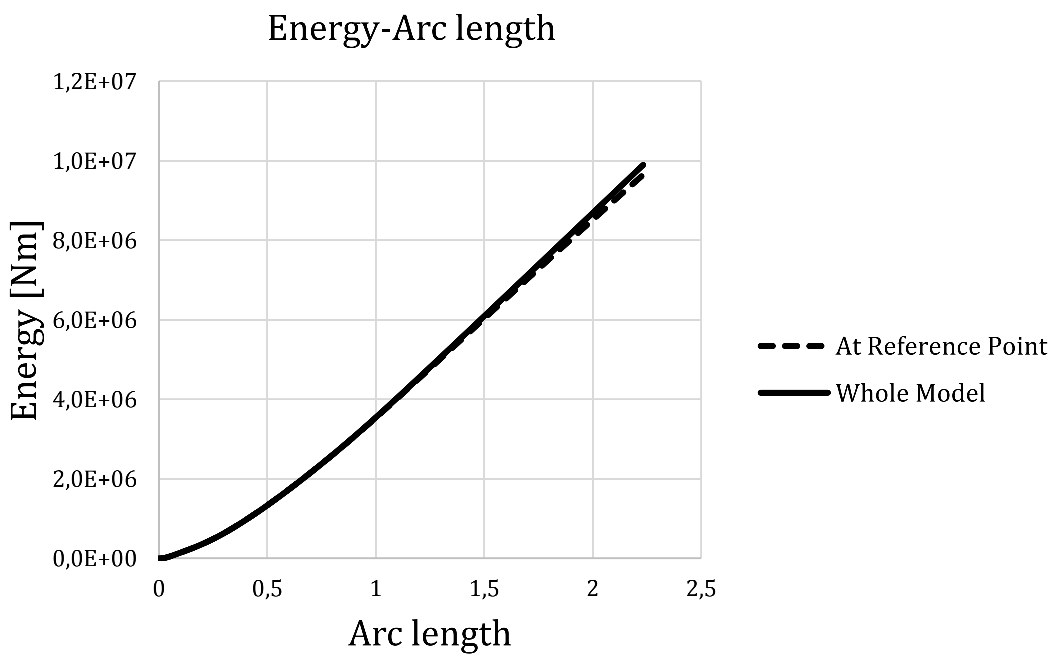

Figure 5.3 Comparison of the hand calculated energy absorption at the reference point and whole models internal energy calculated with ALLIE in Abaqus.

As mentioned in Section 5.1 the overall structural response was investigated at certain points during the analysis. These points were identified at certain arc lengths where interesting structural events occur. The first point was identified at arc length 0.0528, this is the point when the concrete starts cracking in the span. Figure 5.4 shows the areas in tensile plastic strain, i.e. cracked areas, in light grey.

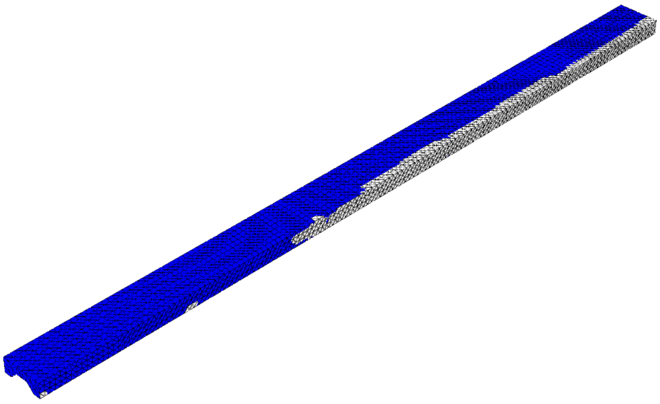

Figure 5.4 Elements in tensile plastic strain i.e. cracked concrete elements (light grey)

The second point was at arc length 0.2023 and this was when the first pile yields see Figure 5.5.

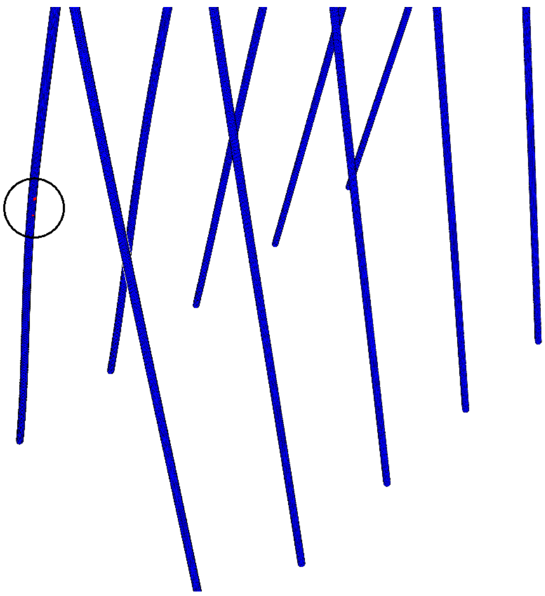

Figure 5.5 Location of the first yielding element of the piles.

The third point was at arc length 0.7363 when the yielding of the Reinforcement starts.

Figure 5.6 Location of the first yielding element of reinforcement.

The fourth point was at arc length 1.954, this was the point when the first clay spring yields and at the fifth point is at the end of the analysis at arc length 2.232. The reaction force and the applied displacement of these structural events are presented in Table 5.1 and shown in Figure 5.7. Complete data regarding the force-displacement curve are appended in Appendix F.

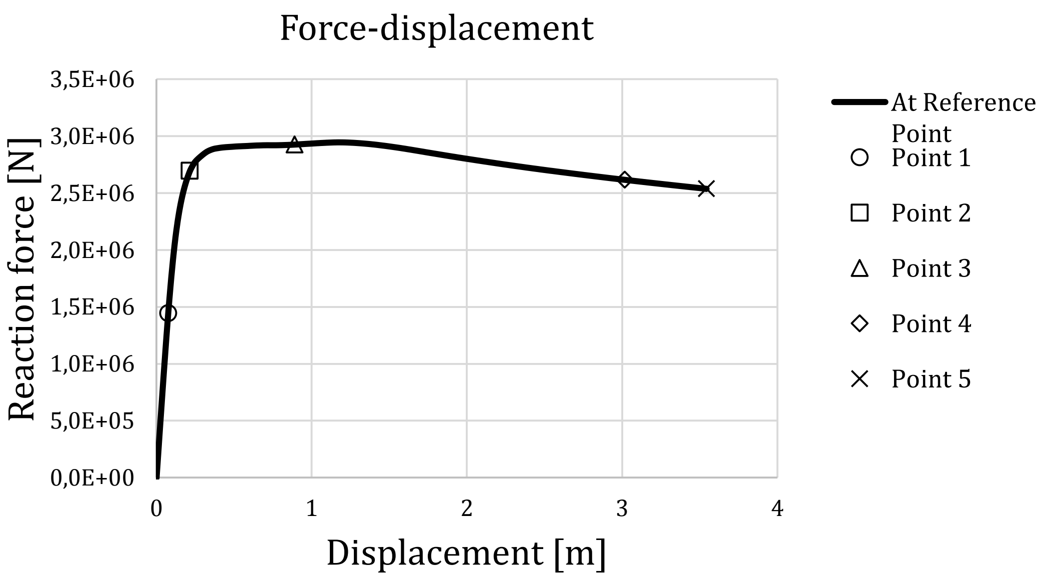

Figure 5.7 Force-displacement curve showing different important structural events. Point 1) First crack of concrete in span, Point 2) First pile yields, Point 3) Reinforcement yields, Point 4) First clay spring yields, Point 5) End of analysis.

A summary of the structural response data at the mentioned structural events is shown in Table 5.1 to get an overview of the structural response of the whole structure. More detailed data on the structural response of the individual parts of the protective pier is presented later in this chapter.

Table 5.1 Structural response for the protective pier at crucial structural events.

	First crack of concrete in span	First pile yields	Reinforcement yields	First clay spring yields	End of analysis
Point	1	2	3	4	5
Arc length	0.0528	0.2023	0.7363	1.954	2.232
Applied displacement [m]	0.075	0.215	0.889	3.017	3.544
Max beam displacement [m]	0.091	0.267	1.101	3.602	4.211
Max pile displacement [m]	0.178	0.979	3.425	7.604	8.446
Total reaction force on structure [kN]	-1447	-2696	-2928	-2618	-2539
Reaction force beam (at fixed end) longitudinal direction [kN]	36.98	-84.00	-138.4	-139.4	-501.2
Reaction force beam (at fixed end) transversal direction [kN]	-15.00	-149.0	-628.0	-569.0	-541.7
Max beam stress [MPa]	10.52	35.22	74.33	131.3	137.1
Max pile stress [MPa]	95.65	350.1	389.7	445.5	453.6
Max reinforcement stress [MPa]	29.20	120.2	500.0	500.0	500.0
Energy absorption [MNm] (ALLIE)	0.056	0.368	2.321	8.454	9.902
Energy absorption [MNm] (hand calculations)	0.056	0.369	2.321	8.294	9.651

5.1.2 Beam

In the following section the results regarding the structural behaviour of concrete beam is presented. This is done in the form of data regarding stresses, displacements and reaction forces.

5.1.2.1 Displacements

Figure 5.8 shows the displacement along the centreline at the top of beam in the direction of the collision. The maximum deflection along this line can be found at the end of the beam and was calculated to 4.037 meters.

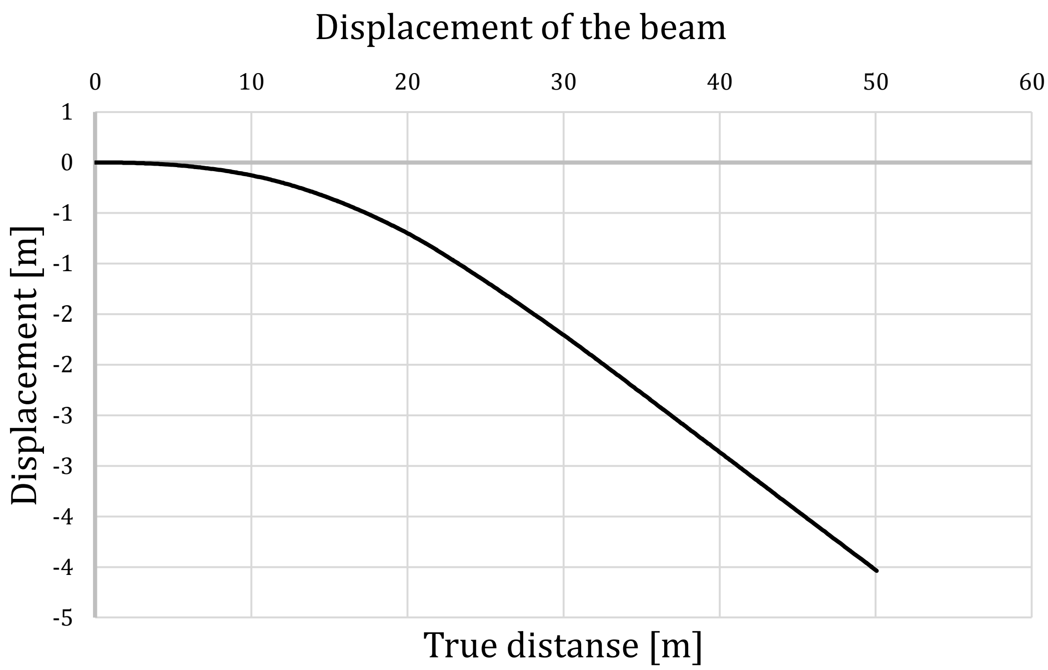

Figure 5.8 Displacement along the beam in the direction of the collision.

The maximum displacements of the beam was also calculated. This was done in Abaqus for all the important arc lengths that was mentioned in Section 5.1.1 and are presented in Table 5.2 along with their location in the model. This was done to see when large displacements occur during the analysis. The locations of theses displacements on the beam are also presented in Figure 5.9.

Table 5.2 Maximum beam displacement, and its location in model.

Arc length	Point	Maximum beam displacement [m]	Node	Part
0.0528	1	0.092	25	BEAM-1
0.2023	2	0.2679	25	BEAM-1
0.7363	3	1.101	25	BEAM-1
1.954	4	3.602	25	BEAM-1
2.232	5	4.211	25	BEAM-1

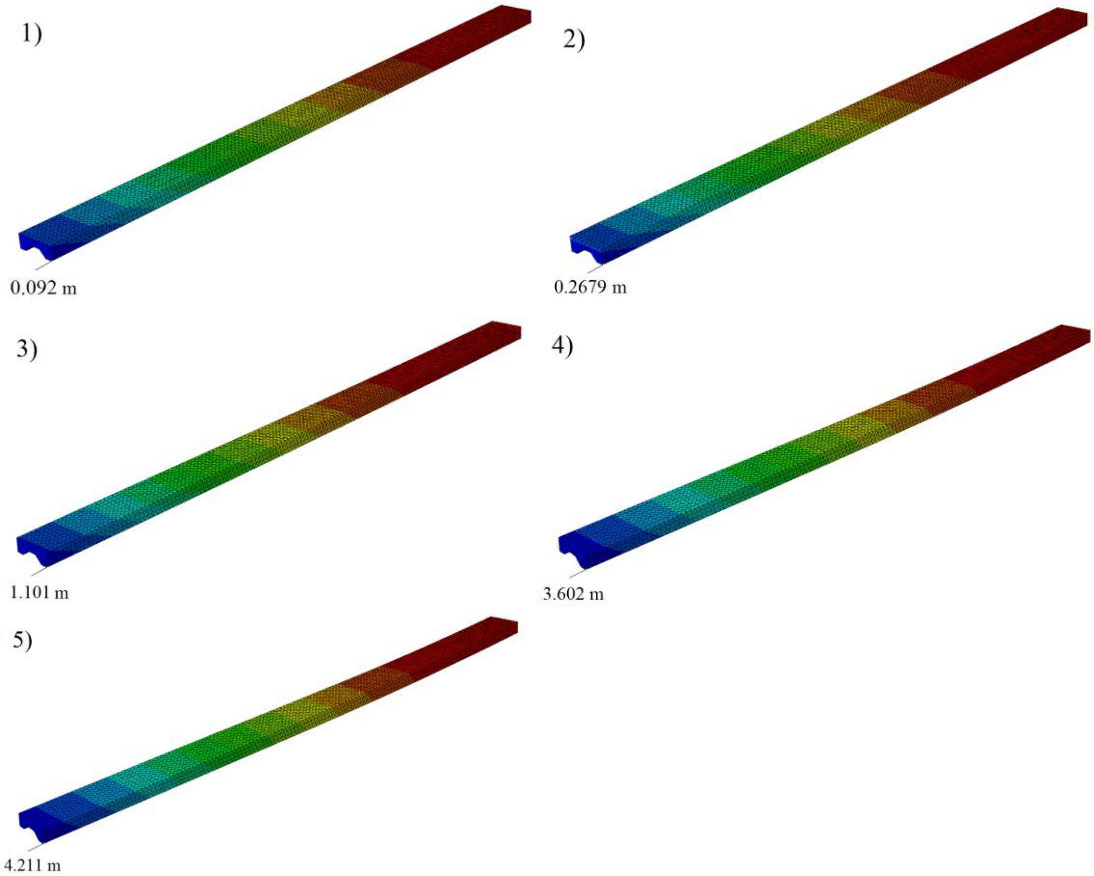

Figure 5.9 Location of maximum beam displacement. 1) Arc length 0.0528, 2) Arc length 0.2023, 3) Arc length 0.7363, 4) Arc length 1.954, 5) Arc length 2.232.

5.1.2.2 Stresses

The maximum stresses in the concrete beam were calculated in Abaqus for the five chosen arc lengths and is presented in Table 5.3 along with their location in the model. These stresses can be compared with the stress-strain curves for compression and tension presented in Appendix E. The location on the beam of these stresses is presented in Figure 5.10.

Table 5.3 Maximum beam stress, and its location in model.

Arc length	Point	Maximum beam stress [MPa]	Element	Node	Part
0.0528	1	10.52	5915	23779	BEAM-1
0.2023	2	35.22	7004	33	BEAM-1
0.7363	3	74.33	4071	37	BEAM-1
1.954	4	131.3	4241	25	BEAM-1
2.232	5	137.1	4241	25	BEAM-1

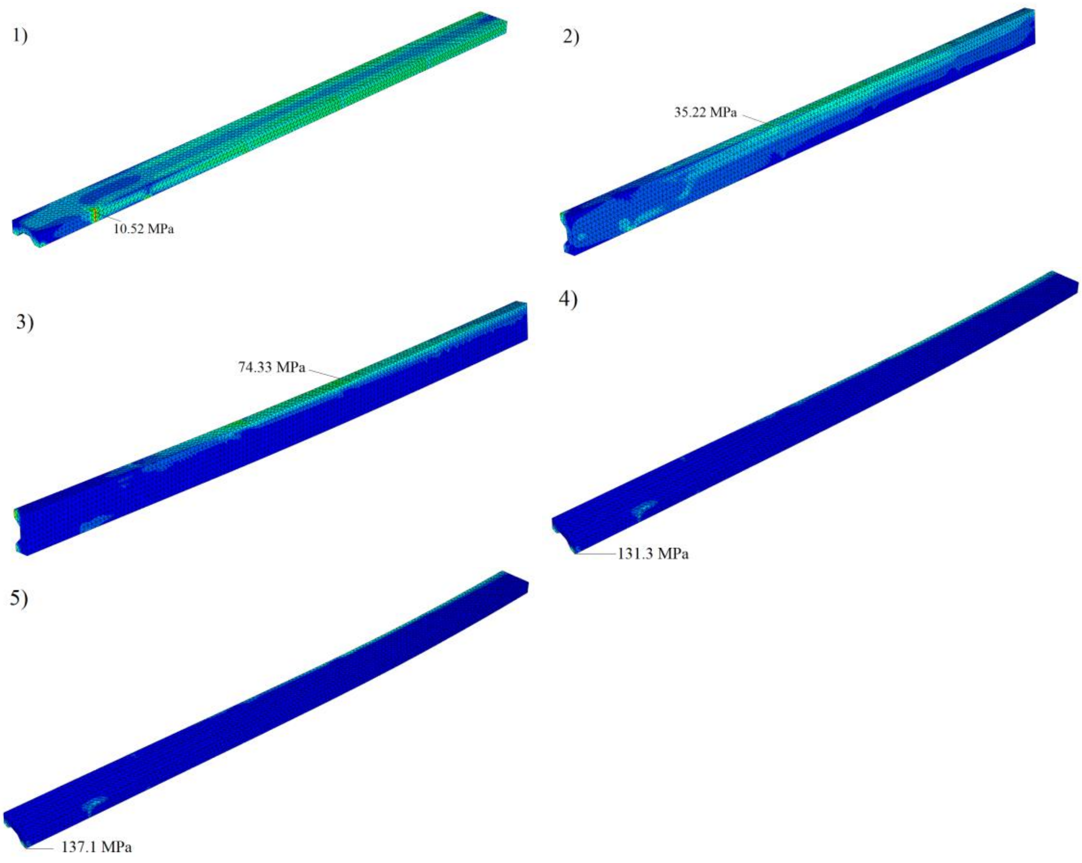

Figure 5.10 Location of maximum beam stress. 1) Arc length 0.0528, 2) Arc length 0.2023, 3) Arc length 0.7363, 4) Arc length 1.954, 5) Arc length 2.232.

The tensile and the compressive behaviour of the concrete are investigated at node 27835 lying on the bottom edge of the beam for tension and node 32684 on the opposite edge for compression.

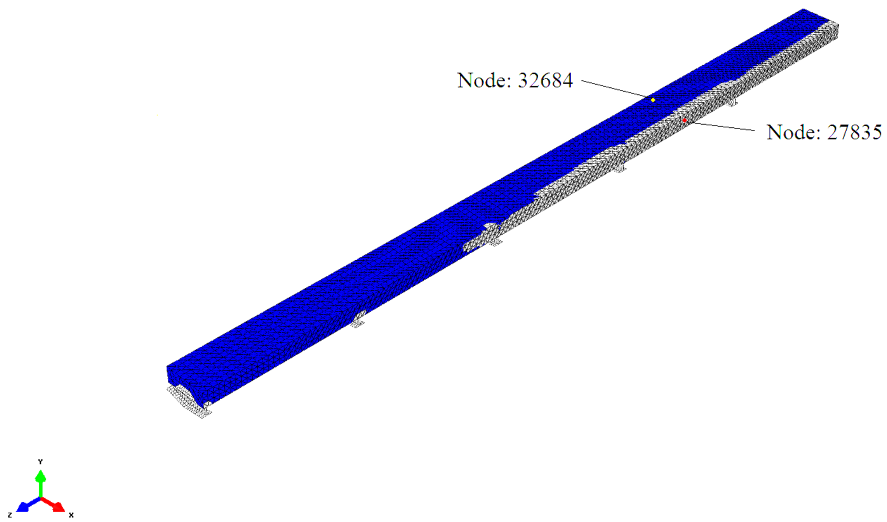

Figure 5.11   Location of nodes 27835 and 32684 on opposite sides of the beam. Picture taken at arc length 0.0528 when the first crack in the concrete appears.

These nodes are deemed to be of interest as they are lying in an area where the curvature of the beam is high. The results of the tensile behaviour is presented in Figure 5.12 and can be compared with the tensile strength of the concrete which was 3.21 MPa. Whereas the results of the compressive behaviour is presented in Figure 5.13 and can be compared with the compressive strength which was 43 MPa. As can be seen in Figure 5.13 the compressive stress exceeds the compressive strength.

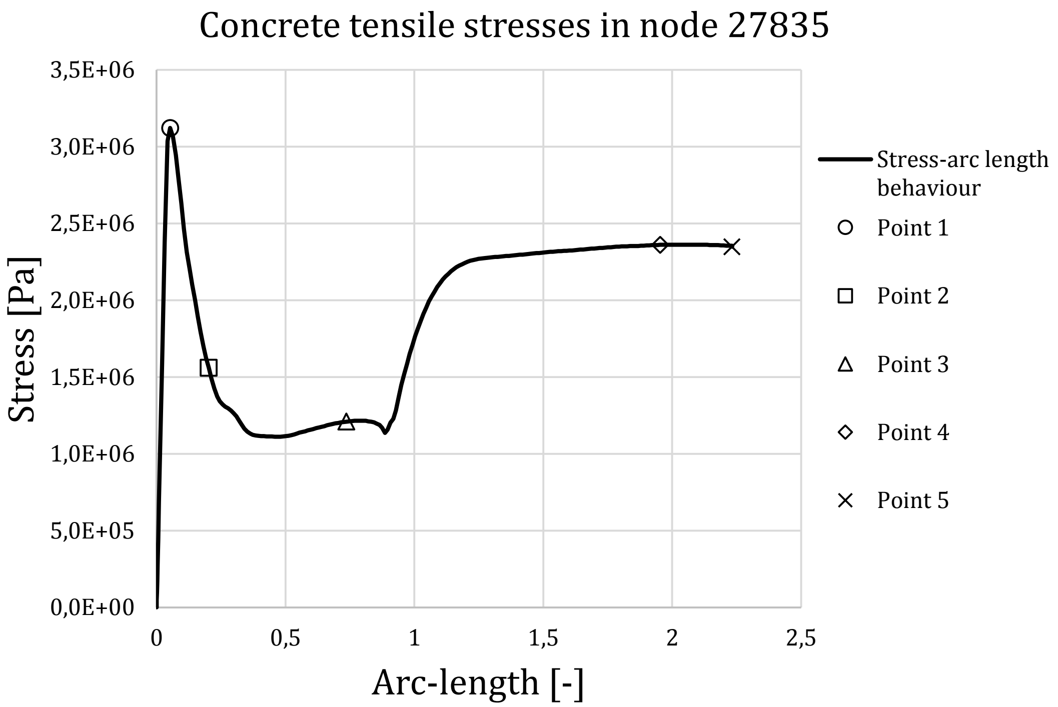

Figure 5.12 Tensile stresses in node 27835 during the analysis. Also showing the structural events, Point 1) First crack of concrete in span, Point 2) First pile yields, Point 3) Reinforcement yields, Point 4) First clay spring yields, Point 5) End of analysis.

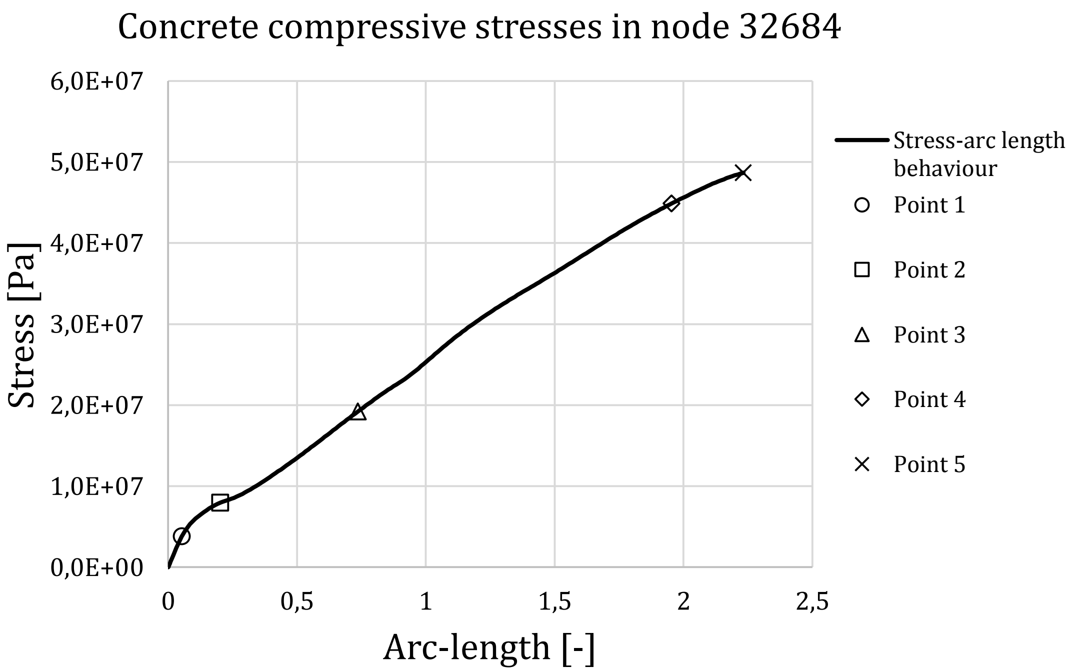

Figure 5.13 Compressive stresses in node 32684 during the analysis. Also showing the structural events, Point 1) First crack of concrete in span, Point 2) First pile yields, Point 3) Reinforcement yields, Point 4) First clay spring yields, Point 5) End of analysis.

5.1.2.3 Reaction forces

The total reaction forces in the longitudinal direction at the fixed end of the beam were calculated in Abaqus and are presented in Table 5.1. Contour plots showing the positive and negative reaction forces along a cut at the fixed end of the beam are presented in Figure 5.14 to see what parts of the beam at the fixed end were in compression and which were in tension.

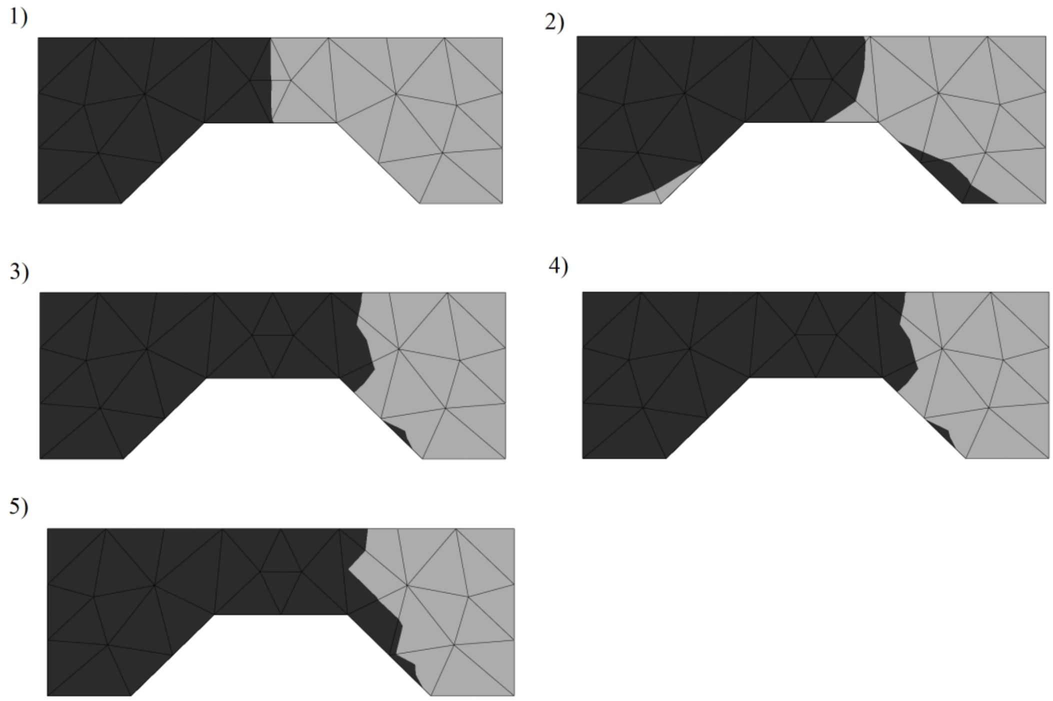

Figure 5.14 Compression zone at the fixed end of the beam where the light grey parts are in compression and the dark grey in tension. 1) Arc length 0.0528, 2) Arc length 0.2023 3) Arc length 0.7362 4) Arc length 1.954 5) Arc length 2.232

5.1.3 Piles

In the model there were 10 piles that are set up in groups of two. To be able to identify the piles a numbering system was decided upon. This numbering system is presented in Figure 5.15. As for the beam all values were calculated for all 5 arc lengths decided in Section 5.1.1.

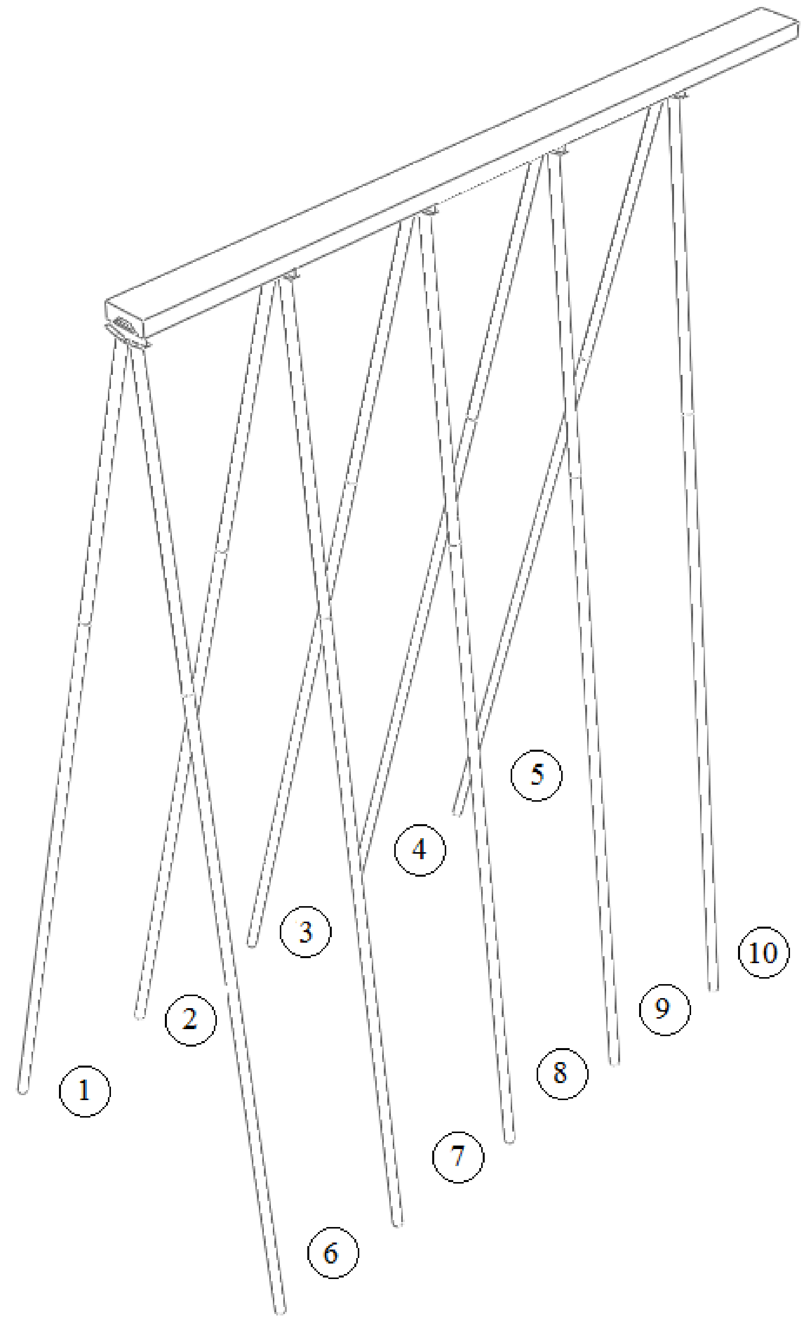

Figure 5.15 Numbering of piles.

5.1.3.1 Displacements

To see the development of the displacement in the piles the maximum displacement are shown in Table 5.4. The table also shows where the maximum displacements occur in the model. The locations on the piles are shown in Figure 5.16.

Table 5.4 Maximum pile displacement, and its location in model

Arc length	Point	Maximum pile displacement [m]	Node	Part
0.0528	1	0.178	3243	PILESTEEL-1
0.2023	2	0.979	2871	PILESTEEL-1
0.7363	3	3.425	2811	PILESTEEL-1
1.954	4	7.604	2883	PILESTEEL-1
2.232	5	8.446	2883	PILESTEEL-1

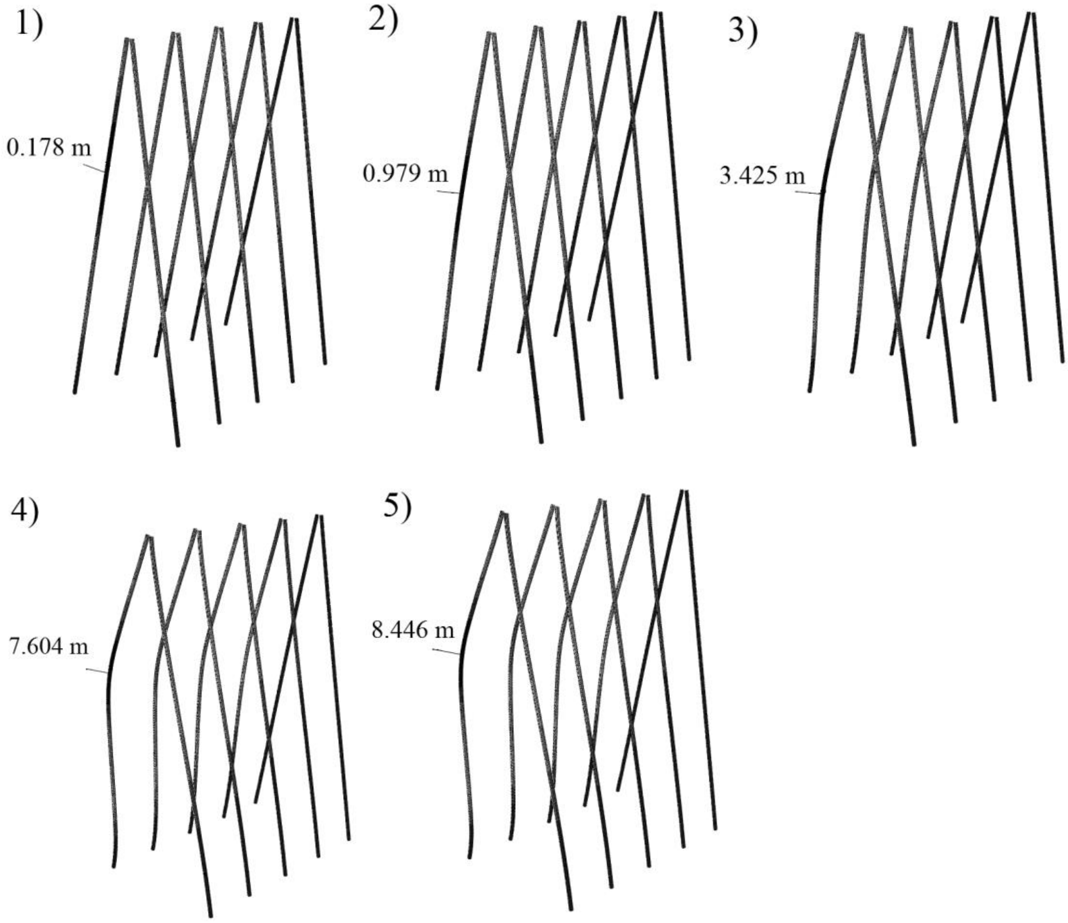

Figure 5.16 Location of maximum pile deflection. 1) Arc length 0.0528, 2) Arc length 0.2023, 3) Arc length 0.7363, 4) Arc length 1.954, 5) Arc length 2.232.

5.1.3.2 Stresses

In Table 5.5 the maximum pile stresses are presented along with the locations of these in the model. These can be compared with the stress-strain curve presented in Appendix E. The locations of the stresses on the piles are presented in Figure 5.17.

Table 5.5 Maximum pile stress, and its location in model

Arc length	Point	Maximum pile stress [MPa]	Element	Node	Part
0.0528	1	95.65	2766	2802	PILESTEEL-1
0.2023	2	350.1	7004	33	PILESTEEL-1
0.7363	3	389.7	4071	37	PILESTEEL-1
1.954	4	445.5	2766	2802	PILESTEEL-1
2.232	5	453.6	2766	2802	PILESTEEL-1

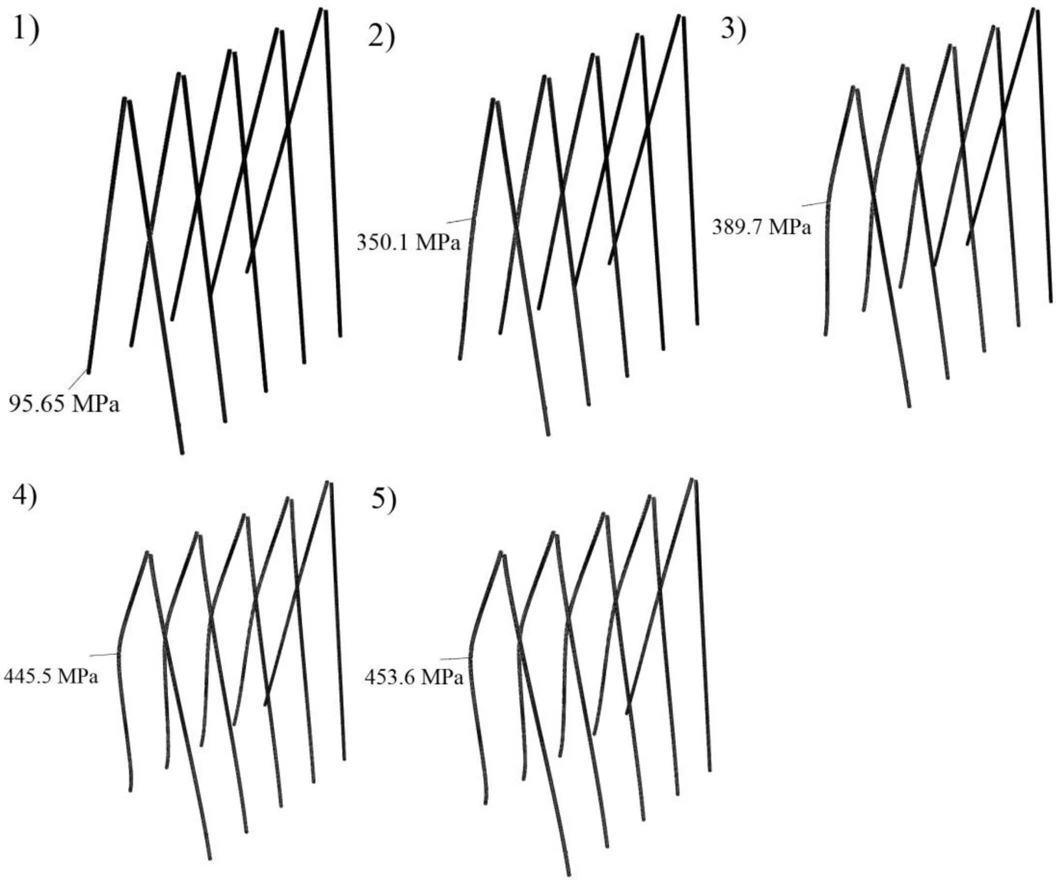

Figure 5.17 Location of maximum pile stress. 1) Arc length 0.0528, 2) Arc length 0.2023, 3) Arc length 0.7363, 4) Arc length 1.954, 5) Arc length 2.232.

5.1.3.3 Reaction forces

The reaction forces were calculated at the fixed end in the bottom of the piles to see if they are lower than the vertical carrying capacity of the clay which where 2527.1 kN in tension and 3610.2 kN in compression. They are presented in Table 5.6-Table 5.10 according to the numbering in Figure 5.15.

Table 5.6 Reaction forces in the piles in point 1, arc length 0.0528

Piles	Reaction force in pile [kN]
Back row	
Pile 1	174.9
Pile 2	120.2
Pile 3	63.26
Pile 4	19.84
Pile 5	-0.513
Front row	
Pile 6	-538.5
Pile 7	-391.2
Pile 8	-239.1
Pile 9	-112.3
Pile 10	-30.6

Table 5.7 Reaction forces in the piles in point 2, arc length 0.2023

Piles	Reaction force in pile [kN]
Back row	
Pile 1	-368.2
Pile 2	-90.53
Pile 3	25.49
Pile 4	5.264
Pile 5	-8.529
Front row	
Pile 6	-1112
Pile 7	-886.2
Pile 8	-561.1
Pile 9	-254.4
Pile 10	-60.40

Table 5.8 Reaction forces in the piles in point 3, arc length 0.7363

Piles	Reaction force in pile [kN]
Back row	
Pile 1	-1489
Pile 2	-1296
Pile 3	-825.0
Pile 4	11.18
Pile 5	388.5
Front row	
Pile 6	-1550
Pile 7	-1367
Pile 8	-1224
Pile 9	-771.7
Pile 10	-208.0

Table 5.9 Reaction forces in the piles in point 4, arc length 1.954

Piles	Reaction force in pile [kN]
Back row	
Pile 1	-1891
Pile 2	-1783
Pile 3	-1594
Pile 4	-1157
Pile 5	276.8
Front row	
Pile 6	-2397
Pile 7	-1986
Pile 8	-1654
Pile 9	-1261
Pile 10	-596.5

Table 5.10 Reaction forces in the piles in point 5, arc length 2.232

Piles	Reaction force in pile [kN]
Back row	
Pile 1	-1938
Pile 2	-1828
Pile 3	-1655
Pile 4	-1261
Pile 5	278.2
Front row	
Pile 6	-2486
Pile 7	-2102
Pile 8	-1741
Pile 9	-1313
Pile 10	-691.2

5.1.4 Reinforcement

Since the displacement of the reinforcement coincides with the displacement of the beam, because of the full interaction between the two, the main focus in this section will be on the stresses of the reinforcement.

5.1.4.1 Stresses

The maximum stresses of the reinforcement at the critical events where obtained from Abaqus and are presented in Table 5.11 along with the location in the model. For comparison the stress-strain behaviour of the reinforcement is presented in Appendix E. These locations are also presented in Figure 5.18.

Table 5.11 Maximum reinforcement stress, and its location in model.

Arc length	Point	Maximum reinforcement stress [MPa]	Element	Node	Part
0.0528	1	29.2	143	144	Reinforcement 20mm-1-lin-4-1-lin-8-1
0.2023	2	120.2	84	85	Reinforcement 20mm-1-lin-4-1-lin-8-1
0.7363	3	500.0	84	85	Reinforcement 20mm-1-lin-2-1-lin-2-1
1.954	4	500.0	65	66	Reinforcement 20mm-1-lin-4-1-lin-7-1
2.232	5	500.0	99	100	Reinforcement 20mm-1-lin-4-1-lin-4-1

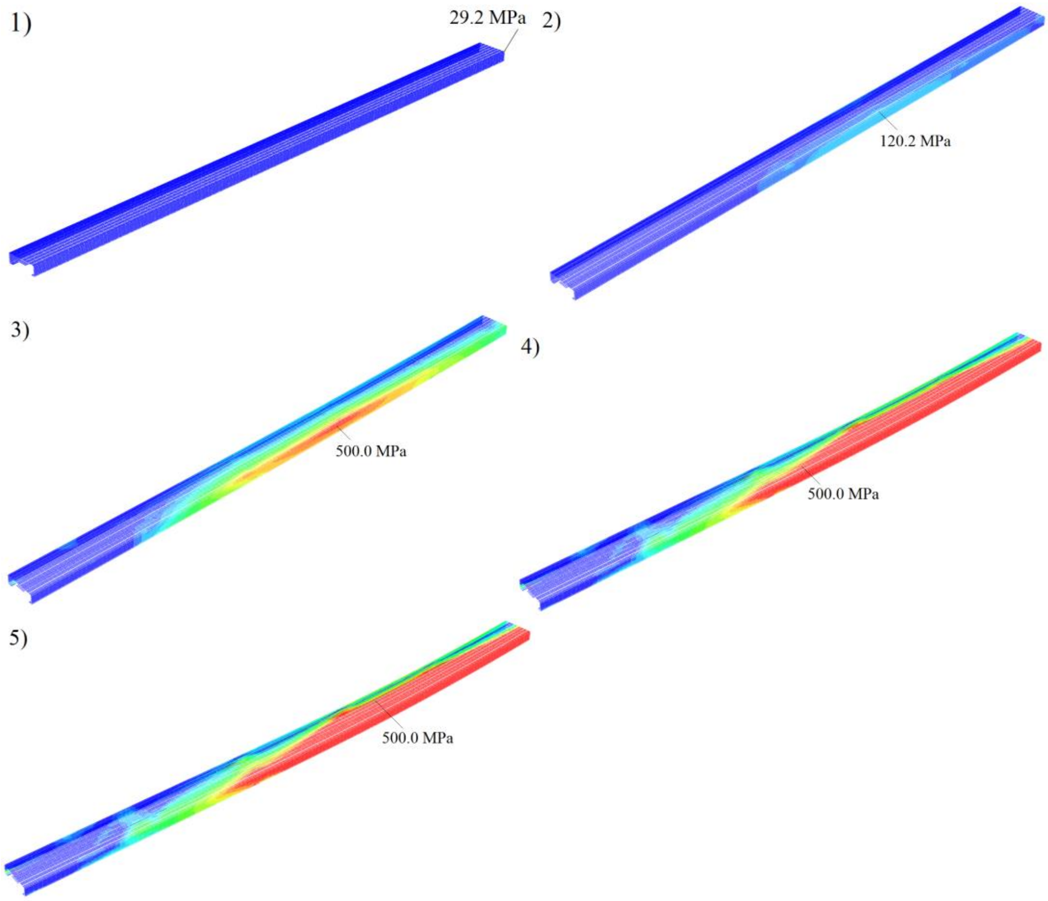

Figure 5.18 Location of Maximum reinforcement stress. 1) Arc length 0.0528, 2) Arc length 0.2023, 3) Arc length 0.7363, 4) Arc length 1.954, 5) Arc length 2.232.

5.1.5 Clay springs

To be able to analyse the behaviour of the clay the stress-strain relationship of the clay springs and the strain behaviour over time were obtained from Abaqus. This data is presented for three different springs denoted Spring-0, Spring-20 and Spring-50 at three different arc lengths 0.0528, 0.7363 and 2,232. These springs are only three of the investigated springs for further results see Appendix G.

The springs that are chosen are located on pile 1 according to Figure 5.19. Spring-0 is the first spring located near the river bottom, Spring-20 is the spring located nearest to the maximum deflection of the pile and Spring-50 is located in the bottom end of the pile.

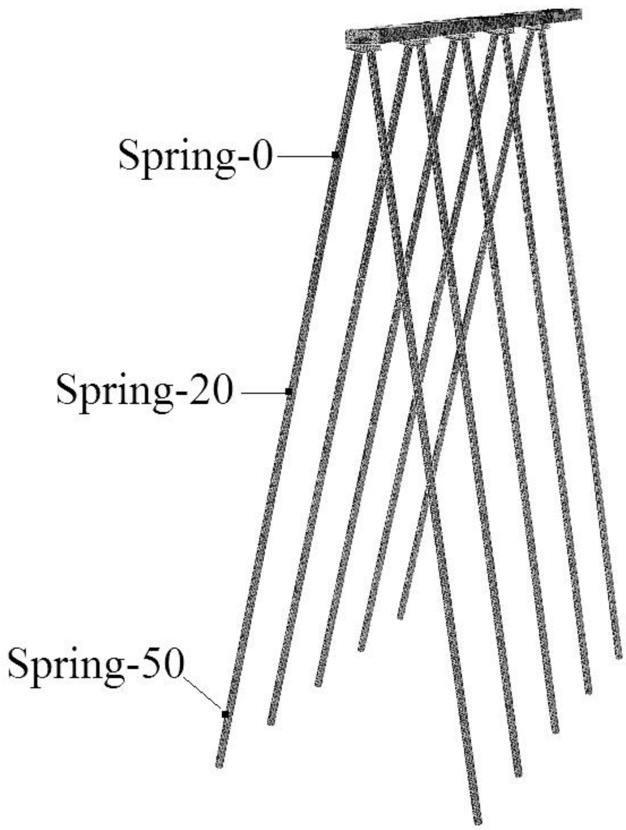

Figure 5.19 Location of the springs on the pile.

5.1.5.1 Stress-strain relationship

Figure 5.20 to Figure 5.22 shows the stress-strain relationship for Spring-0. The yield pressure for Spring-0 was 54.9 kN/m and the displacement of the spring at the time of yielding should be 0.02745 m.

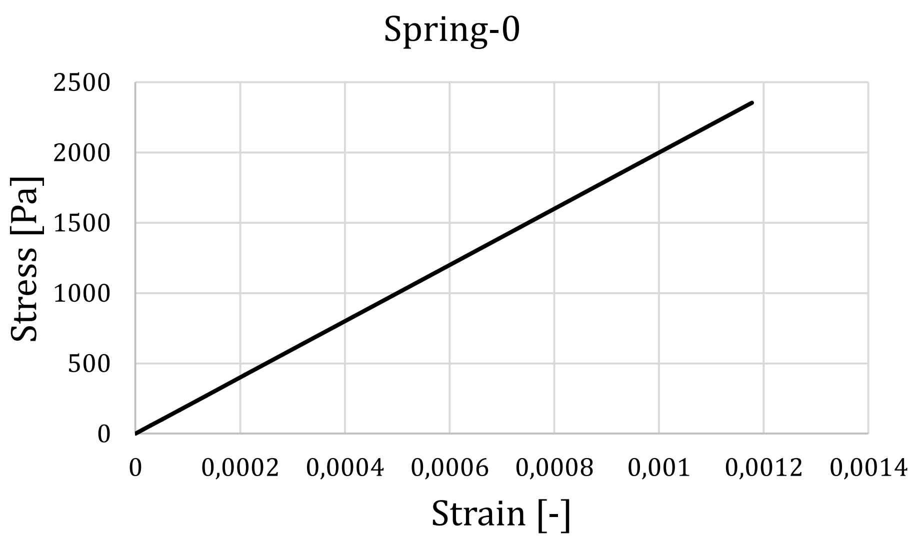

Figure 5.20 Stress-strain relationship for Spring-0 at Arc length 0.0528.

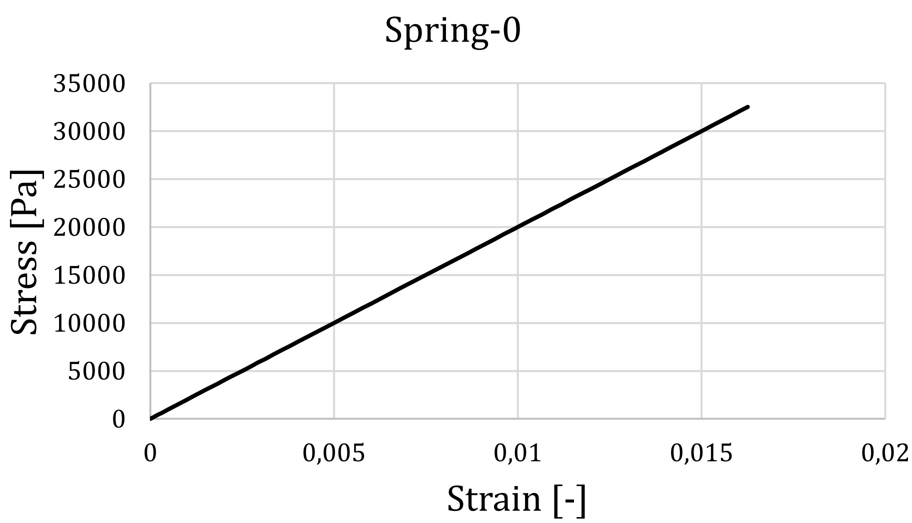

Figure 5.21 Stress-strain relationship for Spring-0 at Arc length 0.7363.

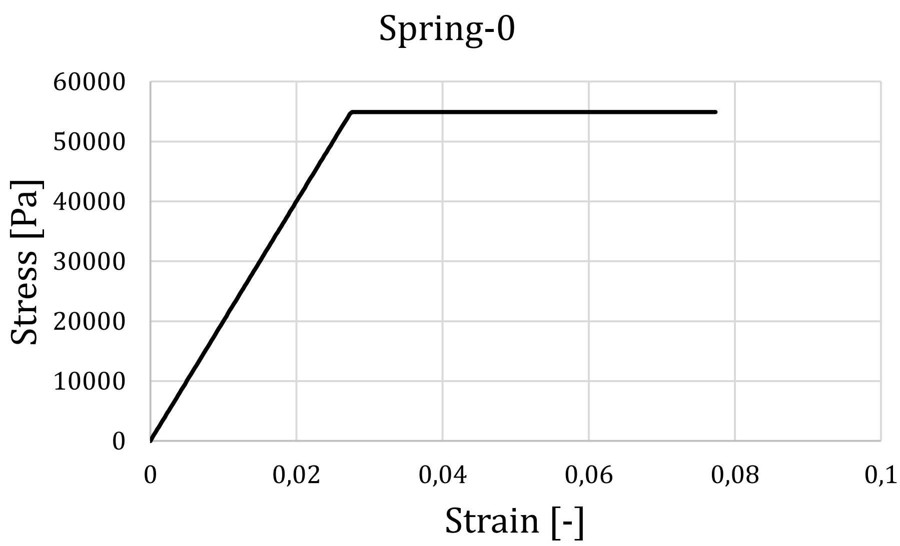

Figure 5.22 Stress-strain relationship for Spring-0 at Arc length 2.232.

Figure 5.23 to Figure 5.25 shows the stress-strain relationship for Spring-20. The yield pressure for Spring-20 was 164.7 kN/m and the displacement of the spring at the time of yielding should be 0.02745 m.

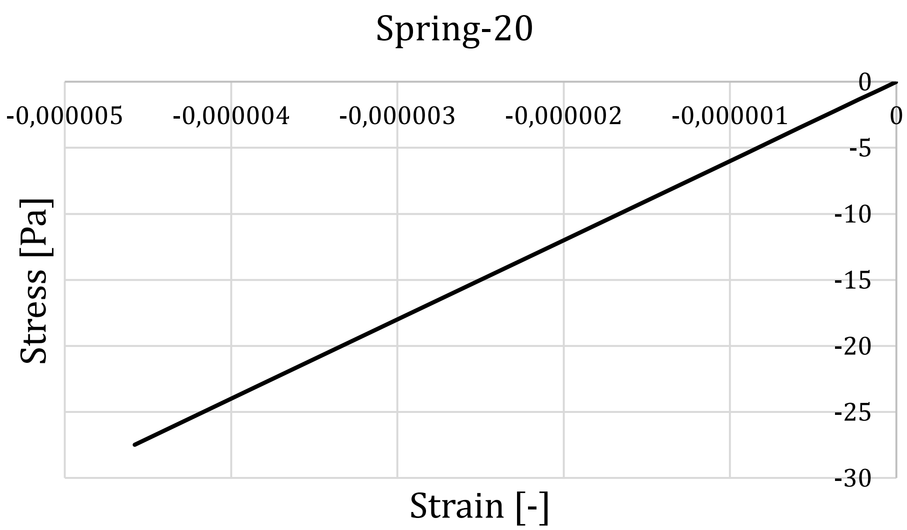

Figure 5.23 Stress-strain relationship for Spring-20 at Arc length 0.0528.

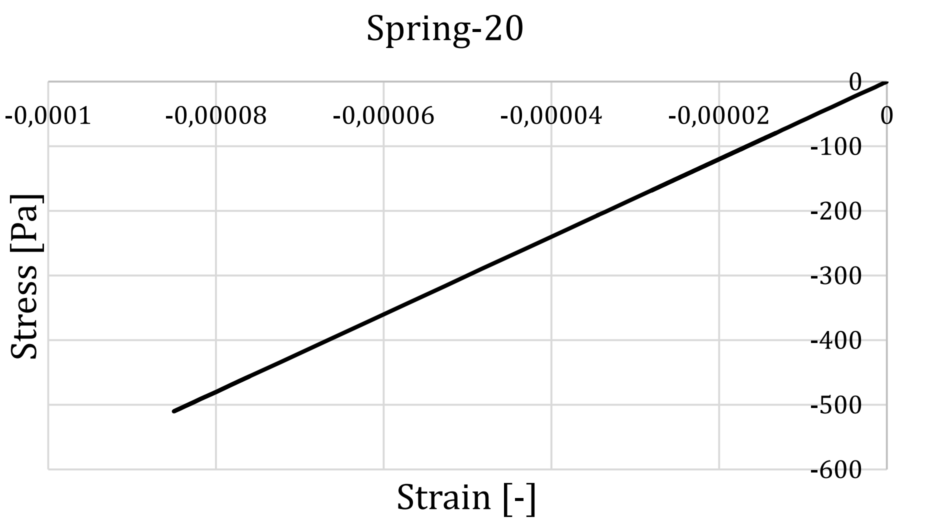

Figure 5.24 Stress-strain relationship for Spring-20 at Arc length 0.7363.

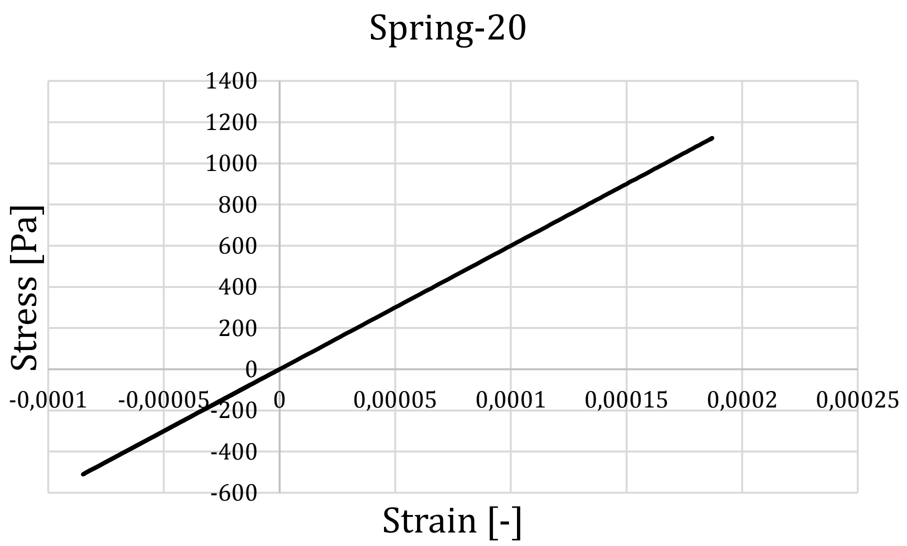

Figure 5.25 Stress-strain relationship for Spring-20 at Arc length 2.232.

Figure 5.26 to Figure 5.28 shows the stress-strain relationship for Spring-50. The yield pressure for Spring-50 was 285.5 kN/m and the displacement of the spring at the time of yielding should be 0.02745 m.

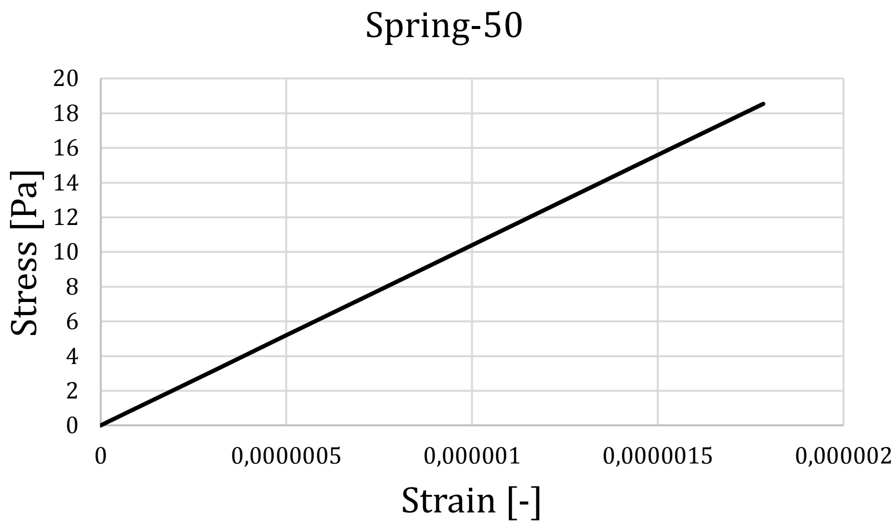

Figure 5.26 Stress-strain relationship for Spring-50 at Arc length 0.053.

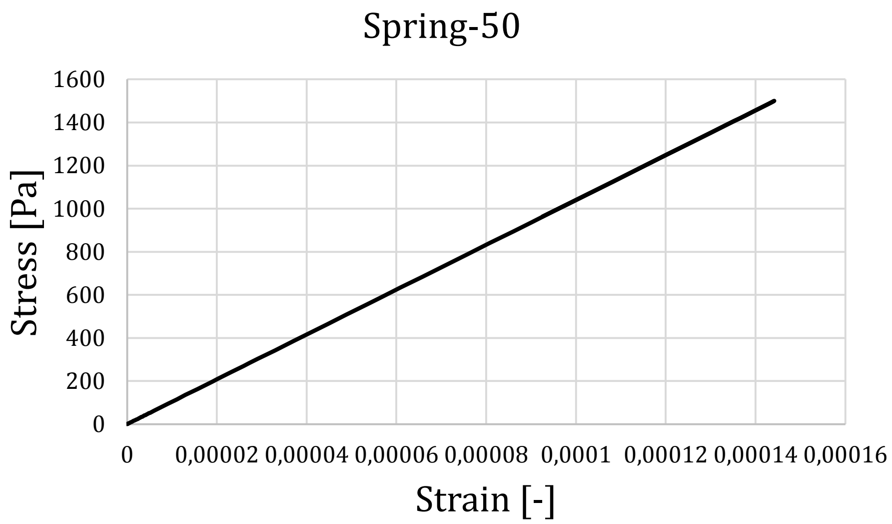

Figure 5.27 Stress-strain relationship for Spring-50 at Arc length 0.7363.

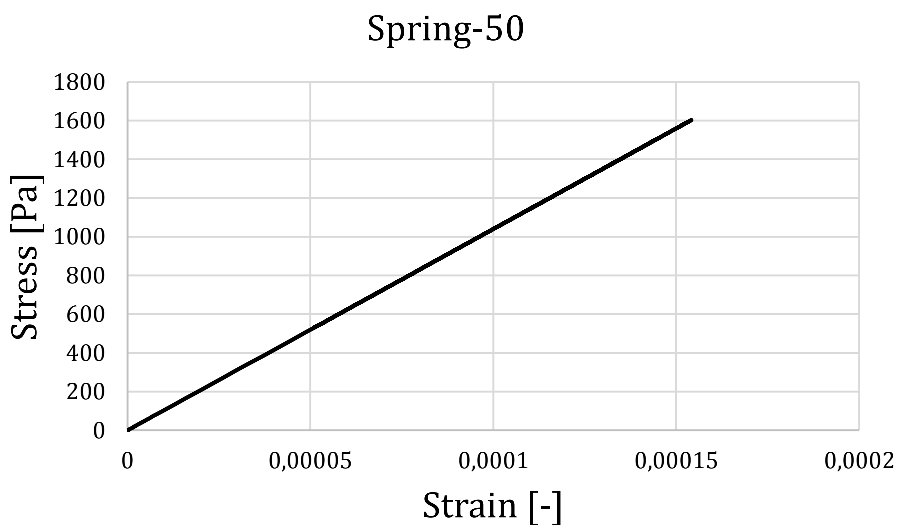

Figure 5.28 Stress-strain relationship for Spring-50 at Arc length 2.232.

5.1.5.2 Strain-arc length relationship

The strain-arc length relationship describes the strain behaviour during the analysis of the model and is shown from the start of the analysis until a specific arc-length.

Figure 5.29 to Figure 5.31 shows the strain-arc length relationship for Spring-0.

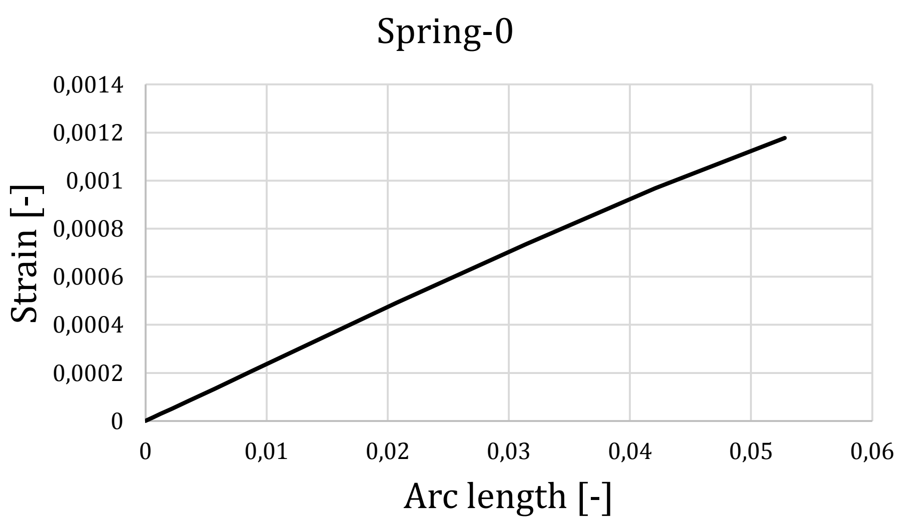

Figure 5.29 Strain-Arc length relationship for Spring-0 at Arc length 0.0528.

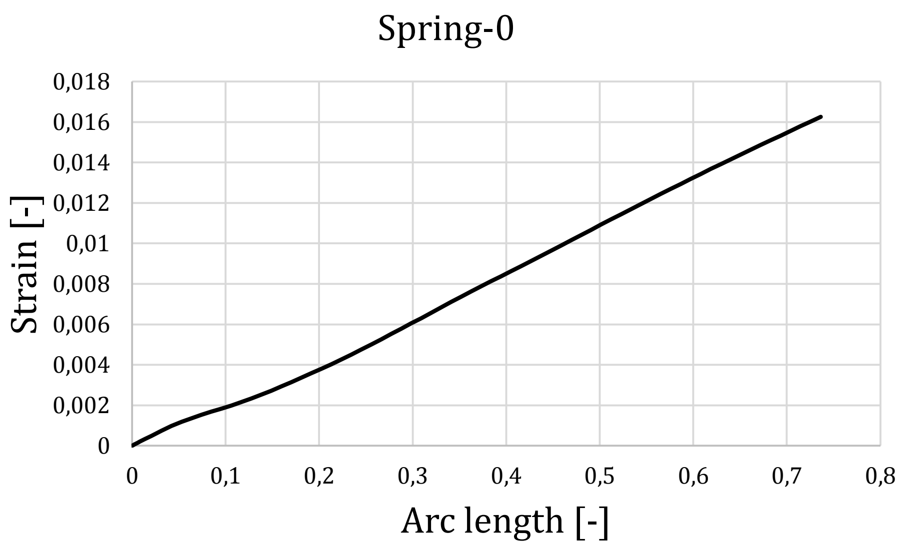

Figure 5.30 Strain-Arc length relationship for Spring-0 at Arc length 0.7363.

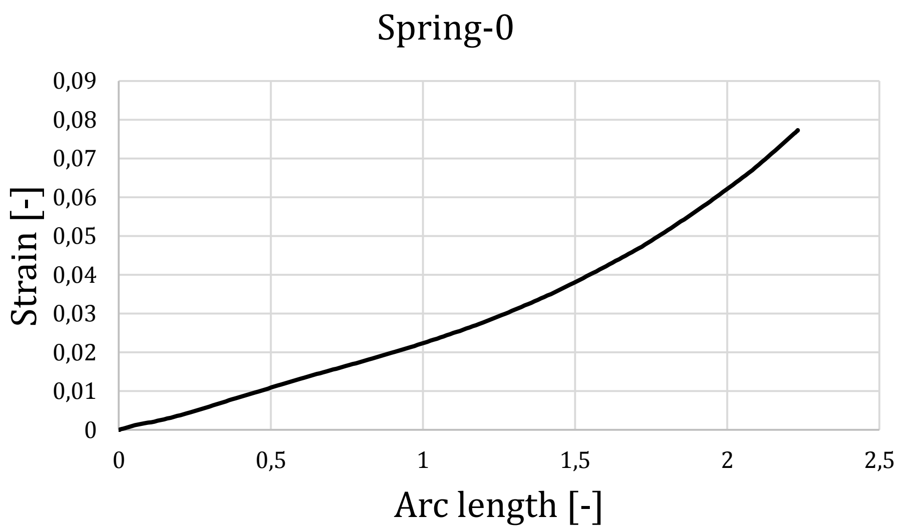

Figure 5.31 Strain-Arc length relationship for Spring-0 at Arc length 2.232.

Figure 5.32 to Figure 5.34 shows the strain-arc length relationship for Spring-20.

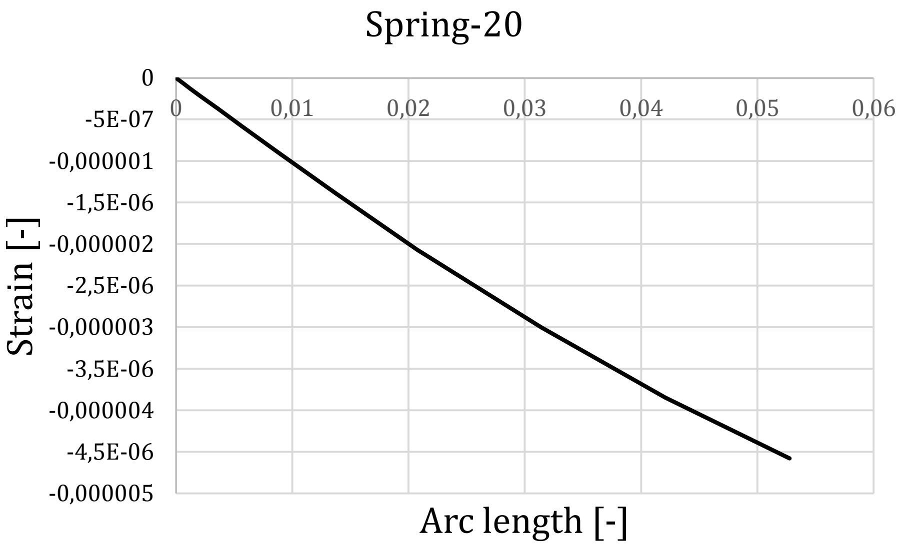

Figure 5.32 Strain-Arc length relationship for Spring-20 at Arc length 0.053.

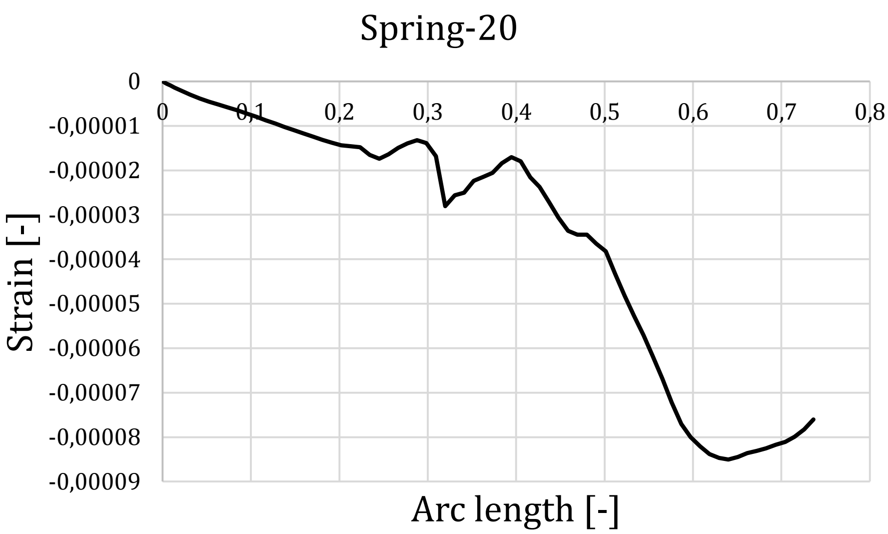

Figure 5.33 Strain-Arc length relationship for Spring-20 at Arc length 0.7363.

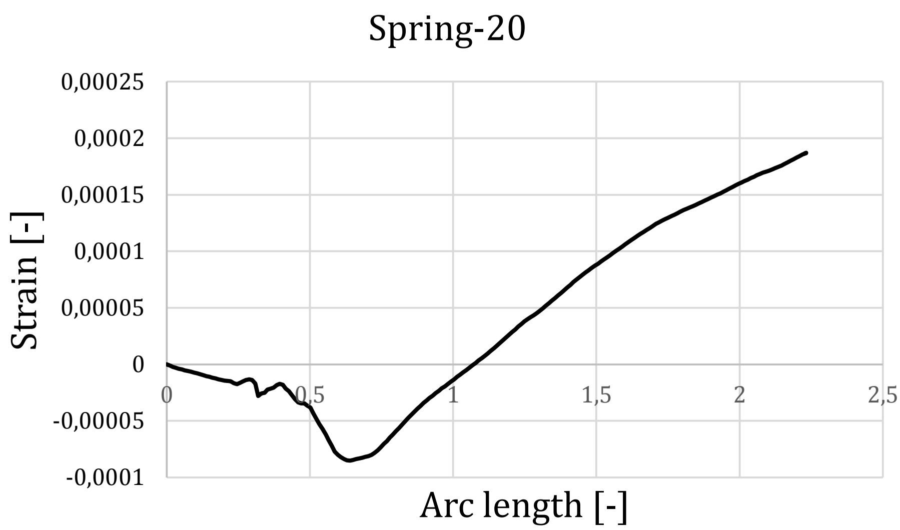

Figure 5.34 Strain-Arc length relationship for Spring-20 at Arc length 2.232.

Figure 5.35 to Figure 5.37 shows the strain-arc length relationship for Spring-50.

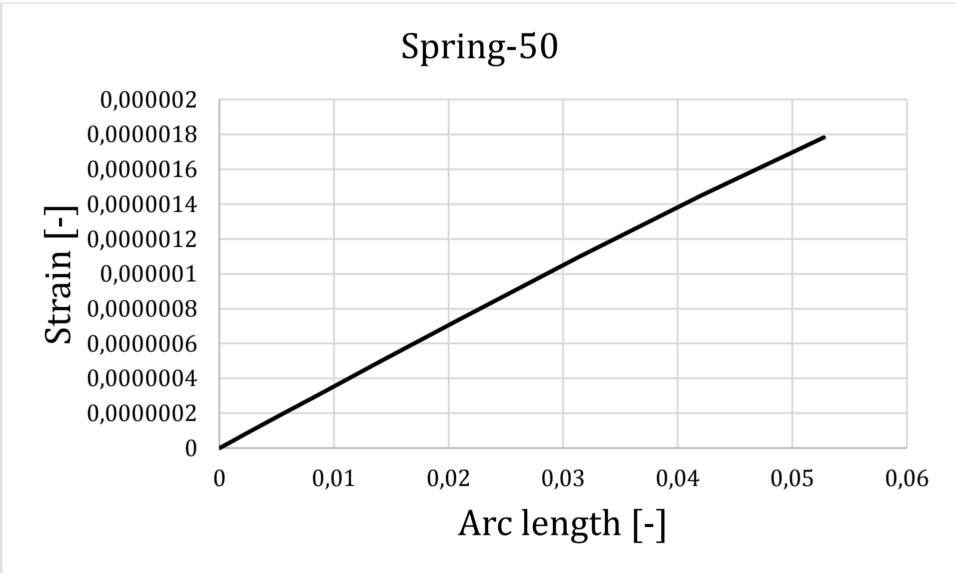

Figure 5.35 Strain-Arc length relationship for Spring-50 at Arc length 0.053.

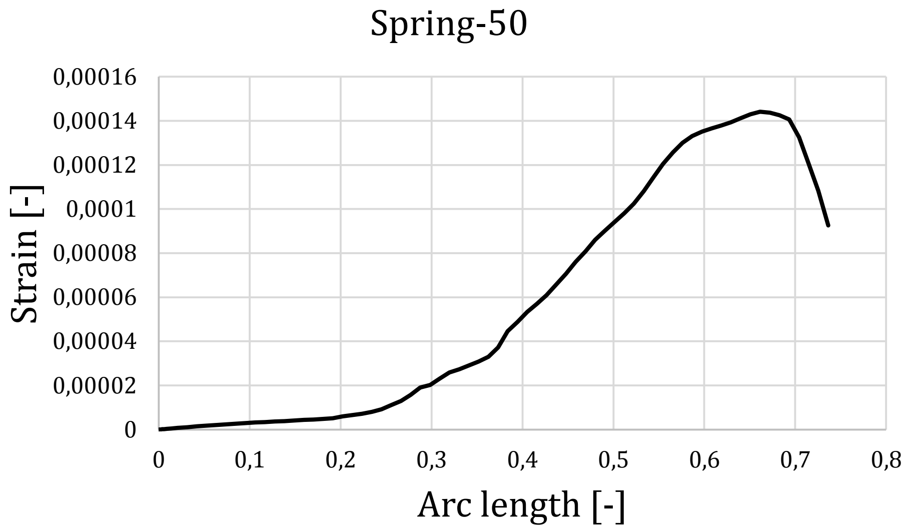

Figure 5.36 Strain-Arc length relationship for Spring-50 at Arc length 0.7363.

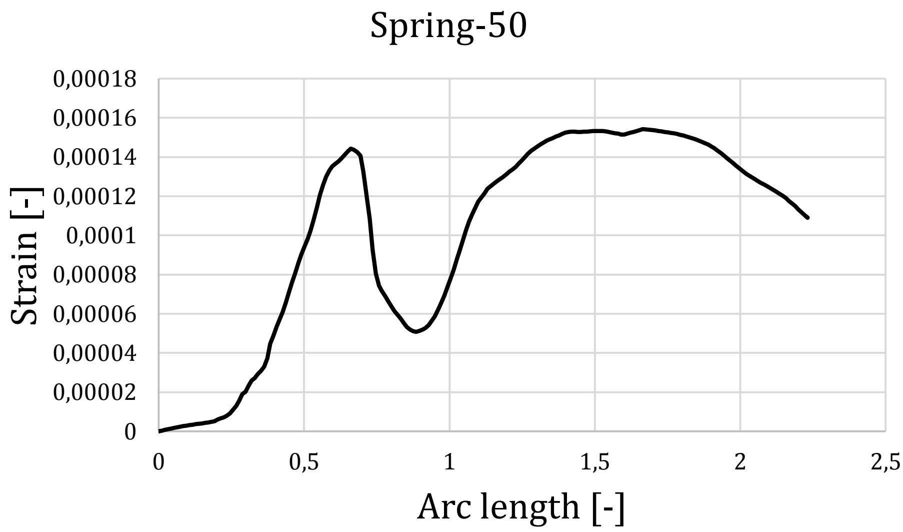

Figure 5.37 Strain-Arc length relationship for Spring-50 at Arc length 2.232.

To be able to investigate that the deformation in the pile was transferred to the spring, the displacement of the nodes where the spring were connected was examined.

Table 5.12 Displacement of the nodes in the pile where the springs were connected.

Arc length [-]	Displacement in pile 1 at Spring-0 [m]	Displacement in pile 1 at Spring-20 [m]	Displacement in pile 1 at Spring-50 [m]
0.0528	-0.1445	-0.1655	-0.0044
0.7363	-1.904	-3.401	-0.1542
2.232	-5.695	-8.333	-0.3810

6 Discussion

This chapter reviews assumptions and reasoning done in the report regarding the mathematical interpretation of the reality and thereby the resulting FE-model. The outcome of the analyses are discussed and judged.

6.1 Modelling

The focus in this report was to model a large part of the structure and allow long computation times to capture the structural response well. An analysis time of 44 hours on a cluster is considered accepted for this thesis work, which is a type of research. This might not be an efficient solution for a design company as increased labour time could increase the project costs. As the mesh convergence study showed, increased mesh accuracy can let the analysis time increase vastly for larger models. The non-linear material properties are probably the governing factor influencing the analysis time negatively in this case study.

There are many assumptions regarding the load and its application that could change the outcome of the analysis. The report treats a load that is constantly acting in the same global direction that is a component of the actual inclined force resultant. A closer prediction discloses an interesting phenomenon which takes place when the protective pier bends back at collision. The transversal force acting on the pier has a potential to increase as the normal to the face of the pier turns towards the incoming ship and hence increases the transversal component of the force, see Figure 6.1. Nevertheless, the ship might be pushed in the right direction during the collision and then the transversal force component decreases.

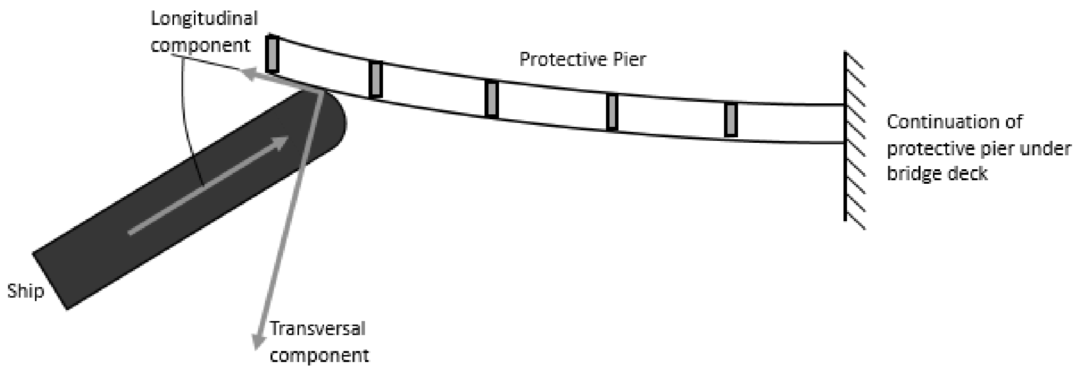

Figure 6.1 Displacement of protective pier due to ship impact with increased transversal force component.

Another aspect is that the ship could be sliding along the pier while the load was resisted and so the structure would behave differently than described in Chapter 5. It is conservative to absorb the load the way it was done in this report, at the end of the pier. If the point of impact was closer to the bridge, more pile groups would work together and also the influence of the fixed support would be greater, resulting in a greater capacity of the pier at that point.

A closer look at the impact area raises the question how the actual collision point would look like. The modelled displacement line allows the concrete beam to rotate freely along with the translation, resembling a hull that partly gets crushed and partly continues to deflect the pier. A stiff ship would be able to load the pier in one point randomly across the concrete face and thereby change the behaviour of the pier deflection. Accidental ship collisions like this would likely have a great impact on the ships' hull though (Hogström, 2015). An inclined hull in the front could possibly produce forces trying to push the protective pier downwards and give rise to other load cases where the piles would need to have a greater load bearing capacity, see Figure 6.2. It is moreover understood that design of piles must be performed to prohibit contact with the ship's bulb as it could destroy the pile and thus reduce the pier's capacity, especially when the piers are displaced backwards. This should not be a concern for the protective piers at Hisingsbron when examining the deformation pattern in Figure 5.1.

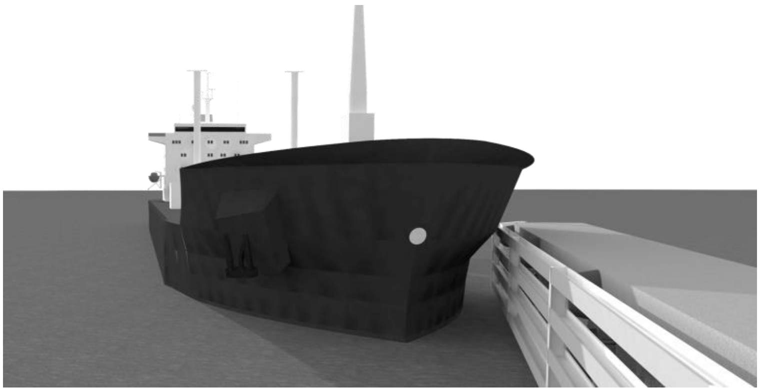

Figure 6.2 Incoming ship before moment of collision.

An assumption was made when modelling the I- and T-beam as totally rigid. These parts could in reality move independently and interact through contact and friction. It is not considered as very possible but this still means that the main beam and the pile groups would not necessarily have the same deformation behaviour. The very complex global behaviour of the protective pier makes it hard to predict what could have occurred if these parts were modelled as in reality. Worth mentioning is that stresses were found to be high in the piles right below the rigid beams which could give rise to these actions.

The chosen method of comparing energies has its limitations in validity as a crucial assumption was made. Protective piers are not necessarily in their original shape when the design collision occurs. If the impact happens after several years it is very probable that several minor hits have taken place (SSPA, 2014). Many small imperfections from these hits could have reduced the capacity of the protective pier that later on would result in more damage at lower loads.

6.2 Structural response

The energy absorbing curve in Figure 5.7 has the expected shape as when comparing to other projects of the same kind (Lindqvist, 2015). Markers in the figure show crucial events for the structure which help explain the response. The curve has a minor shift in inclination at Point 1 when the concrete starts to exceed its tension capacity and cracks. Most eminent change of the slope occurs when the piles start to yield and explains the sudden increase in global displacement at Point 2. Yielding reinforcement could explain the third event along the curve. As more and more of the cross-section's reinforcement yield, the global capacity decreases. This allows more and more force to be resisted by the clay and therefore the clay springs start to reach their max capacity thereafter, at Point 5. The analysis stopped when prescribed displacement got to 3.544 meters as the arc length increment required was smaller than minimum allowed and hence no equilibrium for the system could be found.

6.2.1 Overall structural response

When the result of the calculated energy absorbed by the protective pier was compared to the amount of energy of an incoming ship it was clear that it was not enough. However one have to have in mind that this value is a very conservative one. If this value is used as a design value it is regarded that all of the incoming energy is transferred from the ship to the protective pier. In reality this is not the case since the ship will also absorb energy through deformation and by transferring energy into the water. Some energy will also be released as heat due to friction between the surface of the ship and the surface of the structure. Reasonable assumptions can be that 10-15% of the total energy is released as friction and 20-30% is absorbed as deformations of the ship and energy transfer to the water (Hogström, 2015). That leaves a resulting deformation energy of about 10.4MJ compared to initial 18.9MJ. There are however uncertainties of how Eurocode reduces the total available kinetic energy to deformation energy as it is not purely a force component of the inclined impact. An explanation could be the effects of the above described external dynamics of the impact which is a research area where a lot of knowledge need to be gained.

Additional energy have been absorbed in the neglected events of the collision progress as mentioned in Section 4.1, considering the fenders compression and sheared off bolts between I- and T-beam. This amount of capacity has not been considered in the report but would in reality take care of some load, yet it is still just a fraction of the total. The size and capacity of these parts can however be decided in the design process. Worth mentioning is that by reducing the ship velocity from 8 to 5,8 knots will lower the impact energy by about 43% to 9.9 MJ which is the structure's resisting energy, see Appendix B. The case study treats an accidental load where speed is assumed to be exceeded, but it explains well why the speed limit allowed in the river generally is low.

6.2.2 Structural response in individual parts

One of the simplifications made in this report was to only look at a 50 meter part of the beam, and instead of modelling the rest of the beam it was decided to make a fixed end boundary condition instead. However this may not reflect the reality completely as some rotations and translations possibly could take place during the impact, as the continued pier is not infinitely stiff. The reaction force in the transversal direction at the fixed end was 541.7 kN, this reaction force would probably give rise to some deflection at the fixed end but it is hard to speculate how much since the real behaviour of the boundary is unknown.

The maximum stresses in the beam were unreasonable high throughout the analysis as can be seen in Table 5.3. This was probably due to the fact that the maximum values were from stress concentrations in the interaction between the concrete beam and the rigid beams connecting the concrete to the piles. The tensile behaviour of the stresses described in Figure 5.12 shows an expected behaviour in the beginning. The stress reaches the tensile capacity at the point where cracking starts and after this the stress decreases. In the other half of the curve an unexpected behaviour was found. After the reinforcement yields a sudden increase in the stresses occurred. This increase could be due to the fact that the yield in the reinforcement, which is located over the nearest support, causes a sudden shift in the displacement. This leads to a redistribution and increase of the stresses which the later part of the curve in Figure 5.12 implies. The shape of the curve for the compressive behaviour in the beam described in Figure 5.13 implies that the maximum value was on the verge of being reached when the analysis stopped. This was indicated due to the stabilisation of the values in the last increments. However it was found that the maximum stress exceeds the maximum value calculated for the non-linear behaviour of the compressive concrete, see Appendix E, this could be due to 3D effects where there are compressive stresses in other directions that is favourable to the compressive capacity.

When looking at Figure 5.18 the distribution of the stresses in the reinforcement seems reasonable. Some early stress concentrations are noticed at the fixed end. These are found where the concrete stress limits were reached which is probably the reason for the location and occurrence of these stresses. However, after concrete cracking has begun the increase and distribution of the stresses in the reinforcement at the tensile end of the beam seems reasonable as more and more of the concrete cracks.

The plot in Figure 5.14 shows that most part of the cross-section was in tension as a result of the cracked concrete and yielding reinforcement. Table 5.1 display values supporting this statement.

Studying the deflection of the piles, critical stress areas could be expected at both ends but since both translations and rotations take place in top of the pile, other distributions appear. In addition, the concrete inside the pile strengthen that section and adjusts stress pattern to have higher values just below. That area, approximately in the middle of the pile, has the greatest displacement, Figure 5.16 [5], and highest values of stress, Figure 5.17 [5].

As mentioned in Section 4.3.3 the decision to fix the bottom ends of the piles in the y-direction does not reflect the reality. An alternative solution could be to attach a non-linear spring with its limit at the vertical geotechnical capacity to catch the real behaviour. Because of this the reaction forces in the piles had to be investigated so that the vertical geotechnical capacity had not been exceeded. As a system, piles 1-5 were expected to be in compression and piles 6-10 in tension. But when looking at the results in Table 5.6 to Table 5.10 this is not the case for the later stages of the analysis where piles 1-4 are in tension instead of compression. The phenomenon behind this is not certain but could have its explanations in the displacement of the beam. From Figure 5.1 it can be shown that a rotation of the beam takes place. This rotation is transferred to the pile and forces the pile to bend out and seems to create an uplifting force which would somewhat explain the tensile reaction forces that were measured in piles 1-4. In addition to this the yielding of the pile and the following large deformation of the pile also can have an influence on the increase in tensile reaction forces. Piles 6-10 on the other hand were in tension as expected and the maximum reaction force located in pile 6 was 2486 kN which does not exceed the tensile capacity of the clay which was 2527.1 kN.

While investigating the springs it was found that the springs in the top of the clay deposit had an expected shape to the stress-strain curve. Figure 5.20 to Figure 5.22 shows the uppermost spring at three different arc lengths. Figure 5.20 and Figure 5.21 show the expected linear behaviour before the spring yields and Figure 5.22 shows it after the spring yields. Further investigation showed that the displacement for the pile in the node where the spring is connected, see Table 5.12, was much higher than the measured strain in the spring, see Figure 5.20 to Figure 5.22. These two should be the same since the spring does not have an actual length and it implies that the displacement in the pile was not transferred to the spring.

Though the strain values in the springs and the displacement in the pile did not match, the bi-linear shape of the curve shown in Figure 5.22 was expected for all the springs in the model. Looking at the results of the springs further down it can be concluded that this was not the case. For example when looking at Figure 5.23 to Figure 5.25 describing the stress-strain behaviour for a spring near the maximum displacement of the beam, Spring-20, both the stress and the strain were found to have negative values. This implicates that these springs were active in the opposite direction than the ones further up, which means that they were active in tension rather than compression, which should not be the case. Moreover Figure 5.23 to Figure 5.25 show that the spring was varying between being in compression and in tension which is not an expected behaviour. Since the springs are attached on the same side of the pile and the deflection of the pile is only working in one direction this behaviour should not occur.

The springs in this model were working only in one direction. This means that if there are deflections in any other direction the resistance of the clay is not included. A solution where springs were added in several directions in the node or the whole surface would be to recommend.

7 Conclusion

The results of the analysis show a structural behaviour that contradicts some of the preliminary results obtained by COWI. It is generally concluded that the structural response is complex to predict and interpret. A judgement has been done that the model is not to be fully trusted.

7.1 Modelling

Despite a profound literature study there was not many papers found in the field of protective piers. There are in general little knowledge of these types of structures since there have not been many full scale tests to use as reference. Historical accidents have created the need for protective structures in waterways and thereby driven the engineering knowledge forward to the level so that it is now incorporated in design process of bridges and other exposed constructions from the very beginning. Despite this, the codes are not fully developed to treat this type of structure in detail. The part of Eurocode that was used in the report was an informative annex with no clear information of the impact phenomena. The report clearly states that there are a lot of parameters, which are not treated in the codes. This concludes that a lot of development in this research area ought to be done. It is however not impossible that documentation is kept inside companies.

7.2 Structural response

The analysis performed shows that the protective pier has insufficient energy absorbing capacity even if energy is proposed to partially dissipate into heat, water or hull deformation. However, there should be further studies to confirm these results as there are some issues with the model. Boundary conditions at both the beam end and pile bottoms should be reconsidered. The pile bottoms could include free rotational degrees of freedom and have a non-linear spring in vertical direction to better resemble the reality.

The obtained, indicative, results show that it is possible to connect critical events to the shape of the force-displacement curve for the global structure. It is seen that the piles' response were a ruling factor behind this.

The non-linear horizontal clay springs indicate a malfunction and should be tweaked until a proper behaviour is obtained. Unfortunately, there was no time for this during the master's thesis project time limit. Their behaviour is most likely the cause for many observed results, especially the deformation pattern which involves all parts. Therefore the structural response cannot be trusted and the model should not be used in its current state. When the springs start working, the model is a powerful tool for extracting interesting data. Assumptions and conditions are clearly stated in the report and defines the limits of the model and thereby the output.

It is hard to judge if the model is conservative or not. Largely because it is very unclear what is included in Eurocode whilst calculating the reductions of the incoming energy for a ship colliding with a pier at an angle. Since it is unknown what is included in this calculation the conclusion if the model is conservative or not cannot be made.

8 Further Investigations

This thesis was found to consider a large structure in need of many assumptions along the way to a complete analysis. This means that there were a lot of variables that changed the outcome and hence the results obtained by another group on the same case study could have shown different values. A deep approach into a project with this span required a lot of time and quick decisions to complete the task within the limited period of time. Therefore, several stripped problematic areas are listed below which could be looked into in further investigations on the same scientific subject.

- Ship load application on protective piers.

  Only the load application problem could form a new master's thesis subject. Small scale test, a parametric study and also collaboration with scientists could give essential input for a project like this.

- FE-modelling of steel-concrete piles regarding interaction between materials.

  Previous research on this subject was found during the literature study. A deeper investigation could be done to improve FE-modelling of various applications of these steel-concrete piles.

- Investigation of concrete beam with complex cross-section subjected to loading.

  This report treats a concrete beam with irregular cross-section. The shape has obviously an impact on the deflection. An investigation could be made to map how some arbitrarily shaped cross-sections affect the deflection compared to well-known shaped cross-sections. The result could be a table with different changes in cross-section dimensions and what influence it has on the deflection, used for hand calculations to quickly judge if a value is reasonable or not. The study could include FE-analysis as well as real testing in a lab.

- Investigation regarding methods of calculating the design energy to be absorbed.

  The report considered an energy calculated from a design ship i.e. the largest ship that passes the protective pier. Another way to obtain the design energy is by performing a probability study. In the probability study it is calculated how probable it is for a certain amount of energy to collide with the structure. This is done from data on what kind and how often a ship passes the structure and how probable it is for these types of ships to collide with the structure. From this you get a return period that describes with what reoccurrence a certain energy colliding with the structure occurs (Lindqvist, 2015). Then it is up to the engineer and the contractor to decide the return period to get the design energy.The study could include both methods and involve a comparison of how they affect the protective pier design.

- Alternative modelling of protective pier.

  Investigate how the protective piers could be modelled in an alternative way that would require less effort in time and computational power compared to this thesis model. The comparison could examine the two counterparts, how much less time is spend on modelling and analysis and how much more conservative the results get.

9 References

Adams, V. & Askenazi, A., 1999. *Building Better Products with Finite Element Analysis,* Santa Fe: OnWord Press.

Algers, B., Forsby, L. & Tell, W., 1966. *Bygg.* 3 ed. Stockholm: AB Byggmästarens förlag.

Bathe, K.-J., 1996. *Finite Element Procedures,* New Jersey: Prentice-Hall, Inc.

Brodin, S., 1984. *Tjörnbron.* Västra Aros: Vägverket.

Carlsson, F., Plos, M., Norlin, B. & Thelandersson, S., 2008. *Säkerhetsprinciper för bärighetsanalys av broar med icke-linjära metoder,* s.l.: Lunds Tekniska Högskola, Chalmers Tekniska Högskola, Kungliga Tekniska Högskolan.

COWI, 2014. *Redogörelse för förutsättningar och metoder för dimensionering för ledverk och dykdalb, Hisingsbron, Göteborg.* Göteborg: COWI.

Craig, R. R. & Kurdila, A. J., 2006. *Fundamentals of structural dynamics.* 2nd ed. Hoboken, New Jersey: John Wiley & Sons Inc.

Dai, T.-y., Nie, W., Liu, Y.-j. & Wang, L.-p., 2002. Statistical Analysis of Ship Collisions with Bridges in China Waterway. *Journal of Marine Science and Application,* 1(2), pp. 28-32.

Eurocode, 2010. *SS-EN 1991-1-7:2006,* Stockholm: Swedish Standards Institute.

Flett, I., Carter, M., Hussain, N. & Yeoward, A., 2007. *Incheon Bridge Project - The role of the contractor's checking engineer,* Weimar: IABSE.

Fredriksson, M. & Yhlen, H., 2010. *FE-analysis of cracking in transversal support beams of concrete bridges,* Göteborg: Chalmers Reproservice.

Göteborgs Stad, 2013. *Ny bro över Göta älv,* Göteborg: Göteborgs Stad.

Göteborgs stad, 2015. *goteborg.se.* [Online]
Available at:
http://goteborg.se/wps/portal/enheter/projekt/hisingsbron/!ut/p/b1/jY3LDoIwFES_SHpvb-1jWUEKvhCRRLsxaAwhAd0Y_X1r4tbI7GZyToZ5dpxoQkIQNGUH5m_Ns2ubR3e_Nf2ne3mqEUo9Qwvgyinks71cLzOCwmEAjgHgVIl5lYRJigTyUm9JV8h5Icb5EH8BVxsF-YLbdY0FOuDj_NjZTKgVgF65ANis3pmSCCyN_P8R
[Accessed 20 January 2015].

Johansson, M., 2014. *Beräkningsanvisning för strukturrespons - Strukturrespons vid impulsbelastning,* Karlstad: Myndigheten för samhällsskydd och beredskap.

Johansson, M. & Gylltoft, K., 2002. Mechanical Behavior of Circular Steel-Concrete Composite Stub Columns. *Journal of structural engineering,* 128(8), pp. 1073-1081.

Johansson, M., Reinertsen Sverige AB & LL Engineering, 2012. *Bebyggelsens motståndsförmåga mot extrem dynamisk belastning - del 3,* Karlstad: Myndigheten för samhällsskydd och beredskap.

Kang, B., Choi, W. & Park, G., 2001. Structural optimization under equivalent static loads transformed from dynamic loads based on displacement. *Computers & Structures,* Issue 79, pp. 145-154.

Kuzmanovic, B. O. & Sanchez, M. R., 1992. Design of bridge pier pile foundations for ship impact. *Journal of Structural Engineering,* 118(8), pp. 2151-2167.

Larsen, O. D., 1993. *Ship collision with bridges - The interaction between vessel traffic and bridge structures.* Zürich: International Assosiation for Bridge and Structural Engineering.

Malm, R., 2009. *Predicting shear type crack initiation and growth in concrete with non-linear finite element method,* Stockholm: Royal Institute of Tehcnology (KTH).

Matlock, H., 1970. *Correlations for Design of Laterally Loaded Piles in Soft Clay.* Dallas, Offshore Technology Conference, pp. I-577 - I-594.

Olnhausen, W. v., 1983. Ship collisions with bridges in Sweden. *IABSE reports,* Issue 42, pp. 409-416.

Ottosen, N. & Peterson, H., 1992. *Introduction to the Finite Element Method.* Harlow: Pearson Education Limited.

PIANC, 2001. *Ship Collisions due to the Presence of Bridges,* Brussels: PIANC.

SIMULIA, 2012. *Abaqus 6.12 Online Documentation,* s.l.: Dassult Systèmes.

SSPA, 2009. *Påseglingssannolikhet för Gröndalsbrons bropelare samt dimensioneringskriterier för ledverk,* Göteborg: SSPA.

SSPA, 2014. *Ny Göta Älv bro - Simulering av påsegling av ledverk,* Göteborg: SSPA.

SSPA, 2014. *Risk och säkerhet i Mälarprojektet - Riskanalys för uppgradering av kanal, sluss och farled,* Göteborg: SSPA.

Svensson, H., 2009. Protection of bridge piers against ship collision. *Steel Construction,* 2(1), pp. 21-32.

The International Federation for Structural Concrete (fib), 2012. *Model Code 2010, Final draft volume 1,* Lusanne: The International Federation for Structural Concrete (fib).

Trafikverket, 2011. *TRVK BRO 11,* Borlänge: Trafikverket.

Trafikverket, 2013. *Trafikslagsövergripande stråkstudie och åtgärdsanalys, Göta älv-Vänerstråket,* Göteborg: Trafikverket.

Trafikverket, 2014. [Online]
Available at: http://www.trafikverket.se/Privat/I-ditt-lan/Vastra-gotaland/Vastsvenska-paketet/
[Accessed 21 january 2015].

U.S. Department of Transportation, 1983. *Federal Highway Administration.* [Online]
Available at:
http://www.fhwa.dot.gov/engineering/hydraulics/policymemo/t514019.cfm
[Accessed 27 01 2015].

Vrouwenvelder, A., Stieffel, U. & Harding, G., 2005. *Background Document, Accidental Actions, Eurocode 1 Part 1.7,* s.l.: Finnish Standards Association.

Wang, L. et al., 2008. An impact dynamics analysis on a new crachworthy device against ship-bridge collision. *International Journal of Impact Engineering,* Issue 35, pp. 895-904.

9.1 Oral sources

Darholm, Thomas (Technical Director, Bridge department, COWI).(2015, March 16). Protective piers at Hisingsbron. Interview.

Flansbjer, Mathias (Adjunct Professor, Structural Engineering, Chalmers).(2015, April 24). Concrete filled steel piles. Interview.

Hogström, Per (Lecturer and Masters Programme director, Naval Architecture and Ocean Engineering, Chalmers). (2015, February 10). FEM modelling of ship collision. Interview.

Johansson, Morgan (Adjunct Professor, Structural Engineering, Chalmers).(2015, April 15). Impulse loaded structures. Interview.

Lindqvist, Magnus (Engineer at KFS Anläggningskonstruktörer AB). (2015, March 9). A description of the design process of the protective piers at Gröndalsbron. Interview.

Thorsell, Mikael (Chief Project Manager, Bridge department, COWI). (2015, January 28). Protective piers at Marieholmsbron. Interview.

Appendix A.

Cohesion piles - Protective piers at Hisingsbron

MY	-8	
Pile diameter	0,61	m
k_0	200	[Exceptional design method]
N_c	9	["]
Increase kPa/m	1	

Depth	Level	Corrected cu	Bed module (Bäddmodul)	Beam bed module (Balkbäddmodul)	Clay yield pressure (Lerans flyttryck)	Displacement of spring Ku at py	Characteristic carrying capacity in tension (Kar. bärförmåga i drag)	Characteristic carrying capacity in compression (Kar. bärförmåga i tryck)
			k_u	K_u	py	δ		
m		kPa	kN/m³	kN/m²	kN/m	m	kN	kN
0	-8	10	3278.7	2000	54.9	0.02745		
1	-9	11	3606.6	2200	60.4	0.02745		
2	-10	12	3934.4	2400	65.9	0.02745		
3	-11	13	4262.3	2600	71.4	0.02745	0.0	0.0
4	-12	14	4590.2	2800	76.9	0.02745	20.0	28.6
5	-13	15	4918.0	3000	82.4	0.02745	41.5	59.2
6	-14	16	5245.9	3200	87.8	0.02745	64.4	92.0
7	-15	17	5573.8	3400	93.3	0.02745	88.8	126.9
8	-16	18	5901.6	3600	98.8	0.02745	114.8	163.9
9	-17	19	6229.5	3800	104.3	0.02745	142.2	203.1
10	-18	20	6557.4	4000	109.8	0.02745	171.0	244.3
11	-19	21	6885.2	4200	115.3	0.02745	201.4	287.7
12	-20	22	7213.1	4400	120.8	0.02745	233.2	333.2
13	-21	23	7541.0	4600	126.3	0.02745	266.5	380.8
14	-22	24	7868.9	4800	131.8	0.02745	301.3	430.5
15	-23	25	8196.7	5000	137.3	0.02745	336.9	481.3
16	-24	26	8524.6	5200	142.7	0.02745	373.3	533.3
17	-25	27	8852.5	5400	148.2	0.02745	411.1	587.2
18	-26	28	9180.3	5600	153.7	0.02745	450.2	643.2
19	-27	29	9508.2	5800	159.2	0.02745	490.9	701.2
20	-28	30	9836.1	6000	164.7	0.02745	532.9	761.3
21	-29	31	10163.9	6200	170.2	0.02745	576.4	823.4
22	-30	32	10491.8	6400	175.7	0.02745	621.3	887.5
23	-31	33	10819.7	6600	181.2	0.02745	666.4	952.0

24	-32	34	11147.5	6800	186.7	0.02745	711.8	1016.8
25	-33	35	11475.4	7000	192.2	0.02745	758.5	1083.6
26	-34	36	11803.3	7200	197.6	0.02745	806.6	1152.2
27	-35	37	12131.1	7400	203.1	0.02745	856.0	1222.8
28	-36	38	12459.0	7600	208.6	0.02745	906.8	1295.4
29	-37	39	12786.9	7800	214.1	0.02745	958.9	1369.9
30	-38	40	13114.8	8000	219.6	0.02745	1012.4	1446.3
31	-39	41	13442.6	8200	225.1	0.02745	1067.2	1524.6
32	-40	42	13770.5	8400	230.6	0.02745	1123.4	1604.9
33	-41	43	14098.4	8600	236.1	0.02745	1180.3	1686.1
34	-42	44	14426.2	8800	241.6	0.02745	1237.7	1768.2
35	-43	45	14754.1	9000	247.1	0.02745	1296.5	1852.1
36	-44	46	15082.0	9200	252.5	0.02745	1355.0	1935.7
37	-45	47	15409.8	9400	258.0	0.02745	1413.2	2018.9
38	-46	48	15737.7	9600	263.5	0.02745	1472.6	2103.8
39	-47	49	16065.6	9800	269.0	0.02745	1533.3	2190.5
40	-48	50	16393.4	10000	274.5	0.02745	1595.3	2279.0
41	-49	51	16721.3	10200	280.0	0.02745	1658.5	2369.3
42	-50	52	17049.2	10400	285.5	0.02745	1722.9	2461.4
43	-51	53	17049.2	10400	285.5	0.02745	1788.0	2554.3
44	-52	54	17049.2	10400	285.5	0.02745	1853.1	2647.3
45	-53	55	17049.2	10400	285.5	0.02745	1918.2	2740.3
46	-54	56	17049.2	10400	285.5	0.02745	1983.3	2833.2
47	-55	57	17049.2	10400	285.5	0.02745	2048.3	2926.2
48	-56	58	17049.2	10400	285.5	0.02745	2113.4	3019.2
49	-57	59	17049.2	10400	285.5	0.02745	2180.6	3115.1
50	-58	60	17049.2	10400	285.5	0.02745	2249.9	3214.1
51	-59	61	17049.2	10400	285.5	0.02745	2319.2	3313.1
52	-60	62	17049.2	10400	285.5	0.02745	2388.5	3412.2
53	-61	63	17049.2	10400	285.5	0.02745	2457.8	3511.2
54	-62	64	17049.2	10400	285.5	0.02745	**2527.1**	**3610.2**
70	-78	52	17049.2	10400	285.5	0.02745		

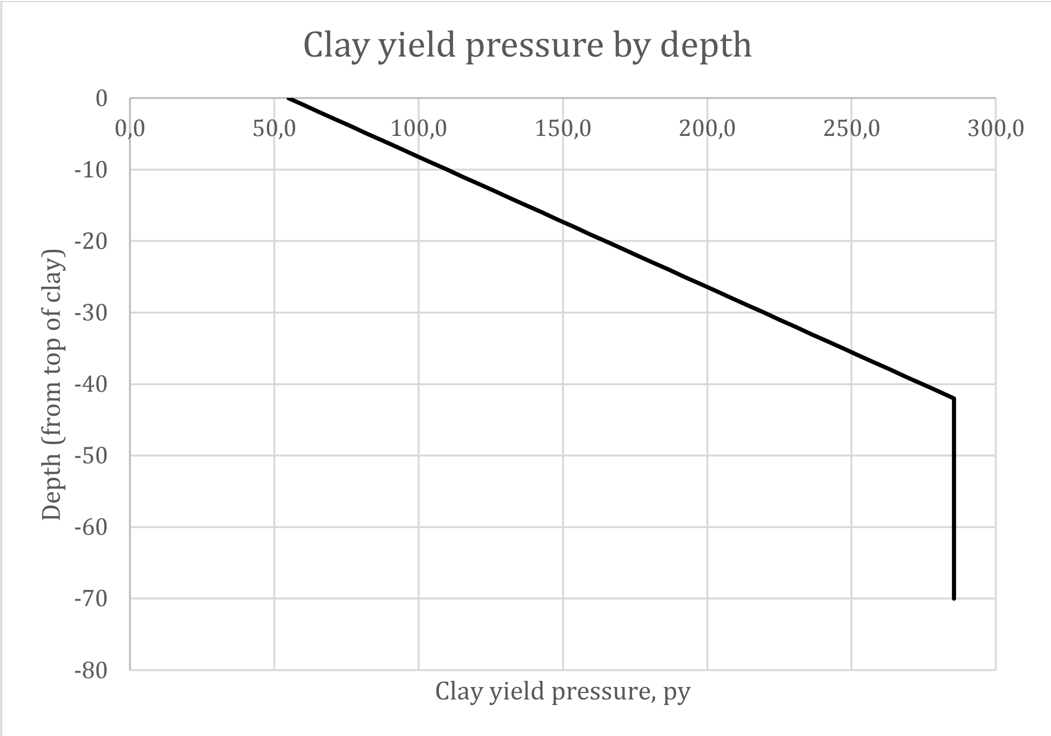

Figure A.1 The yield pressure-clay depth relationship.

Appendix B.

Energy calculations

Action energy from incoming ship:

$m_{tot} := 37000000\text{kg}$

Ship's mass + following water mass [kg] according to (SSPA Ny Göta Älv bro - Simulering av påsegling av ledverk, 2014)

$v_{knot} := 8$

Ship's velocity [knots] according to (SSPA Ny Göta Älv bro - Simulering av påsegling av ledverk, 2014)

$v_{transf} := 0.514444444\,\frac{m}{s}$

Transformation factor from knot to meters/second

$v := v_{knot} \cdot v_{transf} = 4.116 \cdot \frac{m}{s}$

Ship's velocity [m/s]

$E_a := \frac{m_{tot} \cdot v^2}{2} = 313.349 \cdot MN \cdot m$

Total kinetic energy of incoming ship, according to Eurocode 1991-1-7:2006 (C.4.3)

$\alpha := 20°$

Incoming angle of ship according to (SSPA Ny Göta Älv bro - Simulering av påsegling av ledverk, 2014)

(the angle is defined as the angle between the boat and the structure)

$E_{def} := E_a \cdot (1 - \cos(\alpha)) = 18.897 \cdot MN \cdot m$

Deformation energy due to incoming ship at angle of α degrees, according to Eurocode

Following equations are for plotting the speed influence of the incoming energy.

$v_{graph} := 0, 0.2 .. 8$

Speed variable

$v_{transf} := 0.514444444$

Transformation factor from knot to m/s

$$E_{def.graph}(v_{graph}) := \frac{m_{tot} \cdot \left(v_{graph} \cdot v_{transf} \cdot \frac{m}{s}\right)^2}{2} \cdot \frac{(1 - \cos(\alpha))}{10^6}$$

Energy function depending on speed variable

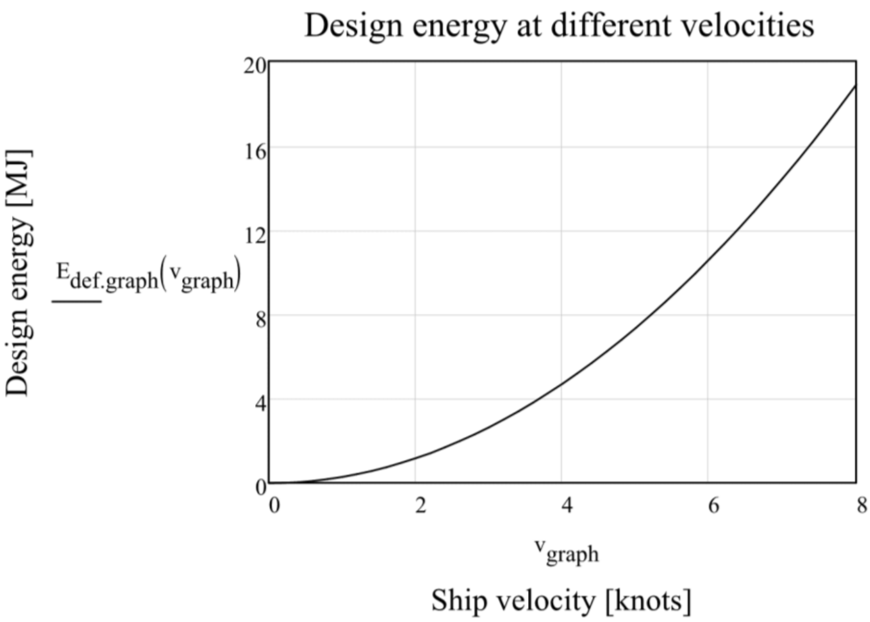

From the equation E.def.graph it is seen that the energy varies exponentially with velocity. This is visualized in the figure above.

Comparison; fender capacity vs incoming energy

$E_{d.fender} := 86\,10^3 J$

Energy absorbing capacity of one fender
Source: Trelleborg AB, Trelleborg Marine System, Product Catalogue 2011.
Fender type: SCN550, E2.8.

$n_{fenders} := 4$

Number of fenders absorbing a collision between two pile groups. (Ship load is distributed by longitudinal beams to 4 fenders).

$E_{tot.fenders} := E_{d.fender} \cdot n_{fenders} = 3.44 \times 10^5 J$

Total absorbing energy of fenders at collision between two pile groups.

$$\frac{E_{tot.fenders}}{E_{def}} = 1.82 \cdot \%$$

The fenders' capacity is neglegible when looking at the amount of energy that needs to be absorbed by the protective pier.

Appendix C.
Verification of pile

Table of contents

Pile deflection

Steel sheet pile:

$b := 0.305\text{m}$	Outer radius of pile
$t := 0.016\text{m}$	Thickness of pile steel
$a := b - t = 0.289\,\text{m}$	Inner radius of pile
$d := 2 \cdot b = 0.61\,\text{m}$	Diameter of pile
$L := 18\text{m}$	Length of pile
$E_s := 210\text{GPa}$	Young's modulus of steel
$P_1 := 20\text{kN}$	Applied force, arbitrary load

There are two types of circular cross-section.
Elementary cases taken from: http://hallf.se/Formelsamling/Formelsamling.html

Massive circular cross-section

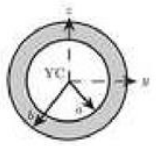

$$\bar{I}_y = \bar{I}_z = \frac{\pi}{4}(b^4 - a^4)$$

$$K_v = \frac{\pi}{2}(b^4 - a^4)$$

Thin-walled circular cross-section

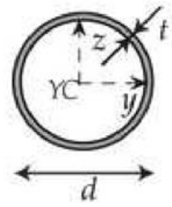

$$t \ll d, \quad A \approx \pi d t$$

$$\bar{I}_y = \bar{I}_z \approx \frac{\pi d^3 t}{8}$$

$$K_v \approx \frac{\pi d^3 t}{4}$$

$$I_{y1} := \frac{\pi}{4}\left(b^4 - a^4\right) = 1.318 \times 10^{-3}\,\mathrm{m}^4$$

$$I_{y1.2} := \frac{\pi d^3 \cdot t}{8} = 1.426 \times 10^{-3}\,\mathrm{m}^4$$

There is a slight difference, choosing massive cross-section model in accordance with previous COWI calculations.

Elementary cases for deflection of console beam

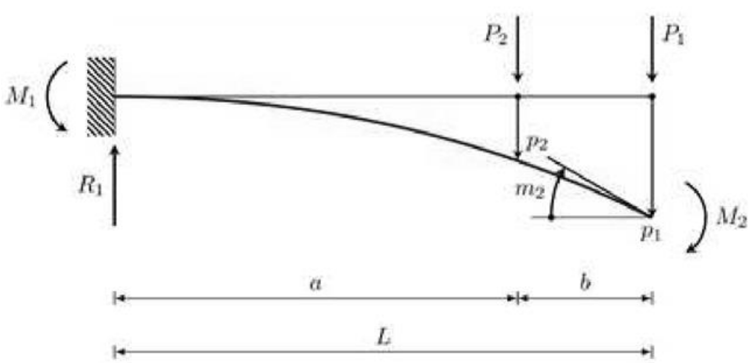

	P_1
$R_1 =$	1
$M_1 =$	L
$p_1 =$	$\frac{L^3}{3EI}$
$p_2 =$	$\frac{a^2 L}{2EI}\left[1 - \frac{a}{3L}\right]$
$m_2 =$	$\frac{L^2}{2EI}$

$$p_{1.hand} := \frac{P_1 \cdot L^3}{3E_s \cdot I_{y1}} = 0.14\,m$$

Deflection at point load (for pure steel pile)

$$p_{1.aba} := 0.140614m$$

Deflection according to Abaqus

$$d_1 := \frac{\left|p_{1.hand} - p_{1.aba}\right|}{p_{1.aba}} = 0.086 \cdot \%$$

Error between hand calculation and Abaqus

Steel sheet, concrete filled pile:

$$a := 0m$$

Inner radius of pile

$$\nu_{btg} := 0.2$$

Poissons ratio for concrete

$$\nu_s := 0.3$$

Poissons ratio for steel

$$E_{cm} := 34GPa$$

Mean Youngs modulus of elsticity for concrete

$$A_{btg} := \pi \cdot (0.289m)^2 = 0.262\,m^2$$

Area of concrete

$$A_s := \pi \cdot (0.305m)^2 - A_{btg} = 0.03\,m^2$$

Area of steel

$$E_{tot} := \frac{E_{cm} \cdot A_{btg} + E_s \cdot A_s}{A_{btg} + A_s} = 51.981 \cdot GPa$$

Combined Youngs modulus

$$\nu_{tot} := \frac{\nu_{btg} \cdot A_{btg} + \nu_s \cdot A_s}{A_{btg} + A_s} = 0.21$$

Combined Poissons ration

(for input in Abaqus properties of mixed material)

$$I_{y2} := \frac{\pi}{4}\left(b^4 - a^4\right) = 6.797 \times 10^{-3}\,m^4$$

Second moment of inertia for combined pile

$$p_{2.hand} := \frac{P_1 \cdot L^3}{3E_{tot} \cdot I_{y2}} = 0.11\,m$$

Deflection at point load (for combined pile)

$$p_{2.aba} := 0.0846801\,m$$

Deflection according to Abaqus (steel with interacting concrete, tie constraint)

$$d_2 := \frac{\left|p_{2.hand} - p_{2.aba}\right|}{p_{2.aba}} = 29.96 \cdot \%$$

Error between hand calculation and Abaqus

$p_{3.aba} := 0.11188\text{m}$ — Deflection according to Abaqus (steel and concrete properties mixed into one material)

$$d_3 := \frac{|p_{2.hand} - p_{3.aba}|}{p_{3.aba}} = 1.636 \cdot \%$$

Error between hand calculation and Abaqus

$p_{4.aba} := 0.0846778\text{m}$ — Deflection according to Abaqus (steel with interacting concrete, tie constraint)

$$d_4 := \frac{|p_{2.hand} - p_{4.aba}|}{p_{4.aba}} = 29.963 \cdot \%$$

Error between hand calculation and Abaqus

$p_{5.aba} := 0.141549\text{m}$ — Deflection according to Abaqus

$$d_5 := \frac{|p_{1.hand} - p_{5.aba}|}{p_{5.aba}} = 0.746 \cdot \%$$

Error between hand calculation and Abaqus

Results & summary

$p_{1.aba}$	$p_{2.aba}$	$p_{3.aba}$	$p_{4.aba}$	$p_{5.aba}$
solid steel elements	solid steel elements solid concrete elements	solid mix elements	shell steel elements solid concrete elements	shell steel elements
$p_{1.hand} = 0.14\,\text{m}$	$p_{2.hand} = 0.11\,\text{m}$	$p_{2.hand} = 0.11\,\text{m}$	$p_{2.hand} = 0.11\,\text{m}$	$p_{1.hand} = 0.14\,\text{m}$
$p_{1.aba} = 0.141\,\text{m}$	$p_{2.aba} = 0.085\,\text{m}$	$p_{3.aba} = 0.112\,\text{m}$	$p_{4.aba} = 0.085\,\text{m}$	$p_{5.aba} = 0.142\,\text{m}$
$d_1 = 0.086 \cdot \%$	$d_2 = 29.96 \cdot \%$	$d_3 = 1.636 \cdot \%$	$d_4 = 29.963 \cdot \%$	$d_5 = 0.746 \cdot \%$

$E_s = 210 \cdot \text{GPa}$	$E_s = 210 \cdot \text{GPa}$ $E_{cm} = 34 \cdot \text{GPa}$	$E_{tot} = 51.981 \cdot \text{GPa}$	$E_s = 210 \cdot \text{GPa}$ $E_{cm} = 34 \cdot \text{GPa}$	$E_s = 210 \cdot \text{GPa}$
$\nu_s = 0.3$	$\nu_s = 0.3$ $\nu_{btg} = 0.2$	$\nu_{tot} = 0.21$	$\nu_s = 0.3$ $\nu_{btg} = 0.2$	$\nu_s = 0.3$

It is concluded that the hand-calculations and Abaqus model give similar values for the deflection in the case of a single material (pile 1,3 & 5). However, the pile with interacting steel and concrete (pile 2 & 4) seem to get a higher stiffness than for the hand-calculated one and hence smaller deflection. This could be expected since the steel properties are concentrated to the edges of the cross section where it resists compression/tension better, than if it would be smeared out as in model to the right.

Comparison between tie and friction model

Abaqus model using shell steel elements and solid concrete elements is tested for two different types of material interaction.

Tie-constraint between surfaces

$p_{2.hand} = 0.11\,m$

$p_{4.aba} = 0.085\,m$

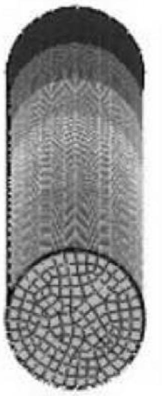

Surface-to-surface contact, frictionless

$p_{2.hand} = 0.11\,m$

$p_{6.aba} := 0.085036m$

$$d_{tie.fric} := \frac{|p_{4.aba} - p_{6.aba}|}{p_{4.aba}} = 0.423 \cdot \%$$

Difference between tie and frictionless model

The two models cmpared are the two extremes, either the materials are fully attached to each other, or they may slide unlimited. A model using frictioncoefficients would be somewhere in between. As the difference is small, less than 1%, a tie model can be used and will reflect the pile response well. This will allow for a simple setup and good computation times.

Check of clay spring functionality

This control concerns the two different modelling techniques of springs in Abaqus. A spring can be modelled in a part's property module or in asembly module. A lot of time and effort is saved if springs are modelled directly onto the pile in property module and then copied in assembly module. The alternative is to model all springs separately in assembly module. This check will model one pile of each case to see if rotation of parts will disturb the direction of the spring. The check is to confirm the already stated fact in Abaqus manual.

Top pile: spring is defined in property module using local attachment point and tie constraint.
Bottom pile: spring is defined in assembly module using global reference point and tie constraint.

The spring is in both cases defined to act in global direction 1 (x).

Spring on top pile is placed i y-direction in property module and then rotated 90 degrees in assembly module to point at x-direction. An arbitrary load and stiffness is applied to the pile and spring respectively. Analysis is performed and values of deflection is probed.

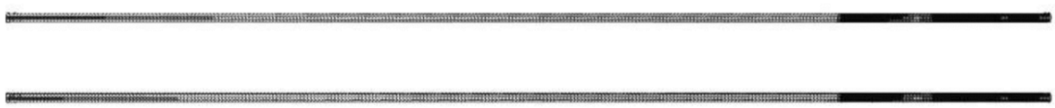

Despite the different setups, the spring is still acting in global direction 1 (x), which is just what was desired.

This concludes that if a spring is defined to act in a certain global direction, it will do this whether the spring is defined in property- or assembly module, and even if the part is rotated in assembly. The clay springs will be modelled in property module in FE-model further on.

Appendix D.

Verification of concrete beam

Table of contents

Comment

The words "beam" and "solid" refers to the element types in FEM-software Abaqus.

Static load, one span, simply supported

Rectangular cross-section <u>without</u> reinforcement

$w := 1m$	Width
$h := 2.8m$	Height
$L := 10m$	Length
$P := 3200kN$	Concentrated force in mid-span
$E_{cm} := 34GPa$	Young's modulus of concrete
$I_I := \frac{w \cdot h^3}{12} = 1.829\,m^4$	Moment of inertia

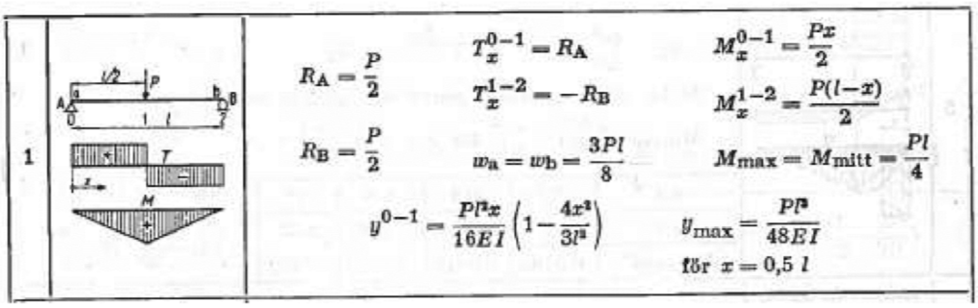

1

$R_A = \frac{P}{2}$ $\quad T_x^{0-1} = R_A$ $\quad M_x^{0-1} = \frac{Px}{2}$

$T_x^{1-2} = -R_B$ $\quad M_x^{1-2} = \frac{P(l-x)}{2}$

$R_B = \frac{P}{2}$ $\quad w_a = w_b = \frac{3Pl}{8}$ $\quad M_{max} = M_{mitt} = \frac{Pl}{4}$

$y^{0-1} = \frac{Pl^2x}{16EI}\left(1 - \frac{4x^2}{3l^2}\right)$ $\quad y_{max} = \frac{Pl^3}{48EI}$

för $x = 0{,}5\ l$

Elementary Case. ["Byggnadsstatistik", avd. 16, kap. 162. Balkar, p. 615]

$d_{hand.rec} := \frac{P \cdot L^3}{48 \cdot E_{cm} \cdot I_I} = 1.072 \cdot mm$	Deflection in mid-span of beam

Comparison between hand calculations and FEM

$d_{aba.rec.beam.euler} := 1.072mm$	Deflection with Euler Bernoulli beam elements
$\frac{d_{aba.rec.beam.euler}}{d_{hand.rec}} - 1 = 0.013 \cdot \%$	There is a good match

$d_{aba.rec.beam.timo} := 1.309mm$

Deflection with Timoshenko beam elements

$$\frac{d_{aba.rec.beam.timo}}{d_{hand.rec}} - 1 = 22.124 \cdot \%$$

There is an obviuos difference between hand calculations and FEM

$d_{aba.rec.solid} := 1.345mm$

Deflection with solid elements

$$\frac{d_{aba.rec.solid}}{d_{hand.rec}} - 1 = 25.483 \cdot \%$$

There is an obvious difference between hand calculations and FEM

$$\frac{d_{aba.rec.solid}}{d_{aba.rec.beam.timo}} - 1 = 2.75 \cdot \%$$

There is almost no difference between solid elements and Timoshenko beam elements in FEM

Rectangular cross-section <u>with</u> reinforcement

$d'_1 := 0.082m$

Reinforcement layer one distance from edge

$d'_2 := 0.172m$

Reinforcement layer two distance from edge

$d_1 := h - d'_1 = 2.718\,m$

Reinforcement distance from opposite edge

$d_2 := h - d'_2 = 2.628\,m$

Reinforcement distance from opposite edge

$E_s := 200GPa$

Young's modulus of reinforcement steel

$$\alpha := \frac{E_s}{E_{cm}} = 5.882$$

Effective-factor for Young's modulus

$\phi := 0.032m$

Reinforcement diameter

$$A_s := \pi \cdot \left(\frac{\phi}{2}\right)^2 = 8.042 \times 10^{-4}\,m^2$$

Reinforcement area of one bar

$$I_I := \frac{w \cdot h^3}{12} + 2\left[(\alpha - 1) \cdot 9 \cdot A_s \cdot \left(d_1 - \frac{h}{2}\right)^2 + (\alpha - 1) \cdot 9 \cdot A_s \cdot \left(d_2 - \frac{h}{2}\right)^2\right] = 2.059\,m^4$$

$$d_{hand.rec.rebars} := \frac{P \cdot L^3}{48 \cdot E_{cm} \cdot I_I} = 0.952 \cdot mm$$

Deflection in mid-span of beam

Comparison between hand calculations and FEM

$$d_{aba.rec.solid.rebars} := 1.209mm$$

Deflection with solid elements

$$\frac{d_{aba.rec.solid.rebars}}{d_{hand.rec.rebars}} - 1 = 26.937 \cdot \%$$

There is an obvious difference between hand calculations and FEM

$$\frac{\frac{d_{aba.rec.solid.rebars}}{d_{hand.rec.rebars}}}{\frac{d_{aba.rec.solid}}{d_{hand.rec}}} - 1 = 1.159 \cdot \%$$

The difference between the unreinforced cross section and the one with reinforcement is almost the same; same error in percentage for both models

Original cross-section <u>without</u> reinforcement

$h_1 := 0.5m$

$h_2 := 0.5m$

$h_3 := h - 2 \cdot h_1 = 1.8\,m$

$b_1 := 1m$

$b_2 := 0.5m$

$b_3 := b_1 - b_2 = 0.5\,m$

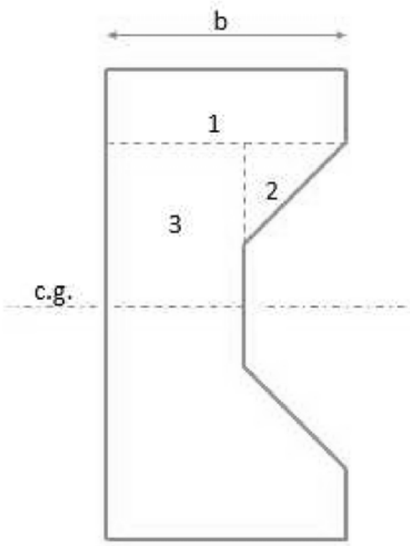

Uncracked section, short-term response:

$$I_I := 2\left[\frac{b_1 \cdot h_1^{\,3}}{12} + b_1 \cdot h_1 \cdot \left(\frac{h - h_1}{2}\right)^2 + \frac{b_2 \cdot h_2^{\,3}}{36} + \frac{b_2 \cdot h_2}{2} \cdot \left(\frac{h}{2} - h_1 - \frac{h_2}{3}\right)^2\right] + \frac{b_3 \cdot h_3^{\,3}}{12}$$

$I_I = 1.724\,m^4$ Moment of inertia, coss-section is symmetric,.

$d_{hand.orig} := \frac{P \cdot L^3}{48 \cdot E_{cm} \cdot I_I} = 1.137 \cdot mm$ Deflection in mid-span due to point-load

Comparison between hand calculations and FEM

$d_{aba.orig.solid} := 1.680mm$ Deflection with solid elements

$\frac{d_{aba.orig.solid}}{d_{hand.orig}} - 1 = 47.734 \cdot \%$ There is an obvious difference between hand calculations and FEM

Lower original cross-section without reinforcement

$h := 1.8m$

$h_1 := 0.35m$

$h_2 := 0.35m$

$h_3 := h - 2 \cdot h_1 = 1.1\,m$

$d_1 := h - d'_1 = 1.718\,m$

$d_2 := h - d'_2 = 1.628\,m$

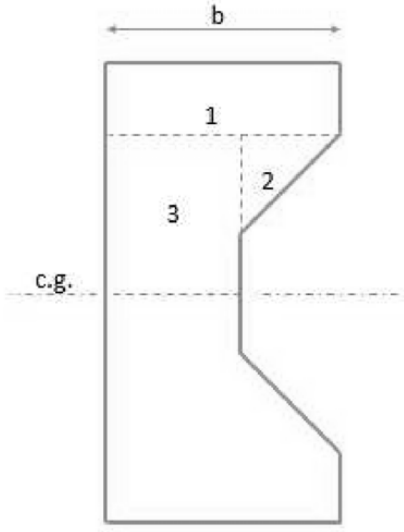

Uncracked section, short-term response:

$$I_I := 2\left[\frac{b_1 \cdot h_1^{\,3}}{12} + b_1 \cdot h_1 \cdot \left(\frac{h - h_1}{2}\right)^2 + \frac{b_2 \cdot h_2^{\,3}}{36} + \frac{b_2 \cdot h_2}{2} \cdot \left(\frac{h}{2} - h_1 - \frac{h_2}{3}\right)^2\right] + \frac{b_3 \cdot h_3^{\,3}}{12}$$

$$I_I = 0.465\,m^4$$

Moment of inertia,
coss-section is symmetric,.

$$d_{hand.low} := \frac{P \cdot L^3}{48 \cdot E_{cm} \cdot I_I} = 4.22 \cdot mm$$

Deflection in mid-span due to point-load

Comparison between hand calculations and FEM

$d_{aba.low.solid} := 4.790mm$

Deflection with solid elements

$$\frac{d_{aba.low.solid}}{d_{hand.low}} - 1 = 13.496 \cdot \%$$

There is an obvious difference between hand calculations and FEM

Original cross-section with reinforcement

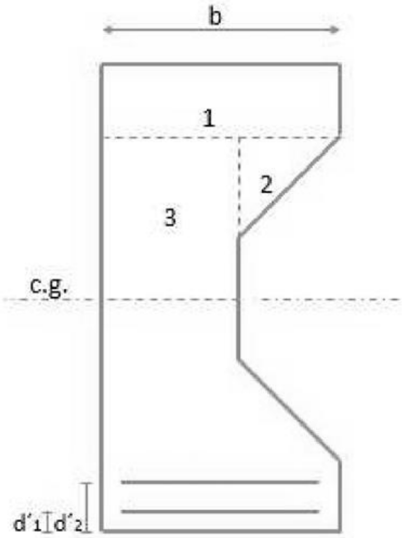

$h := 2.8m$

$h_1 := 0.5m$

$h_2 := 0.5m$

$h_3 := h - 2 \cdot h_1 = 1.8\,m$

$d_1 := h - d'_1 = 2.718\,m$

$d_2 := h - d'_2 = 2.628\,m$

Uncracked section, short-term response:

$$I_I := 2\left[\frac{b_1 \cdot h_1^{\,3}}{12} + b_1 \cdot h_1 \cdot \left(\frac{h - h_1}{2}\right)^2 + \frac{b_2 \cdot h_2^{\,3}}{36} + \frac{b_2 \cdot h_2}{2} \cdot \left(\frac{h}{2} - h_1 - \frac{h_2}{3}\right)^2\right] \dots$$
$$+ \frac{b_3 \cdot h_3^{\,3}}{12} + 2(\alpha - 1) \cdot 9 \cdot A_s \cdot \left(d_1 - \frac{h}{2}\right)^2 + 2(\alpha - 1) \cdot 9 \cdot A_s \cdot \left(d_2 - \frac{h}{2}\right)^2$$

$I_I = 1.954\,m^4$

Moment of inertia, cross section is symmetric

$$d_{hand.orig.rebars} := \frac{P \cdot L^3}{48 \cdot E_{cm} \cdot I_I} = 1.004 \cdot mm$$

Deflection in mid-span due to point-load:

Comparison between hand calculations and FEM

$d_{aba.orig.solid.rebars} := 1.530mm$

Deflection with solid elements

$$\frac{d_{aba.orig.solid.rebars}}{d_{hand.orig.rebars}} - 1 = 52.44 \cdot \%$$

There is an obvious difference between hand calculations and FEM

Cracked section, short-term response:

$x_{II} := 0.55 \cdot m$

Assume a value, update with the solved value until they are the same

$$x_{II} := \mathrm{root}\left[\begin{array}{l}(b_1 \cdot h_1)\cdot\left(x_{II} - \frac{h_1}{2}\right) + \frac{[0.5m - (x_{II} - h_1)]\cdot(x_{II} - h_1)}{2}\cdot\frac{2}{3}\cdot(x_{II} - h_1) \ldots, x_{II} \\ + \frac{[b_1 - [0.5m - (x_{II} - h_1)]]\cdot(x_{II} - h_1)^2}{2} + (\alpha - 1)\cdot 9A_s(x_{II} - d'_1) \ldots \\ + (\alpha - 1)\cdot 9A_s(x_{II} - d'_2) - \alpha\cdot 9A_s\cdot(d_1 - x_{II}) \ldots \\ + -\alpha\cdot 9A_s\cdot(d_2 - x_{II})\end{array}\right]$$

$x_{II} = 0.55\,m$

Compression zone height

$h_2 := x_{II} - h_1 = 0.05\,m$

Compression zone dimensions

$h_3 := h_2 = 0.05\,m$

$b_2 := h_2 = 0.05\,m$

$b_3 := b_1 - b_2 = 0.95\,m$

$$I_{II} := \frac{b_1 \cdot h_1^3}{12} + (b_1 \cdot h_1)\cdot\left(x_{II} - \frac{h_1}{2}\right)^2 + \frac{b_2 \cdot h_2^3}{36} + \left(\frac{b_2 \cdot h_2}{2}\right)\cdot\left(\frac{2 \cdot h_2}{3}\right)^2 \ldots$$
$$+ \frac{b_3 \cdot h_3^3}{12} + (b_3 \cdot h_3)\cdot\left(\frac{h_3}{2}\right)^2 + (\alpha - 1)\cdot 9A_s\cdot(x_{II} - d'_1)^2 \ldots$$
$$+ (\alpha - 1)\cdot 9A_s\cdot(x_{II} - d'_2)^2 + \alpha\cdot 9A_s\cdot(d_1 - x_{II})^2 \ldots$$
$$+ \alpha\cdot 9A_s\cdot(d_2 - x_{II})^2$$

$I_{II} = 0.452\,m^4$

Moment of inertia, cross section is symmetric

$$d_{hand.orig.rebars.crack} := \frac{P \cdot L^3}{48 \cdot E_{cm} \cdot I_{II}} = 4.336 \cdot mm$$

Deflection in mid-span due to point-load:

Comparison between hand calculations and FEM

$d_{aba.orig.solid.rebars.crack} := 2.08mm$

Deflection with solid elements, non-linear analysis

$$\frac{d_{aba.orig.solid.rebars.crack}}{d_{hand.orig.rebars.crack}} - 1 = -52.028 \cdot \%$$

There is an obvious difference between hand calculations and FEM

Original cross-section with reinforcement, check performed using displacement control in Abaqus

$d_{aba.disp.applied} := 2.13397mm$

Applied deflection where load acts in load-controlled case

$R_{tot} := 3198kN$

Total reaction force in supports due to applied deformation, to be compared with applied load in load-controlled case

$$\frac{\left|P - R_{tot}\right|}{P} = 0.063 \cdot \%$$

Error size of load between load-control and displacement-control in Abaqus.

Error is probably due to the not exact match of deflection

$d_{aba.disp.read} := 1.85mm$

Deflection due to applied displacement (read deflection in same place as in load-controlled case)

$$\frac{d_{aba.orig.solid.rebars}}{d_{aba.disp.read}} - 1 = -17.297 \cdot \%$$

Error between load-control and displacement-control in Abaqus

Dynamic load (SDOF), one span, simply supported

Using MSB formulas in document B03-101 & L02-104:

$$k_b := \frac{48 \cdot E_{cm} \cdot I_I}{L^3} = 3.188 \times 10^6 \cdot \frac{kN}{m}$$

Beam stiffness, simply supported with point load in middle

$$\kappa_{mF} := 0.486$$

Transformation factor

$$A_c := h \cdot \frac{b_1}{2} + 2\left(\frac{b_1}{2} \cdot h_1\right) + 2\frac{\left(\frac{b_1}{2}\right)^2}{2} = 2.15\,m^2$$

Beam cross sectional area

$$\rho := 2500 \frac{kg}{m^3}$$

Concrete density

$$m_b := L \cdot A_c \cdot \rho = 5.375 \times 10^4\,kg$$

Beam mass

$$\omega_b := \sqrt{\frac{k_b}{\kappa_{mF} \cdot m_b}} = 349.359\,\frac{1}{s}$$

Angular frequency

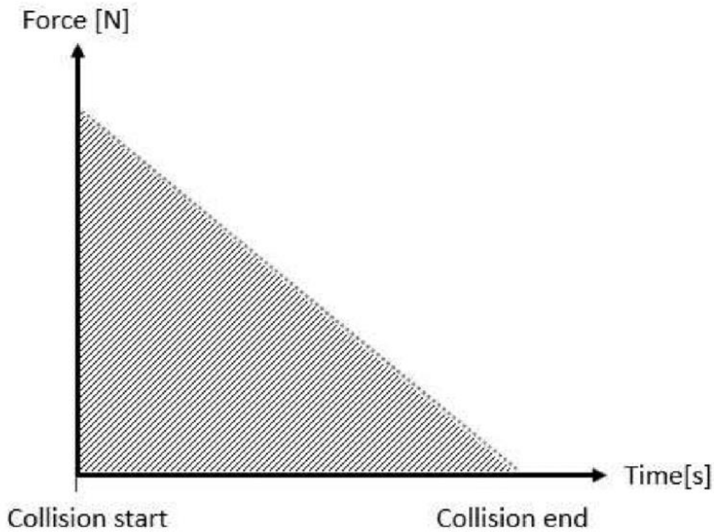

$P := 3200\text{kN}$ Arbitrary peak force

$t_1 := 5\text{s}$ Impact time

$T := \frac{2\pi}{\omega_b} = 0.018\,\text{s}$ Time period

$\frac{T}{t_1} = 3.597 \times 10^{-3}$

This value say that the loading should be treated a pressure load and not an impulse.
After a meeting with Morgan Johansson it is decided to go with Q=2*F for an equivalent static case.

$u_{el} := \frac{2 \cdot P}{\kappa_{mF} \cdot m_b \cdot \omega_b^{\,2}} = 2.007 \times 10^{-3} \cdot \text{m}$ Elastic displacement

Comparison between hand calculations and FEM

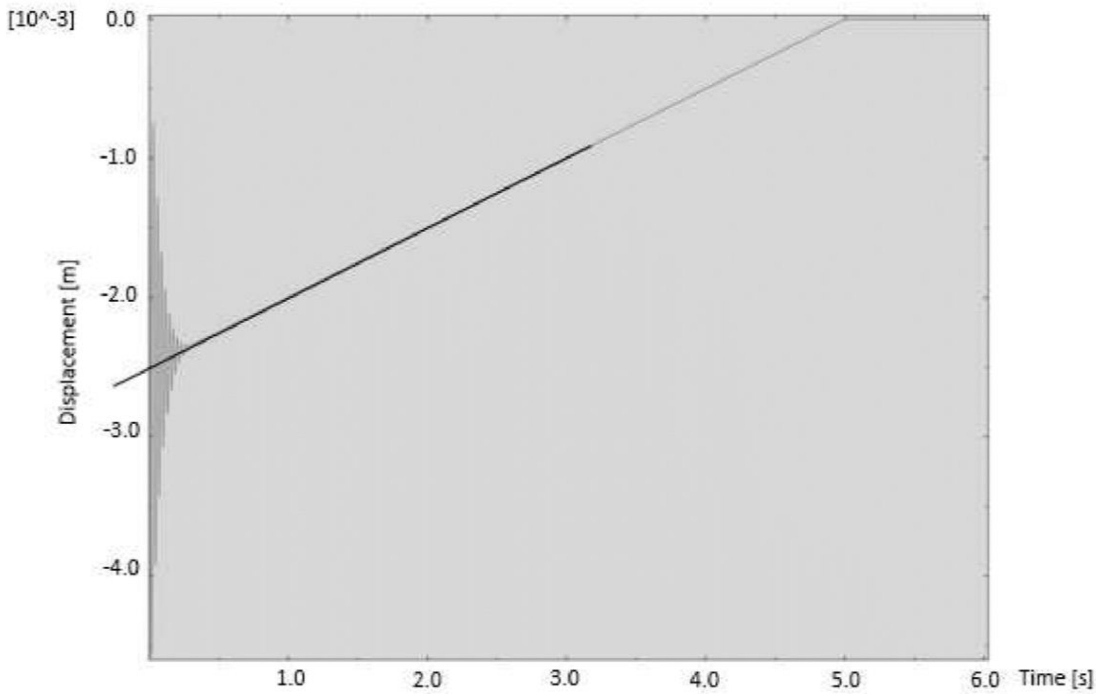

$d_{aba.orig.solid.rebars.dyn} := 2.25\text{mm}$ Deflection with solid elements, non-linear analysis

$\frac{\left|u_{el} - d_{aba.orig.solid.rebars.dyn}\right|}{d_{aba.orig.solid.rebars.dyn}} = 10.785 \cdot \%$

There is certain difference between hand calculations and FEM. The results give a good picture of the dynamic behavior of the beam but is not treated in a particular way and will not affect further modelling.

Appendix E.
Non-linear material parameters

Table of contents

Concrete

Compressive strength

Concrete C 35/45

$f_{ck} := 35\text{MPa}$ — Characteristic compressive strength

$\Delta f := 8\text{MPa}$

$f_{cm} := f_{ck} + \Delta f = 43\cdot\text{MPa}$ — Mean compressive strength

$f_{cc} := f_{cm}$ — Compressive strength

$E_{ci} := 35\text{GPa}$ — Modulus of elasticity in MPa at concrete age of 28 days

(from Table 5.1-7 (fib Model Code 2010 volume 1))

$E_{c1} := 18.2\text{GPa}$ — Secant modulus from the origin to the peak compressive stress

(from Table 5.1-8 (fib Model Code 2010 volume 1))

$\alpha_i := 0.898$ — Reduction Factor

(from Table 5.1-7 (fib Model Code 2010 volume 1))

$E_c := \alpha_i\cdot E_{ci} = 31.43\cdot\text{GPa}$ — Reduced model of elasticity

(from Equation 5.1-23 (fib Model Code 2010 volume 1))

$$\varepsilon_{c1} := 2.311055 \times 10^{-3}$$

Strain at maximum compressive stress

Original value from Table 5.1-8 (fib Model Code 2010 volume 1) modified so that the curves fit together due to the definition of the curve

$$\varepsilon_{c.lim} := 3.5 \times 10^{-3}$$

Ultimate strain

(from Table 5.1-8 (fib Model Code 2010 volume 1))

$$\varepsilon_{c.el} := \frac{0.4 \cdot f_{cc}}{E_c} = 5.472 \times 10^{-4}$$

Elastic strain

(from säkerhetsprinciper kapitel C5.3 sid 35)

$$k := \frac{E_c \cdot \varepsilon_{c1}}{f_{cc}} = 1.689$$

Plasticity number

(from säkerhetsprinciper kapitel C5.3 equation C.39)

$$\varepsilon_{cu} := \varepsilon_{c.lim} = 3.5 \times 10^{-3}$$

Ultimate strain

From säkerhetsprinciper kapitel C5.3 equation C.39

$$\varepsilon_u := \frac{\varepsilon_{cu}}{\varepsilon_{c1}} = 1.514$$

From säkerhetsprinciper kapitel C5.3 equation C.39

$$\zeta := 4\,\frac{\varepsilon_u^{\,2}(k-2) + 2\varepsilon_u - k}{\left[\varepsilon_u \cdot (k-2) + 1\right]^2} = 8.949$$

From säkerhetsprinciper kapitel C5.3 equation C.39

Non-linerar comperssive strength

Part 1

$$\sigma_{c1}(\varepsilon_c) := \frac{\frac{\varepsilon_c}{\varepsilon_{c1}} \cdot \left(k - \frac{\varepsilon_c}{\varepsilon_{c1}}\right)}{1 + \frac{\varepsilon_c}{\varepsilon_{c1}} \cdot (k-2)} \cdot f_{cc}$$

$0 \le \varepsilon_c \le \varepsilon_{cu}$

Describing the first part of the curve

(from Equation 5.1-26 (fib Model Code 2010 volume 1) combined with equation C.39 in säkerhetsprinciper)

Part 2

$$\sigma_{c2}(\varepsilon_c) := \frac{f_{cc}}{(\zeta \cdot \varepsilon_u - 2)\left(\frac{\frac{\varepsilon_c}{\varepsilon_{c1}}}{\varepsilon_u}\right)^2 + (4 - \zeta \cdot \varepsilon_u) \cdot \frac{\frac{\varepsilon_c}{\varepsilon_{c1}}}{\varepsilon_u}}$$

$\varepsilon_c \ge \varepsilon_{cu}$

Describing the second part of the curve

From säkerhetsprinciper kapitel C5.3 equation C.39

$\sigma_{c1}(3.5 \cdot 10^{-3}) - \sigma_{c2}(3.5 \cdot 10^{-3}) = -7.089 \times 10^{-5} \cdot \text{MPa}$ Check for difference between the curves is minimal at ultimate strain

$\sigma_{c1}(3.5 \cdot 10^{-3}) = 21.5 \cdot \text{MPa}$ Compressive stress in part1 of the curve at Ultimate strain after modification of ε_{c1}

$\sigma_{c2}(3.5 \cdot 10^{-3}) = 21.5 \cdot \text{MPa}$ Compressive stress in part2 of the curve at Ultimate strain after modification of ε_{c1}

$\varepsilon_c := 0, 1 \cdot 10^{-5} .. 3.5 \cdot 10^{-3}$ Range for function 1

$\varepsilon_{c2} := 3.5 \cdot 10^{-3}, 3.501 \cdot 10^{-3} .. 10 \cdot 10^{-3}$ Range for function 2

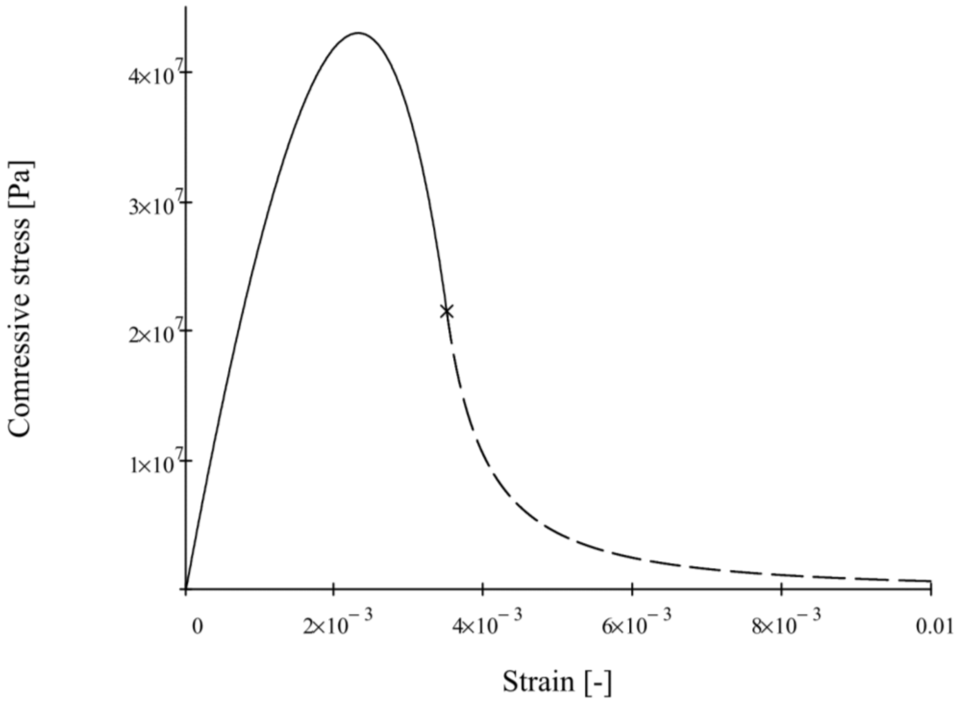

$$\varepsilon_c := \begin{pmatrix} \varepsilon_{c.el} \cdot 10^3 \\ 1.0 \\ 1.3 \\ 1.6 \\ 1.9 \\ 2.2 \\ 2.6 \\ 2.9 \\ 3.2 \\ 3.5 \end{pmatrix} \cdot 10^{-3}$$

Chosen measurment points for the compressive stress in part 1

$$\sigma_{c1} := \begin{pmatrix} \sigma_{c1}(\varepsilon_{c.el}) \\ \sigma_{c1}(1.0\cdot 10^{-3}) \\ \sigma_{c1}(1.3\cdot 10^{-3}) \\ \sigma_{c1}(1.6\cdot 10^{-3}) \\ \sigma_{c1}(1.9\cdot 10^{-3}) \\ \sigma_{c1}(2.2\cdot 10^{-3}) \\ \sigma_{c1}(2.6\cdot 10^{-3}) \\ \sigma_{c1}(2.9\cdot 10^{-3}) \\ \sigma_{c1}(3.2\cdot 10^{-3}) \\ \sigma_{c1}(3.5\cdot 10^{-3}) \end{pmatrix}$$

Compressive stress in part 1

$\sigma_{c1} =$

	0
0	15.964
1	27.011
2	33.026
3	37.814
4	41.173
5	42.859
6	41.966
7	38.422
8	31.832
9	21.5

$\cdot \mathrm{MPa}$

Compressive stress in part 1

$$\varepsilon_{c.el.v} := \frac{\sigma_{c1}}{E_c} =$$

	0
0	$5.079 \cdot 10^{-4}$
1	$8.594 \cdot 10^{-4}$
2	$1.051 \cdot 10^{-3}$
3	$1.203 \cdot 10^{-3}$
4	$1.31 \cdot 10^{-3}$
5	$1.364 \cdot 10^{-3}$
6	$1.335 \cdot 10^{-3}$
7	$1.222 \cdot 10^{-3}$
8	$1.013 \cdot 10^{-3}$
9	$6.841 \cdot 10^{-4}$

Elastic strain for curve 1

$0.4f_{cc} = 17.2 \cdot MPa$

Compressive stress at the limit for elasticity

$$\varepsilon_{ie1} := \varepsilon_c - \varepsilon_{c.el.v} =$$

	0
0	$3.934 \cdot 10^{-5}$
1	$1.406 \cdot 10^{-4}$
2	$2.492 \cdot 10^{-4}$
3	$3.969 \cdot 10^{-4}$
4	$5.9 \cdot 10^{-4}$
5	$8.364 \cdot 10^{-4}$
6	$1.265 \cdot 10^{-3}$
7	$1.678 \cdot 10^{-3}$
8	$2.187 \cdot 10^{-3}$
9	$2.816 \cdot 10^{-3}$

Inelastic strain for part 1

(the first strain is set to 0 and the stress at that point is set to the compressive stress at the limit for elasticity)

$$\varepsilon_c := \begin{pmatrix} 3.5 \\ 3.8 \\ 4.1 \\ 4.4 \\ 4.7 \\ 5.0 \\ 6.0 \\ 7.0 \\ 8.0 \\ 9.0 \end{pmatrix} \cdot 10^{-3}$$

Chosen measurment points for the compressive stress in part 2

$$\sigma_{c2}(\varepsilon_c) = \begin{array}{c|c} & 0 \\ \hline 0 & 21.5 \\ 1 & 13.245 \\ 2 & 9.222 \\ 3 & 6.881 \\ 4 & 5.372 \\ 5 & 4.33 \\ 6 & 2.447 \\ 7 & 1.586 \\ 8 & 1.116 \\ 9 & 0.83 \end{array} \cdot \mathrm{MPa}$$

Compressive stress in part 2

$$\varepsilon_{c.el.v} := \frac{\sigma_{c2}(\varepsilon_c)}{E_c} = \begin{array}{c|c} & 0 \\ \hline 0 & 6.841\cdot10^{-4} \\ 1 & 4.214\cdot10^{-4} \\ 2 & 2.934\cdot10^{-4} \\ 3 & 2.189\cdot10^{-4} \\ 4 & 1.709\cdot10^{-4} \\ 5 & 1.378\cdot10^{-4} \\ 6 & 7.784\cdot10^{-5} \\ 7 & 5.047\cdot10^{-5} \\ 8 & 3.551\cdot10^{-5} \\ 9 & 2.64\cdot10^{-5} \end{array}$$

Elastic strain in part 2

$$\varepsilon_{ie2} := \varepsilon_c - \varepsilon_{c.el.v} = \begin{array}{c|c} & 0 \\ \hline 0 & 2.816\cdot10^{-3} \\ 1 & 3.379\cdot10^{-3} \\ 2 & 3.807\cdot10^{-3} \\ 3 & 4.181\cdot10^{-3} \\ 4 & 4.529\cdot10^{-3} \\ 5 & 4.862\cdot10^{-3} \\ 6 & 5.922\cdot10^{-3} \\ 7 & 6.95\cdot10^{-3} \\ 8 & 7.964\cdot10^{-3} \\ 9 & 8.974\cdot10^{-3} \end{array}$$

Inelastic strain in part 2

Tensile strength

$$f_{ctm} := 0.3MPa \cdot \left(\frac{f_{ck}}{MPa}\right)^{\frac{2}{3}} = 3.21 \cdot MPa$$

Mean tensile strength

$$\varepsilon_{t.el} := \frac{f_{ctm}}{E_c} = 1.021 \times 10^{-4}$$

Elastic strain

$$\varepsilon := \begin{pmatrix} 0 \\ \varepsilon_{t.el} \\ 2 \cdot \varepsilon_{t.el} \\ 4\varepsilon_{t.el} \\ 6 \cdot \varepsilon_{t.el} \\ 10 \cdot \varepsilon_{t.el} \end{pmatrix} = \begin{pmatrix} 0 \\ 1.021 \times 10^{-4} \\ 2.043 \times 10^{-4} \\ 4.085 \times 10^{-4} \\ 6.128 \times 10^{-4} \\ 1.021 \times 10^{-3} \end{pmatrix}$$

According to (Carlson, et al. 2008) plastic part of the stress-strain curve for concrete in tension can be decided by calculating the strain at the maximum tensile strength and multiplying this by 10. These two values will indicate the start and end point for the plastic part of the curve and will give a curve that has a reasonable fracture energy. In they also mention that the shape of the curve between these two values is of little significance but if the curve has too much hang it will be hard to reach convergence. Due to this the values used in this model has been chosen so that the curve has a moderate hang

$$\sigma_t := \begin{pmatrix} 0 \\ f_{ctm} \\ \frac{f_{ctm}}{2} \\ \frac{f_{ctm}}{5} \\ \frac{f_{ctm}}{16.5} \\ \frac{f_{ctm}}{100} \end{pmatrix} = \begin{pmatrix} 0 \\ 3.21 \\ 1.605 \\ 0.642 \\ 0.195 \\ 0.032 \end{pmatrix} \cdot MPa$$

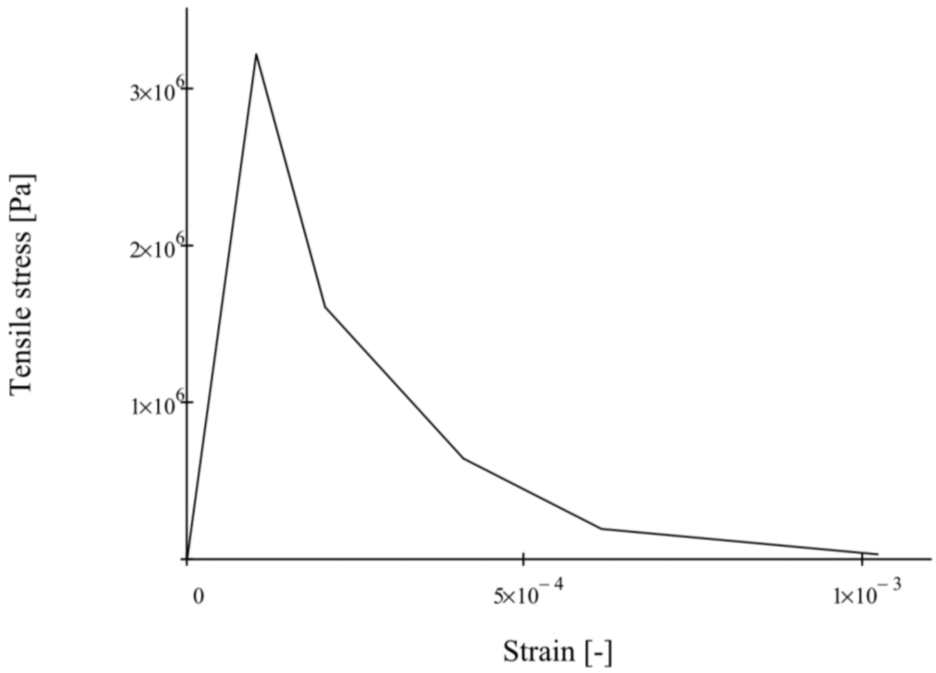

$$G_F := 73\left(\frac{f_{cm}}{MPa}\right)^{0.18}\cdot\frac{N}{m} = 143.664\cdot\frac{N}{m}$$ Fracture energy

Reinforcement

$f_y := 500\text{MPa}$ Yield strength

$E_s := 200\text{GPa}$ Youngs modulus of elasticity

$\varepsilon_y := \frac{f_y}{E_s} = 2.5 \times 10^{-3}$ Yield strain

Indata for bi-linear stress strain curve

$$\varepsilon := \begin{pmatrix} 0 \\ \varepsilon_y \\ 50 \times 10^{-3} \end{pmatrix}$$

$$\sigma := \begin{pmatrix} 0 \\ f_y \\ f_y \end{pmatrix}$$

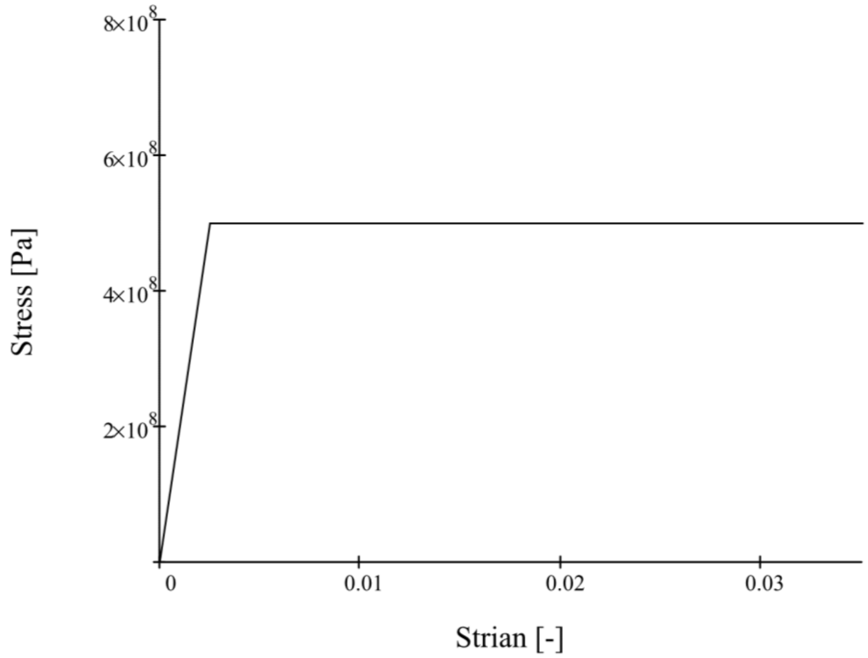

Steel

S355

$f_y := 355MPa$		Yield strength
$f_u := 490MPa$	t < 16mm	Ultimate strength
$E_s := 210GPa$		Youngs modulus of elasticity
$E_h := 3500MPa$		Tagent modulus for the strain hardening curve in the point where strain hardening begins
$\varepsilon_y := \frac{f_y}{E_s} = 1.69 \times 10^{-3}$		Yield strain

$$\varepsilon_h := 0.025 - 5 \cdot \frac{f_u}{E_s} = 0.013$$

$$\varepsilon_3 := 0.02 + 50 \cdot \frac{f_u - f_y}{E_s} = 0.052$$

Non-linear strength of steel

Part 1

$$\sigma_{s1}(\varepsilon) := E_s \cdot \varepsilon$$ if $\varepsilon<\varepsilon_y$

Part 2

$$\sigma_{s2}(\varepsilon) := f_y$$ if $\varepsilon_y<\varepsilon<\varepsilon_h$

Part 3

$$\sigma_{s3}(\varepsilon) := f_y + E_h \cdot (\varepsilon - \varepsilon_h)\left[1 - E_h \cdot \frac{\varepsilon - \varepsilon_h}{4 \cdot (f_u - f_y)}\right]$$ if $\varepsilon>\varepsilon_h$

$$\varepsilon_1 := 0, 1 \cdot 10^{-5} .. \varepsilon_y$$ Range for part 1

$$\varepsilon_2 := \varepsilon_y, \left(\varepsilon_y + 1 \cdot 10^{-5}\right) .. \varepsilon_h$$ Range for part 2

$$\varepsilon_3 := \varepsilon_h, \left(\varepsilon_h + 1 \cdot 10^{-5}\right) .. 0.5$$ Range for part 3

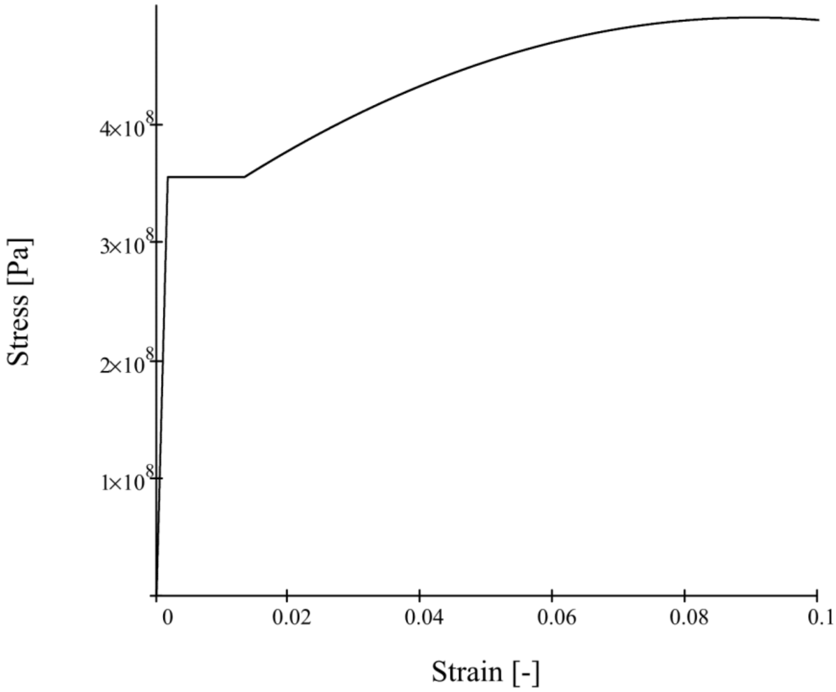

$$\varepsilon := \begin{pmatrix} 0.015 \\ 0.03 \\ 0.06 \\ 0.08 \\ 0.1 \\ 0.12 \\ 0.15 \end{pmatrix}$$

Chosen measurment points for the stress in part 3

$$\sigma_{s3} := \begin{pmatrix} \sigma_{s3}(0.015) \\ \sigma_{s3}(0.03) \\ \sigma_{s3}(0.06) \\ \sigma_{s3}(0.08) \\ \sigma_{s3}(0.1) \\ \sigma_{s3}(0.12) \\ \sigma_{s3}(0.15) \end{pmatrix} = \begin{pmatrix} 360.77 \\ 407.032 \\ 468.93 \\ 487.51 \\ 487.942 \\ 470.226 \\ 409.624 \end{pmatrix} \cdot \text{MPa}$$

Stress in part 3 of the curve

$$\varepsilon_{ie} := \varepsilon - \varepsilon_y = \begin{pmatrix} 0.013 \\ 0.028 \\ 0.058 \\ 0.078 \\ 0.098 \\ 0.118 \\ 0.148 \end{pmatrix}$$

Inelastic strain

Appendix F.

Force-Displacement

arc length	reaction force [N]	applied displacement [m]	energy (area under graph) [Nm]	energy (area under graph) [Nm]	internal energy (ALLIE) [Nm]
	(at displacement RP)	(at displacement RP)	(Riemannsum of values to left)	(total to current timestep)	(abaqus calculated for whole model)
0	0	0	0	0	0
0.000625	1.89E+04	0.000944285	8.905787906	8.9058	8.89082
0.00125	3.77E+04	0.00188847	26.71302365	35.619	35.5583
0.0021875	6.60E+04	0.00330447	73.4363796	109.055	108.87
0.00359375	1.08E+05	0.00542764	185.1392563	294.194	293.692
0.00570313	1.72E+05	0.00860968	445.9756342	740.170	738.901
0.00886719	2.67E+05	0.0133739	1045.381827	1785.55	1782.48
0.0136133	4.09E+05	0.0204907	2404.111974	4189.66	4182.47
0.0207324	6.18E+05	0.0310704	5433.37421	9623.04	9606.68
0.0314111	9.20E+05	0.0465792	11932.23809	21555.3	21519.6
0.0420898	1.20E+06	0.0613955	15699.78115	37255.1	37190.9
0.0527686	1.45E+06	0.0753136	18411.69777	55666.8	55565
0.0634473	1.66E+06	0.0882681	20124.81575	75791.6	75643.5
0.074126	1.84E+06	0.100248	20963.44731	96755.0	96552.7
0.0848047	1.99E+06	0.11134	21228.59058	117983.6	117722
0.0954834	2.11E+06	0.121711	21256.71273	139240.3	138911
0.106162	2.21E+06	0.131544	21260.56845	160500.9	160101
0.116841	2.30E+06	0.141015	21368.51756	181869.4	181393
0.12752	2.37E+06	0.150266	21608.57831	203478.0	202922
0.138198	2.44E+06	0.159405	21971.61824	225449.6	224812
0.148877	2.49E+06	0.168515	22444.26145	247893.9	247172
0.159556	2.54E+06	0.177654	22996.19153	270890.1	270083
0.170234	2.59E+06	0.186864	23607.39435	294497.5	293604
0.180913	2.63E+06	0.196173	24255.71658	318753.2	317774
0.191592	2.66E+06	0.205603	24934.9003	343688.1	342623
0.202271	2.70E+06	0.215158	25599.70822	369287.8	368139
0.212949	2.72E+06	0.224835	26220.50889	395508.3	394276
0.223628	2.75E+06	0.23468	26931.53898	422439.8	4.21E+05
0.234307	2.77E+06	0.244716	27684.60708	450124.4	4.49E+05
0.244985	2.79E+06	0.254947	28418.85332	478543.3	4.77E+05
0.255664	2.80E+06	0.265394	29179.82911	507723.1	5.06E+05
0.266343	2.81E+06	0.276068	29960.58375	537683.7	5.36E+05
0.277021	2.83E+06	0.286971	30746.24194	568429.9	5.67E+05
0.2877	2.84E+06	0.298102	31529.94888	599959.9	5.98E+05

0.298379	2.85E+06	0.309447	32275.6174	632235.5	6.30E+05
0.309058	2.86E+06	0.320989	32969.1459	665204.7	6.63E+05
0.319736	2.87E+06	0.332731	33658.26687	698862.9	6.97E+05
0.330415	2.88E+06	0.344684	34361.05004	733224.0	7.31E+05
0.341094	2.88E+06	0.356811	34943.7686	768167.7	7.66E+05
0.351772	2.89E+06	0.369108	35505.1281	803672.9	8.02E+05
0.362451	2.89E+06	0.381558	36002.0385	839674.9	8.38E+05
0.37313	2.90E+06	0.394172	36516.39474	876191.3	8.74E+05
0.383809	2.90E+06	0.406938	36991.46373	913182.8	9.11E+05
0.394487	2.90E+06	0.419851	37450.79912	950633.6	9.48E+05
0.405166	2.90E+06	0.43285	37728.10262	988361.7	9.86E+05
0.415845	2.90E+06	0.445968	38095.65585	1026457.3	1.02E+06
0.426523	2.91E+06	0.4592	38445.04672	1064902.4	1.06E+06
0.437202	2.91E+06	0.472576	38879.41728	1103781.8	1.10E+06
0.447881	2.91E+06	0.48608	39267.80896	1143049.6	1.14E+06
0.45856	2.91E+06	0.499725	39695.28352	1182744.9	1.18E+06
0.469238	2.91E+06	0.513508	40115.35259	1222860.2	1.22E+06
0.479917	2.91E+06	0.527424	40518.10392	1263378.3	1.26E+06
0.490596	2.91E+06	0.541465	40894.34229	1304272.7	1.30E+06
0.501274	2.91E+06	0.55561	41209.1943	1345481.9	1.34E+06
0.511953	2.91E+06	0.569858	41520.59548	1387002.5	1.38E+06
0.522632	2.92E+06	0.584225	41879.5895	1428882.1	1.43E+06
0.533311	2.92E+06	0.598704	42220.8364	1471102.9	1.47E+06
0.543989	2.92E+06	0.613289	42545.46595	1513648.4	1.51E+06
0.554668	2.92E+06	0.627975	42855.73061	1556504.1	1.55E+06
0.565347	2.92E+06	0.642743	43110.08104	1599614.2	1.60E+06
0.576025	2.92E+06	0.657569	43291.10457	1642905.3	1.64E+06
0.586704	2.92E+06	0.672488	43572.05843	1686477.3	1.68E+06
0.597383	2.92E+06	0.687485	43809.01145	1730286.3	1.73E+06
0.608062	2.92E+06	0.702561	44047.32306	1774333.7	1.77E+06
0.61874	2.92E+06	0.717721	44297.0652	1818630.7	1.82E+06
0.629419	2.92E+06	0.732956	44515.60355	1863146.3	1.86E+06
0.640098	2.92E+06	0.748274	44755.51968	1907901.9	1.91E+06
0.650776	2.92E+06	0.763674	44994.796	1952896.7	1.95E+06
0.661455	2.92E+06	0.779152	45224.93603	1998121.6	2.00E+06
0.672134	2.92E+06	0.794706	45451.74326	2043573.3	2.04E+06
0.682813	2.92E+06	0.810334	45675.09606	2089248.4	2.09E+06
0.693491	2.92E+06	0.826031	45886.41222	2135134.8	2.13E+06
0.70417	2.92E+06	0.841788	46073.54679	2181208.4	2.18E+06
0.714849	2.93E+06	0.857611	46279.90155	2227488.3	2.23E+06
0.725527	2.93E+06	0.873502	46494.36453	2273982.7	2.27E+06
0.736206	2.93E+06	0.889459	46705.58051	2320688.2	2.32E+06
0.746885	2.93E+06	0.905482	46918.86906	2367607.1	2.37E+06
0.757563	2.93E+06	0.921564	47113.18392	2414720.3	2.41E+06
0.768242	2.93E+06	0.937706	47311.31419	2462031.6	2.46E+06

0.778921	2.93E+06	0.953919	47541.94735	2509573.5	2.51E+06
0.7896	2.93E+06	0.970199	47760.7174	2557334.3	2.56E+06
0.800278	2.94E+06	0.986538	47955.53687	2605289.8	2.61E+06
0.810957	2.94E+06	1.00294	48162.34074	2653452.1	2.66E+06
0.821636	2.94E+06	1.01941	48384.5778	2701836.7	2.70E+06
0.832314	2.94E+06	1.03593	48553.6842	2750390.4	2.75E+06
0.842993	2.94E+06	1.05252	48780.9042	2799171.3	2.80E+06
0.853672	2.94E+06	1.06919	49037.22215	2848208.5	2.85E+06
0.864351	2.94E+06	1.08592	49233.96415	2897442.5	2.90E+06
0.875029	2.94E+06	1.10272	49458.864	2946901.4	2.95E+06
0.885708	2.95E+06	1.1196	49711.7688	2996613.1	3.00E+06
0.896387	2.95E+06	1.13654	49903.7154	3046516.8	3.05E+06
0.907065	2.95E+06	1.15357	50181.36435	3096698.2	3.10E+06
0.917744	2.95E+06	1.17066	50366.4517	3147064.7	3.15E+06
0.928423	2.95E+06	1.18782	50574.81	3197639.5	3.20E+06
0.939102	2.95E+06	1.20505	50777.41305	3248416.9	3.25E+06
0.94978	2.95E+06	1.22236	51004.9536	3299421.8	3.31E+06
0.960459	2.95E+06	1.23973	51168.3723	3350590.2	3.36E+06
0.971138	2.94E+06	1.25718	51385.5385	3401975.7	3.41E+06
0.981816	2.94E+06	1.2747	51569.5944	3453545.3	3.46E+06
0.992495	2.94E+06	1.29228	51720.9753	3505266.3	3.51E+06
1.00317	2.94E+06	1.30994	51927.8172	3557194.1	3.57E+06
1.01385	2.94E+06	1.32766	52072.878	3609267.0	3.62E+06
1.02453	2.94E+06	1.34545	52244.2488	3661511.3	3.67E+06
1.03521	2.93E+06	1.3633	52382.69925	3713894.0	3.73E+06
1.04589	2.93E+06	1.38122	52546.9952	3766441.0	3.78E+06
1.05657	2.93E+06	1.39918	52619.3876	3819060.3	3.83E+06
1.06725	2.93E+06	1.41719	52717.34115	3871777.7	3.89E+06
1.07792	2.92E+06	1.43527	52870.8016	3924648.5	3.94E+06
1.0886	2.92E+06	1.4534	52962.9877	3977611.5	3.99E+06
1.09928	2.92E+06	1.47157	53023.5123	4030635.0	4.05E+06
1.10996	2.91E+06	1.4898	53139.99425	4083775.0	4.10E+06
1.12064	2.91E+06	1.50806	53166.3638	4136941.3	4.15E+06
1.13132	2.91E+06	1.52638	53277.3996	4190218.7	4.21E+06
1.142	2.90E+06	1.54473	53298.95125	4243517.7	4.26E+06
1.15268	2.90E+06	1.56313	53376.468	4296894.2	4.32E+06
1.16335	2.90E+06	1.58158	53451.58725	4350345.7	4.37E+06
1.17403	2.89E+06	1.60006	53466.1512	4403811.9	4.43E+06
1.18471	2.89E+06	1.61857	53478.62925	4457290.5	4.48E+06
1.19539	2.88E+06	1.63712	53518.51225	4510809.0	4.53E+06
1.20607	2.88E+06	1.65571	53556.95345	4564366.0	4.59E+06
1.21675	2.87E+06	1.67433	53565.3643	4617931.4	4.64E+06
1.22743	2.87E+06	1.69298	53572.96425	4671504.3	4.70E+06
1.23811	2.87E+06	1.71167	53608.527	4725112.8	4.75E+06
1.24878	2.86E+06	1.73038	53586.09485	4778698.9	4.81E+06

1.25946	2.86E+06	1.74913	53620.6875	4832319.6	4.86E+06
1.27014	2.85E+06	1.76791	53626.3839	4885946.0	4.92E+06
1.28082	2.85E+06	1.78671	53603.312	4939549.3	4.97E+06
1.2915	2.84E+06	1.80555	53637.009	4993186.3	5.03E+06
1.30218	2.84E+06	1.82441	53613.6049	5046799.9	5.08E+06
1.31286	2.84E+06	1.8433	53618.98165	5100418.9	5.14E+06
1.32354	2.83E+06	1.86222	53624.5776	5154043.5	5.19E+06
1.33421	2.83E+06	1.88117	53630.2055	5207673.7	5.25E+06
1.34489	2.82E+06	1.90015	53636.0565	5261309.8	5.30E+06
1.35557	2.82E+06	1.91915	53613.915	5314923.7	5.36E+06
1.36625	2.82E+06	1.93818	53620.2601	5368543.9	5.41E+06
1.37693	2.81E+06	1.95724	53626.9301	5422170.9	5.47E+06
1.38761	2.81E+06	1.97632	53605.8324	5475776.7	5.52E+06
1.39829	2.80E+06	1.99543	53613.00945	5529389.7	5.58E+06
1.40896	2.80E+06	2.01456	53592.40805	5582982.1	5.63E+06
1.41964	2.80E+06	2.03372	53600.0042	5636582.1	5.69E+06
1.43032	2.79E+06	2.0529	53579.4259	5690161.5	5.74E+06
1.441	2.79E+06	2.07211	53586.77525	5743748.3	5.80E+06
1.45168	2.78E+06	2.09135	53594.0782	5797342.4	5.85E+06
1.46236	2.78E+06	2.11061	53573.4234	5850915.8	5.91E+06
1.47304	2.78E+06	2.12989	53552.8992	5904468.7	5.96E+06
1.48372	2.77E+06	2.1492	53560.147	5958028.9	6.02E+06
1.49439	2.77E+06	2.16853	53539.75075	6011568.6	6.07E+06
1.50507	2.76E+06	2.18788	53519.68125	6065088.3	6.13E+06
1.51575	2.76E+06	2.20726	53527.2693	6118615.6	6.18E+06
1.52643	2.76E+06	2.22666	53507.334	6172122.9	6.24E+06
1.53711	2.75E+06	2.24608	53487.7292	6225610.6	6.29E+06
1.54779	2.75E+06	2.26552	53468.6508	6279079.3	6.35E+06
1.55847	2.74E+06	2.28498	53450.1009	6332529.4	6.40E+06
1.56915	2.74E+06	2.30446	53431.7894	6385961.2	6.46E+06
1.57982	2.74E+06	2.32396	53413.5225	6439374.7	6.51E+06
1.5905	2.73E+06	2.34348	53395.3008	6492770.0	6.57E+06
1.60118	2.73E+06	2.36303	53404.735	6546174.7	6.62E+06
1.61186	2.73E+06	2.38259	53359.8756	6599534.6	6.68E+06
1.62254	2.72E+06	2.40218	53369.8206	6652904.4	6.73E+06
1.63322	2.72E+06	2.42178	53325.622	6706230.1	6.79E+06
1.6439	2.72E+06	2.4414	53309.0115	6759539.1	6.85E+06
1.65458	2.71E+06	2.46104	53292.7472	6812831.8	6.90E+06
1.66525	2.71E+06	2.4807	53276.9289	6866108.7	6.96E+06
1.67593	2.70E+06	2.50037	53234.39625	6919343.1	7.01E+06
1.68661	2.70E+06	2.52007	53246.2435	6972589.4	7.07E+06
1.69729	2.70E+06	2.53978	53204.28705	7025793.7	7.12E+06
1.70797	2.69E+06	2.55951	53189.61375	7078983.3	7.18E+06
1.71865	2.69E+06	2.57926	53175.19625	7132158.5	7.23E+06
1.72933	2.69E+06	2.59903	53160.83805	7185319.3	7.29E+06

1.74	2.68E+06	2.61881	53119.5856	7238438.9	7.34E+06
1.75068	2.68E+06	2.6386	53078.5611	7291517.5	7.40E+06
1.76136	2.68E+06	2.65841	53064.55175	7344582.0	7.46E+06
1.77204	2.67E+06	2.67823	53023.7523	7397605.8	7.51E+06
1.78272	2.67E+06	2.69807	53009.9008	7450615.7	7.57E+06
1.7934	2.67E+06	2.71791	52942.9408	7503558.6	7.62E+06
1.80408	2.66E+06	2.73778	52956.23245	7556514.8	7.68E+06
1.81476	2.66E+06	2.75765	52889.66795	7609404.5	7.73E+06
1.82543	2.66E+06	2.77754	52876.3716	7662280.9	7.79E+06
1.83611	2.65E+06	2.79744	52836.689	7715117.6	7.84E+06
1.84679	2.65E+06	2.81735	52797.338	7767914.9	7.90E+06
1.85747	2.65E+06	2.83728	52784.605	7820699.5	7.95E+06
1.86815	2.64E+06	2.85722	52745.3877	7873444.9	8.01E+06
1.87883	2.64E+06	2.87718	52732.7232	7926177.6	8.07E+06
1.88951	2.64E+06	2.89715	52693.8405	7978871.5	8.12E+06
1.90019	2.63E+06	2.91714	52681.54605	8031553.0	8.18E+06
1.91086	2.63E+06	2.93714	52643.1	8084196.1	8.23E+06
1.92154	2.63E+06	2.95715	52604.8893	8136801.0	8.29E+06
1.93222	2.62E+06	2.97718	52593.27175	8189394.3	8.34E+06
1.9429	2.62E+06	2.99721	52529.4762	8241923.7	8.40E+06
1.95358	2.62E+06	3.01727	52544.5622	8294468.3	8.45E+06
1.96426	2.61E+06	3.03733	52481.3732	8346949.7	8.51E+06
1.97494	2.61E+06	3.0574	52444.7163	8399394.4	8.57E+06
1.98562	2.61E+06	3.07749	52434.39775	8451828.8	8.62E+06
1.99629	2.61E+06	3.09759	52398.087	8504226.9	8.68E+06
2.00697	2.60E+06	3.1177	52361.8147	8556588.7	8.73E+06
2.01765	2.60E+06	3.13781	52299.57425	8608888.3	8.79E+06
2.02833	2.60E+06	3.15794	52289.4867	8661177.8	8.84E+06
2.03901	2.59E+06	3.17808	52253.5321	8713431.3	8.90E+06
2.04969	2.59E+06	3.19823	52217.81825	8765649.1	8.95E+06
2.06037	2.59E+06	3.21839	52182.3456	8817831.5	9.01E+06
2.07104	2.58E+06	3.23857	52172.8675	8870004.3	9.07E+06
2.08172	2.58E+06	3.25875	52111.6212	8922115.9	9.12E+06
2.0924	2.58E+06	3.27895	52101.86	8974217.8	9.18E+06
2.10308	2.57E+06	3.29915	52040.654	9026258.5	9.23E+06
2.11376	2.57E+06	3.31937	52031.2161	9078289.7	9.29E+06
2.12444	2.57E+06	3.33959	51970.455	9130260.1	9.34E+06
2.13512	2.57E+06	3.35982	51935.56865	9182195.7	9.40E+06
2.1458	2.56E+06	3.38006	51900.926	9234096.6	9.45E+06
2.15647	2.56E+06	3.40031	51866.42625	9285963.0	9.51E+06
2.16715	2.56E+06	3.42057	51832.0697	9337795.1	9.57E+06
2.17783	2.55E+06	3.44083	51772.3027	9389567.4	9.62E+06
2.18851	2.55E+06	3.46111	51763.686	9441331.1	9.68E+06
2.19919	2.55E+06	3.48139	51704.1642	9493035.3	9.73E+06
2.20987	2.55E+06	3.50168	51670.514	9544705.8	9.79E+06

2.22055	2.54E+06	3.52198	51637.11	9596342.9	9.84E+06
2.22322	2.54E+06	3.52706	12912.8266	9609255.7	9.86E+06
2.22589	2.54E+06	3.53214	12909.1944	9622164.9	9.87E+06
2.22655	2.54E+06	3.53341	3226.73345	9625391.7	9.87E+06
2.22722	2.54E+06	3.53468	3226.5112	9628618.2	9.88E+06
2.22789	2.54E+06	3.53595	3226.2826	9631844.4	9.88E+06
2.22856	2.54E+06	3.53722	3226.054	9635070.5	9.88E+06
2.22922	2.54E+06	3.53849	3225.83175	9638296.3	9.89E+06
2.22989	2.54E+06	3.53976	3225.6095	9641521.9	9.89E+06
2.23056	2.54E+06	3.54103	3225.3809	9644747.3	9.89E+06
2.23123	2.54E+06	3.5423	3225.15865	9647972.5	9.90E+06
2.23189	2.54E+06	3.54357	3224.9364	9651197.4	9.90E+06
2.23193	2.54E+06	3.54359	50.7834	9651248.2	9.90E+06
2.23198	2.54E+06	3.54361	50.7808	9651299.0	9.90E+06
2.23199	2.54E+06	3.54362	25.3895	9651324.4	9.90E+06
Total progress	**Total reactionforce**	**Total deformation**		**Total energy**	**Total energy**
(1.00 = 6m)	**(at displacement RP)**	**(at displacement RP)**		**(calculated from DisplacementRP values)**	**(calculated from abaqus values):**

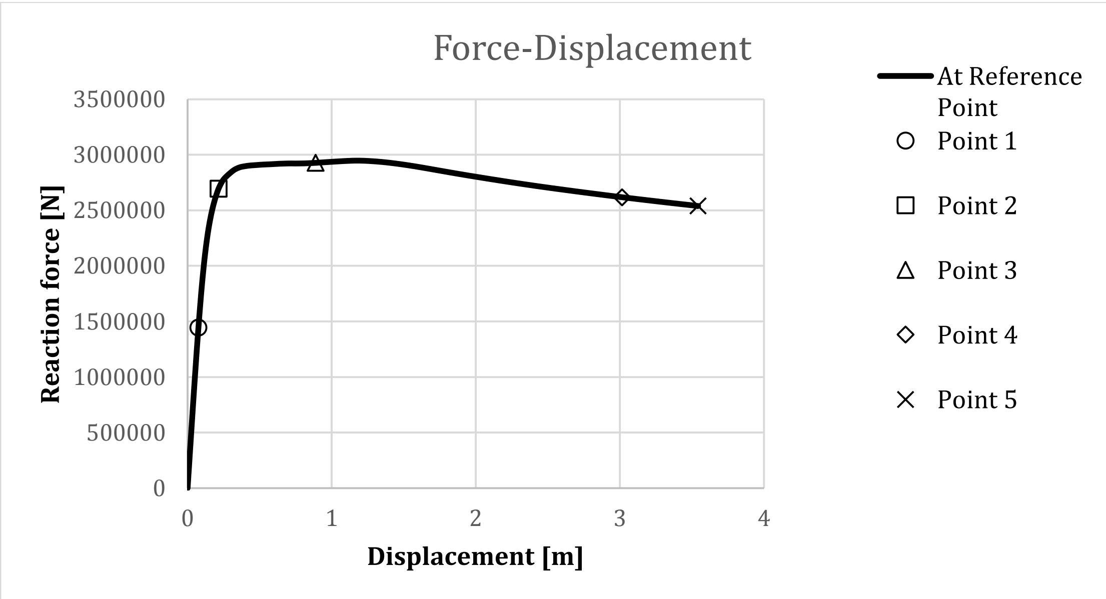

Figure F.1

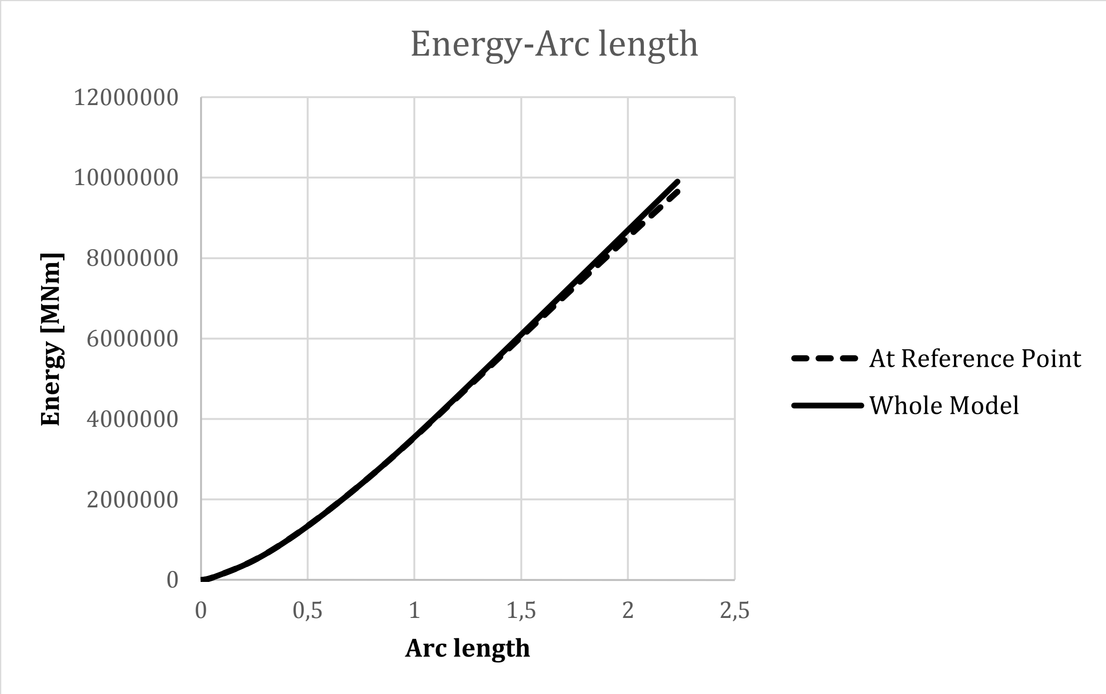

Figure F.2 The absorbed energy by the protective pier calculated with ALLIE (solid line) and by hand (dashed line).

Appendix G.
Clay springs

Stress-strain

<u>Arc length 0.0528</u>

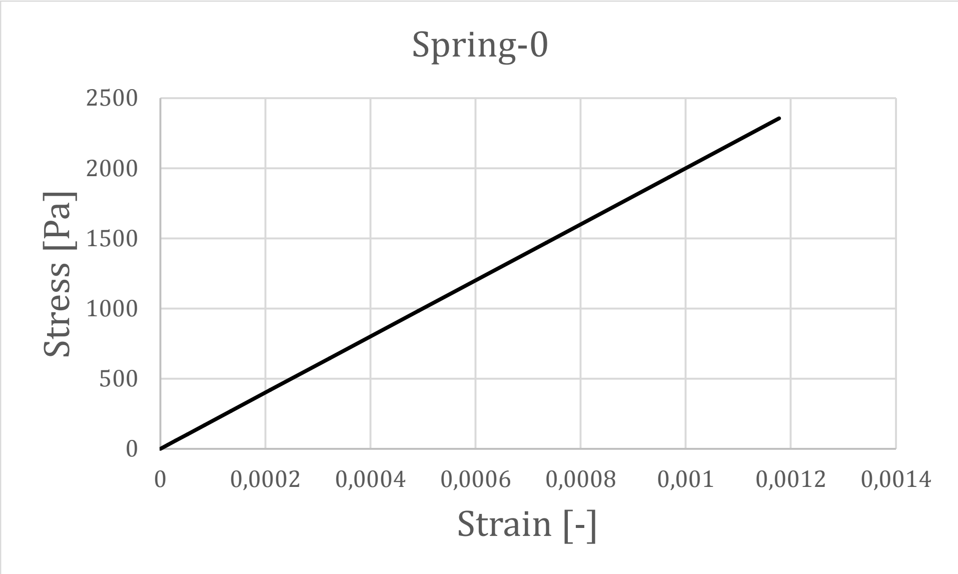

Figure G.1 Stress-strain relationship for Spring-0 at Arc length 0.0528.

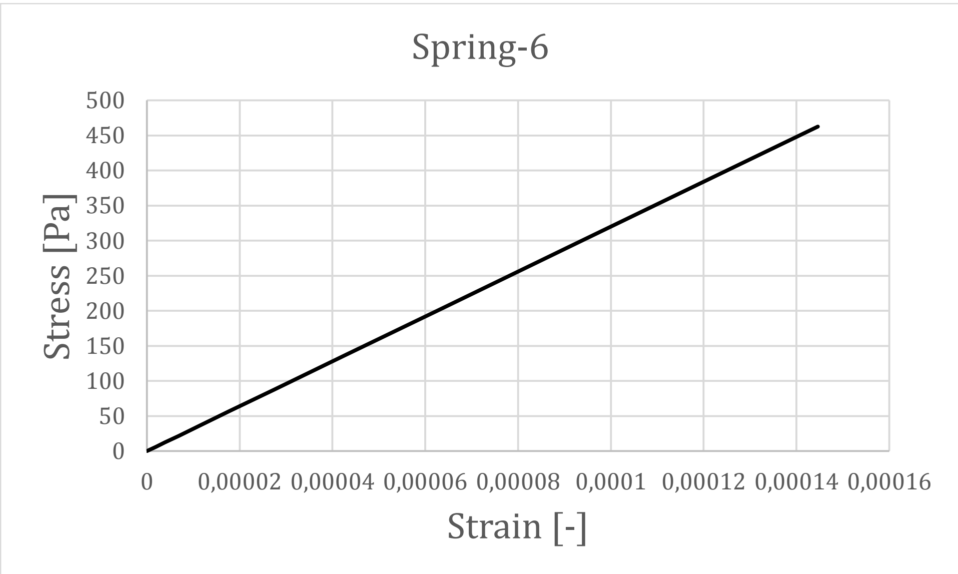

Figure G.2 Stress-strain relationship for Spring-6 at Arc length 0.0528.

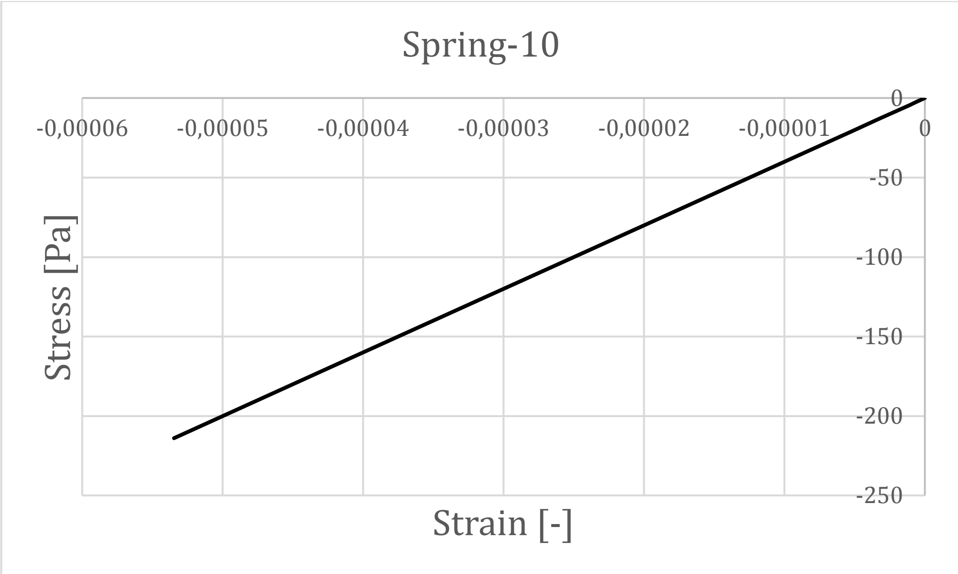

Figure G.3 Stress-strain relationship for Spring-10 at Arc length 0.0528.

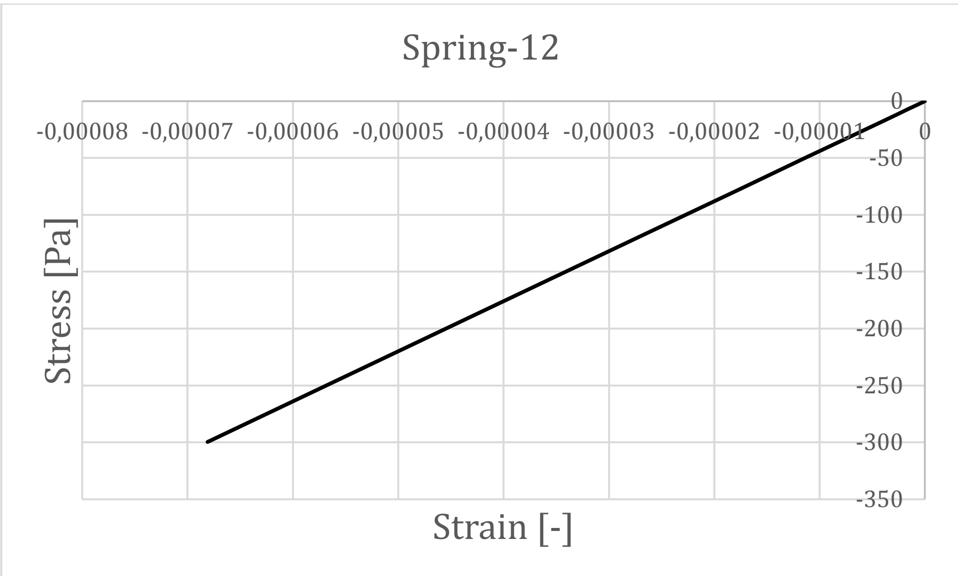

Figure G.4 Stress-strain relationship for Spring-12 at Arc length 0.0528.

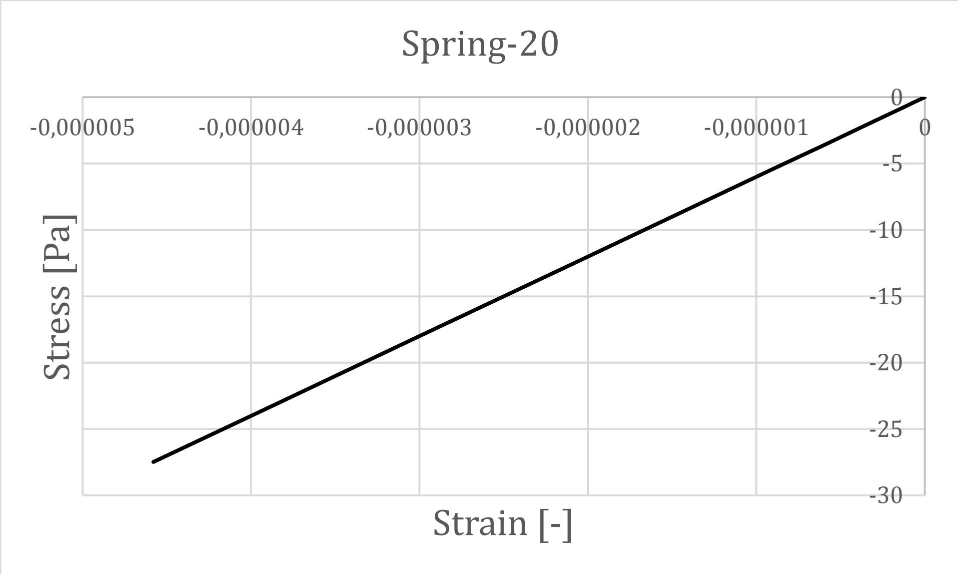

Figure G.5 Stress-strain relationship for Spring-20 at Arc length 0.0528.

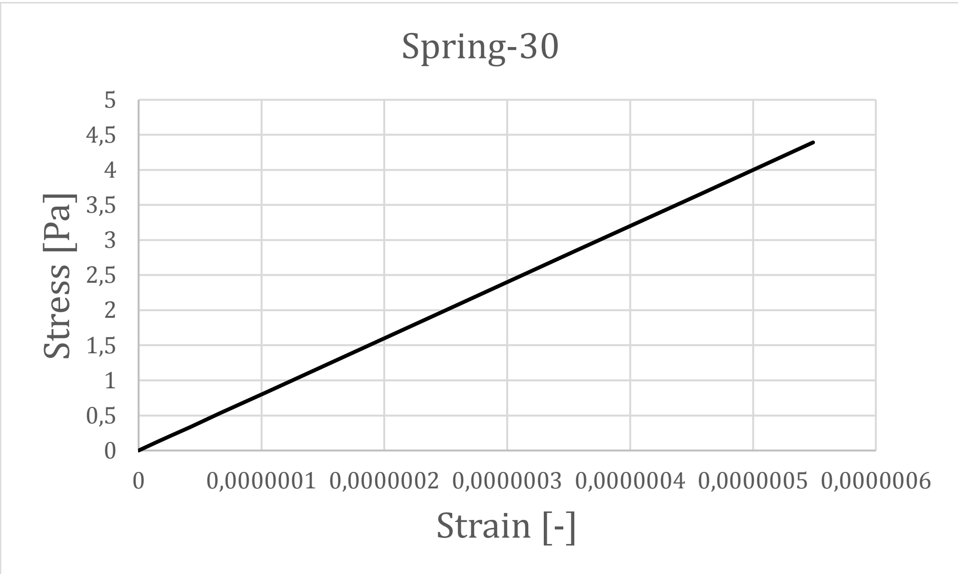

Figure G.6 Stress-strain relationship for Spring-30 at Arc length 0.0528.

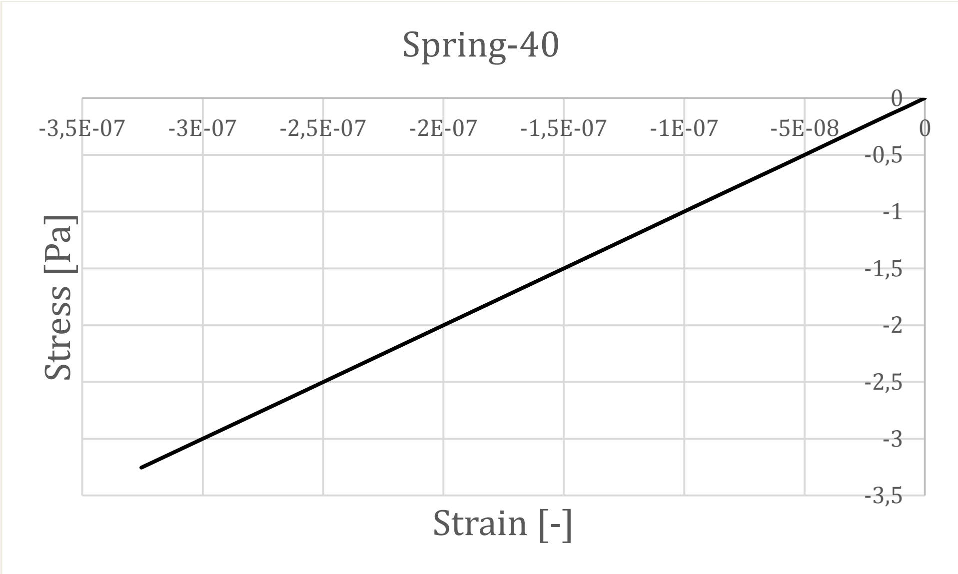

Figure G.7 Stress-strain relationship for Spring-40 at Arc length 0.0528.

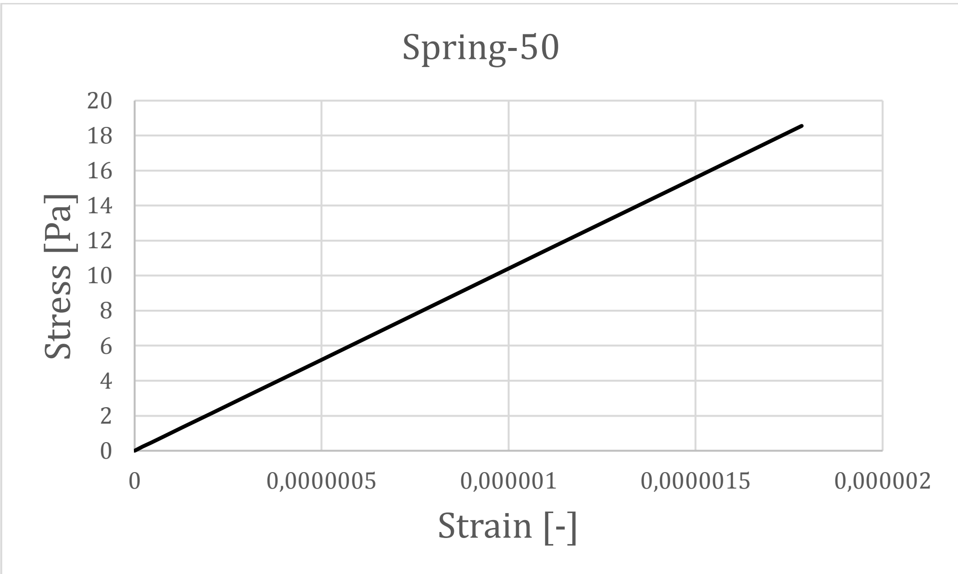

Figure G.8 Stress-strain relationship for Spring-50 at Arc length 0.0528.‘

Arc length 0.2023

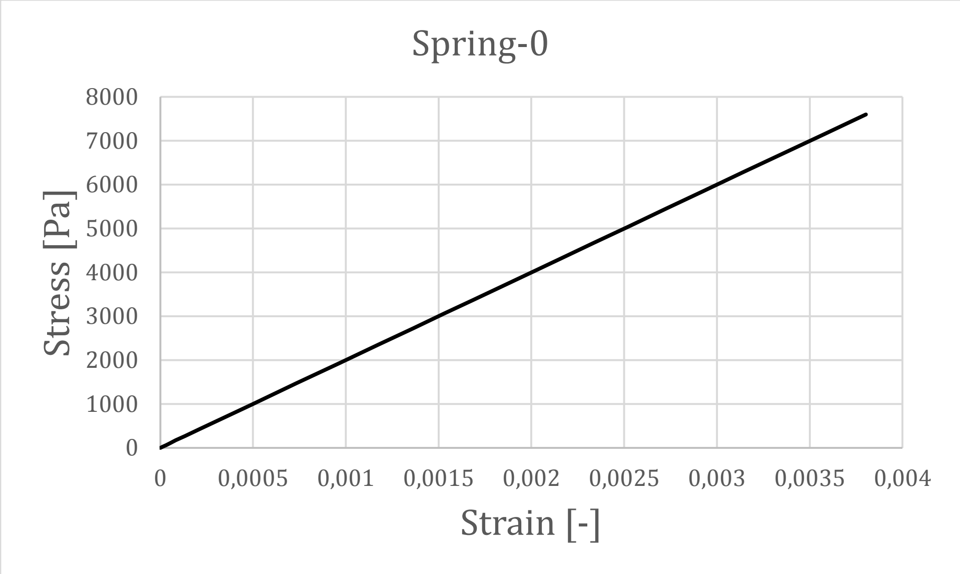

Figure G.9 Stress-strain relationship for Spring-0 at Arc length 0.2023.

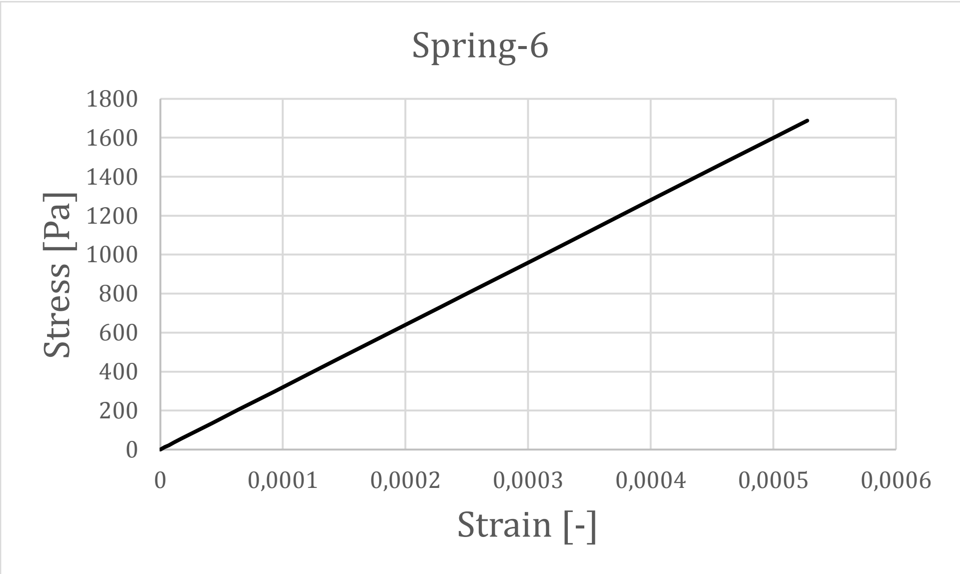

Figure G.10 Stress-strain relationship for Spring-6 at Arc length 0.2023.

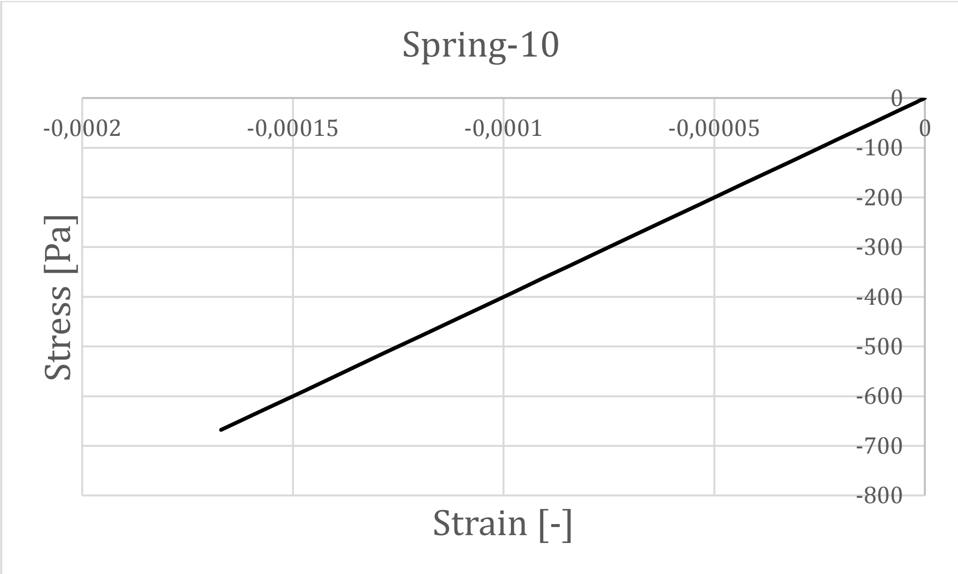

Figure G.11 Stress-strain relationship for Spring-10 at Arc length 0.2023.

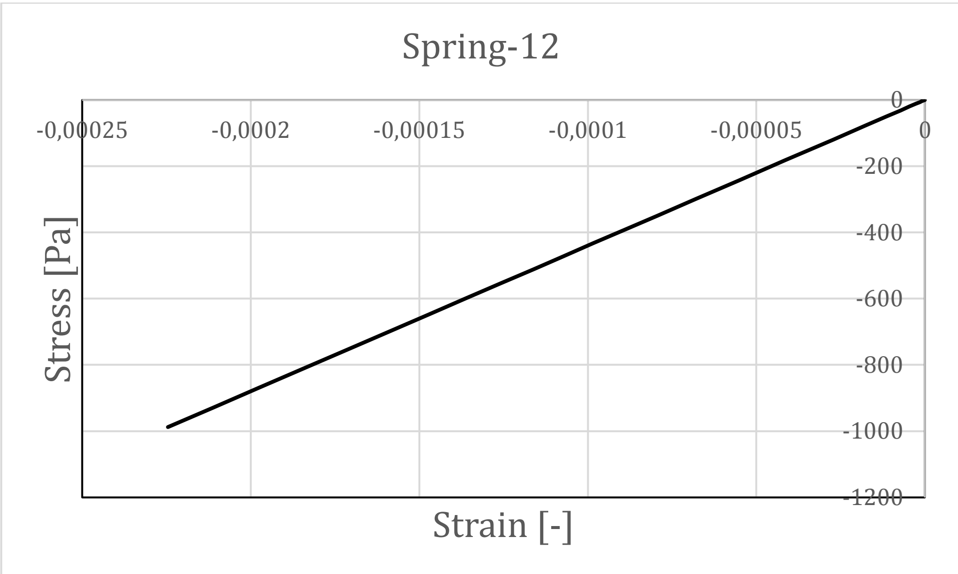

Figure G.12 Stress-strain relationship for Spring-12 at Arc length 0.2023.

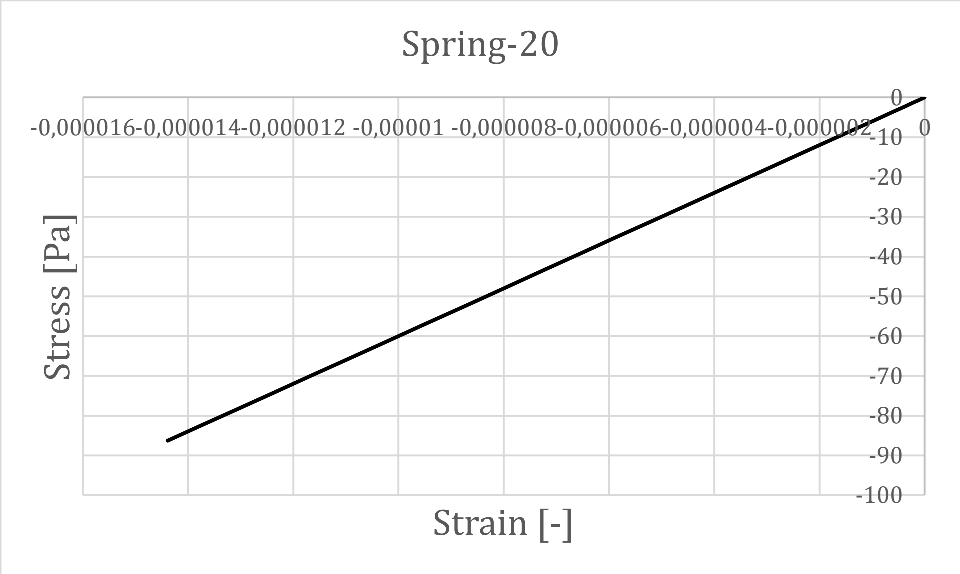

Figure G.13 Stress-strain relationship for Spring-20 at Arc length 0.2023.

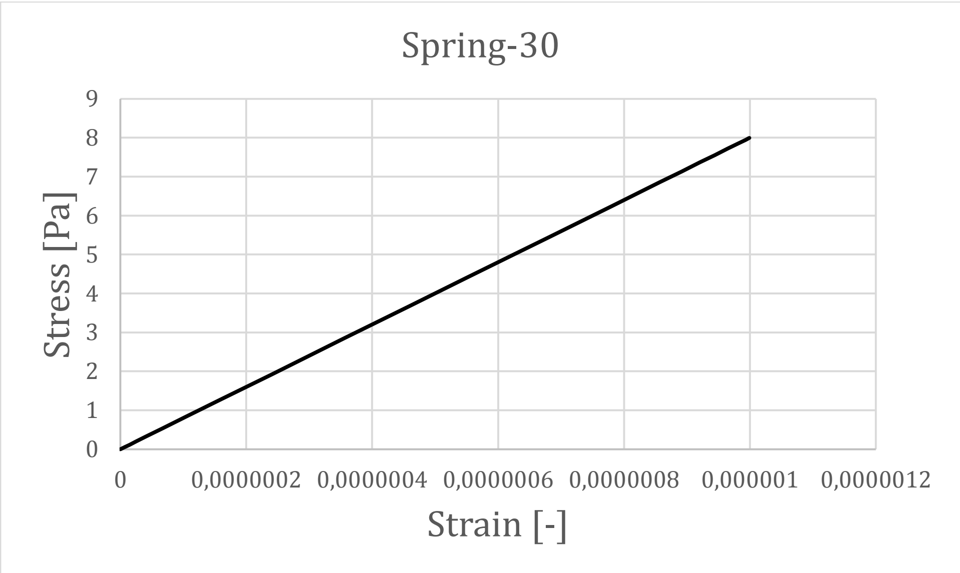

Figure G.14 Stress-strain relationship for Spring-30 at Arc length 0.2023.

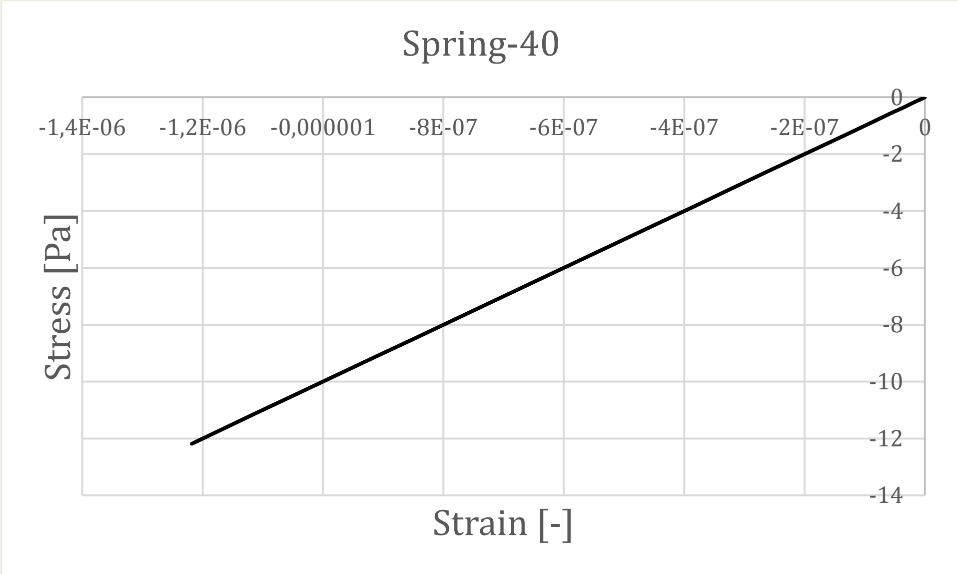

Figure G.15 Stress-strain relationship for Spring-40 at Arc length 0.2023.

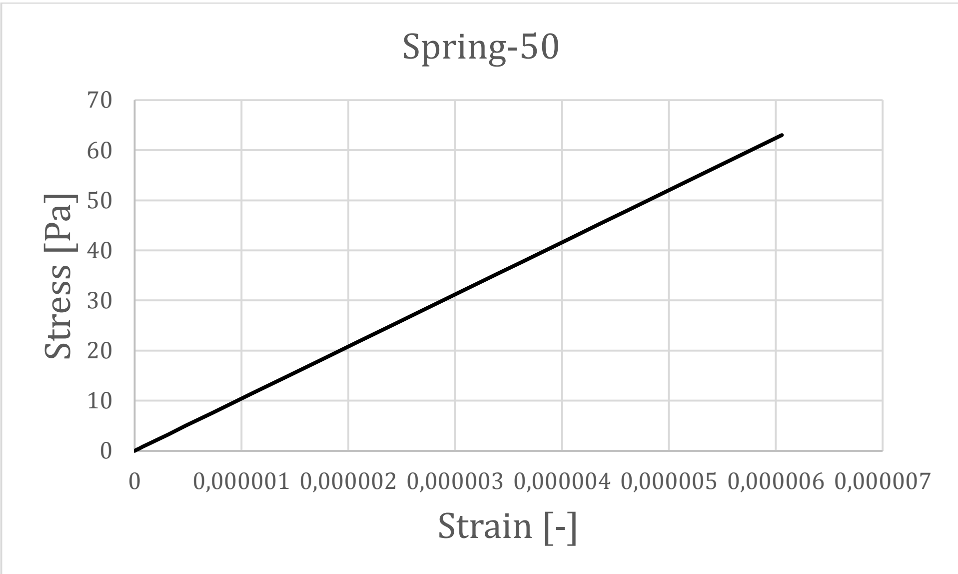

Figure G.16 Stress-strain relationship for Spring-50 at Arc length 0.2023.

Arc length 0.7363

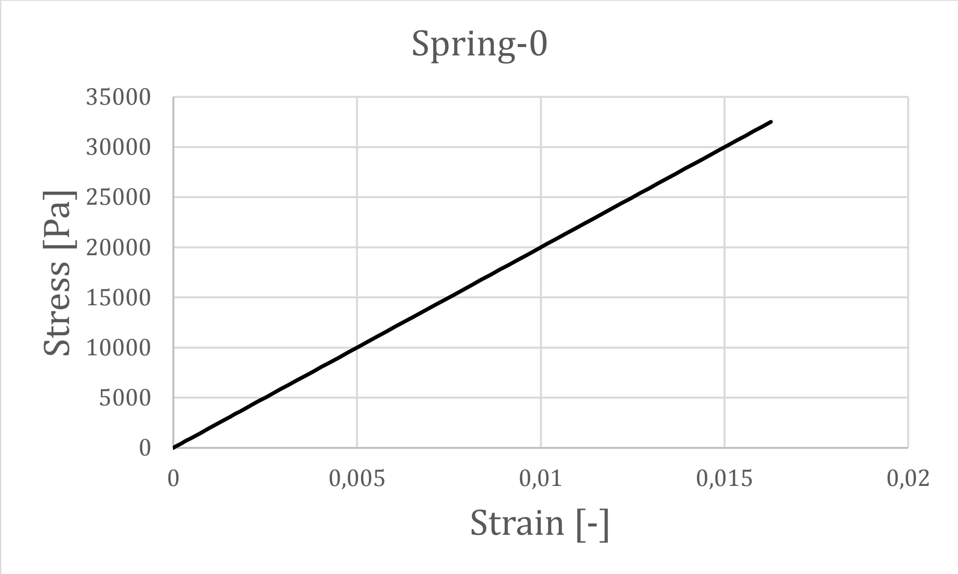

Figure G.17 Stress-strain relationship for Spring-0 at Arc length 0.7363.

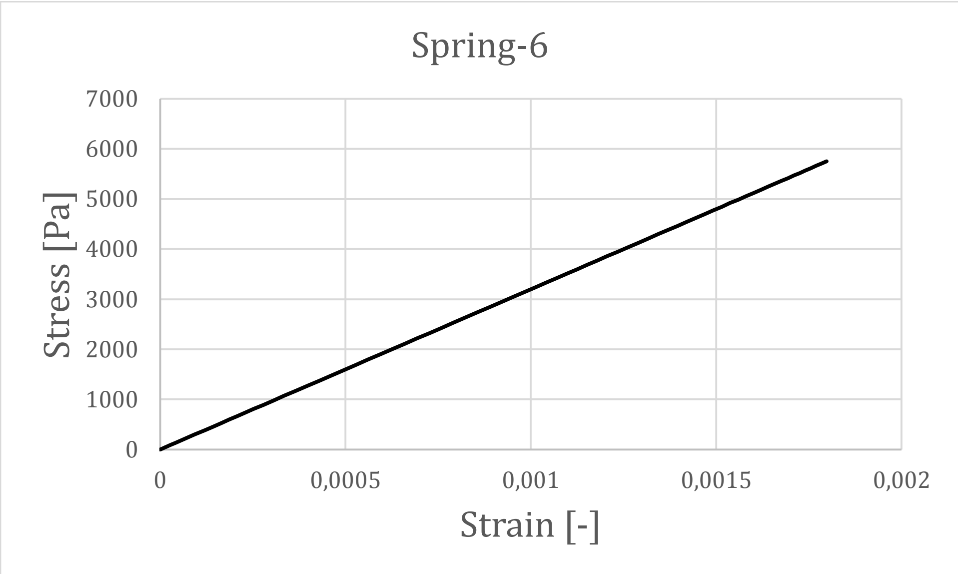

Figure G.18 Stress-strain relationship for Spring-6 at Arc length 0.7363.

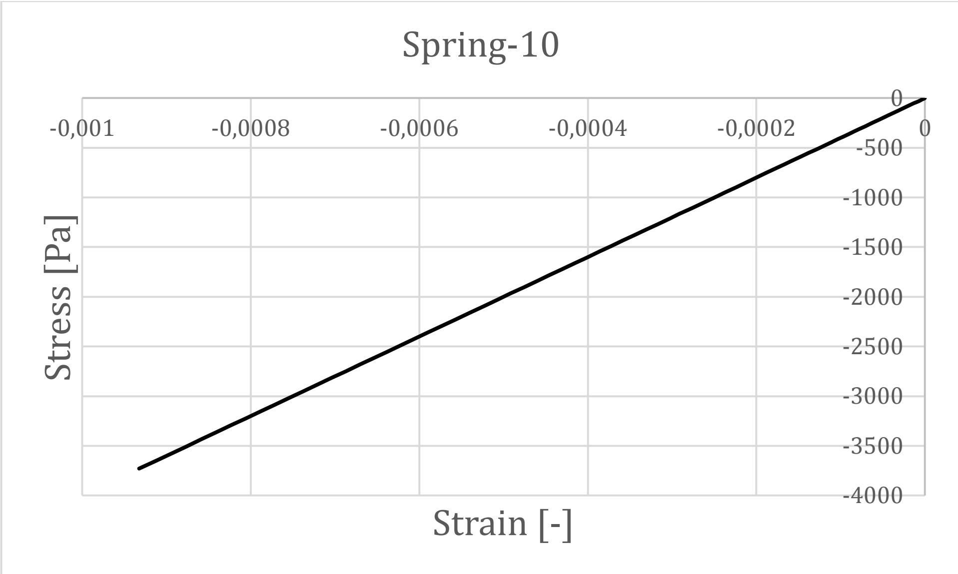

Figure G.19 Stress-strain relationship for Spring-10 at Arc length 0.7363.

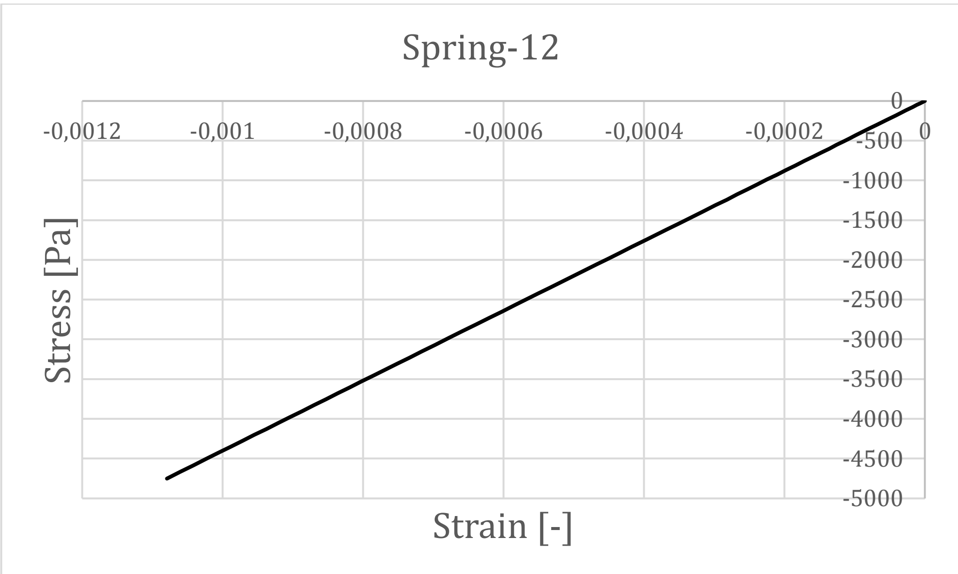

Figure G.20 Stress-strain relationship for Spring-12 at Arc length 0.7363.

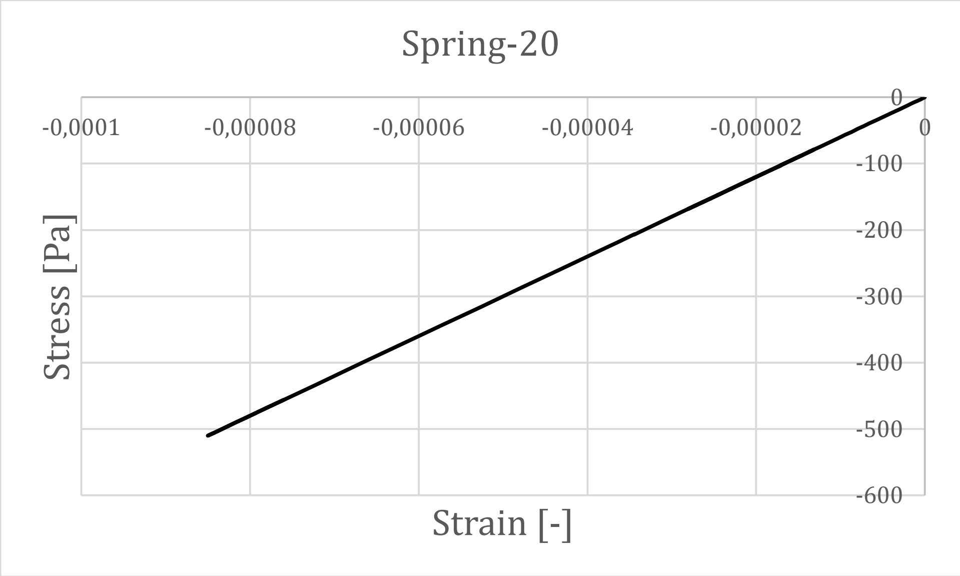

Figure G.21 Stress-strain relationship for Spring-20 at Arc length 0.7363.

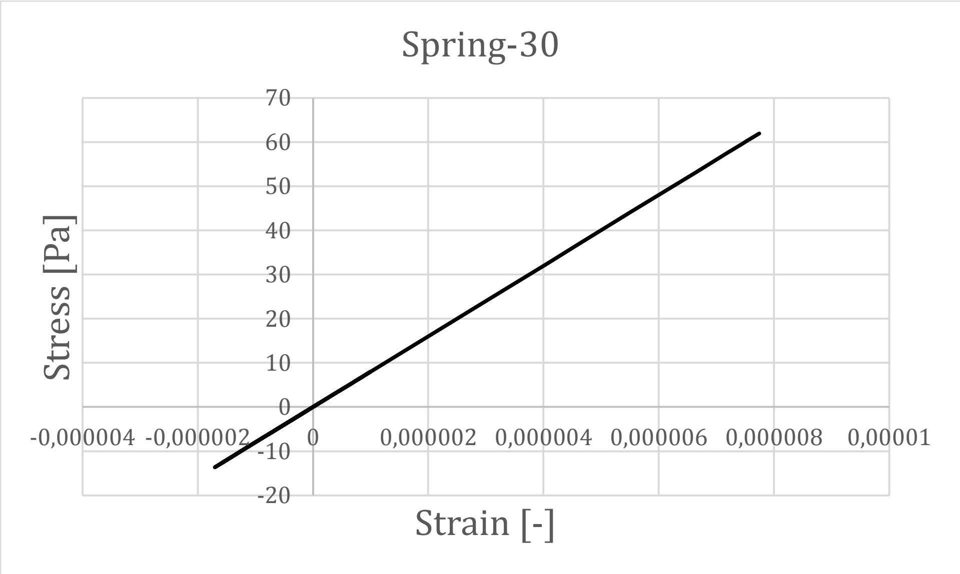

Figure G.22 Stress-strain relationship for Spring-30 at Arc length 0.7363.

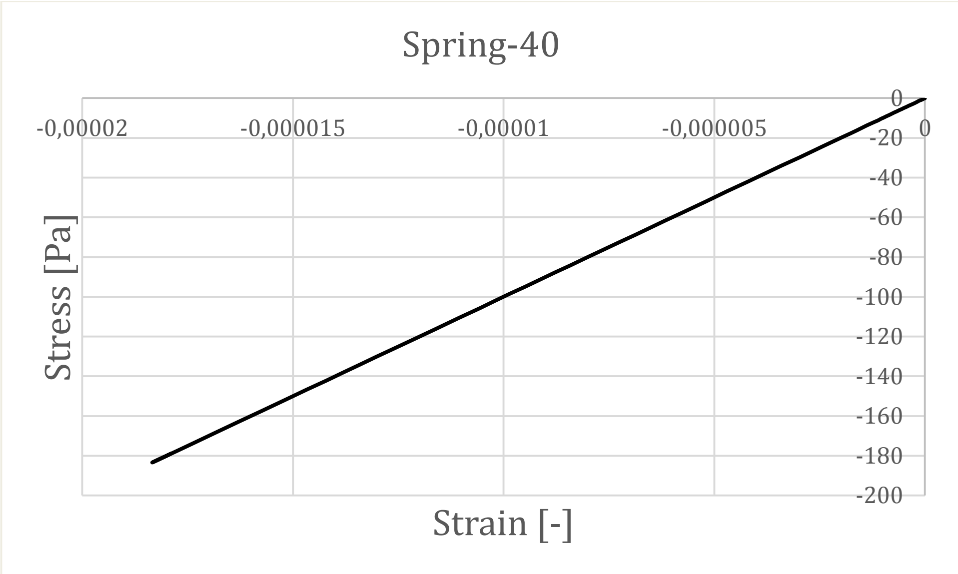

Figure G.23 Stress-strain relationship for Spring-30 at Arc length 0.7363.

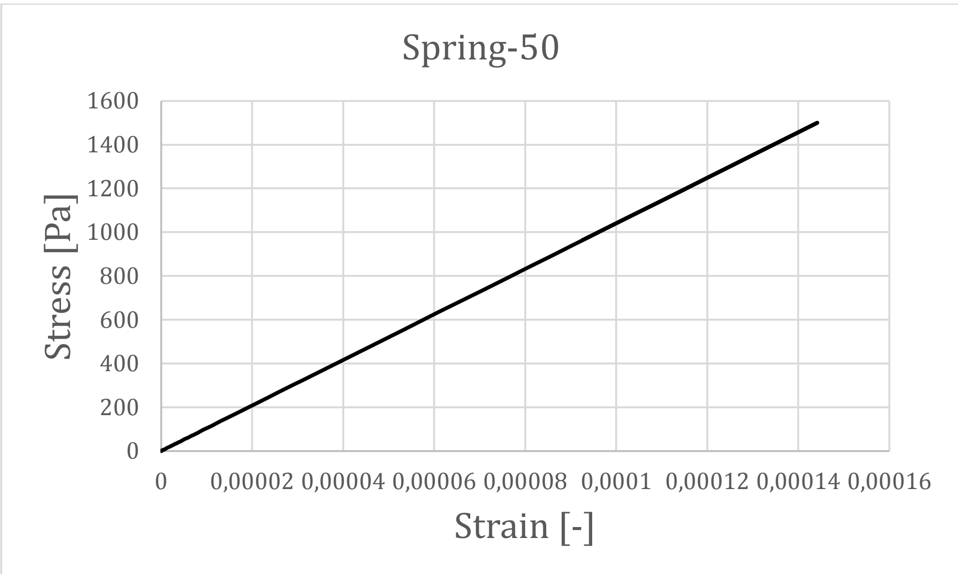

Figure G.24 Stress-strain relationship for Spring-50 at Arc length 0.7363.

Arc length 1.954

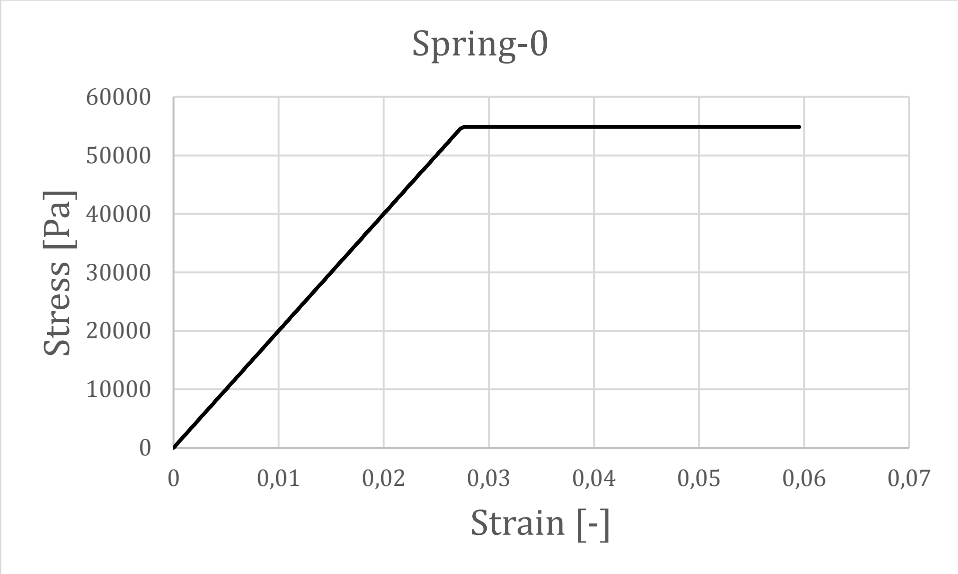

Figure G.25 Stress-strain relationship for Spring-0 at Arc length 1.954.

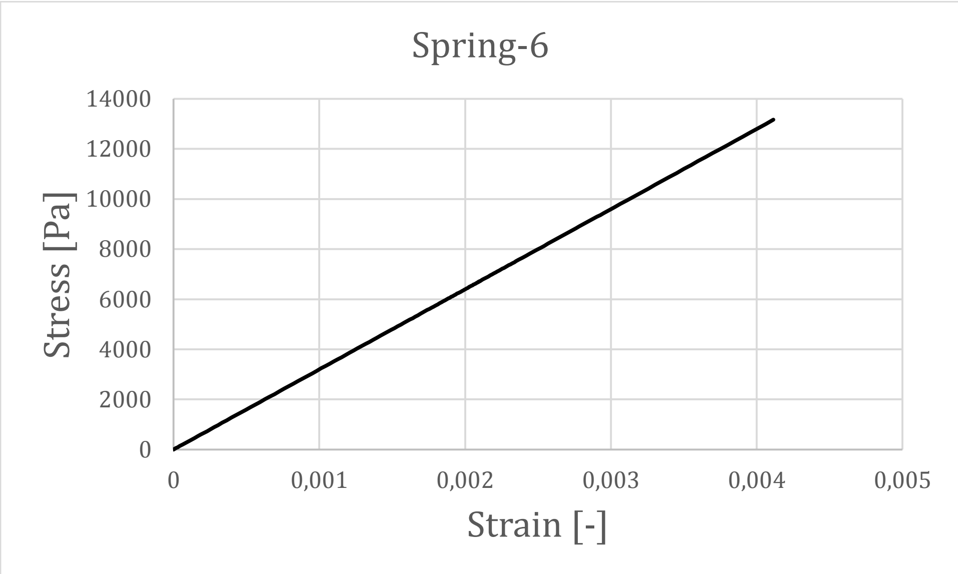

Figure G.26 Stress-strain relationship for Spring-6 at Arc length 1.954.

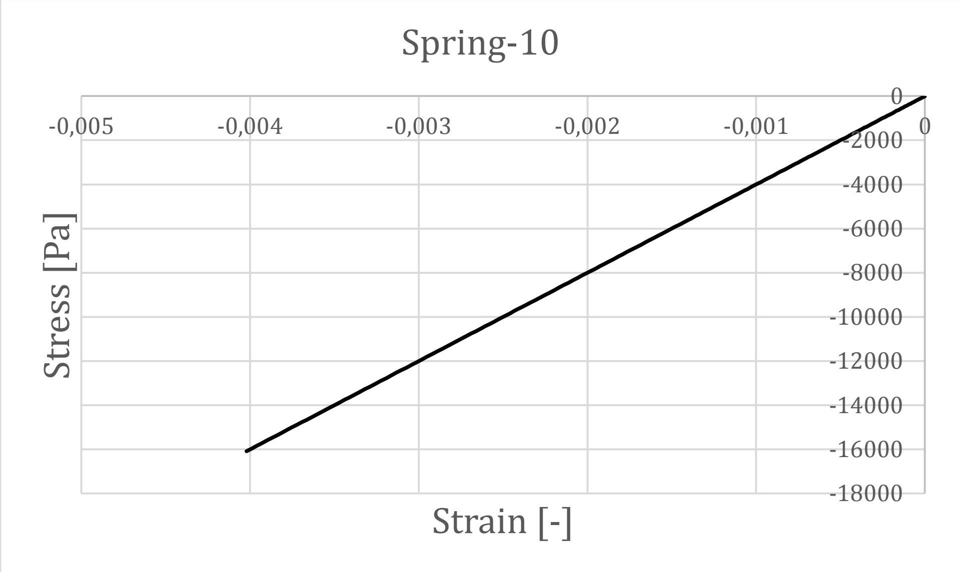

Figure G.27 Stress-strain relationship for Spring-10 at Arc length 1.954.

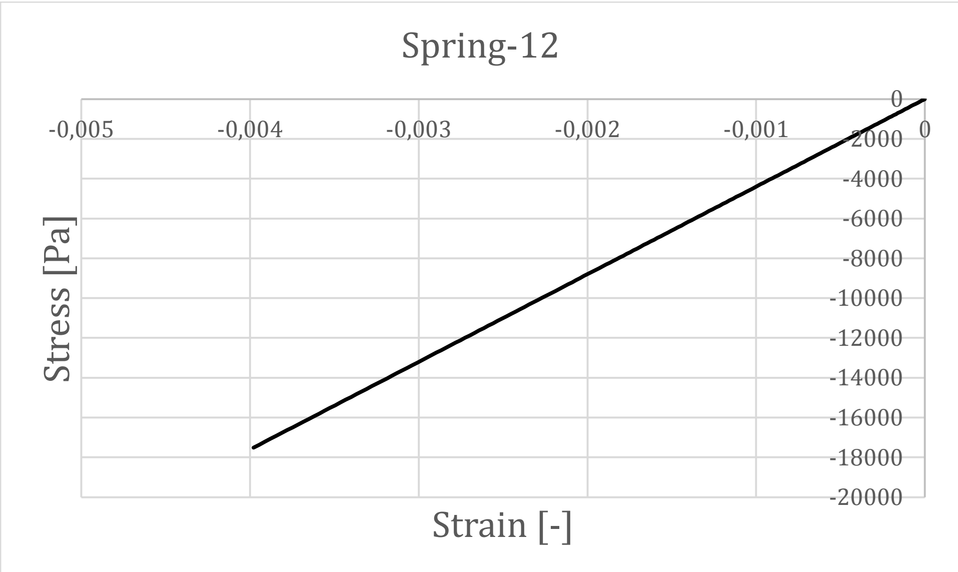

Figure G.28 Stress-strain relationship for Spring-12 at Arc length 1.954.

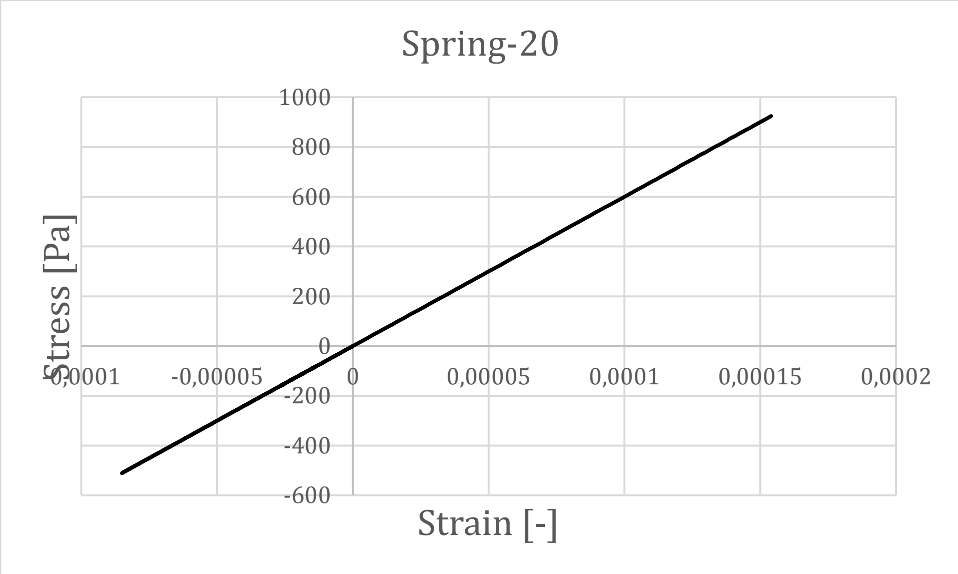

Figure G.29 Stress-strain relationship for Spring-20 at Arc length 1.954.

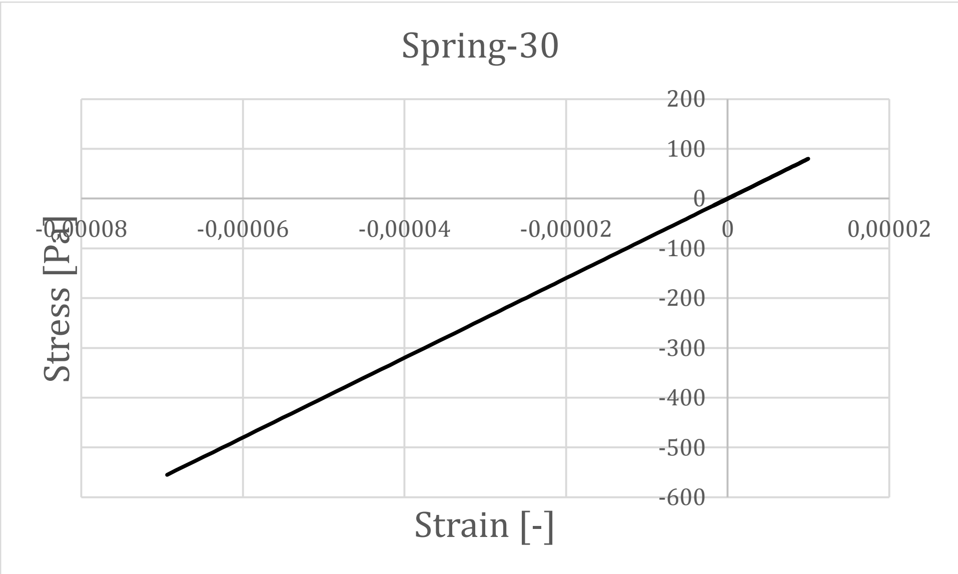

Figure G.30 Stress-strain relationship for Spring-30 at Arc length 1.954.

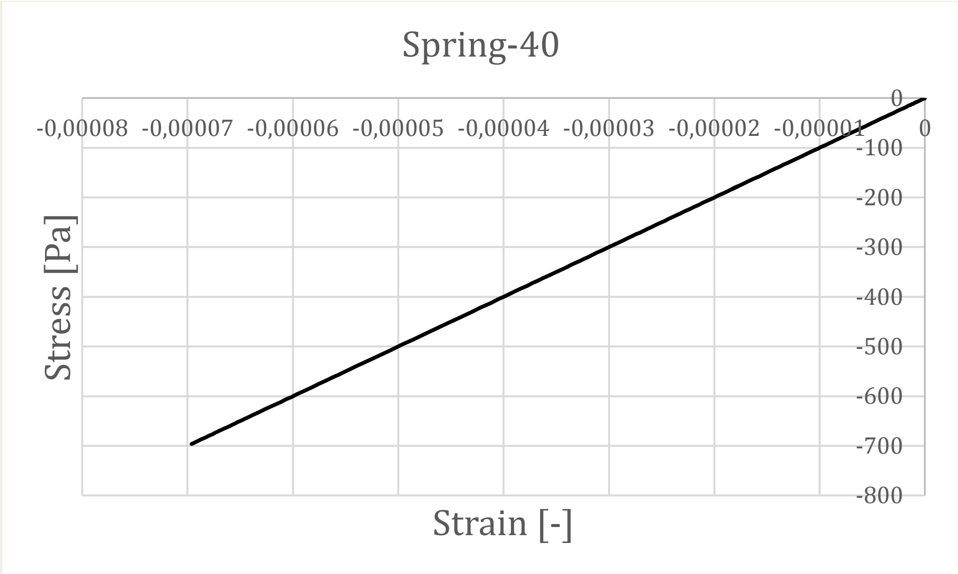

Figure G.31 Stress-strain relationship for Spring-40 at Arc length 1.954.

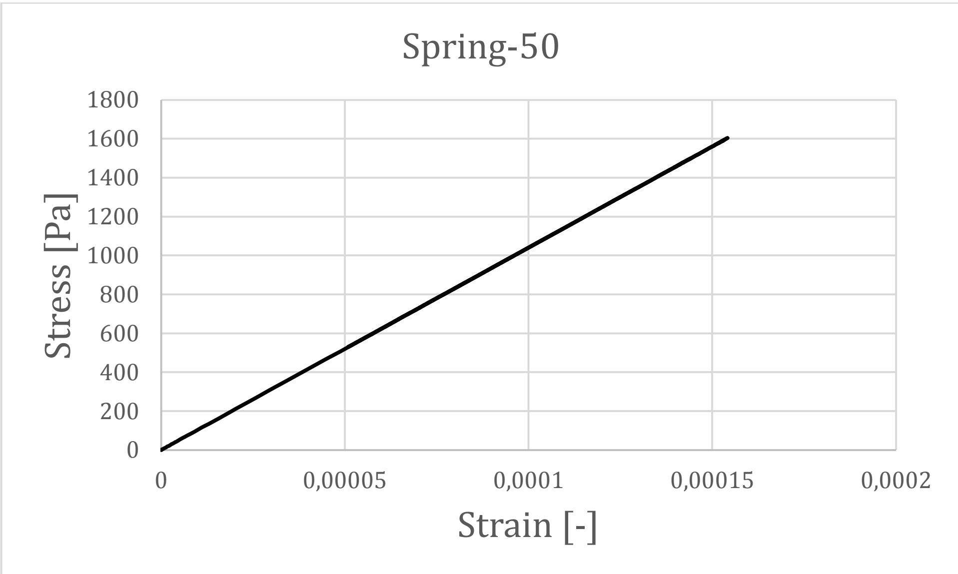

Figure G.32 Stress-strain relationship for Spring-50 at Arc length 1.954.

Arc length 2.232

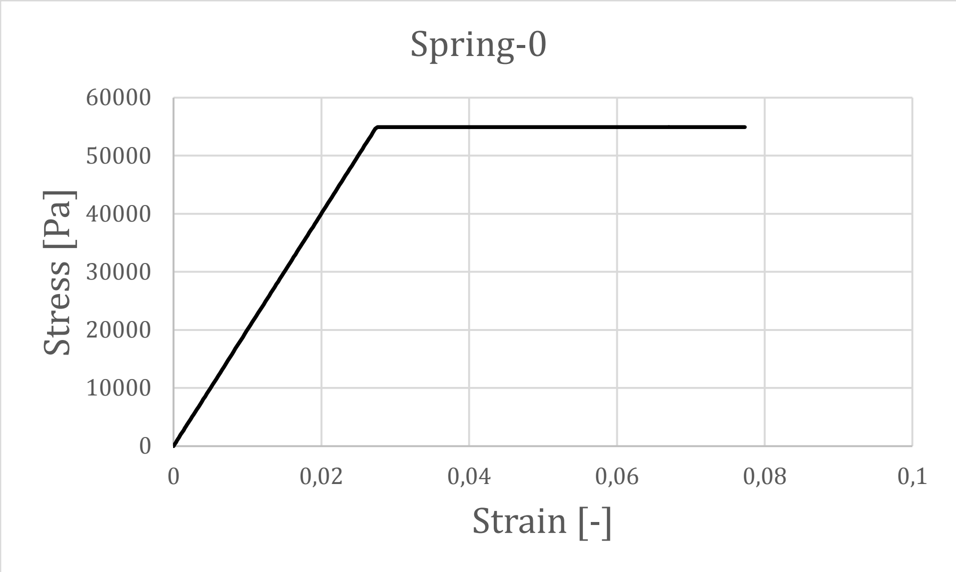

Figure G.33 Stress-strain relationship for Spring-0 at Arc length 2.232.

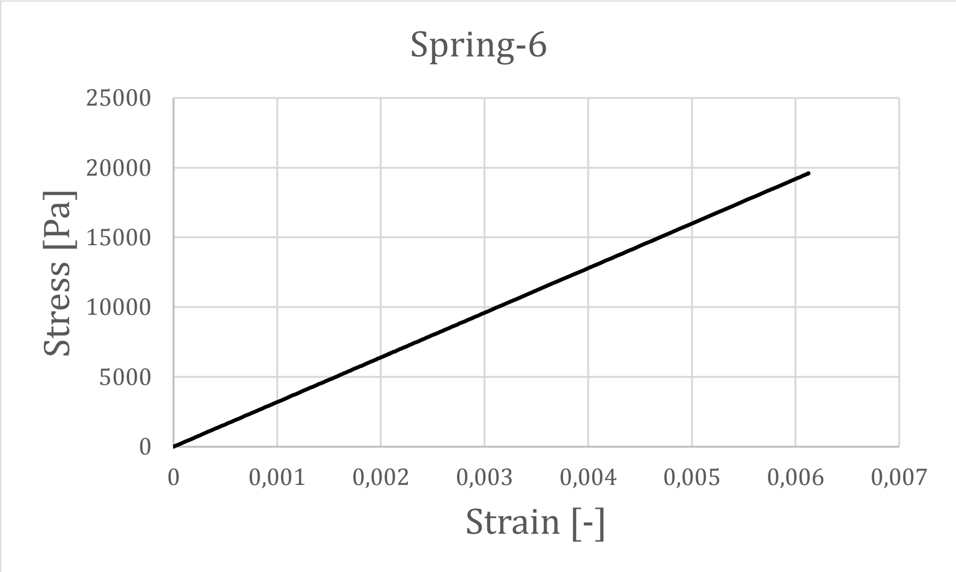

Figure G.34 Stress-strain relationship for Spring-6 at Arc length 2.232.

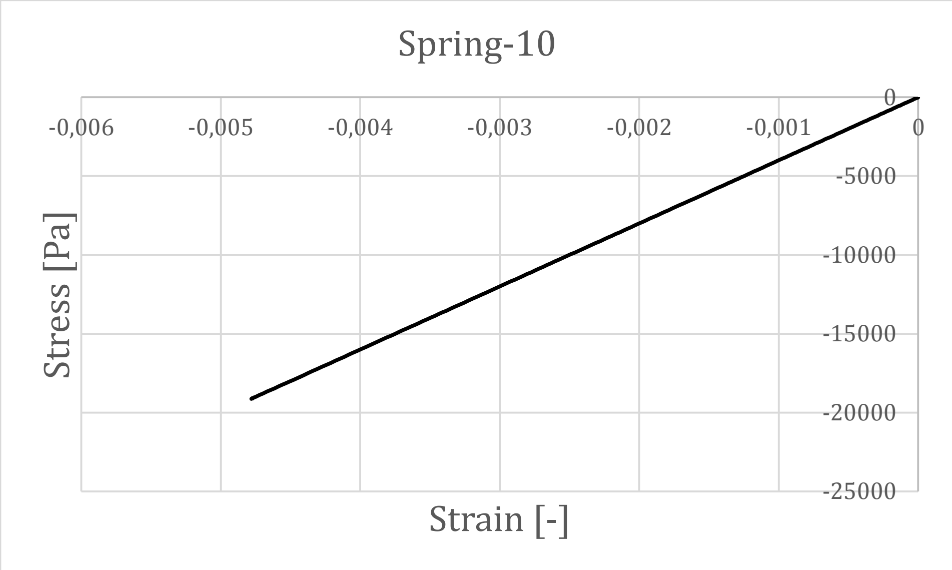

Figure G.35 Stress-strain relationship for Spring-10 at Arc length 2.232.

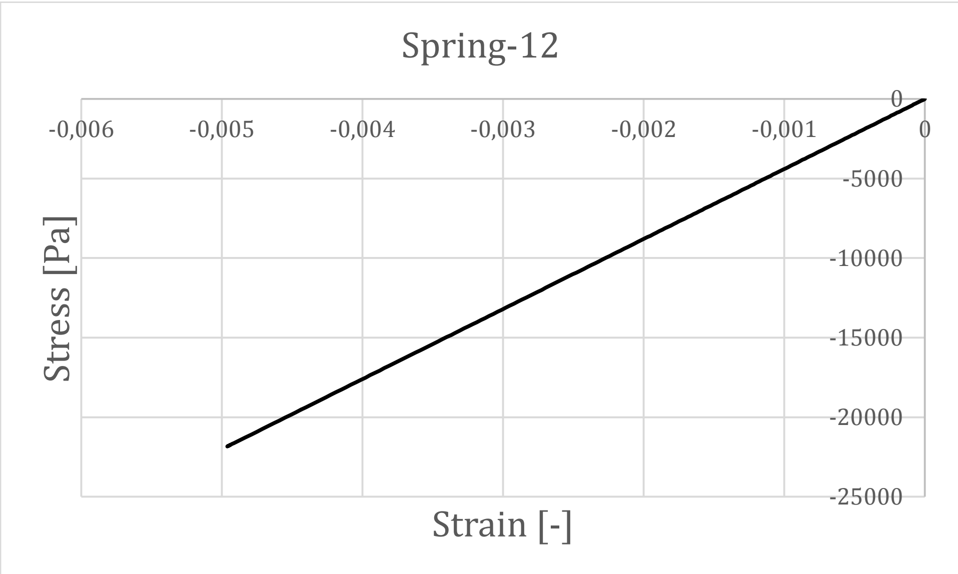

Figure G.36 Stress-strain relationship for Spring-12 at Arc length 2.232.

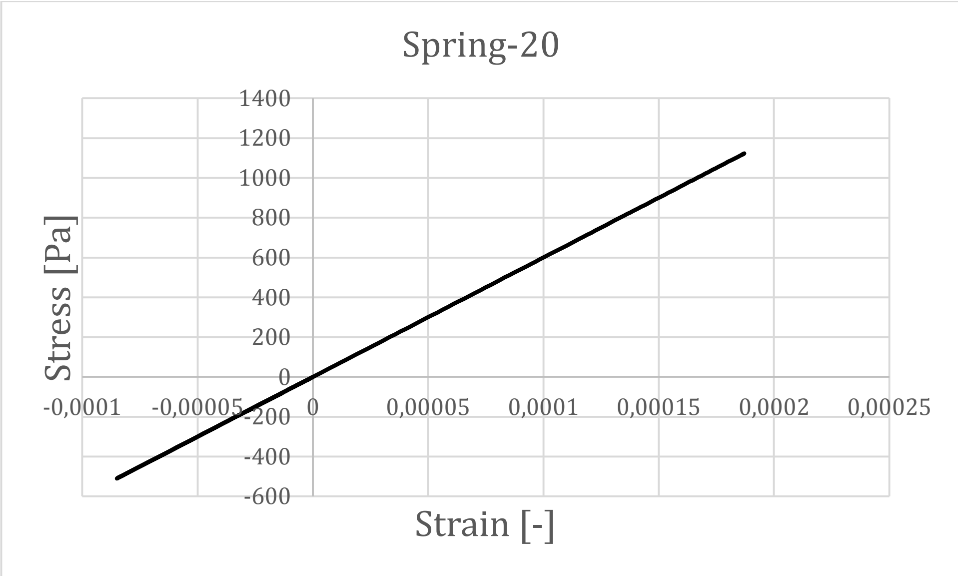

Figure G.37 Stress-strain relationship for Spring-20 at Arc length 2.232.

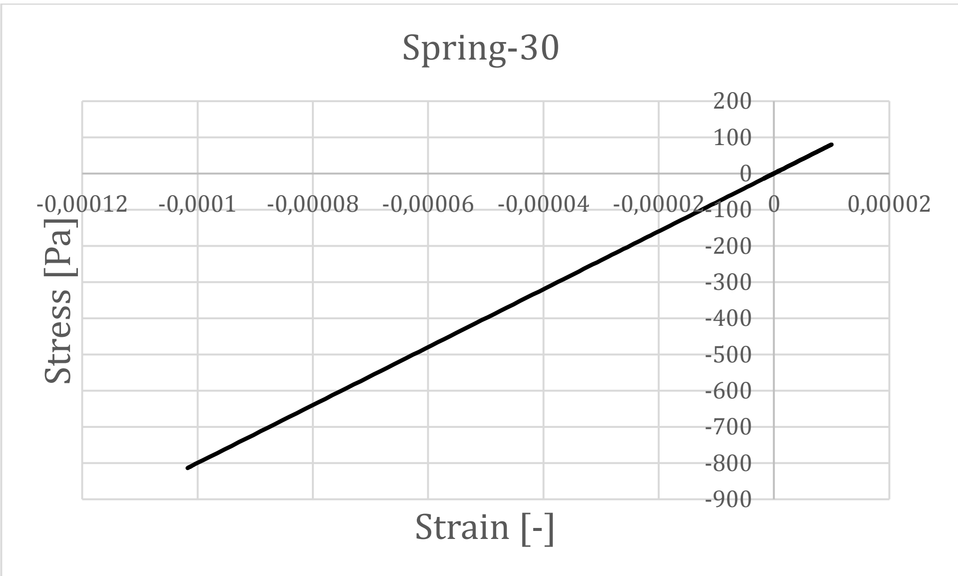

Figure G.38 Stress-strain relationship for Spring-30 at Arc length 2.232.

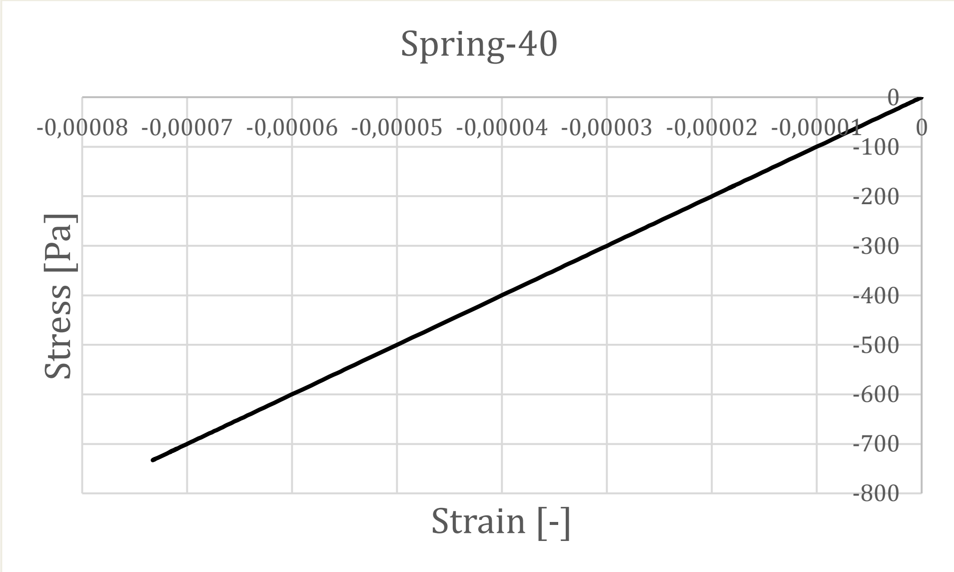

Figure G.39 Stress-strain relationship for Spring-40 at Arc length 2.232.

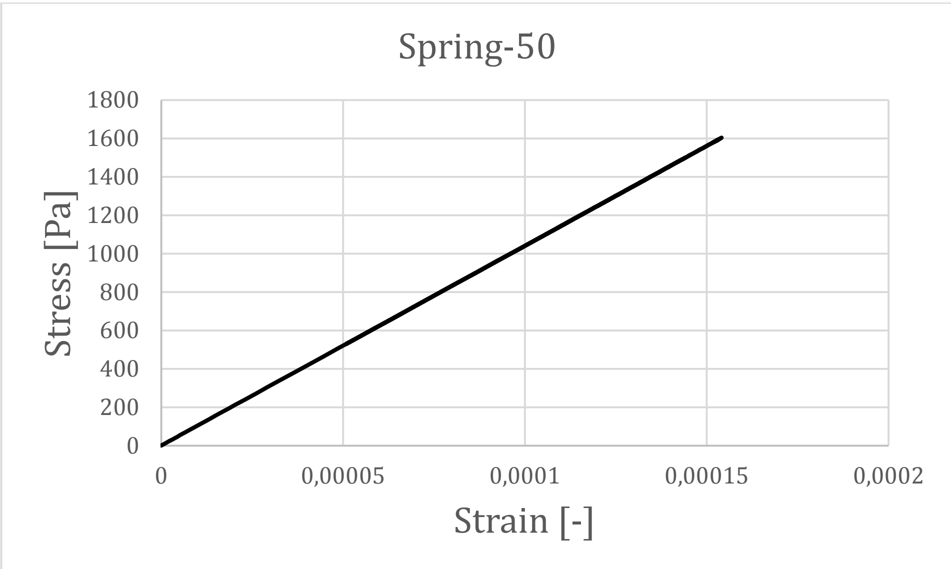

Figure G.40 Stress-strain relationship for Spring-50 at Arc length 2.232.

Strain-arc length

Arc length 0.0528

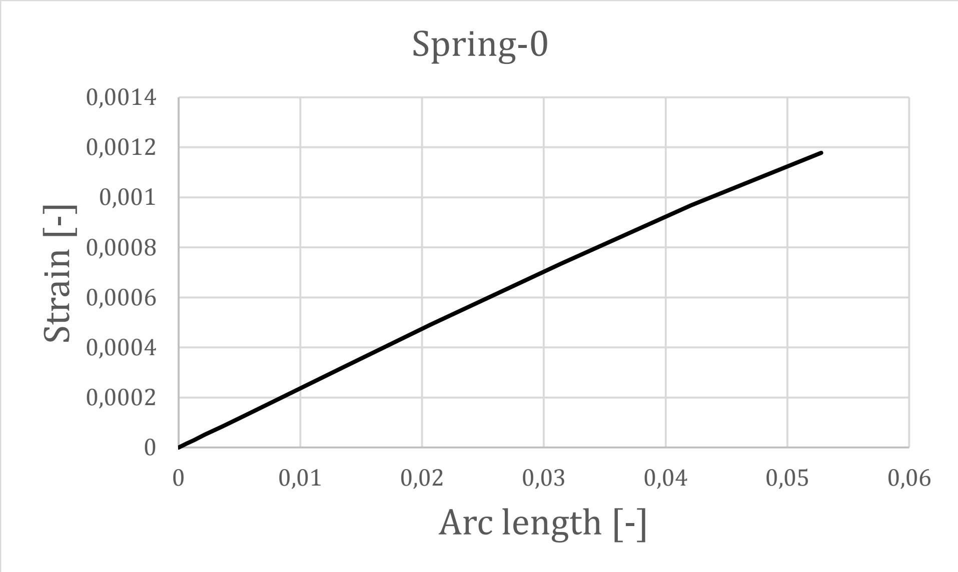

Figure G.41 Strain-arc length relationship for Spring-0 at Arc length 0.0528.

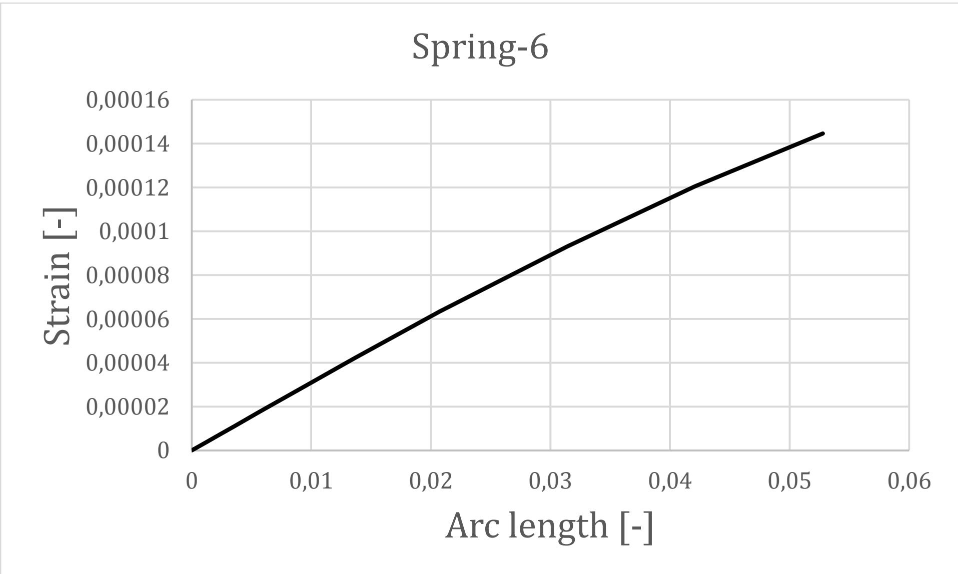

Figure G.42 Strain-arc length relationship for Spring-6 at Arc length 0.0528.

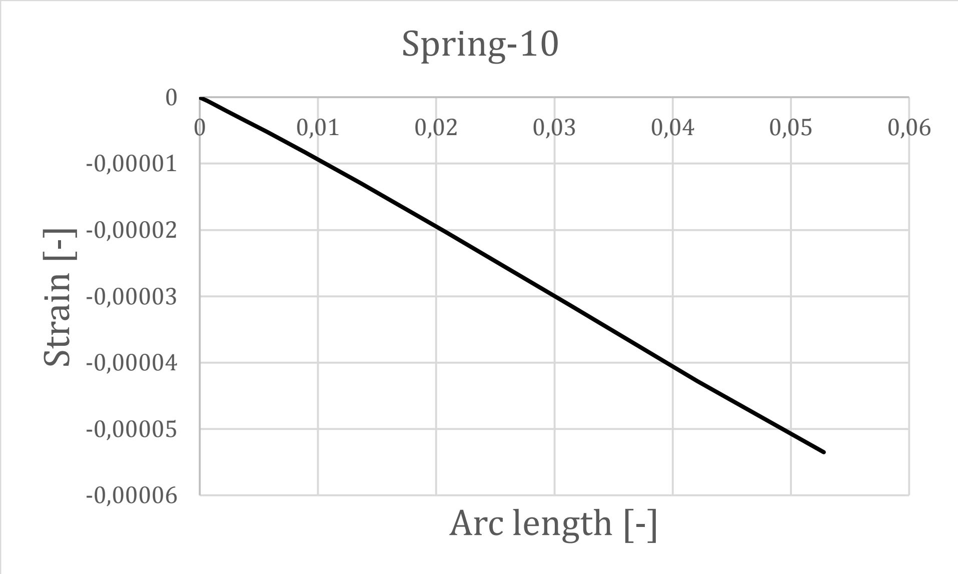

Figure G.43 Strain-arc length relationship for Spring-10 at Arc length 0.0528.

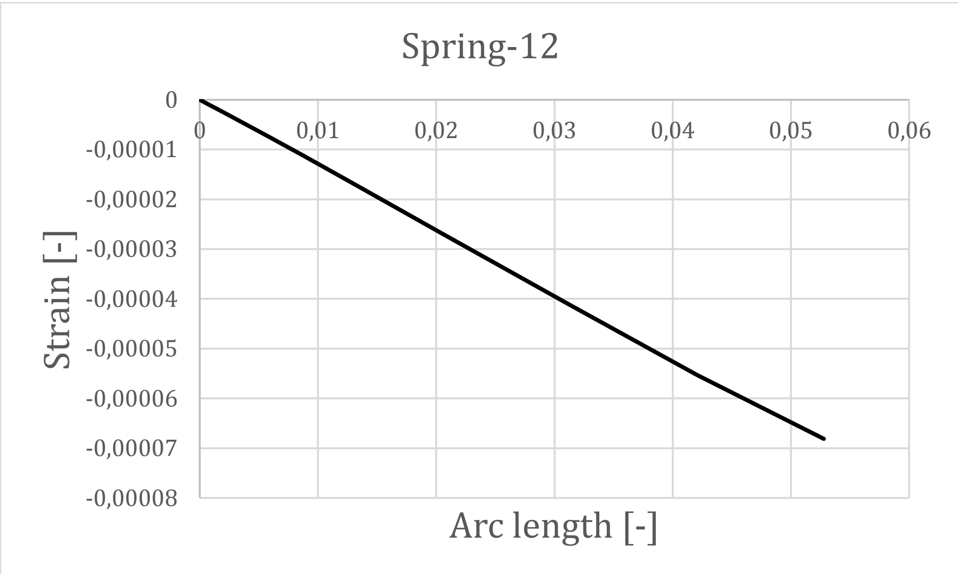

Figure G.44 Strain-arc length relationship for Spring-12 at Arc length 0.0528.

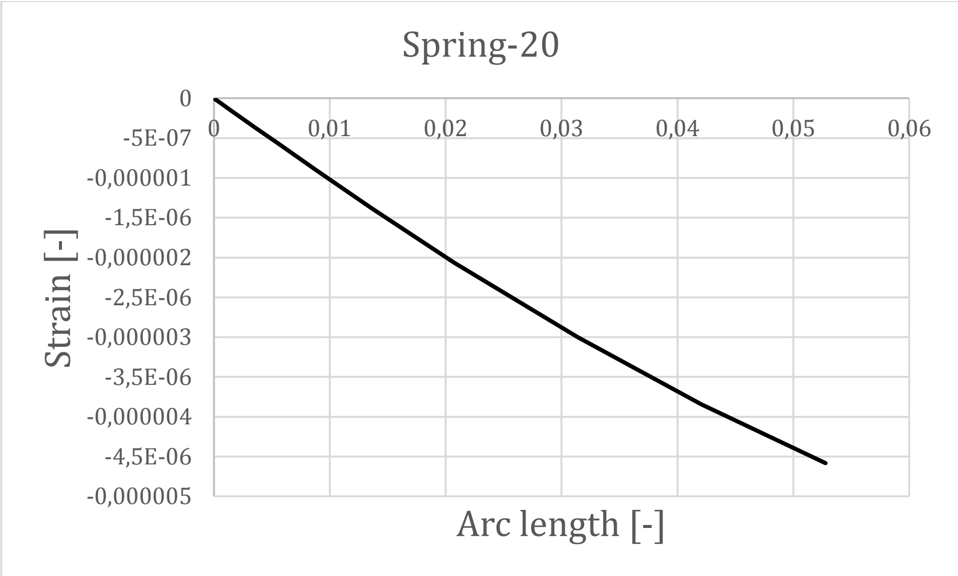

Figure G.45 Strain-arc length relationship for Spring-20 at Arc length 0.0528.

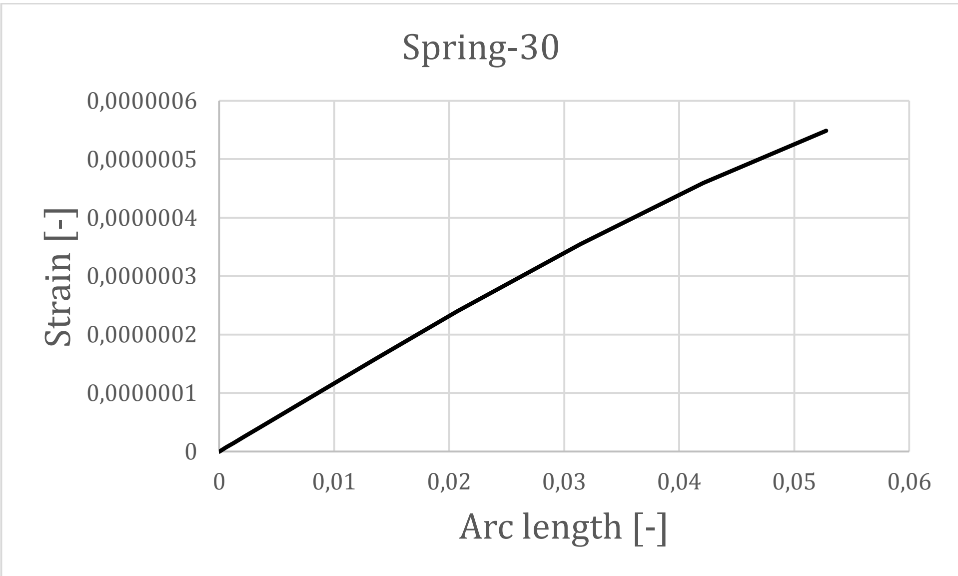

Figure G.46 Strain-arc length relationship for Spring-30 at Arc length 0.0528.

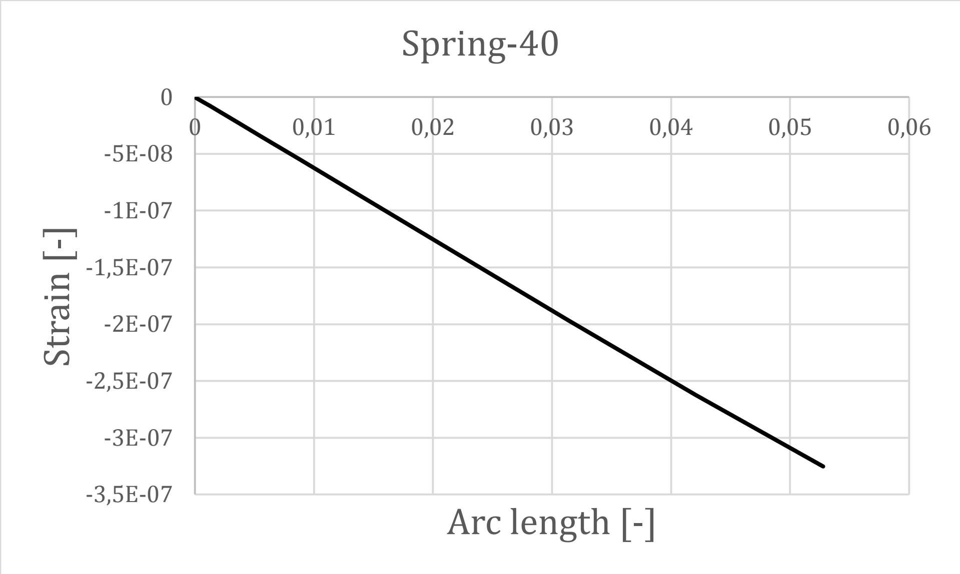

Figure G.47 Strain-arc length relationship for Spring-40 at Arc length 0.0528.

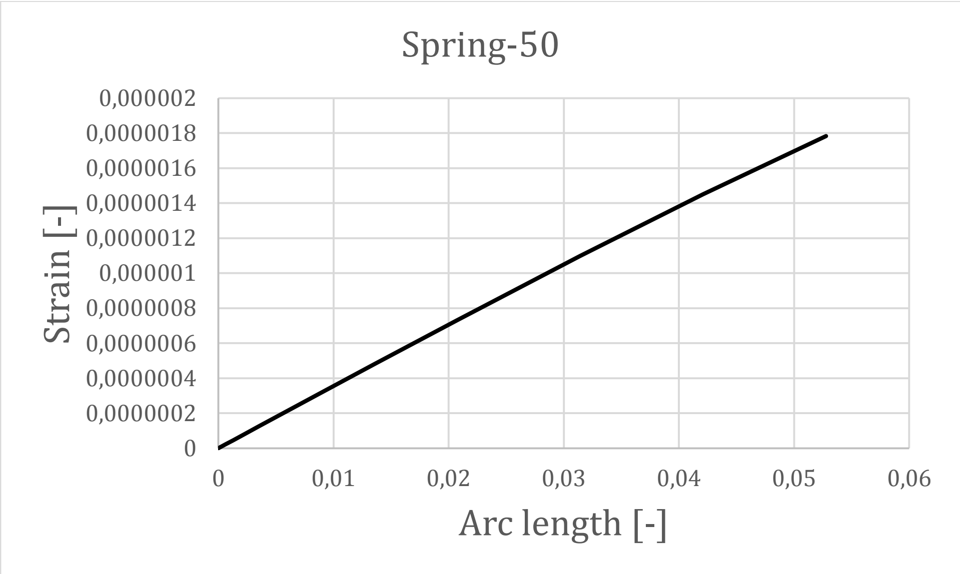

Figure G.48 Strain-arc length relationship for Spring-50 at Arc length 0.0528.

Arc-length 0.2023

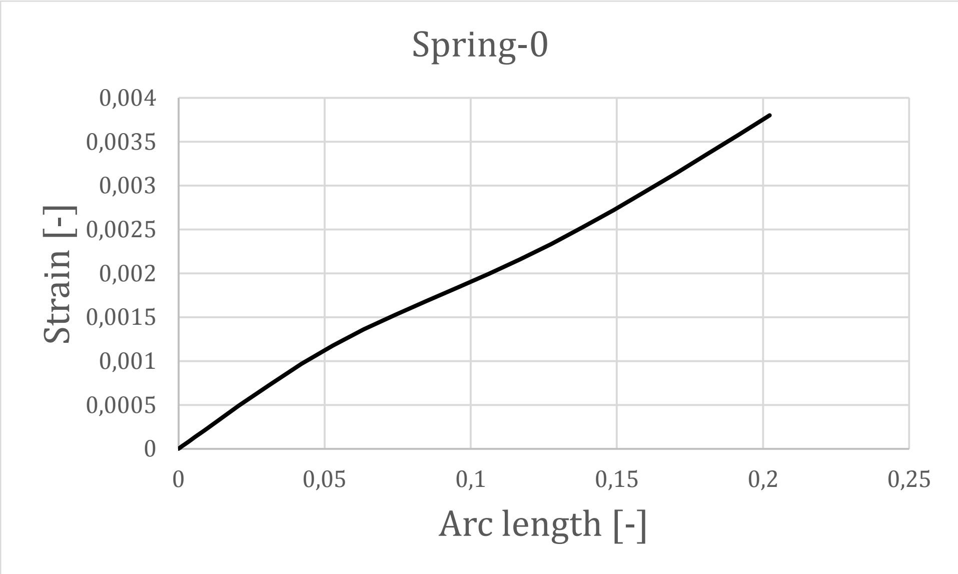

Figure G.49 Strain-arc length relationship for Spring-0 at Arc length 0.2023.

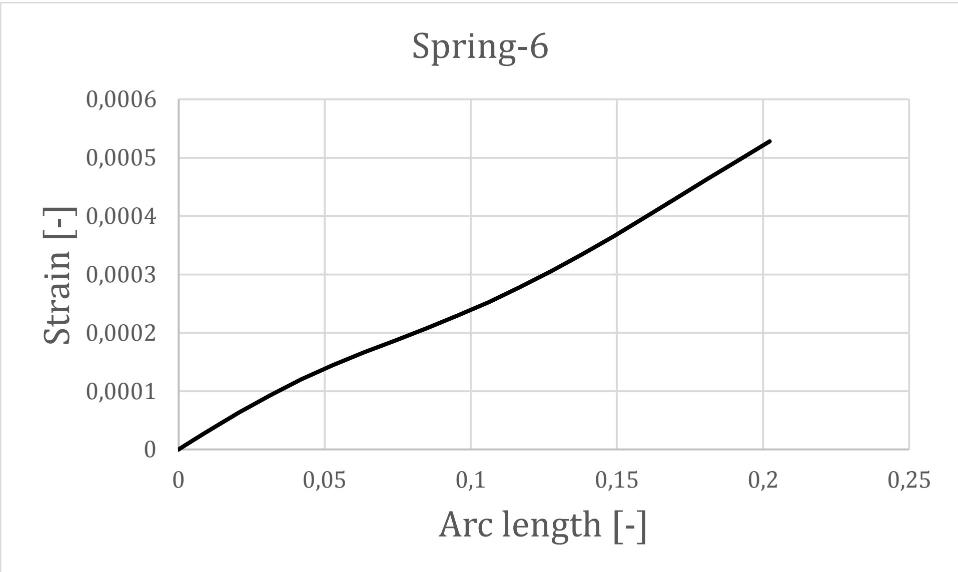

Figure G.50 Strain-arc length relationship for Spring-6 at Arc length 0.2023.

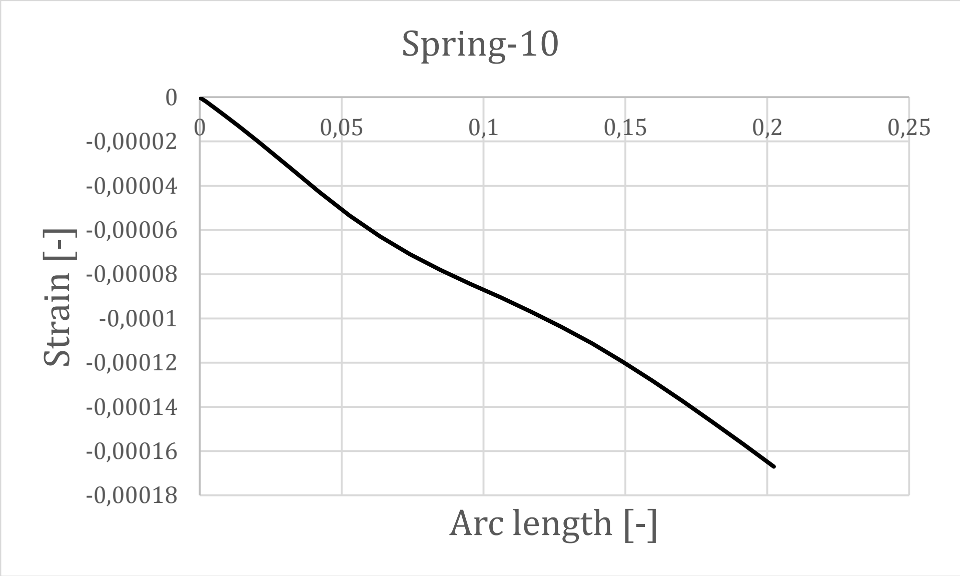

Figure G.51 Strain-arc length relationship for Spring-10 at Arc length 0.2023.

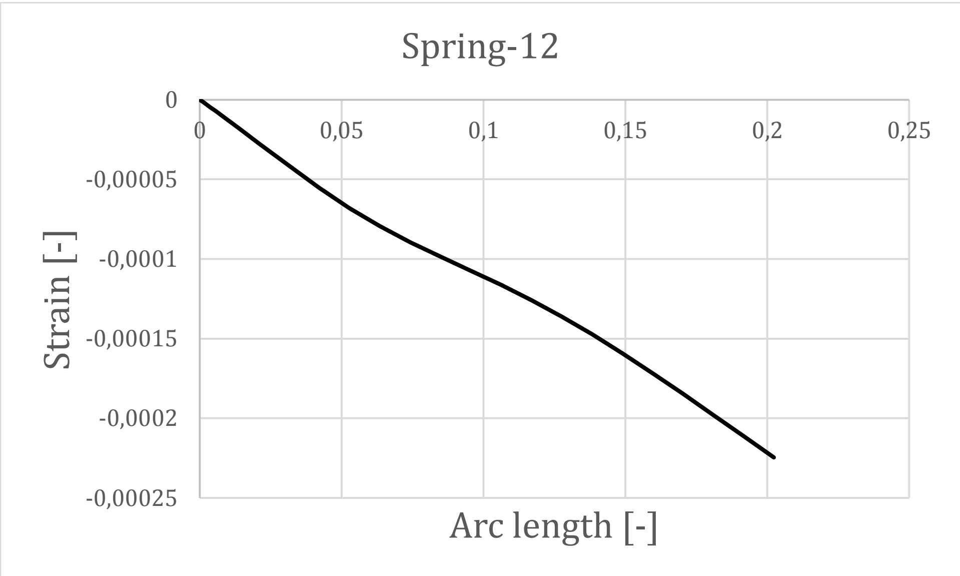

Figure G.52 Strain-arc length relationship for Spring-12 at Arc length 0.2023.

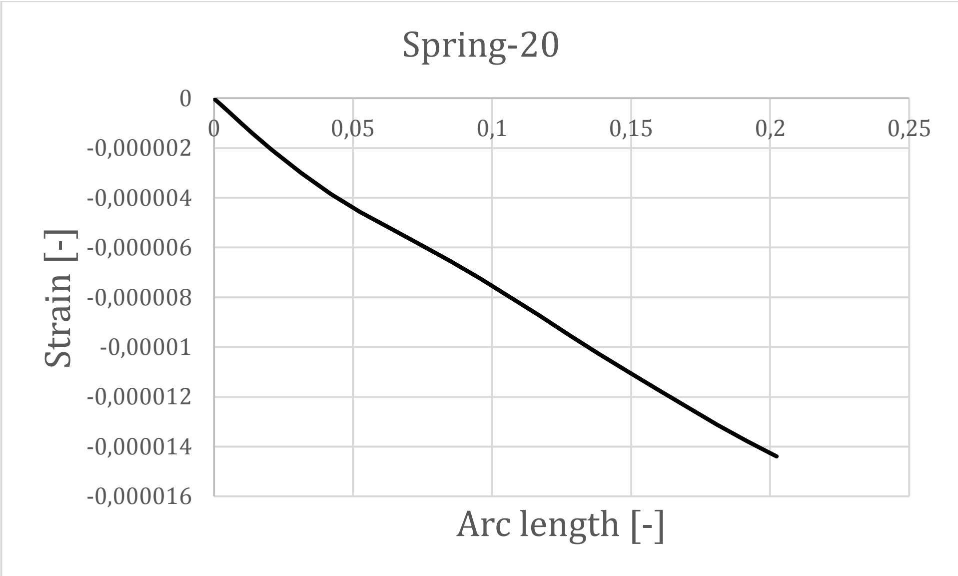

Figure G.53 Strain-arc length relationship for Spring-20 at Arc length 0.2023.

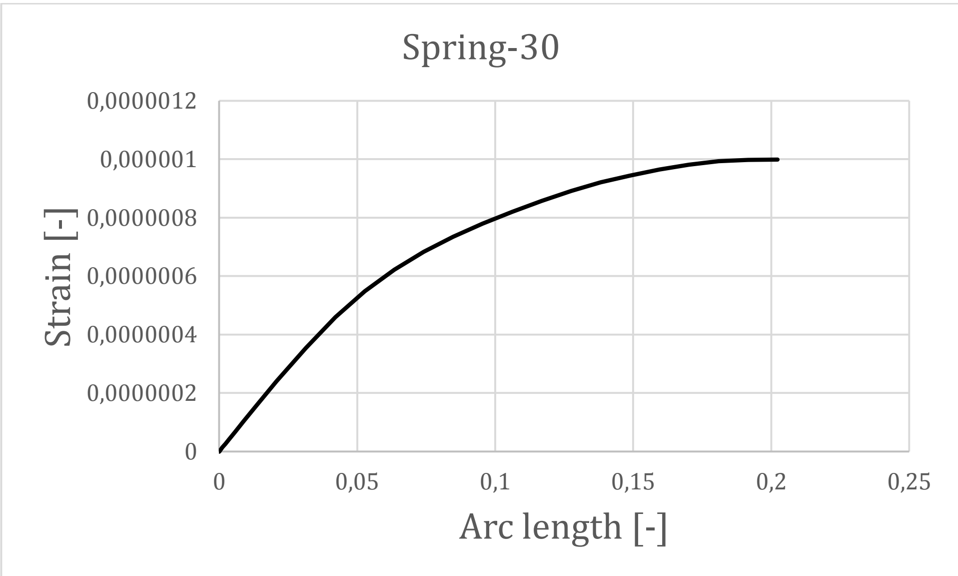

Figure G.54 Strain-arc length relationship for Spring-30 at Arc length 0.2023.

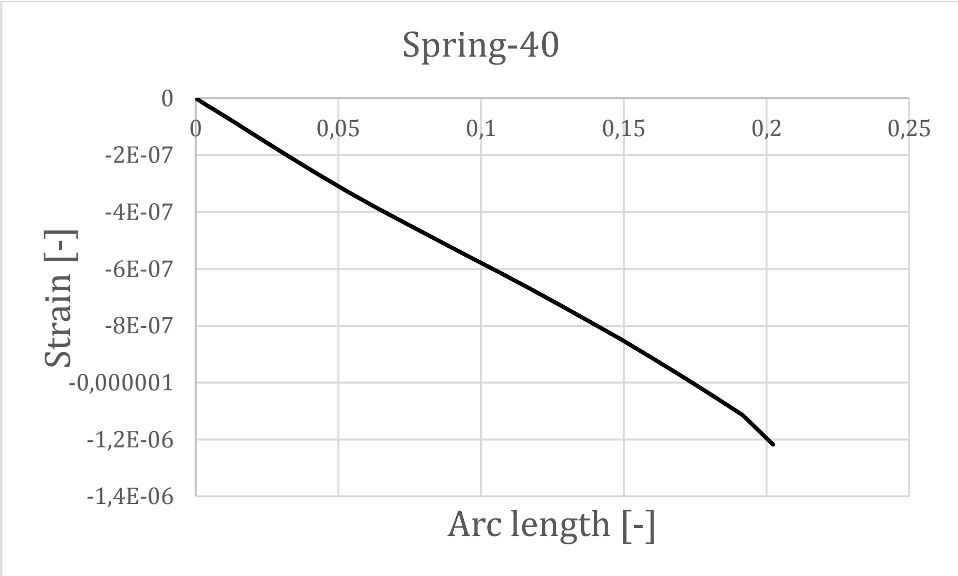

Figure G.55 Strain-arc length relationship for Spring-40 at Arc length 0.2023.

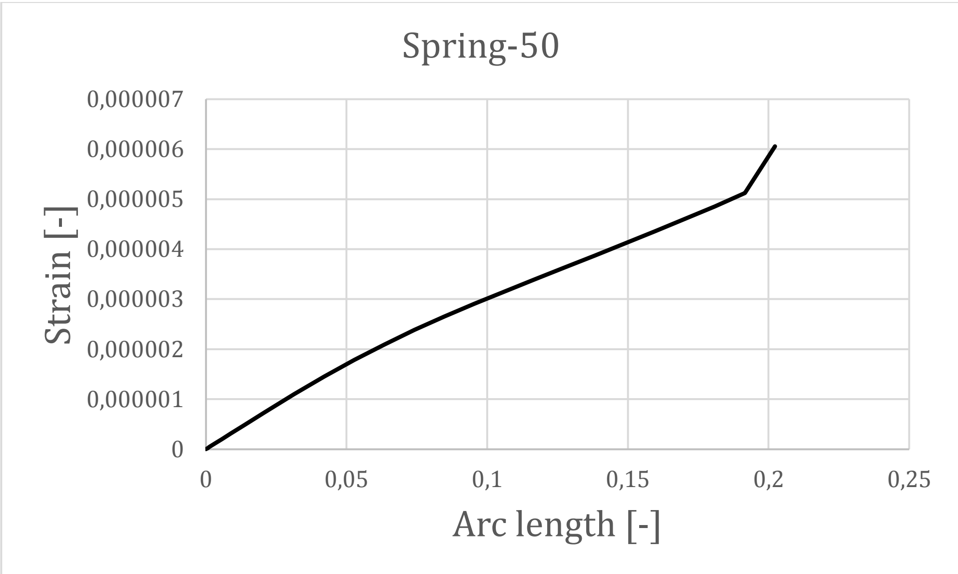

Figure G.56 Strain-arc length relationship for Spring-50 at Arc length 0.2023.

Arc-length 0.7363

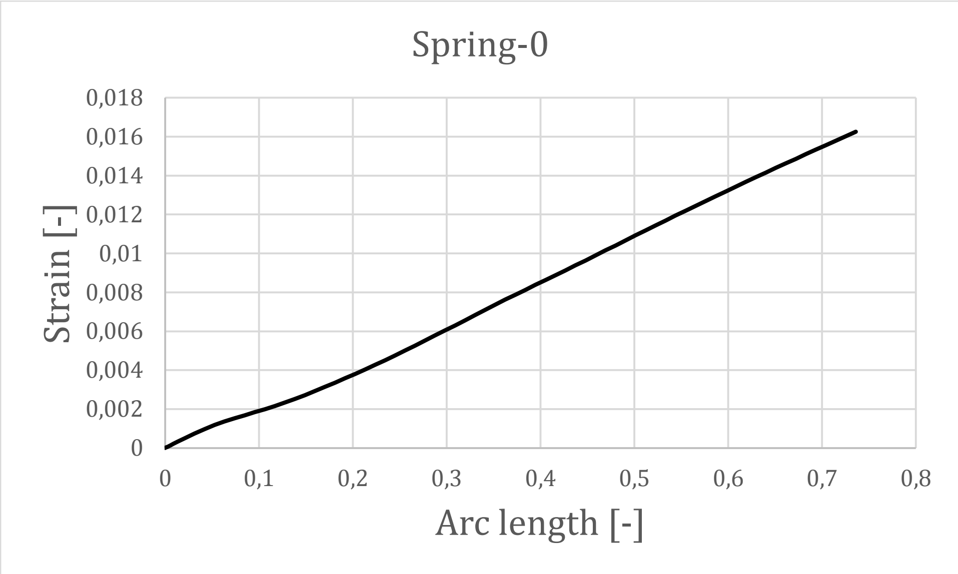

Figure G.57 Strain-arc length relationship for Spring-0 at Arc length 0.7363.

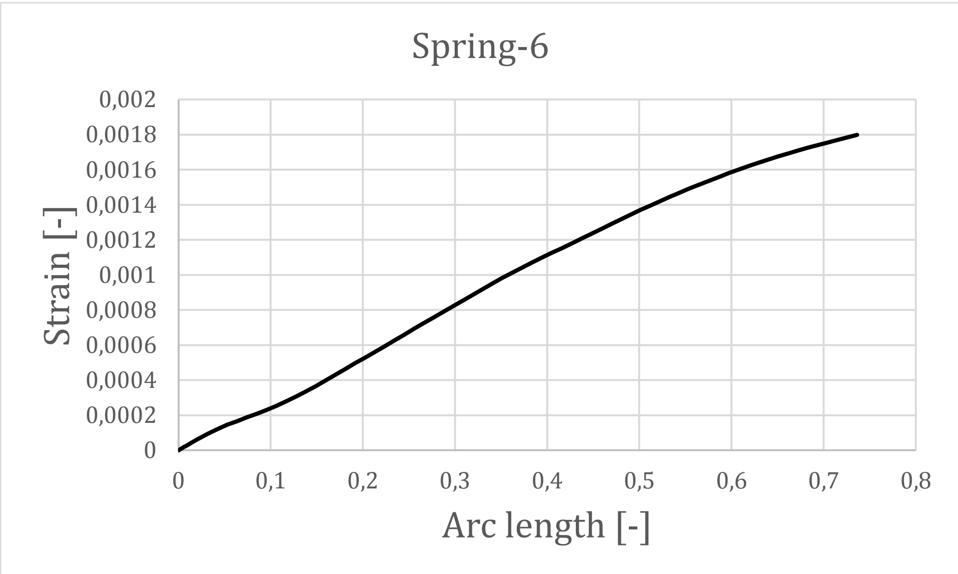

Figure G.58 Strain-arc length relationship for Spring-6 at Arc length 0.7363.

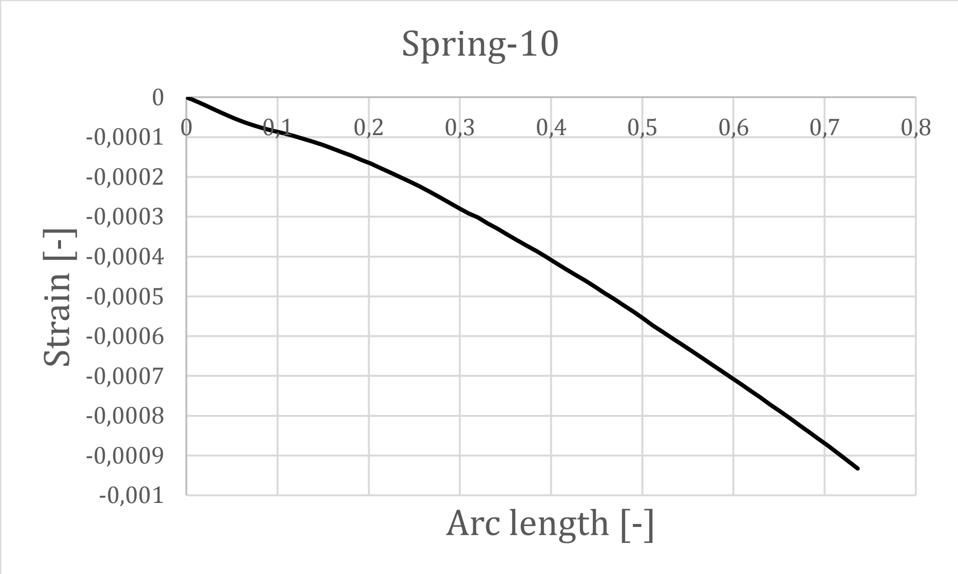

Figure G.59 Strain-arc length relationship for Spring-10 at Arc length 0.7363.

Figure G.60 Strain-arc length relationship for Spring-12 at Arc length 0.7363.

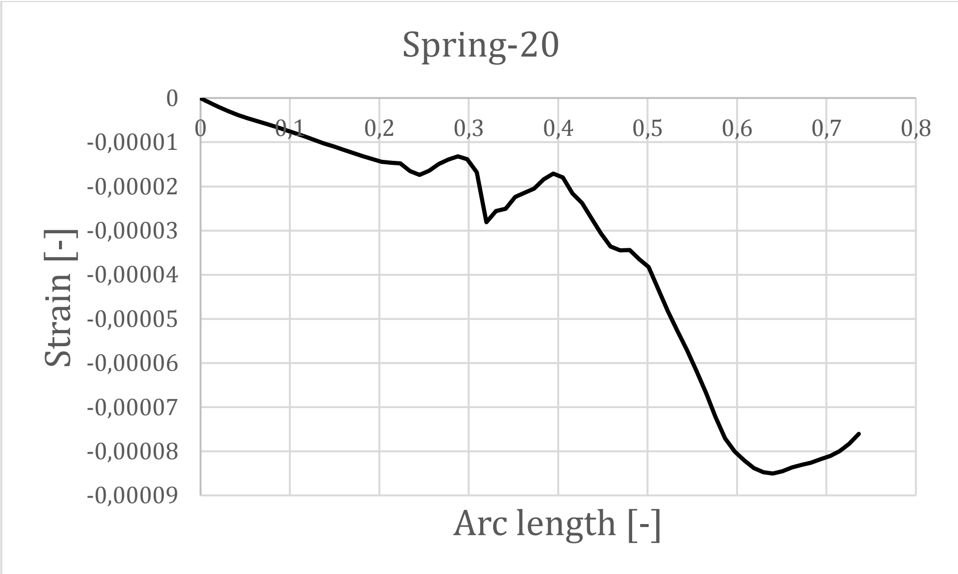

Figure G.61 Strain-arc length relationship for Spring-20 at Arc length 0.7363.

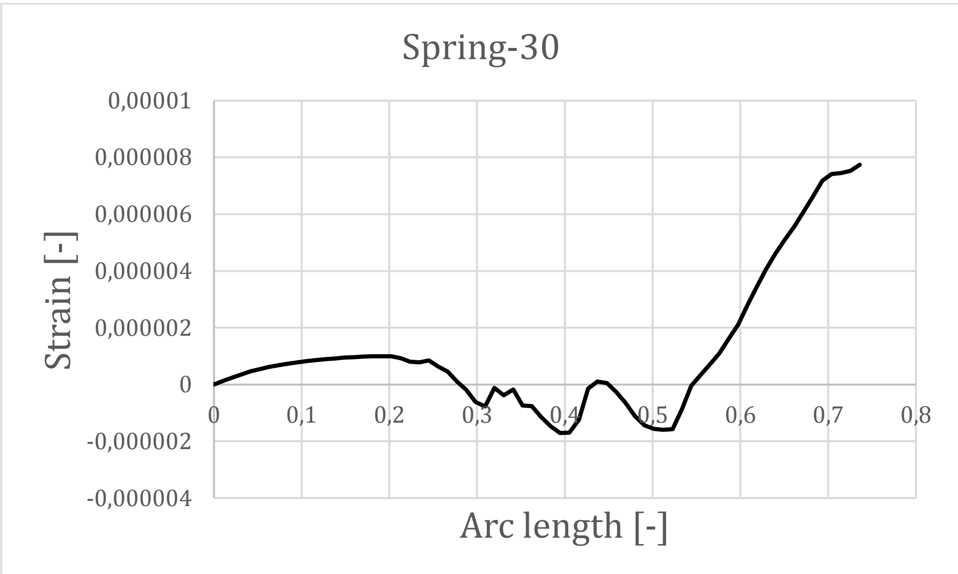

Figure G.62 Strain-arc length relationship for Spring-30 at Arc length 0.7363.

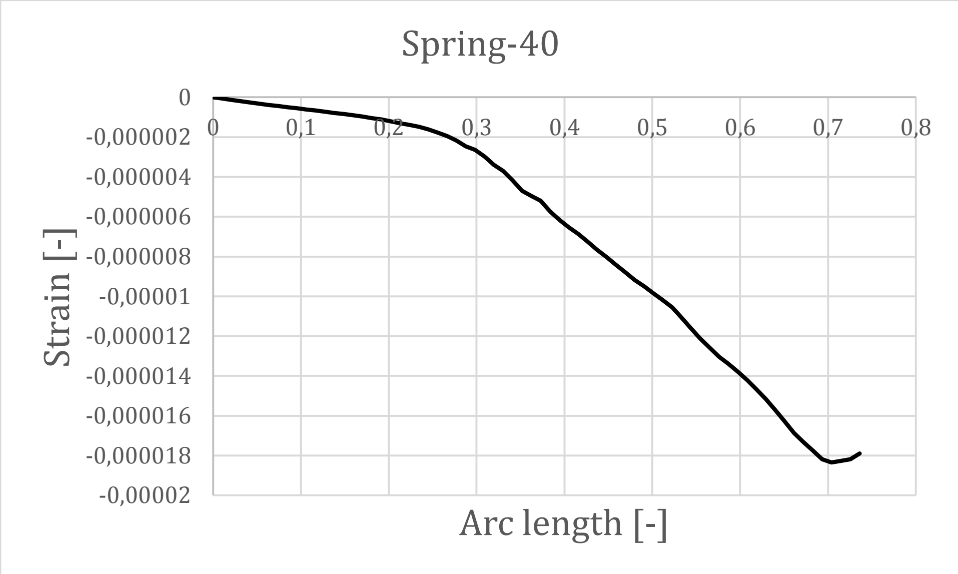

Figure G.63 Strain-arc length relationship for Spring-40 at Arc length 0.7363.

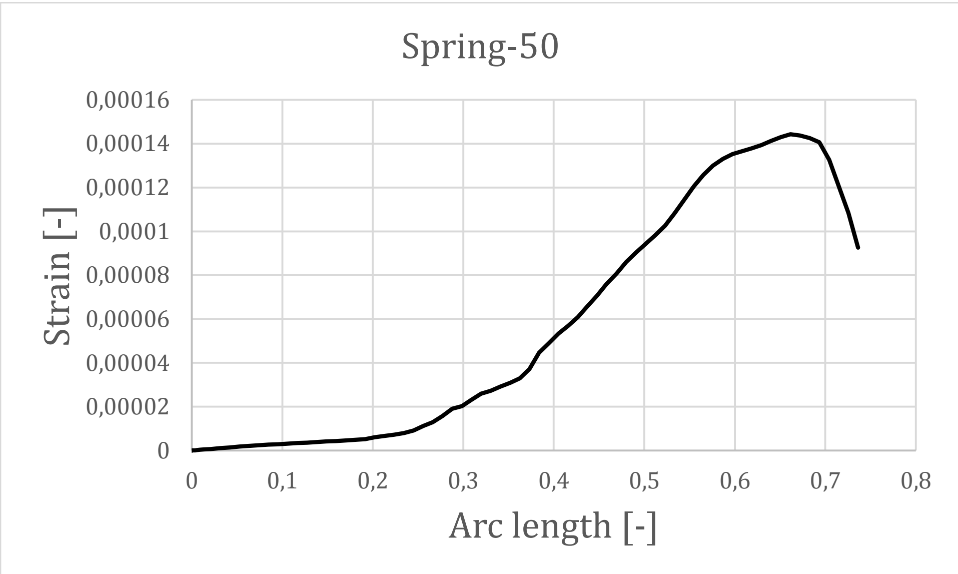

Figure G.64 Strain-arc length relationship for Spring-50 at Arc length 0.7363.

Arc-length 1.954

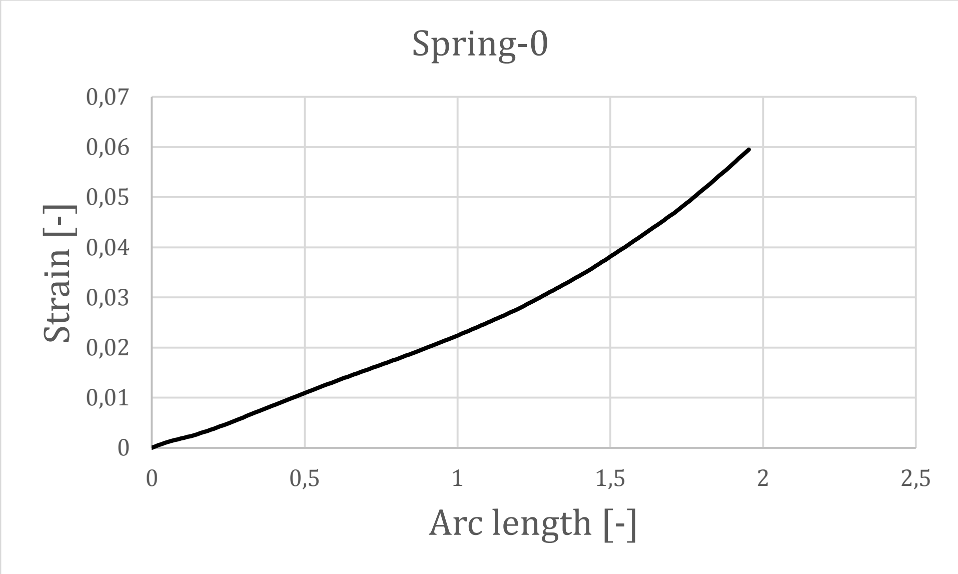

Figure G.65 Strain-arc length relationship for Spring-0 at Arc length 1.954.

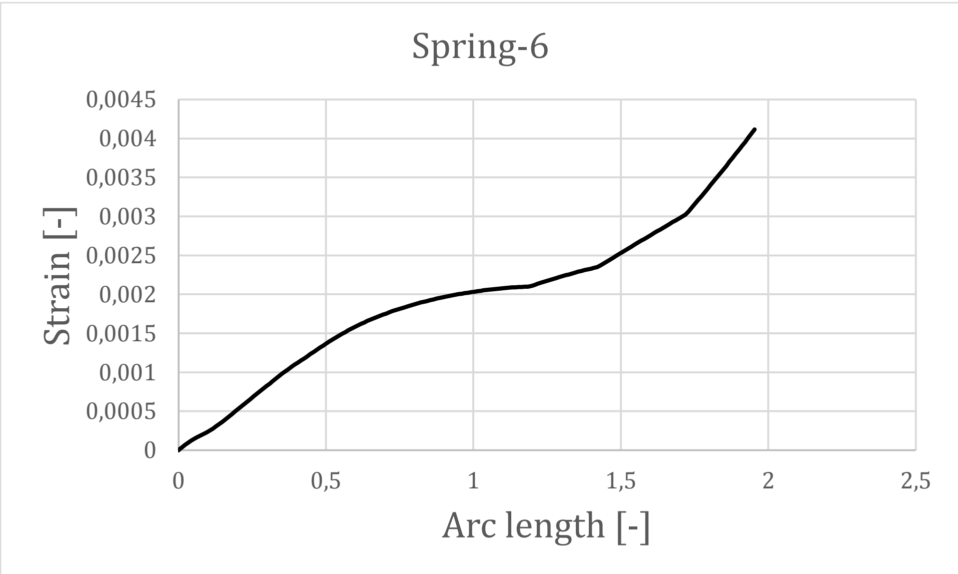

Figure G.66 Strain-arc length relationship for Spring-6 at Arc length 1.954.

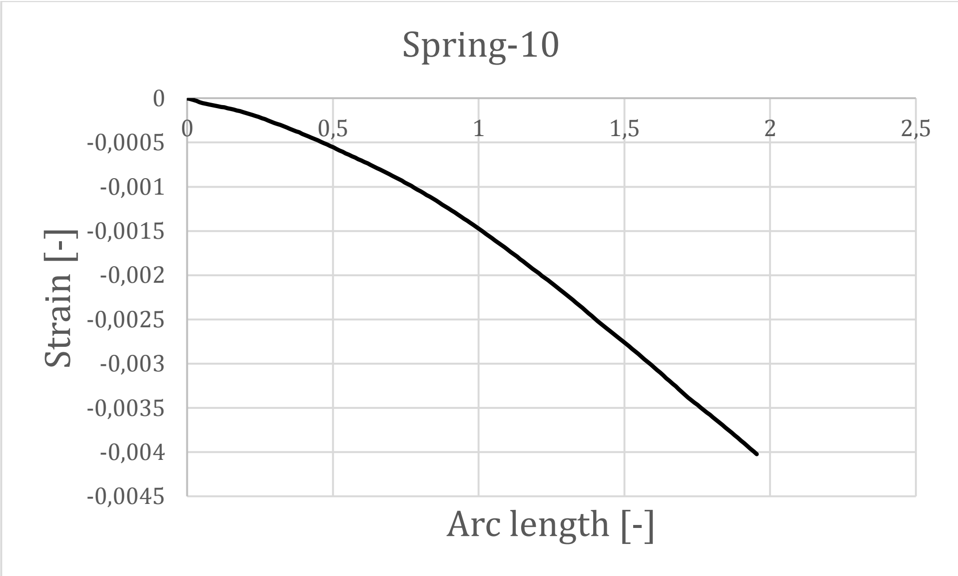

Figure G.67 Strain-arc length relationship for Spring-10 at Arc length 1.954.

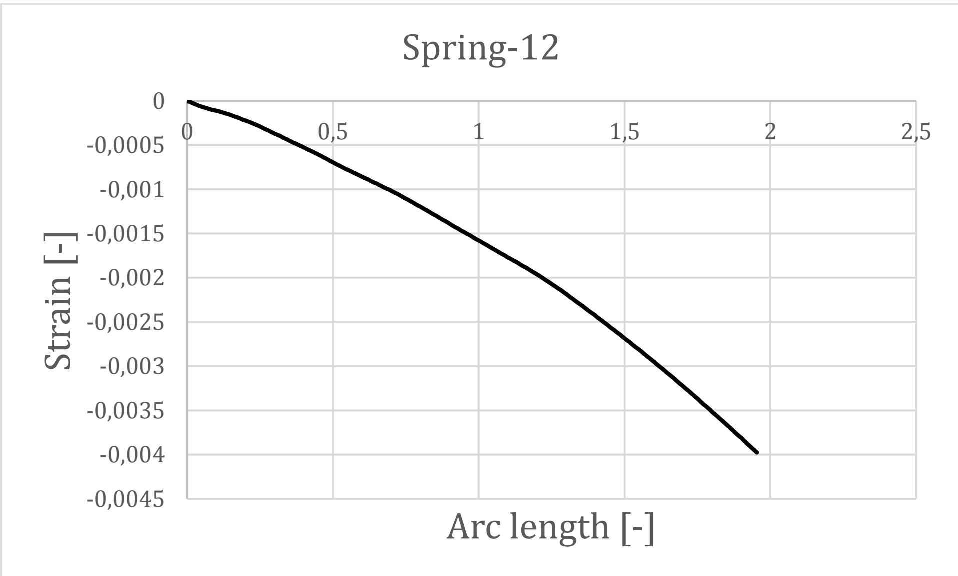

Figure G.68 Strain-arc length relationship for Spring-12 at Arc length 1.954.

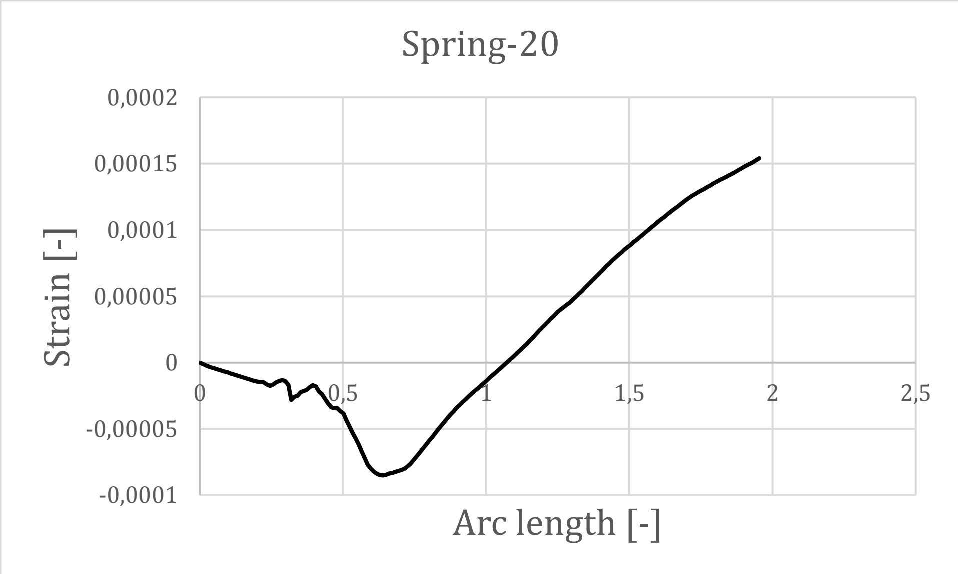

Figure G.69 Strain-arc length relationship for Spring-20 at Arc length 1.954.

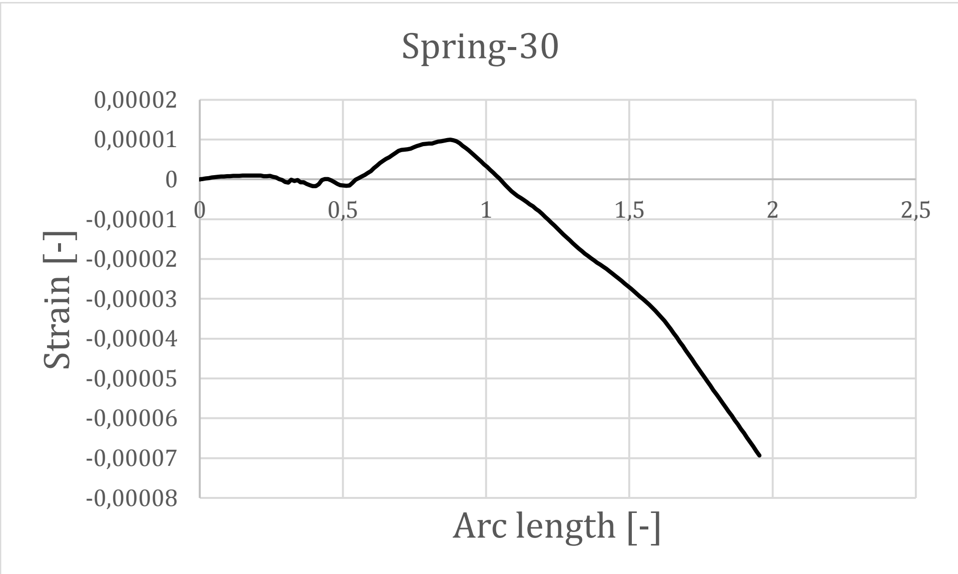

Figure G.70 Strain-arc length relationship for Spring-30 at Arc length 1.954.

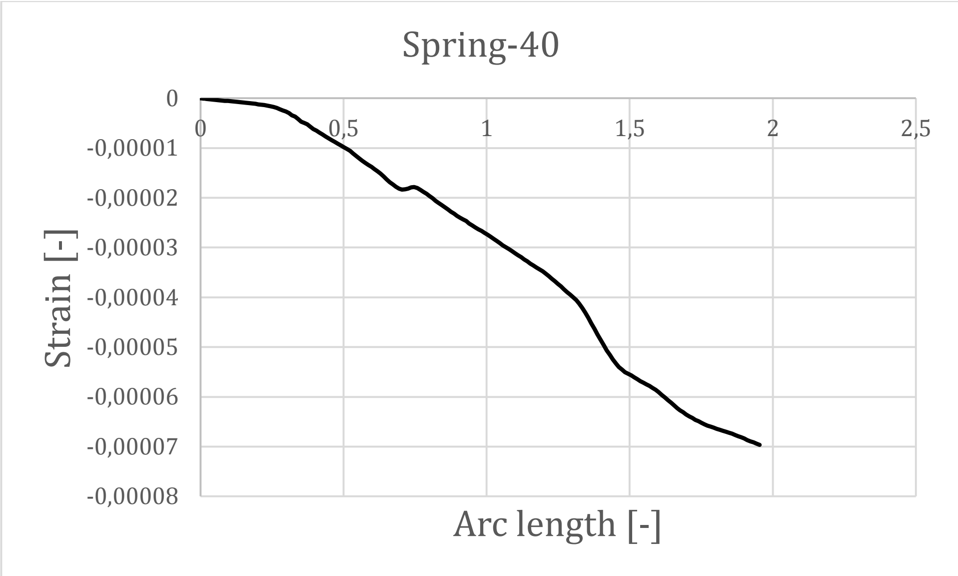

Figure G.71 Strain-arc length relationship for Spring-40 at Arc length 1.954.

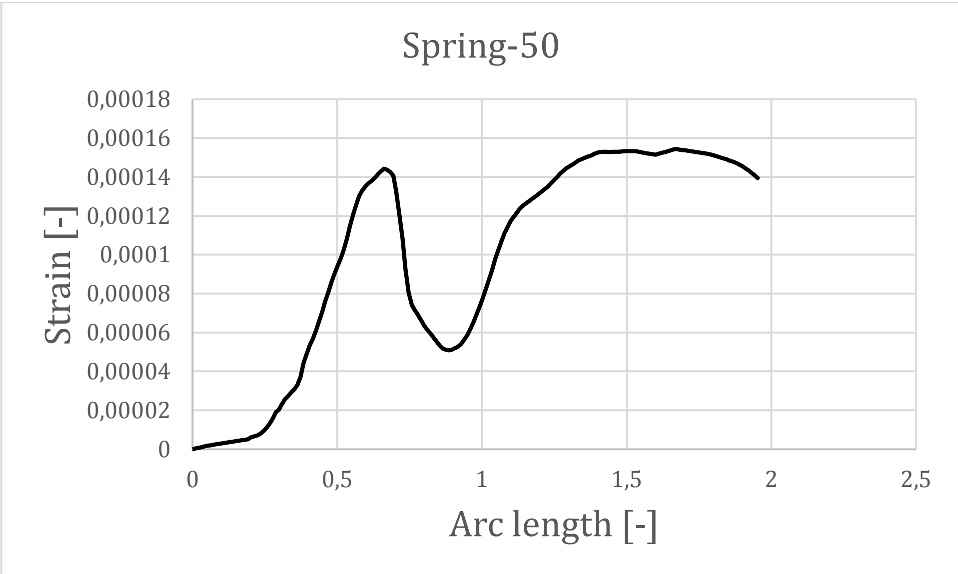

Figure G.72 Strain-arc length relationship for Spring-50 at Arc length 1.954.

Arc-length 2.232

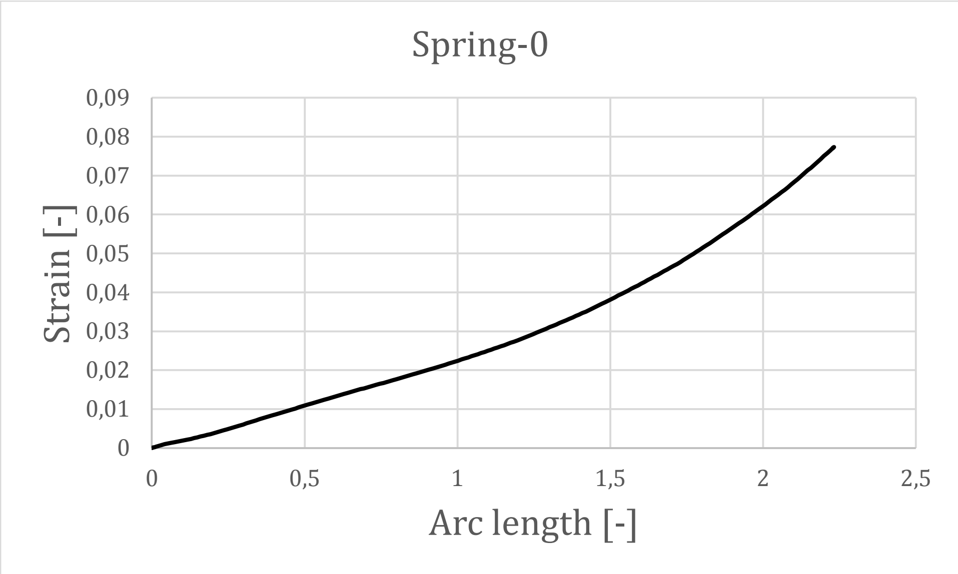

Figure G.73 Strain-arc length relationship for Spring-0 at Arc length 2.232.

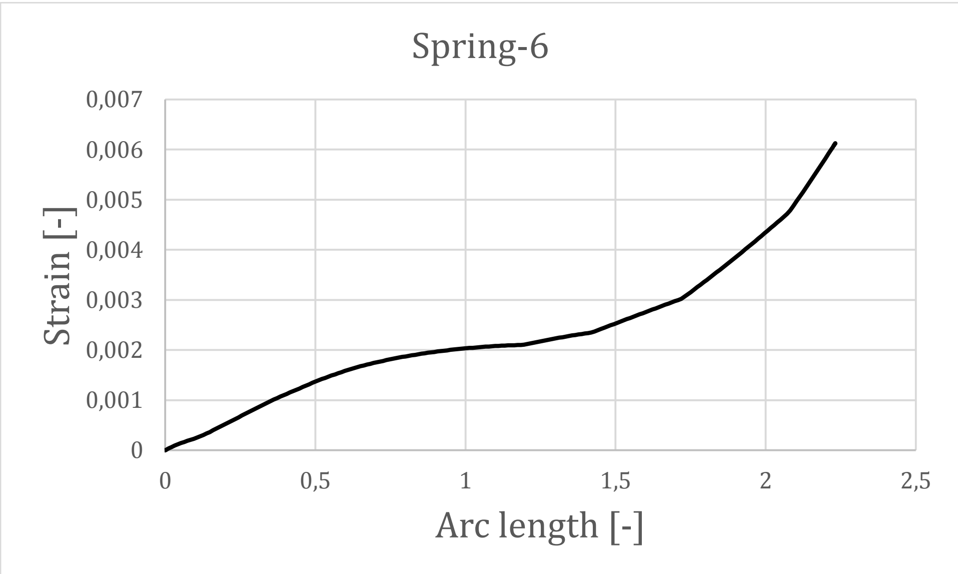

Figure G.74 Strain-arc length relationship for Spring-6 at Arc length 2.232.

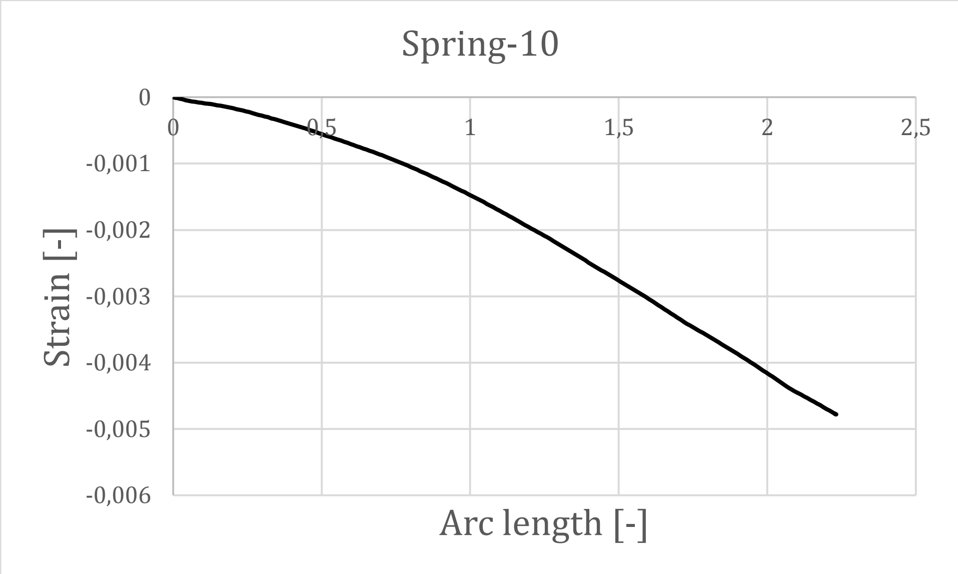

Figure G.75 Strain-arc length relationship for Spring-10 at Arc length 2.232.

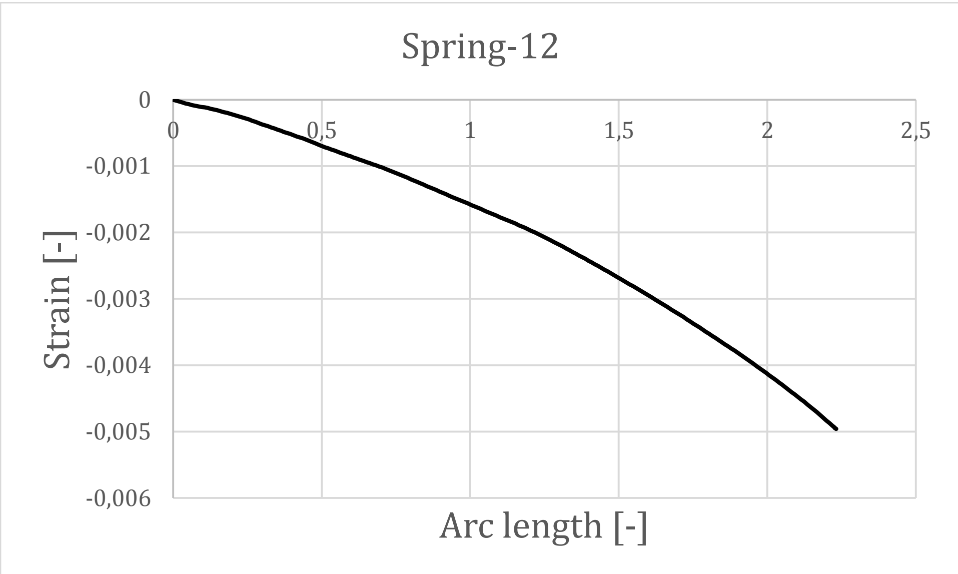

Figure G.76 Strain-arc length relationship for Spring-12 at Arc length 2.232.

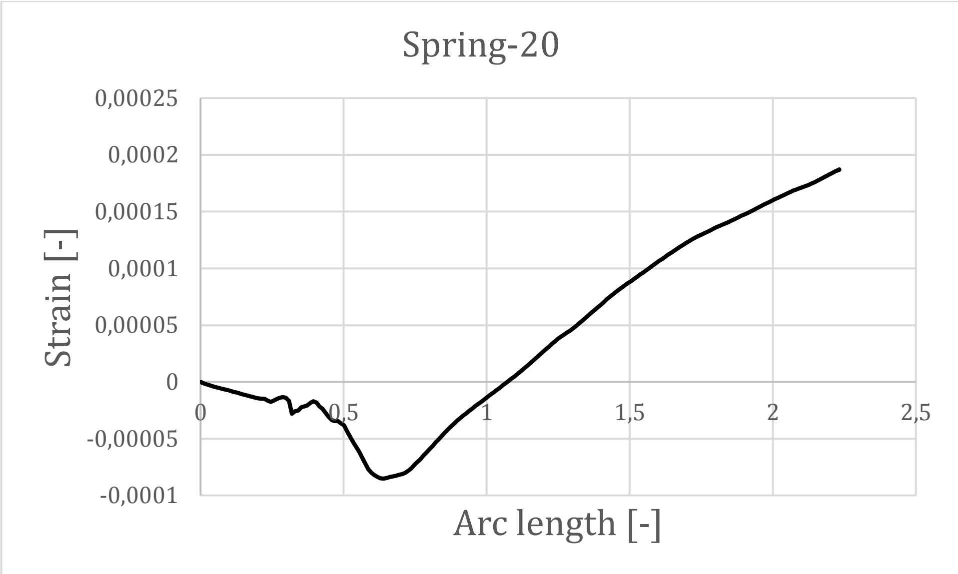

Figure G.77 Strain-arc length relationship for Spring-20 at Arc length 2.232.

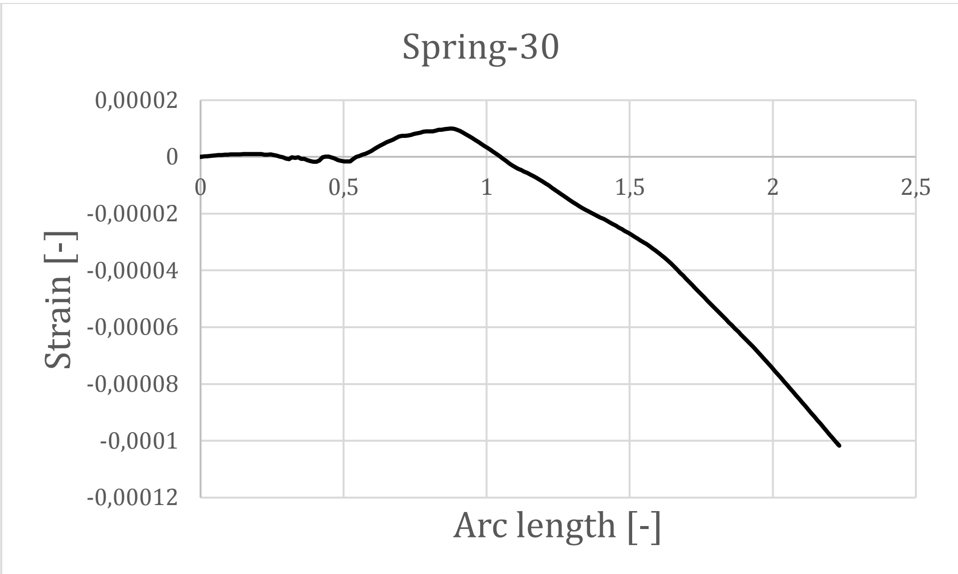

Figure G.78 Strain-arc length relationship for Spring-30 at Arc length 2.232.

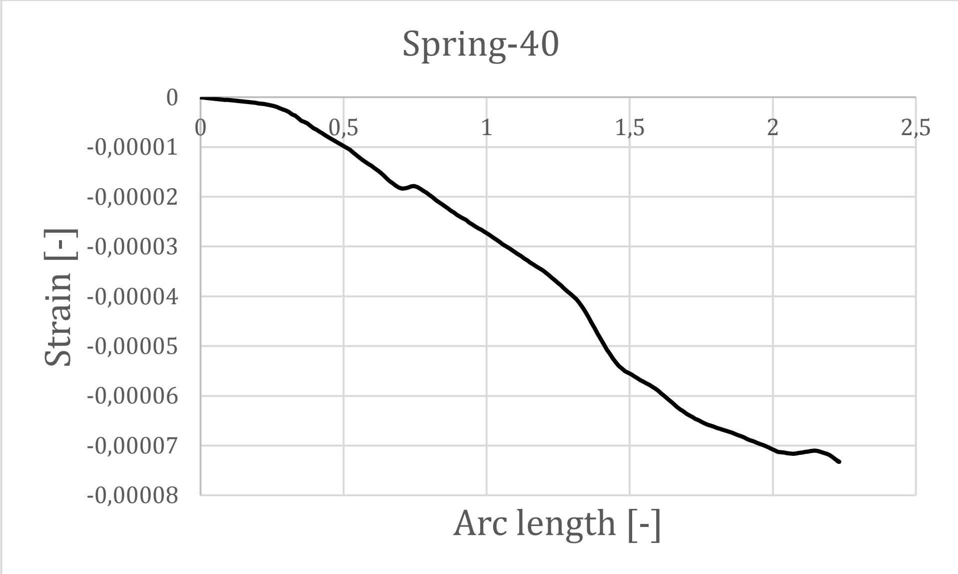

Figure G.79 Strain-arc length relationship for Spring-40 at Arc length 2.232.

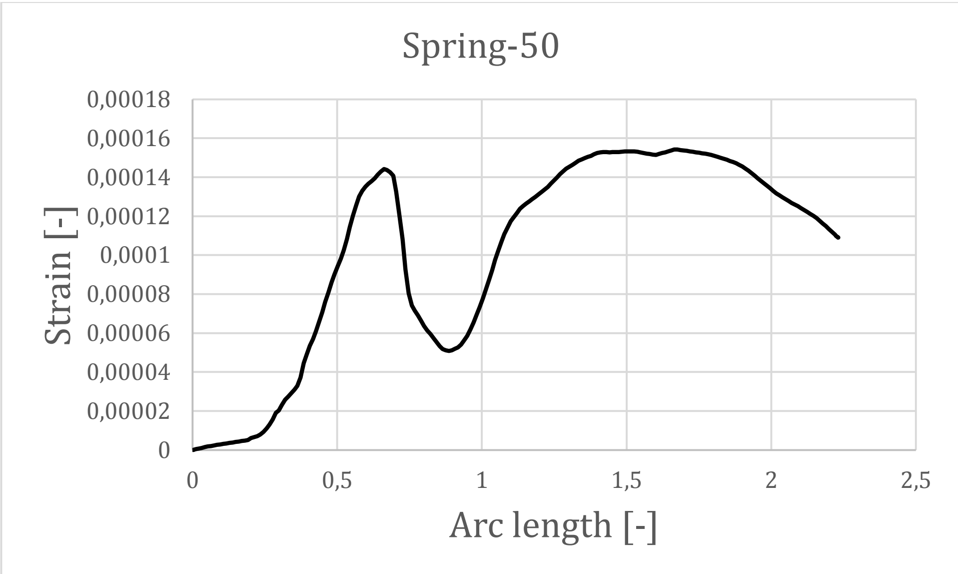

Figure G.80 Strain-arc length relationship for Spring-50 at Arc length 2.232.